Thermodynamics of Helium and Hydrogen Films Adsorbed on Single-Walled Carbon Nanotube Bundles

Tate Wilson

A dissertation submitted in partial fulfillment
of the requirements for the degree of

Doctor of Philosophy

University of Washington

2004

Program Authorized to Offer Degree: Physics

ProQuest Information and Learning Company
300 North Zeeb Road
P.O. Box 1346
Ann Arbor, MI 48106-1346

University of Washington
Graduate School

This is to certify that I have examined this copy of a doctoral dissertation by

Tate Wilson

and have found that it is complete and satisfactory in all respects,
and that any and all revisions required by the final
examining committee have been made.

Chair of Supervisory Committee:

Oscar Vilches

Oscar Vilches

Reading Committee:

Oscar Vilches

Oscar Vilches

L B Sorensen

Larry Sorensen

J G Dash

Greg Dash

Date: 8/20/04

In presenting this dissertation in partial fulfillment of the requirements for the Doctoral degree at the University of Washington, I agree that the Library shall make its copies freely available for inspection. I further agree that extensive copying of this dissertation is allowable only for scholarly purposes, consistent with "fair use" as prescribed in the U.S. Copyright Law. Requests for copying or reproduction of this dissertation may be referred to Bell and Howell Information and Learning, 300 North Zeeb Road, Ann Arbor, MI 48106-1346, to whom the author has granted "the right to reproduce and sell (a) copies of the manuscript in microform and/or (b) printed copies of the manuscript made from microform."

Signature____________________

Date 8/20/04

University of Washington

Abstract

Thermodynamics of Helium and Hydrogen Films Adsorbed on Single-Walled Carbon Nanotube Bundles

by Tate Wilson

Chair of Supervisory Committee:

Professor Oscar Vilches
Physics

Adsorption of Helium and Hydrogen on bundles of single walled carbon nanotubes (SWCNs) has been studied via heat capacity and volumetric isotherm measurements. These measurements allow conclusions regarding the growth of the films, the dimensionality as a function of density, and the structure of the films. Comparisons can then be made, both quantitative and qualitative, to theories regarding ideal and real one-dimensional systems, as well as the theory of adsorption specifically on the SWCNs.

In this thesis I describe the experiments, focusing mostly on the heat capacity measurements. These are the first systematic measurements of the heat capacity of this system as a function of both coverage and temperature. The data support some of the earlier conclusions about growth of the films, in particular the 1-line → 3-line → monolayer progression with little or no adsorption in interstitial sites. There are also new mysteries presented. Most importantly we see no evidence of a gas phase at all, and instead have small and increasing heat capacity, indicative of a solid, or at least immobile system. This observation is inconsistent with all of the predictions so far, as well as with a previous experiment (Lasjaunias *et al.*, 2003). Finally, the helium film is one dimensional at very low density,

as expected, but also at roughly 3/4 of a monolayer, whereas hydrogen appears to be two dimensional at all coverages. These surprising facts need further theoretical development.

TABLE OF CONTENTS

LIST OF FIGURES

LIST OF TABLES

GLOSSARY

Terms

ADSORPTION: process in which molecules from the gas phase of one species form bound states on the surface of the condensed phase of another species.

PHYSISORPTION: when the forces involved in adsorption are of the weak van der Waals type, the system is said to be physically adsorbed or physisorbed, as distinct from chemical adsorption.

Abbreviations and Acronyms

AD: Arc-Discharge. A method for making tubes in which an electric arc is struck between an electrode of carbon and catalyst, and one of cooled copper. Carbon evaporates from the electrode and collects on the copper in the form of tubes. Our sample of AD tubes was made at Montpellier and was donated to us.

CVD: Chemical Vapor Deposition. A method for making tubes in which a hydrocarbon is decomposed in the gas phase and deposited on a cold substrate. This method is typically used to make a few nanotubes at a time on a substrate.

LA: Laser Ablation. A method for making tubes in which a pellet containing carbon and catalyst is vaporized by heating with a laser. Our sample of LA tubes was purchased from Carbon Nanotechnologies Incorporated.

SWCNs: Single-Walled Carbon Nanotubes. I will occasionally use this to mean bundles as well, as single-wall tubes which are not associated in bundles are not discussed in this thesis.

TPD: Temperature Programmed Desorption. An experimental technique in which the temperature of a sample with an adsorbed film is raised at a constant rate and the rate at which the film is desorbed is measured as a function of temperature.

Symbols

k_B: The Boltzmann constant, which in effect sets the SI scale of temperature to the Kelvin. $k_B = 1.38 * 10^{-23}$, in Joules per Kelvin.

q_{st}: Isosteric Heat of Adsorption. The derivation of this is in Section 5.2.

ACKNOWLEDGMENTS

I began my long education as a scientist by taking a few 'self improvement' courses at a community college. I soon took an interest in physics and calculus, and after some time, almost by accident, I had a bachelor degree. I determined to go to graduate school, not to become a physicist, but only because I was not yet done studying physics. At that point I had worked for Oscar Vilches in his lab for a few years. When he took me aside one day and told me that he hoped I would stay at UW and work with him as a graduate student, he set the course of a drifting boat.

I have had a great deal of support from various people in the UW physics department. Thanks to Bob Morley for quickly and expertly fixing all my glass, and then not getting frustrated when I broke it again. Thanks to Bryan Venema for many hours of troubleshooting electronics and for making the excellent schematics for this thesis. Thanks to the many professors in the condensed matter group for their interest and for many helpful discussions. And many thanks to Kim Hawley and Nichole Fernkes for keeping the bureaucracy under control and letting me focus on my work.

I think it is fair to say that, in general, friends, regardless of intention, can only impede one's progress toward a doctoral degree. In my case there are several notable exceptions. Everyone who goes through this process experiences their own private misery along the way. It always seemed that my trials were well matched to those of Richard Elliott, and commiserating with him was indispensible therapy. Neal Weiner, on the other hand, set an example and made an indelible impression by proving that one can go through this process and remain a whole and happy person. Whether in course work, lab skills, programming and software issues, or even using LaTeX to format a thesis, Clark Griffith always seemed to be one step ahead of me, and from that vantage point was able to teach me a great deal. Suzanne Joneson has tireless worked to teach me that, no matter how hard I work, I still need to love. And in the last desperate days when I was too consumed with this thesis to even care for myself, my good friend Jack Millard let his parents Robert and Lisa house and feed me.

No matter how many times I change direction, or redefine the goal, my family has never given up hope.

This work was funded by the NSF, DMRs 9876763, 0245423, and 0115663

Chapter 1

INTRODUCTION

In the last ten years the physics of real, weakly interacting, one-dimensional systems has become the subject of experimental tests. We hope that fundamental ideas about one dimensional systems, as well as results of some 'toy' models which were never thought to represent real systems, will now be checked.

This thesis is concerned with experimental measurements of the thermodynamic properties of films of helium and hydrogen adsorbed on bundles of carbon nanotubes, and the connection of these measurements to the physics of real one-dimensional systems. This is a very narrow slice of the much larger field of studies of physisorption, which has a rich history, mostly in the past four decades. In this chapter I will present some of the key motivations for studying adsorption specifically on nanotubes. Then I'll give a cursory history of studies of physisorption, focusing almost exclusively on the results which are of direct relevance to this study. I'll use this opportunity to introduce many of the key concepts and terminology. Finally I'll introduce nanotubes and nanotube bundles and compare these to their close relative and the canonical substrate for studies of physisorption, graphite.

1.1 Motivation

1.1.1 Applications

There are several reasons, some applied and some more esoteric, to study adsorption on nanotube bundles. While my own research is concerned with the quantum mechanical and statistical properties of condensed systems in restricted geometries, I will list here several other motivations which have been expressed in the relevant literature. These include, on the applied side:

- Hydrogen storage for fuel cell applications.

  The Department of Energy has set target values for density and mass percent of hydrogen storage in fuel tanks to be used on fuel cell powered vehicles. Previously, chemically stored hydrogen in metal hydrides have achieved the highest densities, with the greatest technical challenge being the manufacture of materials with larger surface area to mass ratios. Hydrogen chemically adsorbed in this way can also be difficult to recover in a controlled way.

  The very large surface area to mass ratios for SWCN bundles, together with high calculated binding energies for some of the adsorption sites, has spurred interest in these materials as an absorbent for hydrogen. The capacity of current, 'as prepared' samples is shown on the chart, Figure 1.1. The capacity of the material can be increased by chemical treatments which open the tubes for adsorption on the inner surface, but the open tubes are highly reactive and prone to re-close on contact with other reactive molecules. It has been shown recently that under very high pressure the hydrogen molecule can dissociate and the hydrogen atoms chemisorb on the surface, thus greatly increasing the binding energy, but again making it very difficult to recover the hydrogen for use [18]. The targets have not been reached using carbon nanotubes, however, the DOE remains hopeful and continues to fund research in this area.

- Chemical sensing.

  Nanotubes and nanotube bundles may be very sensitive detectors of particular chemical species in a gas. Practically, this detection may be accomplished in two ways. One either measures the electrical transport properties of a single tube in the presence of the gas to be tested, or adsorbs a large quantity of the sample into bundles of tubes and determines later during desorption which species were present.

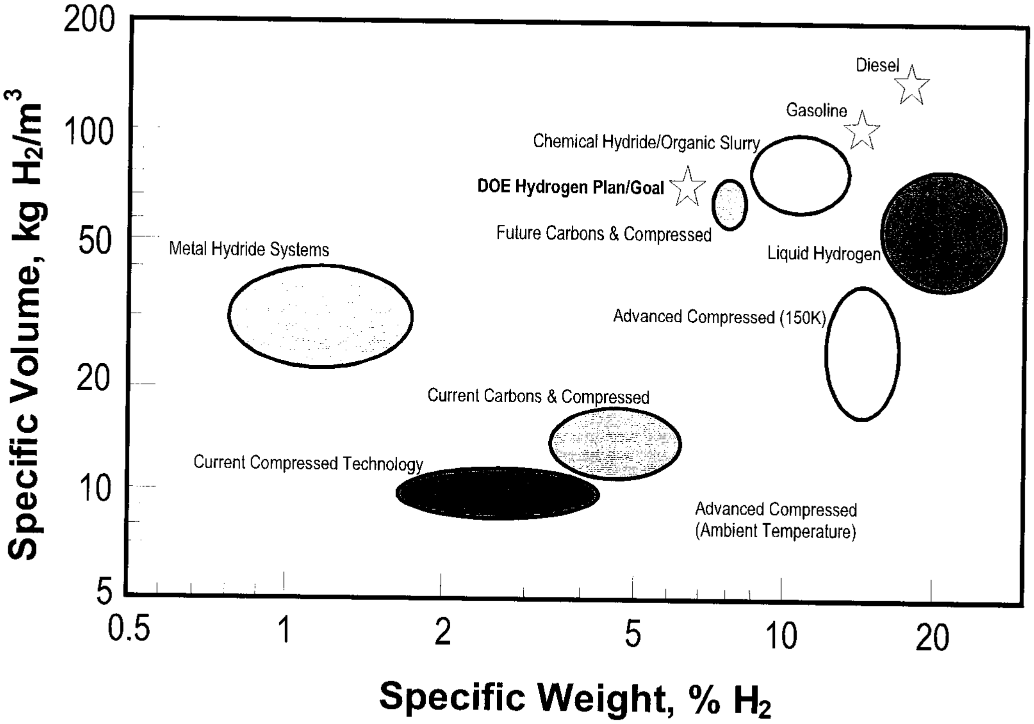

Figure 1.1: The hydrogen storage density of various technologies, shown with the Department of Energy target value. Note the very optimistic projection for "Future Carbons and Compressed". This figure is from a DOE report from 2002.

A single, single-walled nanotube displays a very complex band structure, which is very sensitive to defects in the tube structure. The small perturbation that an adsorbed molecule makes in this band structure can be sensitively detected. If these properties are sensitive even to the type of molecules adsorbed, extremely sensitive detectors could be made from single tubes [16, 49, 36, 10]. Even if the chemical species cannot be distinguished in this way, it may be possible to make highly sensitive pressure gauges, for very low pressures.

Atoms or molecules of different species are adsorbed to a given surface with varying strength. The binding energy depends on the strength of the interaction with individual substrate atoms, as well as some considerations of geometry. For example, on a porous substrate, atoms clearly must fit into the pores to be adsorbed strongly. In general, substrates with higher binding energies also have a larger spread in binding energies for differing adsorbates. In a temperature-programmed desorption experiment (see Section 1.2.2) the various gasses will be desorbed at different temperatures. If a sample of unknown gas mixture were adsorbed on a strong binding substrate, the various components can be identified by the location of peaks in the desorption.

- Gas purification.

  In the same way that chemical species can be detected during desorption as described above, gasses can be separated into constituent elements by collecting and sequestering that portion of the gas that desorbs at a particular temperature. Isotopes can also be separated by porous media through a process called quantum sieving, similar to molecular sieving except that the particles have the same (classical) size [81, 6]. There are estimates that the selectivity of this type of separation may be as much as 10^6 times that of traditional techniques.

- Nanotechnology.

Progress is well underway on nano-electronics and nano-optics made of carbon nanotubes. Because the electronic transport properties of the tubes can be strongly affected by the presence of adsorbates [16], it is important to study adsorption to develop an understanding of the impact that environmental conditions may have on such devices.

1.1.2 Restricted Geometries

The main scientific interest in adsorption on carbon nanotubes arises from the narrow channels and very high aspect ratios present in the nanotube bundles (Section 1.5). Adsorption phenomena and the refinement of substrate fabrication have long allowed researchers to probe the physics of systems in reduced dimensions [21, 13]. The unique geometry of the nanotube bundles extends the possibilities for reduction of dimensionality.

On planar surfaces the potential may be such that atoms on the surface have discrete energy levels for excitations in the direction perpendicular to the surface, so that for low temperatures these excitations are effectively 'frozen', and the film remains in the ground state in this direction. Films on planar surfaces have very complicated behavior, which is intimately tied to the fine details of the structure of the surface, but they do make contact with the physics of idealized 2-D systems in important ways, as well as with 'toy' models. When Ising models first came into common use, it is doubtful that anyone foresaw that the 2-D lattice gas was a real system that would be experimentally studied. With the SWCN substrates we may be able to study the same model systems in 1-D.

There have been 1-D experimental systems available already, but with limitations. There are 1-D electrons on nanowires and nanotubes, but these are a very strongly interacting system of very few particles [1, 34, 5, 10, 36, 49]. Helium adsorbed in the pores in Vycor and FSM-16 can be treated theoretically like a system that approaches one dimensionality, but the behavior is significantly more complicated than this [86, 31, 32], see Section 3.5. For one thing the properties of the film depend very sensitively on the radius of the pore, and most samples have a range of pore sizes. There are odd crystals like the Mercury salt, $Hg_{3-\delta}AsF_6$

[17, 67, 26]. This crystal has one dimensional chains of mercury which are embedded in channels in the AsF_6 lattice, but are not commensurate with it. The Hg chains necessarily interact weakly[1] with the lattice because they are not commensurate. Experimentally this system is lacking because the 'background' cannot be measured separately and the density and temperature cannot be varied independently.

1.2 Physical Adsorption

1.2.1 Forces

Adsorption occurs when atoms or molecules from the gas phase of one species are attracted to and can form bound states on the surface of a condensed phase of a second species. The possible adsorbed systems are divided into two categories, physical and chemical, based on the strength of the binding to the surface and also on the degree to which individual adsorbate particles retain their chemical identity. There is a large gray area at medium energies in which the distinction between physical and chemical adsorption is not sharp and is largely a matter of taste. Far from this gray area the distinction can be made clear by choosing the underlying interaction to be chemical (or ionic) binding for chemisorption, and induced dipole-dipole interactions (van der Waals forces) for physisorption. By this criteria one would assume that the noble gasses and many other inert, light atomic and molecular gasses would be physisorbed on solid, relatively inert substrates. This has been a standard assumption in the majority of physisorption studies and has been well born out by the results. The issue becomes a bit trickier when the substrate is 'soft', such as a liquid or a film of another adsorbed species. This is because we intend to measure the properties of the substrate with no film, then add a film, remeasure, subtract the extensive properties of the two systems, and assign the difference to the 'film'. It is always an approximation that the properties of the substrate do not change with the addition of the adsorbate. This is important only because what we wish to measure needs to have some connection to a

---

[1] Here, 'weakly' means not chemically bound.

theoretical model. In particular, we are interested in the properties of systems of particles of the adsorbate in a static external potential. This is the system which can be theoretically modeled as a separate film and substrate. If the approximation is bad, we measure instead a system of particles of both the adsorbate and substrate atoms, in no external potential. As I will discuss in Section 7.4, the approximation may not be very good in the present study, due to the weak binding between tubes in the bundles.

The underlying interaction between a physisorbed particle and an atom in the substrate is due to the correlation of the 'random' motions of the electrons in each. The leading term in this interaction is the dipole term, so this is usually thought of as an attraction between correlated fluctuating electric dipoles, known as London dispersion forces [51].

This is the attractive part of the interaction, but of course the atoms or molecules cannot occupy the same space, so there must also be a repulsive part of the interaction which prevents the particles from overlapping. A standard approximation to the repulsive interaction is to add a term with r^{-12} to the van der Waals potential. This leads to the two parameter Lennard-Jones potential [50],

$$V(r) = 4\epsilon\left[\left(\frac{\sigma}{r}\right)^{12} - \left(\frac{\sigma}{r}\right)^{6}\right] \tag{1.1}$$

where ϵ is the depth at the minimum of the potential, which occurs at $2^{1/6}\sigma$, Figure 1.2.

The Lennard-Jones potential is conceptually clean, and is a good enough approximation for many qualitative features of an interaction. With the advent of computers, calculations with more realistic potentials (such as the Aziz potential [4]) have become tractable, and many such potentials are employed to solve the more current problems in adsorption. It is interesting that a recent calculation [43, 44] shows a condensed phase at T = 0 for one dimensional helium using either the Morse or Aziz potentials, but the same calculation arrives at no condensed phase if the L-J potential is used.

The van der Waals interaction is an interaction between two neutral particles. In a system of many particles it is sometimes assumed, as a rough approximation, that the total interaction is a pair-wise sum of van der Waals interactions. With this assumption, along

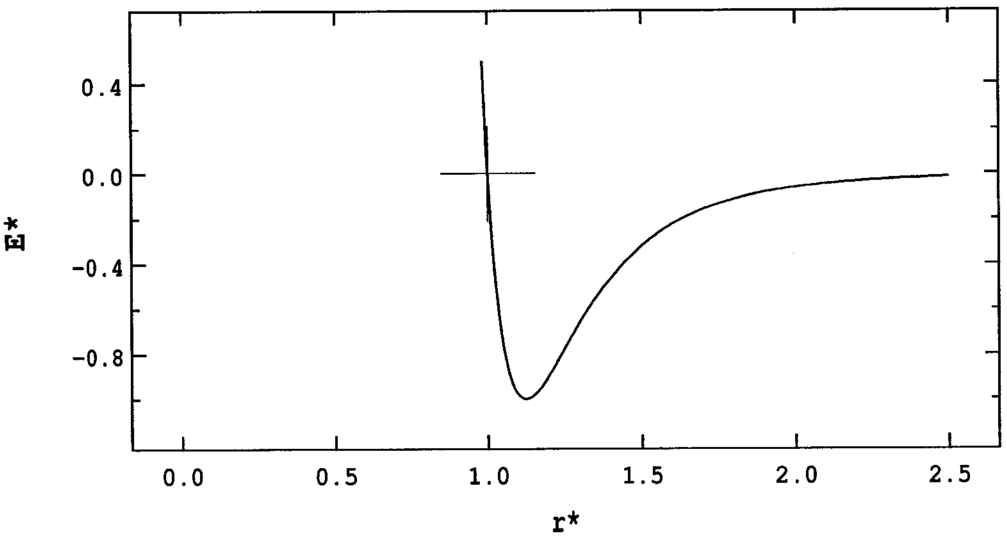

Figure 1.2: The Lennard-Jones potential, plotted in the dimensionless parameters $\mathbf{r}^* = r/\sigma$ and $\mathbf{E}^* = \mathrm{E}/\epsilon$. The zero crossing occurs at $\mathbf{r}^* = 1$ and the minimum of the potential occurs at $\mathbf{r}^* = 2^{1/6}$.

with some mathematical form for the pair interaction, one can use the geometry of the substrate to calculate a potential for adsorption to the surface. An alternative derivation of the potential treats the surface as a continuous dielectric medium, with an effective adsorbate interaction based on the average pair potential.

The pair-wise summation of the adsorption potential is an approximation. The correlation of the instantaneous dipole moment of the adsorbate atom with one of the substrate atoms modifies its interactions with other substrate atoms, as well as influencing the interaction between the substrate atoms themselves. It can be shown by calculating the contribution of 3-body interactions that the depth of the potential is over-estimated by the pairwise summation method [42, 13].

Now that we have confinement of the atoms on the surface, we can worry about their interactions. Given that the substance is of a type that is physisorbed on the surface, these inter-adsorbate interactions will necessarily be due to van der Waals type forces. Treating these forces theoretically involves the same complications as the adsorption potential, plus a few more. One uses an approximate form such as the L-J potential, and then could make a pairwise summation, in the situation that the film is solid, which is also approximate. The film needn't be solid, and is therefore much more complicated than the adsorption potential. In this case a mean field theory is usually required, though occasionally the film can be very simple, such as an ideal gas. Two dimensional helium and hydrogen gasses on graphite have successfully been treated as quantum virial gasses [66, 53].

The extent to which the film is two dimensional, or how closely two dimensional calculations approximate the measured properties of the real film, depends on how important are the fine details of the substrate which are neglected in the calculations. Hence the 'dimensionality' of adsorbed films is found experimentally to vary greatly depending on the adsorbate/substrate combination.

1.2.2 Experimental Techniques

I include here a *very* brief review here of some of the techniques traditionally used to study adsorbed films. We have used 3 of these techniques; heat capacity and vapor pressure isotherms presented in this thesis, and neutron scattering studies completed with our collaborators in Marseille [8, 39]. At least these three experiments are necessary to establish a phase diagram such as the ones in Figure 1.3. The over simplified view is that the heat capacity measurements establish the vertical boundaries, isotherms establish the horizontal ones, and scattering experiments determine the structure within the regions bounded. Each of these experiments is richer than this view suggests, and the results overlap and reinforce one another.

Vapor Pressure Isotherms

A physisorbed film always coexists with a 3-D vapor of the same species. We take advantage of this to measure the chemical potential of the film as a function of density. The chemical potential of the 3-D vapor, and therefore of the film, is proportional to the log of the pressure and is thus easily measured. The quantity adsorbed in the film may be measured many ways. We use the volumetric method described in Section 4.1. The coverage may also be monitored by micro-balance or surface scattering techniques.

The vapor pressure isotherm was the first experiment used studies of physisorption, and continues to be the mainstay. It is easy to measure and contains a wealth of information. It was also the first place where good quantitative contact was made between theory and experiment, with the pioneering work of Langmuir in 1916 and Brunauer, Emmett and Teller in 1938.

Heat Capacity

The thermodynamic definition of the constant volume heat capacity is $C_V \equiv [\partial U/\partial T]_V$. Experimentally, there are several methods for measuring C_V which approximate the thermodynamic definition:

- DC Calorimetry 1, Adiabatic heat pulse.

  This is the method used extensively in our laboratory for the measurement of the heat capacity of 2-D adsorbed films. The thermodynamic definition of the heat capacity is approximated by $C_A \sim \left(\frac{\Delta Q}{\Delta T}\right)_A$, with ΔQ the heat input form an electric heater, $(\Delta Q = I^2 R_{heater} \Delta t)$, and ΔT is the measured change of the sample temperature. For details of the method see the thesis of Roberto Ramos [60]. This method was not used in the experiments described in this thesis.

- DC Calorimetry 2, Relaxation time constant.

  The calorimeter cell is connected through a thermal resistance R to a heat bath at constant temperature T_0. Beginning at time $t = 0$ heat is supplied to the cell at a constant rate from an electric heater, $\left[\dot{Q} = I^2 R_{heater}\right]$, producing a rise in the cell temperature asymptotically approaching T_F with a time constant $\tau = RC$. One obtains $R = (T_F - T_0)/\dot{Q}$, and τ from the measured time to reach equilibrium, and finally $C = \tau/R$.

We used this method to check that the magnitude of our AC measurements was correct, but the method is not well suited to our cryostat and cell. The application of this method in our system is described in detail in Appendix B.

- AC Calorimetry.

  Here the cell is again linked to a heat bath through a thermal resistance. An oscillating voltage is applied to an electric heater on the cell, resulting in an oscillating heat input which can be separated conceptually into a DC and a sinusoidal part. The DC part leads to an offset of the cell temperature from that of the bath and the AC part leads to oscillations of the cell temperature around this offset value. From the value of the sinusoidal part of the heat signal and the measured oscillatory part of the temperature response we can extract the heat capacity. This is described in detail in Appendix A. The advantage of the AC technique is that the temperature response can be averaged over many cycles to improve sensitivity. The main disadvantage is that it places severe restrictions on the design of the cell (see Appendix A).

Scattering

The many scattering techniques can be loosely grouped in two categories based on the depth to which the scattered particles penetrate the sample. Atoms and electrons can be scattered from the surface, or reflected, with information gleaned both from Bragg reflections and in some cases from polarization of the reflected particles. This requires very clean, well oriented surfaces. Neutrons, electrons, and x-rays can be transmitted through the sample. This allows the use of powder samples without special orientation of the surfaces, but in exchange requires that the surface area to volume ratio be very large.

Desorption

In a temperature programmed desorption experiment, on begins with the film adsorbed on the substrate and held at a low temperature. Then the sample is heated so that the rate of change of the temperature is constant. During the process the cell is evacuated through a mass-flow meter or mass spectrometer, or through some other means of determining the rate at which gas evolves in the cell due to desorption. There will be a peak in the desorption rate at some temperature, which can be related to an average heat of adsorption for the film. By repeating the experiment with different initial densities of the film, the heat of adsorption vs. coverage can be mapped, similar to typical measurements of the isosteric heat of adsorption from vapor pressure isotherms.

Other

The heat of adsorption can sometimes be measured directly. With a very low mass sample attached to a sensitive bolometer, one allows short bursts of adsorption by, for example, exposing the sample to a pulsed molecular beam. If all of the molecules were adsorbed, the energy deposited in the bolometer is the heat of adsorption, with the complication then being to determine the number adsorbed. In general, not all of the molecules are adsorbed, but this is an experimental complication which can be solved.

There are many other experiments commonly used to study adsorbed films. The selection presented here is based on relevance to our own studies, not a judgement of the value of the techniques.

1.3 Helium as Adsorbate

The unique combination of closed electronic shells, which leads to very weak interactions, with very light masses makes the two helium isotopes the most ‘quantum’ naturally occurring substances. They have no solid-liquid-vapor triple point, and no solid even at T=0 (except for ^{4}He at pressures above ~26 atmospheres). The critical temperature is 5.2 K for ^{4}He and 3.1 for ^{3}He, far lower than for any other substance.

Helium is the only substance for which a superfluid has been observed, though such a state should in principle be possible for other substances. The mechanism by which superfluidity is achieved in the bulk does not work in the restricted geometry of a thin film, and it was once thought that for this reason superfluidity could not exist in two dimensions. Superfluidity was observed however in films even down to one atomic layer, and it was eventually understood as a manifestation of the Kosterlitz-Thouless transition [21]. This mechanism too cannot work in 1-D, yet superfluidity of helium in pores as small as 18 Å, thought to be small enough to be quasi-one-dimensional, has been observed [86].

1.4 Hydrogen as Adsorbate

Hydrogen has the lowest solid-liquid-vapor triple point at 13.8 K in the bulk. It is also a boson (molecular hydrogen, of course), and if it could be kept fluid to lower temperatures, it is predicted to have a superfluid transition at 6 K. Confining H_2 to a 2-D film lowers the triple point significantly. T_t varies with substrate, but has been observed as low as 5.74 K on D_2 plated graphite [11]. Unfortunately the temperature of the hypothetical superfluid transition also moves to lower temperature in 2-D, still lower than the observed S-L-V triple point temperatures. A superfluid transition has not yet been observed for H_2.

H_2 is much lighter than ^{4}He, making it more 'quantum', but on the other hand it is more strongly interacting due to its greater polarizability, which tends to wash out some quantum effects. D_2 has the similar interaction strength to H_2, but almost the same mass as ^{4}He, and is again a boson. So by using these three species it is possible experimentally to change one at a time the two most important parameters governing the behavior of the quantum fluid.

Using hydrogen also in a sense lowers our effective operating temperature. It is an oversimplification to say that whatever behavior helium displays will be repeated for hydrogen at a higher temperature, but many qualitative features of the phase diagrams for the two adsorbates on graphite are simply shifted in temperature, Figure 1.3. It is possible then that features we might miss in helium, because they are below our temperature range, might be seen for hydrogen without having to go colder.

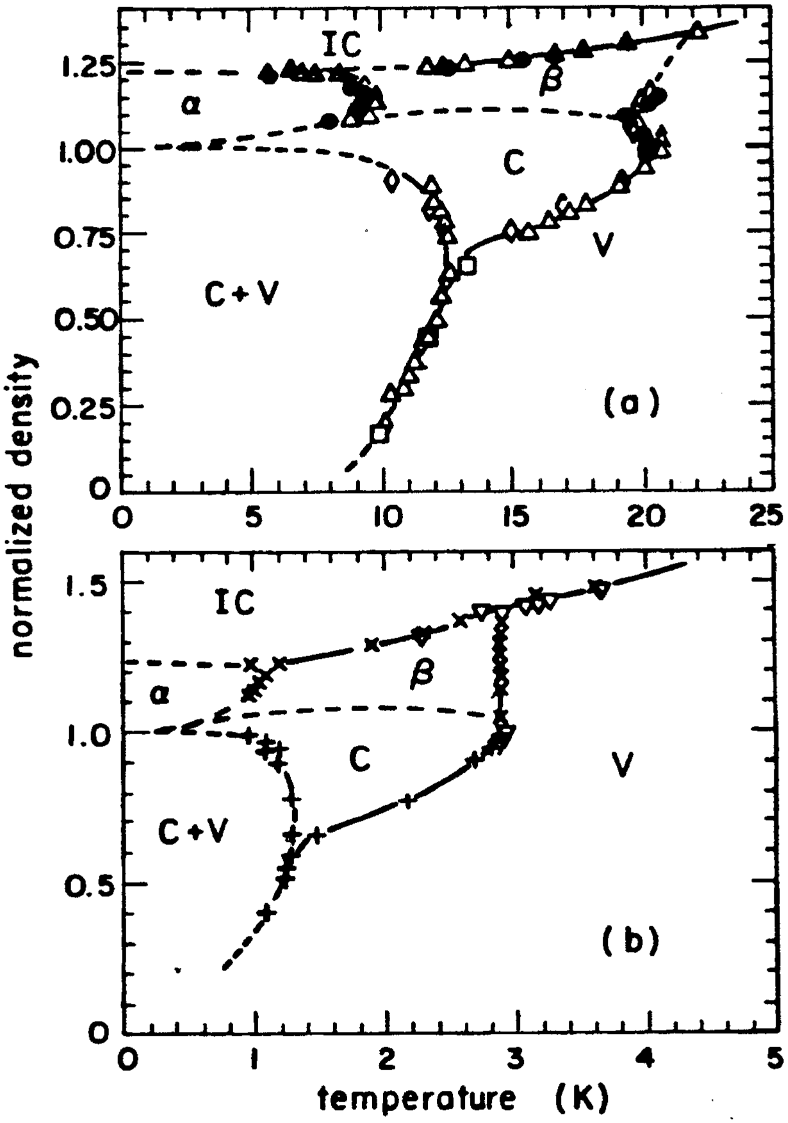

Figure 1.3: A comparison of the phase diagrams of H2 (top) and ^{4}He (bottom) on graphite, from the thesis of Frederick Motteler [55]. C, IC, and V denote the commensurate solid, incommensurate solid, and vapor. α and β are complicated 'exotic' phases which are not completely understood and are not the same for helium and hydrogen.

1.5 Nanotubes as Substrate

Nanotubes are a novel 'solid'[2] carbon material. A closely related solid carbon structure, graphite, has a long and rich history as a substrate for adsorption studies. As such, it will be useful here to review some of the main features of adsorption on graphite. Then I'll describe carbon nanotubes and discuss what we expect to be the similarities and differences from graphite as a substrate.

1.5.1 Graphite

Graphite has been a very important substrate for studies of adsorption and particularly for studies of two dimensional systems. The graphene planes within the graphite crystal are very flat, and exert one of the stronger binding potentials for adsorption. With the advent of Grafoil™ and graphite foam, substrates with exceptionally high surface area to mass ratios (up to 30 m^2/g) became available.

The graphite surface is strongly corrugated. This is a nusance of sorts, for studies of reduced dimensions, but it also leads to an experimental advantage which can hardly be overestimated. Many adsorbates form a commensurate phase in this corrugated potential, and from the maximum filling of this phase the *exact* surface area of the substrate can be found, regardless of the adsorbate used.

The adsorption potential of graphite is very well understood theoretically, including the details of the corrugation. Often, in summing the pair-wise interactions to get a substrate potential, the variations of the potential with position laterally on the surface are averaged to get a potential only as a function of z, the height above the surface.

The large body of knowledge of adsorption on graphite will be important in this study, because of the expected similarity of the adsorption properties of the curved graphene sheets that form the outer surface of the bundle.

---

[2] Carbon nanotubes exist in a new gray-area between crystals and molecules. What is clear is that they have a rigid structure and are so heavy (up to millions of carbon atoms each) that they behave essentially as a solid.

Helium and Hydrogen on Graphite

Helium is not expected to form a solid in two dimensions. Hydrogen is, but at even lower temperature than in 3-D, where it already has the lowest solid-liquid-vapor triple point of any substance. The classical expectation of T_t for H_2 is 8.2 K, from scaling the 3-D value. Substrates have a strong influence on the behavior of adsorbed systems. In the first layer of ^{4}He and H_2 a solid structure, commensurate with the substrate is observed (density of 0.036 $Å^{-2}$). This commensurate structure overrides the triple point of hydrogen, and prevents helium from remaining fluid to T=0. On other substrates the triple point of hydrogen has been observed, and is as low as 5.74 K on D_2 'plated' graphite [11].

Increasing the density from that of the commensurate phase, several exotic phases are encountered on the way to the incommensurate solid (IS), which begins at about 0.078 $Å^{-2}$ for both species. The maximum densities reached before the second layer begins are 0.120 $Å^{-2}$ for ^{4}He and 0.094 $Å^{-2}$ for H_2.

Two dimensional Debye temperatures (see Section 7.2) have been extracted for the helium and hydrogen incommensurate solids. These are shown for helium together with the 3-D values on a common molecular area scale in Figure 1.4.

1.5.2 Nanotubes

Carbon nanotubes were discovered by Iijima in 1991 [37], as an offshoot of experiments studying the formation and properties of Fullerenes. They are long cylindrical structures of graphitic carbon (the carbon bonds form hexagons, as they do in the planes of a graphite crystal), closely related to the Fullerenes except in aspect ratio. Figure 1.5 shows how the tubes can be thought of as a strip of a graphene sheet, rolled into a cylinder. The rolling vector must be a sum of integral multiples of the two graphene lattice vectors (a and b in the figure), in order to satisfy all the bonds of each carbon atom's hybridized p-orbital (also shown in the figure). This leads to a discrete set of possible tubes, which can be labeled by the coefficients n and m of the rolling vector. These can then be further grouped into three categories based on chirality: 1) $n = m$ → armchair tubes, 2) $m = 0$ → zig-zag

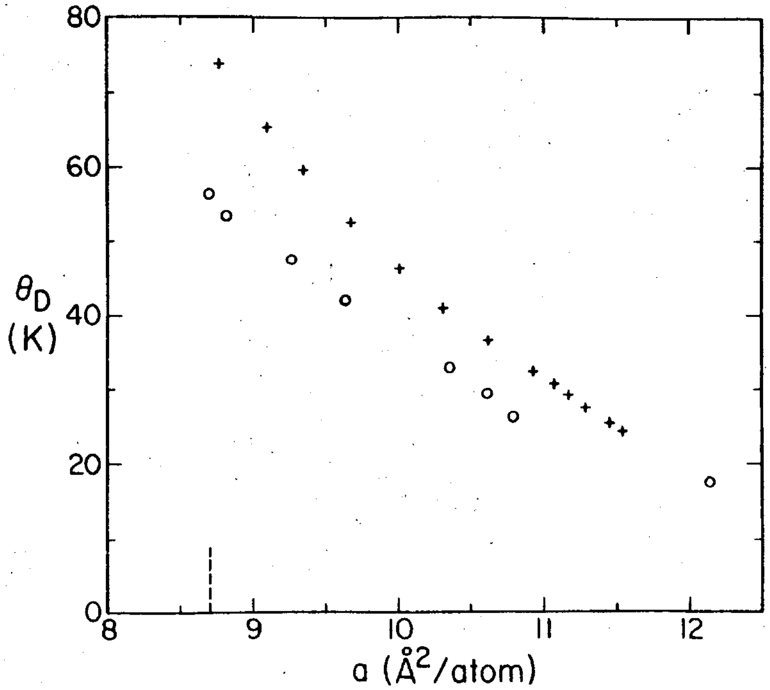

Figure 1.4: Comparison of the Debye temperatures for ^{4}He in the bulk, for 2-D solid on graphite. The plusses are bulk and the open circles are the 2-D values. The figure is from the thesis of Robert Elgin [25].

tubes, and 3) the rest are 'chiral' tubes. When the tubes get large enough the discreteness is not apparent in the diameter, as there is a large number of possible combinations of n and m leading to similar diameters. On the other hand, properties which depend on the chirality, such as the electrical transport, are very sensitive to this discreteness. The spread of chiralities may play a role in the heterogeneity of our samples, as discussed in Sections 5.2 and 7.5. The tubes are closed, as suggested in the figure, in order to satisfy the bonds of all the carbon atoms. They can be opened by chemical or other treatments. The tubes in our samples are not open.

In the first experiments mostly multi-walled tubes were created. The techniques were quickly refined to create single-walled tubes [7, 38]. Single walled tubes can be made by carbon arc-discharge, laser ablation, or chemical vapor deposition. AD and LA tubes are typically made in large quantities while CVD is typically, though not exclusively, used to make a few tubes at a time on a substrate. In the large samples of AD and LA tubes, bundles of parallel tubes, close packed in a hexagonal lattice are created. An early paper in which these bundles of single-walled tubes had been seen reported a "web-like deposit" [7]. The authors report that the "tubules are mostly coated with non-graphitic carbon". The early bundles made by the AD process were characterized by neutron diffraction, and found to have and average tube diameter of ~13.8 Å with a spread of about 1 Å, and 37 tubes per bundle on average, but with a huge spread. Reports of the bundles size have been 10 to 100 tubes. The tubes are arranged in the bundle in a hexagonal close packed lattice, Figure 1.6 shows schematically such a bundle with 37 tubes, and Figure 1.7 shows dramatically that such bundles do exist.

The properties of the bundles themselves have received some attention. There are some measurements of the bundle heat capacity [54, 35] and comparisons to that of graphite and multi-walled single nanotubes. Also important to our study are the measurements of the thermal conductivity of the bundles [36]. In this study the bundles are prepared aligned by deposition in a strong magnetic field. We have difficulty with our experiment, with the thermal link between the cell and the sample. This probably has little to do with

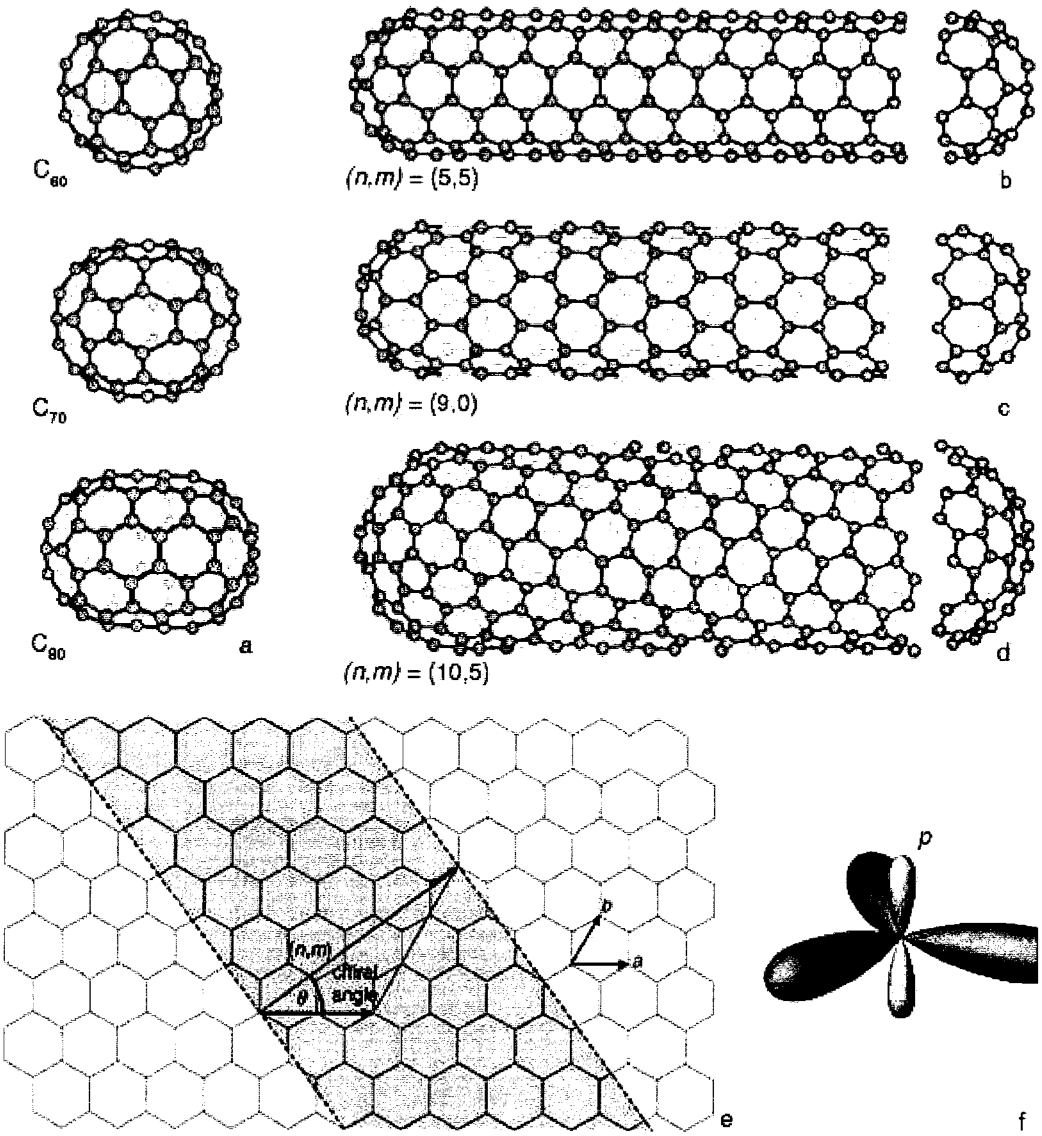

Figure 1.5: The 3 basic types of nanotubes. They can be thought of as rolled graphene sheets with a rolling vector n, m as shown, or as extended Fullerenes. Also shown is the hybridized p-orbital responsible for the hexagonal structure of graphene. Image courtesy of Dr. Richard Smalley and Rice University.

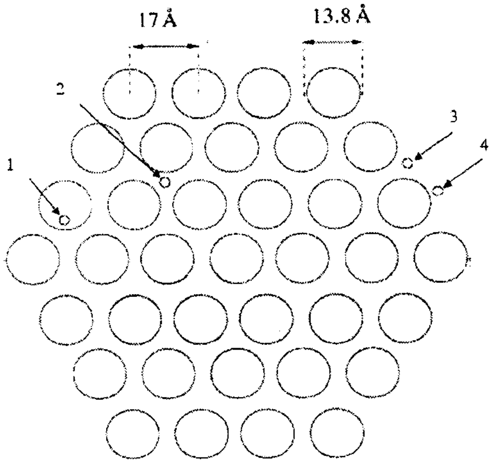

Figure 1.6: Schematic of the structure of an idealized SWCN bundle. The geometrically distinct sites for adsorption are: 1. Inside the individual tubes. 2. In the interstitial channels in the interior of the bundle. 3. In the grooves on the outer surface of the bundle, where two tubes meet. 4. The rest of the bundle surface. This figure is an adaptation of one in a review by Gatica *et al.* [29].

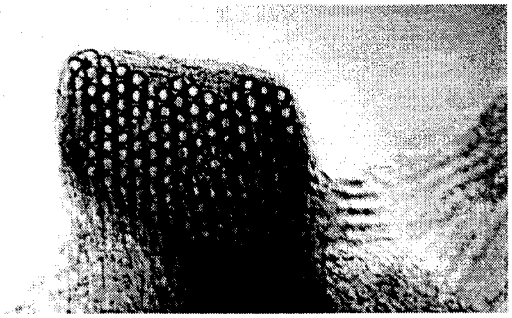

Figure 1.7: Transmission Electron Microscope image of a nanotube bundle, showing the hexagonal lattice of the bundle, as well as defects in the bundle, and junk surrounding the bundle which may block some of the sites. Image courtesy of Dr. Richard Smalley and Rice University [77].

the intrinsic conductivity of the nanotubes and is more likely dominated by the contact resistance from the copper container to the sample.

Considering the geometry of SWCN bundles, we see that there are two distinct locations for adsorption which should have potentials of the correct form to confine the adsorbate in two directions, leaving it only one degree of freedom. In the first of these, the interstitial channels, the confinement is obvious. The adsorbate exists in a narrow 'pipe', in which there simply is no room to move laterally. In the second, the grooves on the outer surface of the bundle where two tubes meet, the confinement perpendicular to the bundle axis is the same as that for planar surfaces. That is, the potential well for adsorption is deep enough to raise the level for excitations in this directions to the point where it can be 'frozen' for sufficiently low temperatures. In the other direction, parallel to the surface but perpendicular to the groove, the confinement is somewhat weaker but arises essentially for the same reason. Motion in this direction is suppressed by the favorability of being adsorbed to two tubes at once, instead of just one, see Figure 2.2.

There is one more potentially 1-D adsorption site on the bundles, in the interior of individual tubes. There the behavior may be one dimensional or two dimensional, with a strong dependence on the radius of the tube and on the temperature. Understanding this behavior is of incidental interest to this study, as we believe that our tubes are all closed and no adsorption occurs there. I should note however that there is a great deal of theory and experiment related to this topic, both due to the possibility of samples of chemically opened tubes, as well as the applicability to adsorption on porous substrates such as Vycor and FSM-16.

As an experimental substrate, nanotubes present some challenges. The samples are not well characterized - average properties are known, but not details. The samples are not homogeneous - there is a small spread in the size of tubes and a large spread in the size of bundles. The samples are powder - it is always very difficult to make good thermal contact with a powder, if you need to keep the sample clean. Perhaps worst, it is not at all clear that the separation of the substrate and film into independent systems is always a good approximation in the case of SWCNs. It was thought that Argon adsorbed in significant amounts in the ICs. The evidence for this was a measured 'dilation' of the bundle. In other words, the lattice spacing of the bundle itself was significantly changed by the presence of the adsorbate. This is certainly not a negligible effect on the substrate system! This effect was later explained another way, and it was found that Argon was not adsorbed in the ICs (or at least did not cause a dilation), but the point I want to make is that with binding energies of the adsorbate so high, and cohesive energy of the substrate so low [54], the possibility of a profound effect on the substrate is very real. I'll discuss this again in the analysis of the heat capacity, Section 7.4.

The nanotubes used in the experiments presented here are commercially available from Carbon Nanotechnologies Incorporated, and were made by the patented HiPco™ process. A paper was recently brought to our attention characterizing these tubes [19]. Here the average diameter is reported at 1.1 nm, as opposed to 1.3 for the tubes made by laser ablation. Where any of our analysis has depended on the diameter of the tubes we have used 1.3 nm, as that was the best information we had at the time.

1.6 Scope of Research

In this thesis I will present the results of two kinds of thermodynamic measurements of the properties of films adsorbed on SWCNs. These measurements are repeated for the two most 'quantum' adsorbates, ^{4}He and H_2. These results will be compared to a large body of theoretical predictions for this system. The results will also be compared to other experiments. Some of them are similar types of measurements on the same system, some on other adsorbates, and some are very different types of experiments on the same system. Tentative conclusions about the growth, structure, and dimensionality of the films will be presented, as well as the suitability of the carbon nanotube substrates for the original goal - to achieve an experimental one-dimensional system.

If the substrate is suitable, and the system is one dimensional, what do we expect to see? First, let's assume for a moment that things are as simple as we can imagine them.

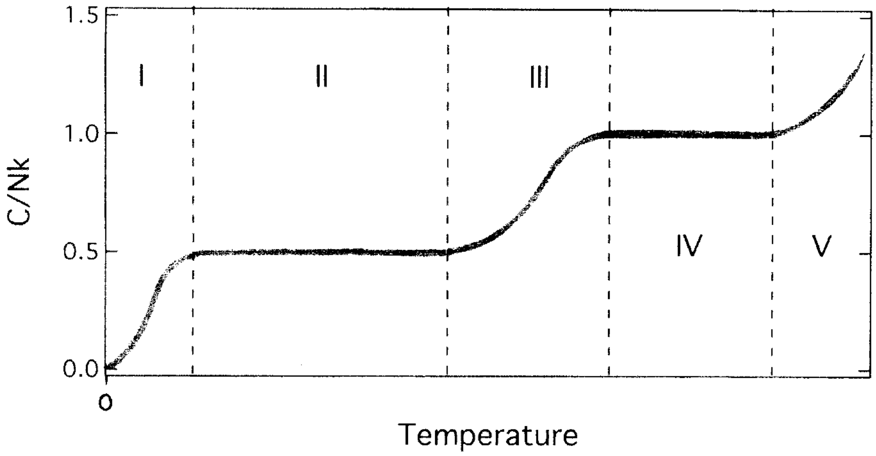

Figure 1.8: Schematic of the expected heat capacity behavior of a low coverage helium film on nanotube bundles. The various regimes are: I) The heat capacity goes to zero as T goes to zero, II) The (ideal) 1-D gas, III) Crossover to two dimensional behavior, IV) The (ideal) 2-D gas, and V) Desorption.

Also, just for this discussion, we assume nothing goes in the ICs. For coverages low enough that all the adsorbate can fit in the grooves and not be very dense, there will be some temperature for which it is effectively all in the grooves and behaves as an ideal 1-D gas (i.e. the heat capacity is constant at 1/2 Nk_B). Likely the system will not be an ideal gas for all temperature and density, though there are very nearly ideal regimes for helium on graphite. Even helium has interactions, so the way in which this specific heat deviates from 1/2 should be an interesting finding of this experiment.

At some temperature higher than that for the 1-D gas, the film must become free of the groove, but possibly not free of the surface altogether (though the amount of desorption at this stage depends on how strong the outer surface potential is, compared to the groove). This may lead to a crossover of the dimensionality from one to something larger but less than two. The groove potential still exerts its influence on the film and there will be a preferred direction for excitations, but not strict confinement to one dimension. What this crossover might look like and what the effective dimensionality is remains to be seen and should be one of the key findings of this experiment.

Lastly, as the temperature goes to zero, the heat capacity must go to zero too. It would be interesting to see at what temperature and in what way this departure takes place. It has been found that ideally 1-D helium should have a self-bound fluid, in equilibrium with its own zero pressure vapor, at T=0. Such things as finite size effects, boundaries, non-ideality of the gas (interactions), corrugation of the substrate, screening by the substrate, inter-channel interactions, and so on are bound to take their toll on the 'neat' properties of 1-D systems. What *really* happens as $T \rightarrow 0$ is a hopeful target of this study, though our apparatus likely does not go cold enough.

There should be another dimensional crossover as a function of density. When the coverage is such that not all of the adsorbate can fit in a groove, we naturally assume that the film will be less one dimensional. As the coverage approaches this regime, or when the adsorbate can all fit in the groove, but must squeeze to do so, the behavior may be very complicated, and we hope to map it out here.

Chapter 2

THEORY OF REAL AND IDEAL 1-D BEHAVIOR

One of the first steps to understanding complicated phenomena has long been to solve a related but simpler system. In the case of condensed matter and statistical physics this simpler system is sometimes one with the same or similar interactions, but fewer dimensions (eg. the Ising models). Over the course of the last half century, as surface preparations and measurement techniques improved, it was realized that the two dimensional systems which had been a theoretical convenience, were becoming themselves testable in the laboratory. This contact with experiment accelerated and matured the theory of two dimensional systems to the point where entirely new phenomena were explained (eg. the Kosterlitz-Thouless transition).

Recently it has been realized that it may be possible to prepare systems which are one dimensional, at least in the same sense that physisorbed systems can be two dimensional. That is, in one or more directions the energy for excitations is so high that, for sufficiently low temperatures, the system remains in the ground state in these directions. Just as planar substrates can have potentials for adsorption that form a well deep enough that motion of the adsorbate in the z direction is essentially 'frozen', carbon nanotube bundles have both interstitial channels and grooves in which the motion of an adsorbate can be frozen in two directions. This possibility, that the properties of real 1D systems will soon be measured, has encouraged a number of theoretical investigations of the properties not only of ideal 1D systems but of realistic systems, using the known 3D interactions and potentials as a starting point. Many calculations have even included in depth analysis of the effect of the details of the substrate, thus putting theory far ahead of experiment in this area. On the experimental side attempts are still underway to determine if the substrate samples as prepared are really suitable for the investigation we have in mind, and if so, how we have to handle them to get the best results. There are however already results which connect the experiments to theory (Chapter 3).

In this chapter I will review many results from the theory of 1-D systems, both ideal and realistic, as well as results from the theory of adsorption on nanotubes. By the time we get to the tubes we are discussing very complex systems with a very rich predicted behavior. The predictions are variously more or less connected with the physics of 1-D systems. Most compelling, in my own opinion, are the predictions of quasi-1-D Bose-Einstein condensation, mediated by weak inter-channel interactions.

I would like to point out here that, had the experiment shown the very simplest possible, purely 1-D behavior, it would still be a very worthwhile and valuable experiment. It is a matter of the highest principle that, when theoretical results can be tested, they must be. Only measurements can be 'true', not calculations. Most of us have no doubt that a perfect 1-D system is a disordered fluid at all temperatures and densities, but until it is measured this is, as a matter of principle, not known.

Naturally, physical theories which cannot be tested can still be useful. 1-D theories and models, for example, have been invaluable as both pedagogical tools and as testing grounds for mathematics which will eventually be applied to other systems. With the possibility of experimental tests, 1-D physics may soon join the realm of the known.

2.1 1-D in Principle

There can be no phase coexistence in the thermodynamic limit in one dimension. This is a well known and unassailable principle. It is also known that there cannot be long range positional order in two dimensions, and this was once thought to imply that there could be no phases in two dimensions. Still, the measurements of experimentally realizable systems were made, and all the properties one would expect from finite examples of 'ideal' 2D crystals were found, as well as superfluid, normal liquid, and 'exotic' fluid phases. Of course the theoretical underpinnings allowing such phases to exist were soon found, and a piece of that work, the Kosterlitz-Thouless transition, stands out conspicuously as one of the greatest achievements in condensed matter theory.

The argument against the existence of phases (not just crystals) in one dimension is much stronger, however, and must be addressed seriously. I will present next three common ways to approach the argument that there can be no phases in 1-D.

2.1.1 Spatial Correlations

As a thought experiment, imagine starting with a 1-D ordered system, and try to measure the position of the n_{th} atom. Random fluctuations cause the deviations from the equilibrium position of neighbors to go up and up until some atom has an appreciable chance of being on the adjacent lattice site, meaning the order is lost. If you measure from the known position of one atom, the position of its nearest neighbor is some distance d away, plus or minus an amount δ that depends on the size of the fluctuations[1]. The position of the next nearest neighbor is uncertain by an amount δ as well, but relative to the nearest neighbor, not the starting point. So the position of the next nearest neighbor is $2d$ plus or minus 2δ. The third neighbor is uncertain by 3δ and so on. No matter how small δ is, $N\delta$ must eventually be larger than d for some N. Then the Nth neighbor's position is not known to within a lattice spacing.

If you can't have order, you can only have disorder. This leaves gas and liquid as the possible phases, it doesn't completely rule out any kind of transition. It is an argument against the existence of 1-D crystalline solids, rather than against 1-D phases of any kind.

2.1.2 Entropy

There is an elegant argument, often attributed to Landau (though it differs in subtle but essential ways from the argument in his book on statistical physics), which again shows that there cannot be unlimited long range order in 1-D. Perhaps due to its similarity to Landau's

---

[1] There is really a Gaussian distribution of the position of the neighbor, but the gist of the argument doesn't depend on the details.

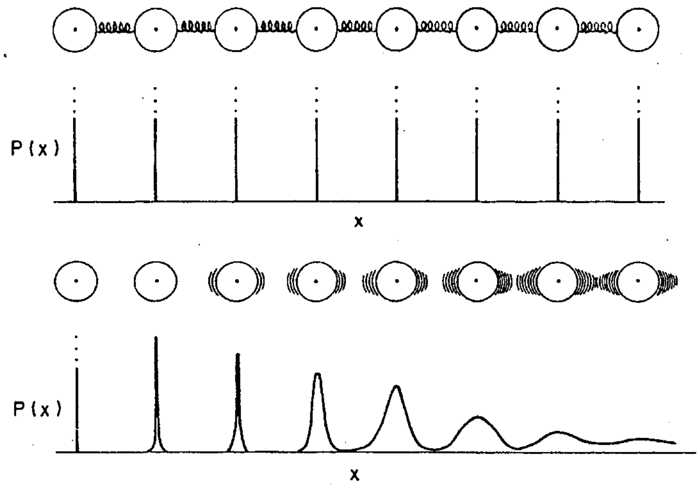

Figure 2.1: An illustration of the breakdown of 1-D order, from a review article by J. G. Dash [22].

argument, this reasoning is sometimes mistakenly used to argue against the existence of phases in 1-D.

Consider a system consisting of a long line of particles in one ordered phase. Now insert an interface which separates the system into two uncorrelated sections of the same phase. The energy cost to create the interface was ΔE, independent of the number N of particles in the system, but because there are N equivalent points at which to place the interface, the entropy is increased by $k_B \ln N$. The system will try to increase the entropy, and lower the energy. Because the entropy increase depends on N and the energy does not, long correlated sections are disfavored. Hence the interfaces will multiply until the correlated regions are 'short'.

I think it is important to point out here that short means $k_B \ln N \sim \Delta E$, not $N = 0$. This may relate to the results of Phillips and Dash [58], who found solid-like clustering of helium at finite temperatures in a Monte Carlo study. This result is discussed in Section 2.3.1.

2.1.3 Landau's Argument

In Landau's book on statistical physics [46] he presented an argument which is superficially very similar to the entropy argument presented above. The essential difference is that here the boundaries are between different phases, not uncorrelated regions of the same phase. In this way it is an argument that honestly addresses the issue of phase coexistence, not only long range order.

Landau uses his formalism of dilute mixtures to argue that the phase boundaries are favored and multiply at will until there is nothing but boundaries, and therefore no phases. I present his argument here, reworded but essentially unchanged. Every detail presented here can be found in Statistical Physics, Landau and Lifshitz, Sections 87 and 163.

Consider a line of atoms or molecules consisting of alternating long sections of two phases 'A' and 'B'. The phases meet at point interfaces. We will consider these points to be a dilute solute, the solvent being all the particles in both phases. The assumption that the solute is dilute allows us to ignore interactions between individual solute 'particles'. The thermodynamic potential of the system can then be written as the sum of the potential from the pure solvent and a term which is the number of solute particles times the effect that one of them has on the potential of the solvent. Let $\Phi_0(P,T,N)$ be the potential of the pure solvent, n the number of interfaces, and $\alpha(P,T,N)$ the effect on the pure solvent potential when one solute particle is added. For any pure substance, $\Phi_0(P,T,N) = N\mu_0(P,T)$. We don't have the partition function for the solute, but we know by construction that by adding n distinguishable particles to the system we would add $n\alpha$ to the potential of the system. We also know that to take account of indistinguishability we would divide the partition function by $n!$. Since the free energy is $F = -T \ \ln \ Z$, this leads to an additional term of $T \ \ln \ n!$ in the potential, which we can write as $Tn\ln(n/e)$, because n is a very large number, even though it is much less than N. We thus arrive at

$$\Phi = N\mu_0(P,T) + n\left[\alpha(N,P,T) + T\ln(n/e)\right] = \Phi_0 + nT\ln\left[(n/e)e^{\alpha/T}\right]. \qquad (2.1)$$

Because Φ must be a homogeneous function of 1st order in n and N, the term $e^{\alpha/T}$ must have the form $f(P,T)/N$, or

$$\Phi = \Phi_0 + nT \ln\left[\left(\frac{n}{eN}\right) f(P,T)\right] = \Phi_0 + nT\ln\left(\frac{n}{eN}\right) + n\psi(P,T), \tag{2.2}$$

where $\psi(P,T) \equiv T\ln\left[f(P,T)\right]$. The change in this potential with the number of interfaces is

$$\frac{\partial\Phi}{\partial n} = T\ln\left(n/N\right) + \psi(P,T). \tag{2.3}$$

When the relative number of interfaces n/N is small, or in other words when the single phase 'domains' are large, $\ln(n/N)$ is a large negative number and therefore $\partial\Phi/\partial n < 0$. Since the potential must tend to a minimum, and it decreases with increasing n, it follows that the number of interfaces increases, or the domains intermingle in shorter and shorter sections, and therefore do not coexist.

2.1.4 Ramifications

Once the argument is established that there can be no phases in 1-D, it is often inferred that the system is a gas at all temperatures, densities, and pressures. The reasoning is that, in the high temperature limit the behavior must be gas-like. Therefore, if it can have no phase transitions, the system must be a gas at all temperatures. This reasoning may be inadequate in the case that complications in the film behavior arise from effects which resist a description 'in the thermodynamic limit'. In particular, the clustering on short length scales found in the simulations of Phillips and Dash [58] do not contradict the above arguments. Then there are purely experimental complications which can defeat the thermodynamic arguments, for example, there is some average and some spread in the length of uniform 1-D segments in our samples. If this length is short, we have a few particles in a box, rather than a statistical ensemble which can adequately be treated thermodynamically. How long this needs to be for the thermodynamic limit, and how long it is in our samples, is not clear. It is likely that, even if our samples have 'long' sections, the ends of the 'box' and the finite size cause noticeable effects.

2.2 1-D in Models

In many 1-D models it can be proved unambiguously that there is no phase transition.

It can be rigorously shown that the 1-D Ising model has no phase transitions. This follows from the fact that the free energy can be solved exactly, and that the resulting expression is analytic at all temperatures. The disordered Ising chain shows slightly more complicated behavior, but once again no phase transition, rather it is a glass. Finally, a different extension of the Ising model uses Heisenberg spins (fixed magnitude and continuous orientation) in place of the spin 1/2 particles. Again the free energy can be solved exactly and is analytic for all temperatures.

The failure of the 1-D Ising model to display a phase transition convinced Ising himself that his model was not applicable to studies of real magnetic phenomena [52]. Long after Ising abandoned the subject, it was found that, not only does his model have a phase transition in 2-D, but it can be productively applied to study a wide range of phenomena, in addition to magnetism.

2.3 1-D in Reality

Encouraged by the advent of carbon nanotubes, there are many recent studies revisiting the properties of real 1-D systems (ie. those which use the known 3-D interaction of the particles and take into account that the confining potential is not perfect) as well as systems which are ideally confined, but have the interactions known from the 3-D system. Among these there are predictions that there can be phases, both in ideal systems at zero temperature, and in realistic 1-D systems at finite temperature.

Here I'll present a sweeping overview of the theoretical and calculational work to date, listing a few of the key results of each study. This is not meant to substitute for reading the studies themselves. I just mean to give a feeling for state of the art in this field.

2.3.1 Ideal 1-D Helium

Zero Temperature State

First to revisit the physics of 1-D helium were Krotscheck and Miller [43]. In particular their conclusion that there is a self-bound fluid at zero temperature and very low density was completely unexpected. Because this is a zero temperature study, the result does not directly contradict any of the arguments above. This study was inspired by adsorption studies of helium in FSM-16, which consists of honeycomb of hexagonal tubes of approximately 18 Å diameter.

The helium in this study is 'quasi' one-dimensional, in the sense that they used an extension of the Jastrow-Feenberg variational method to inhomogeneous geometries, to approximate the wave functions of helium confined in narrow tubes, which is of course different from eliminating two of the dimensions altogether. Then they use a purely one dimensional Hamiltonian, using the Aziz potential, for the helium-helium interactions. The conclusion is that the zero-temperature equation of state shows a many body bound state and dimers. They note that in one dimension, if the low lying excitations are phonons, there is no optimal pair function, and that this implies the absence of Bose condensation (details in an appendix of the paper). This is not in contradiction to the prediction of BEC from Cole's group [3, 2] because they include interactions between individual 1-D channels. Of particular interest here, they note that "in the presence of an external periodic perturbing potential, questions of commensurate and incommensurate competing phases become an interesting possibility".

Simulation of Finite Temperature States

Phillips and Dash [58] have studied finite temperature helium and hydrogen in one dimension by Monte Carlo simulation. They find that the particles can cluster in a solid-like 'phase', but with finite extent, which could account for the lack of a gas in our experiments, as well as for the low and linearly increasing heat capacity. Later this will be contrasted with the possibility that our linear heat capacity is simply due to heterogeneity. Also there is a kind of interrelation between heterogeneity and the clustering in the model. The right kind of heterogeneity can create a 1-D pressure, and raise the temperature at which the clusters can dissociate.

2.3.2 Helium on Tubes

Tube Interiors

Perhaps the first paper on adsorption on nanotubes is by Breton, Gonzalez-Platas, and Girardet [12] in 1994, only 3 years after the discovery of nanotubes. They described the quality of continuum approximations of the graphene sheet and predicted energies for various adsorbates. A key motivation here is the notion that chemistry, and catalysis in particular, may be modified in 1-D. This study was done with the helium in the interior of tubes, both single and multi-walled.

Gordillo, Boronat, and Casulleras have employed diffusion Monte Carlo techniques to compare strictly 1-D ^{4}He with ^{4}He in a tube of radius 3.42 Å, with the aim of characterizing the 'quasi-one-dimensionality' of ^{4}He adsorbed in nanotubes [31]. The choice of radius corresponds to a very narrow nanotube, the 5, 5 armchair tube, much smaller than in our samples, but larger than the interstitial channels. They use an Aziz potential for the He-He interaction, and the He-tube interaction is an averaged pair-wise summation of He-C interactions, simulating a smooth 'continuum-carbon' tube. For 1-D He this study verifies the self-bound fluid found by Krotscheck and Miller [43], though with small discrepancies which are attributed to the details of the interaction potential used. The same condensed phase is found in the tube, but with a larger binding energy. The tube system is found to be poorly represented by the 1-D system.

More importantly, both in 1-D and in the the tube a liquid-solid phase transition (as a function of density) is found for high densities, $\lambda > 0.358$ Å^{-1}. At high enough densities the ideal and tube systems differ greatly due to the transverse freedom of the tube system.

There is also a finite temperature grand canonical Monte Carlo study by Firlej and

Kuchta [28], for helium adsorption inside and outside of individual single walled tubes, not in bundles. The tubes used here are quite large (12, 12 armchair). They find that when the corrugation of the substrate is included there is commensuration on the tubes. We have expected also to see commensuration in the part of the film that is away from the grooves on the outer surface, but we have no evidence for this so far.

Interstitial channels

Milton Cole's group was early into the fray, and has remained prolific on the topic of SWCN adsorption [29, 15, 14]. An early paper from this group predicted that, in the ICs, "There can result extraordinary anisotropic liquids or crystalline phases, depending on the magnitude of the corrugation within the interstitial channels" [69]. In this same paper the first simple estimations of the effect of corrugation are discussed, with the tentative conclusion that localization may be so strong as to result in a real lattice gas. The same group predicted a BEC transition for hydrogen at 10 mK (in the ICs) [3].

Antonio Šiber has published papers on the calculated specific heat of helium [79] and Xenon, Krypton, and Argon [80]. His predictions for helium can, of course, be directly compared to our results. The other predictions are interesting, because he assumes a solid phase and breaks up the specific heat into contributions from different phonon modes.

Grooves

The adsorption potential in the grooves has qualitatively the same form for a large number of adsorbates. Figure 2.2 shows such a calculation for CH_4 [14]. The potentials for helium and hydrogen also show a deep triangular well inside the groove, smoothly changing to isopotentials which are parallel to the surface away from the groove.

From the Monte Carlo simulations of Milton Cole's group [29, 14], they arrive at typical density contours for adsorption in the groove, Figure 2.3, showing the 3-line phase in the first layer and the 1-line phase in the second layer. Some adsorbates show a stable 5-line or 6-line phase as well in the first layer.

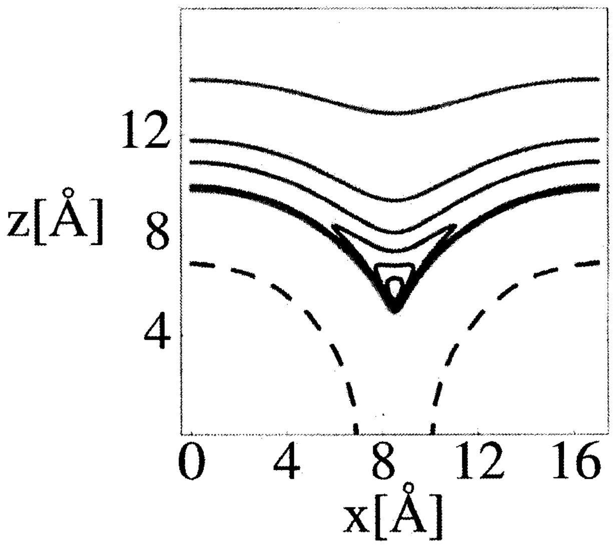

Figure 2.2: Plot of typical isopotential contours for adsorption on the outer surface of the bundle, with the dashed lines representing the locations of the carbon atoms on two neighboring tubes, from Calbi and Cole [14]. Other adsorbates show a similar form, differing only in the depth of the potential and the position of the minimum relative to the tube surfaces.

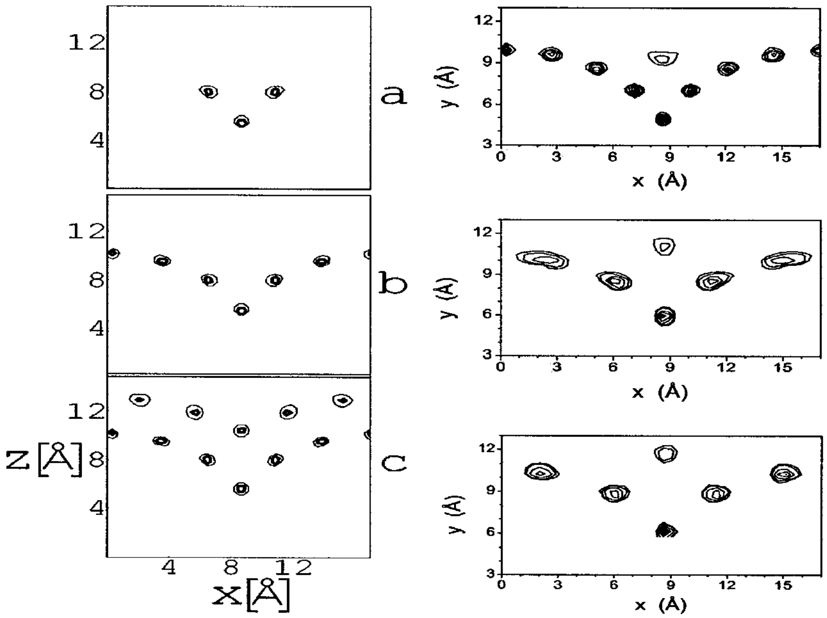

Figure 2.3: Density contours as a function of coverage on the outer surface of the bundle from Monte Carlo simulations. On the left is Argon on the first layer, from Gatica *et al.* [29], and on the right is (from top to bottom) Neon, Methane, and Xenon, all showing a second layer 1-line phase, from Calbi *et al.* [14].

Outer surface and second layer

Kostov *et al.* have found that cohesion is enhanced on a cylindrical surface [41], that is, the film is bound to itself tighter if the surface is curved. On the other hand, the film is less bound to the surface. The Monte Carlo study of Firlej and Kutchta [28] was also for the outer surface of a tube, where they find that the commensurate phase similar to that on graphite is possible

2.3.3 Hydrogen on Tubes

Gordillo *et al.*, mentioned above for DMC calculations for ^{4}He in the interior of tubes, have also published a paper on hydrogen [32], and one [33] where they discuss specifically 'isotopic effects' by comparing H2 and D2. These are again DMC calculations, and again compare ideal 1-D systems and adsorbed systems in tubes. They find that H_2 and D_2, like ^{4}He, is a self-bound liquid at low density, and has a liquid-solid phase transition at higher density. In the narrow, (5, 5) nanotube, hydrogen is found to be a much better realization of a 1-D system than is helium. This is attributed to the difference in the hard-core size of the H_2-C interaction, vs. that for ^{4}He-C, making the tubes effectively smaller for H_2.

The isotopic comparison is made to find the dependence of the properties of a 1-D quantum fluid on the mass of the constituent particles. The comparison is also made with ^{4}He, which has almost the same mass as D_2 but very different interactions, to find the dependence on interaction strength. It is found that D_2 is denser than H_2 in the liquid, showing that the mass difference plays a role, but the differences with ^{4}He show that the interaction potential dominates the properties.

There are also things that are predicted for hydrogen that have little to do with a comparison to helium, for example the hindered rotation in the ICs [40].

2.3.4 Pores, and Other Cylindrical Geometries

Even before the discovery of carbon nanotubes, there were studies of adsorption and wetting on cylinders and spheres which may be relevant in this context [30, 68]. Likewise the large body of knowledge for adsorption in porous media [27, 24] may be relevant. In particular, as discussed with John Wettlaufer, confinement enhanced pre-melting may be evidence for the unfavorability of solids in 1-D [62, 82].

2.3.5 Realistic Bundles

Many groups have used a distribution of tube sizes to get an imperfect bundle, before starting to add adsorbate, in an attempt to bring the model closer to reality, see Figure 2.4. One, by Mark Johnson and coworkers [39] lets the tubes themselves relax and 'ovalize'. Another, by Wei Shi and Karl Johnson [65], compares their large ICs to CH_4, Ar, and Xe experiments. Another from Bienfait *et al.* [8] retains the ideal 37 tube bundle (for purposes of the figure at least) but allows the known variation of size, in part to retain the lattice of the bundle that they know is seen in the scattering.

2.4 Possible Quasi-One Dimensional Phases

In addition to the varied behavior predicted for helium and hydrogen in strictly one dimensional geometries, the tube bundles also allow slight departures from this geometry with interesting effect. Here the interplay between theory and experiment is strongest, with many of the theoretical ideas arising in attempts to explain observed behavior. There are phenomena like the 3-line phase, zig-zag phase, and possible phases due to communication between the channels predicted, which have little to do with reduced dimensions, but are only possible due to the restriction of the adsorbate into high aspect ratio channels.

2.4.1 Zig-zag phase

The zig-zag phase was first used by Bienfait's group to explain scattering data [56]. This is important to our interpretation, because they couldn't have seen this if the film was not compressed on the surface. We believe that we see solid behavior at low coverage, and at temperatures much too high for the self-binding of helium alone. This suggests that there

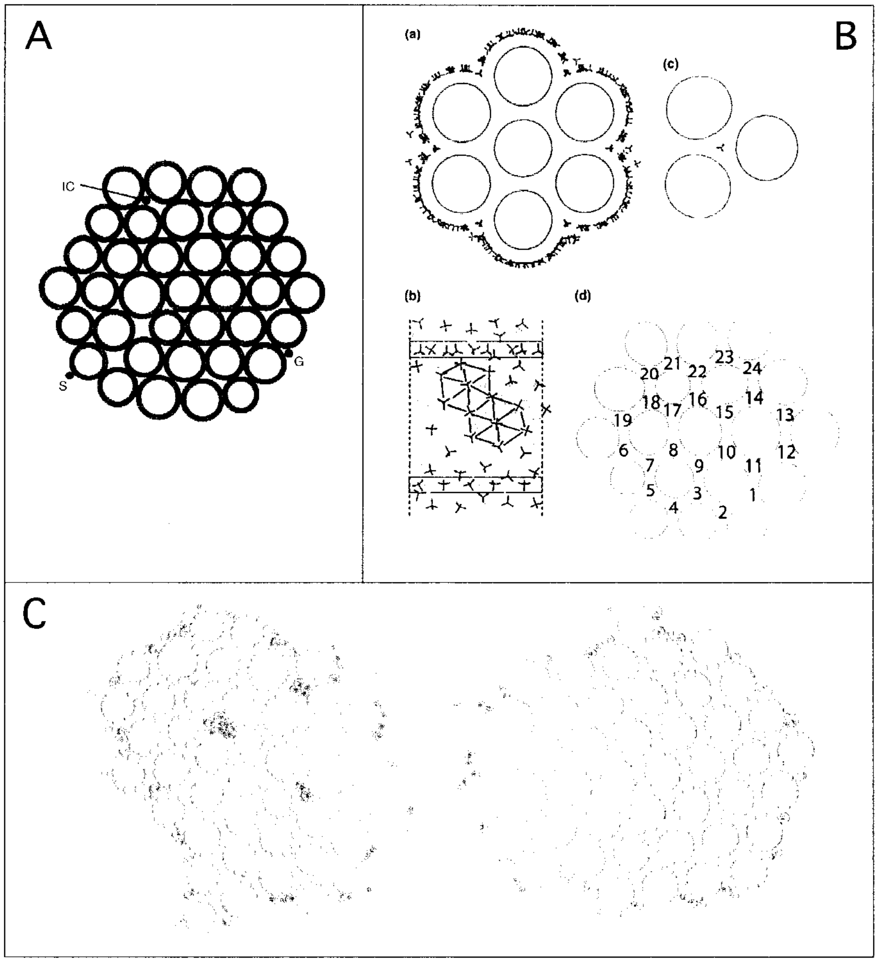

Figure 2.4: Schematics of realistic bundles, from various groups: A) Bienfait *et al.*, from a review article attempting to condense what is so far known to be universal behavior in nanotube adsorption, B) Johnson *et al.*, numerical modelling of methane adsorption, and C) Shi and Johnson, looking specifically for the effect of realistic bundles on universal adsorption properties.

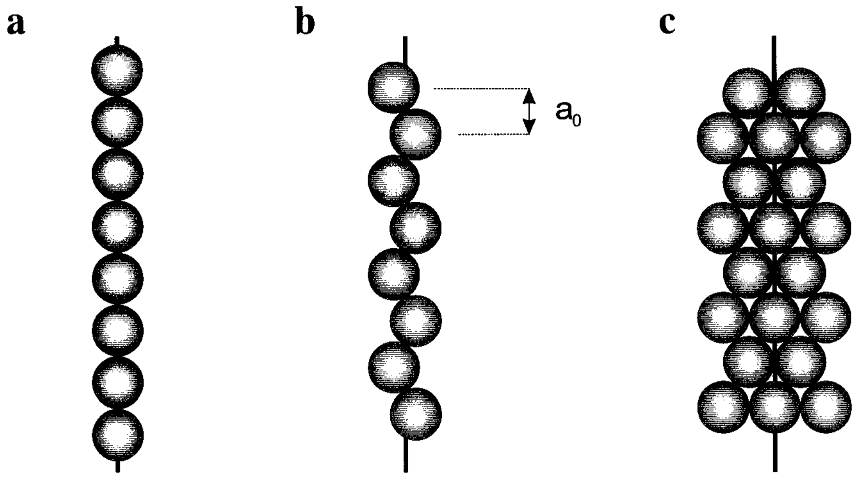

Figure 2.5: Schematic of the proposed zig-zag phase, used to explain the neutron scattering data on D_2 and CD_4. **a** linear chain; **b** single zig-zag chain; **c** stripe of 2.5 parallel zig-zag chains. As more chains are added the film approaches the hexagonal packing that is proposed for the structure of the film near monolayer completion.

is a significant pressure in the grooves due to heterogeneity. The zig-zag phase likewise requires significant in channel pressure to form.

It is relevant to this study not only because this phase may exist in our system, but also because if the molecules can be pushed out of the center of the groove at high density, it is possible that at lower density they also have low energy excitations in this direction. This suggests that the real film may include transverse phonon modes, though a strictly 1-D system does not. Our analysis in Section 7.2 of the Debye temperature of a one dimensional solid film assumes that there are no low energy transverse modes.

2.4.2 3-line phase

This is simply the prediction that, after forming a single line in the grooves, the next stage of film growth is still to crowd into the groove rather than to evenly coat the rest of the outer surface. This is seen from steps in vapor pressure isotherms described in the next chapter. The Monte Carlo predictions of this phase were shown earlier in this chapter, Figure 2.3.

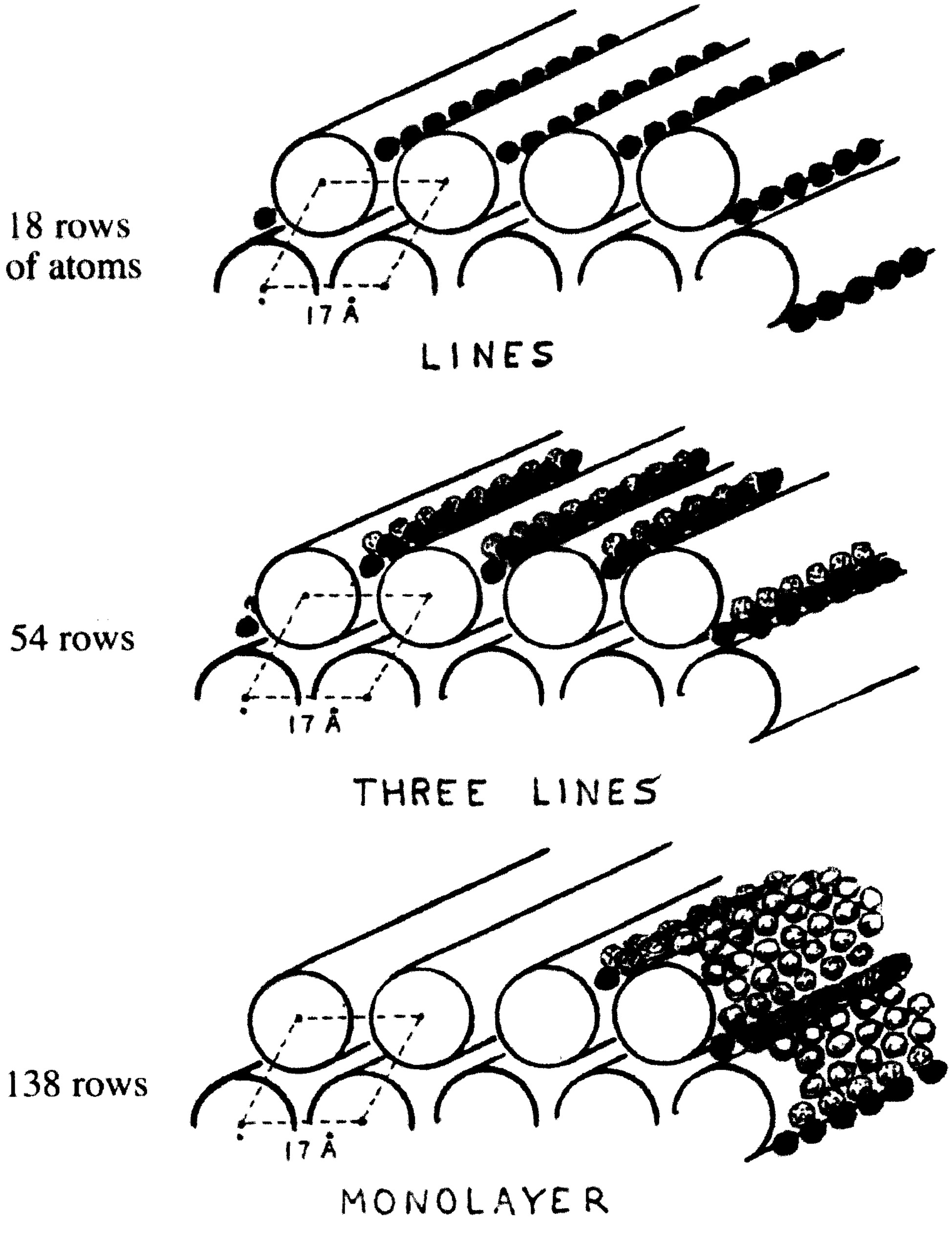

Figure 2.6: A cartoon of 3 stages of the growth of films on the SWCN bundle surface, from Oscar Vilches [78]. The numbers of rows are for an ideal bundle of 37 tubes, arranged as in Figure 1.6

2.4.3 Dilation induced phases

Calbi, Toigo and Cole have calculated the effect of a dilation of the bundle lattice on an adsorbate film within the ICs [16]. They find that, for densities of the adsorbate greater than a minimum density ρ_c, the ground state of the system is a dense phase of the adsorbate in the ICs of the swollen bundle. They find that a region in the phase diagram of coexistence between a dense phase and a dilute, quasi-1D gas exists, with critical temperatures for ^{4}He and H2 of 5.4 K and 398.4 K respectively.

This calculation was inspired to some extent by experimental results from neutron scattering experiments [9], which seemed to show a dilation of the bundle for Argon adsorption. A reinterpretation of the the scattering data shows that it can be explained another way [8]. Talapatra *et al.* have reported isotherm measurements for Xe, CH_4, and Ne, from which they conclude that there is no adsorption in the ICs [74].

This group also looked at the effect this dilation would have on the breathing mode frequency for the tubes and found that it is as large as 3%, or as great as that due to the tubes' mutual interaction. If the breathing mode of the tubes is a significant contributor to the heat capacity of the bundles at low temperature, this will surely not be a negligible effect in our experiments. Even if it is not, this suggests a similar effect on the breathing modes of the bundle itself, which may be of comparable energy to that of the individual tubes.

2.4.4 Phases due to inter-channel interactions

There are several papers exploring the possibility of a mixture of 1-D and more complicated physics, due to the weak interactions of separate but nearby lines of atoms [69, 40, 15, 2]. These interactions lead to crystalline phases and even superfluid, both of which are not possible in 1-D. The calculations were inspired by the possibility of adsorption in the interstitial channels, where we believe we see little adsorption under our experimental conditions. Still, there may be some connection with our system, where the grooves each have only two nearest neighbors and are spaced further apart, but must still interact at some level. It is

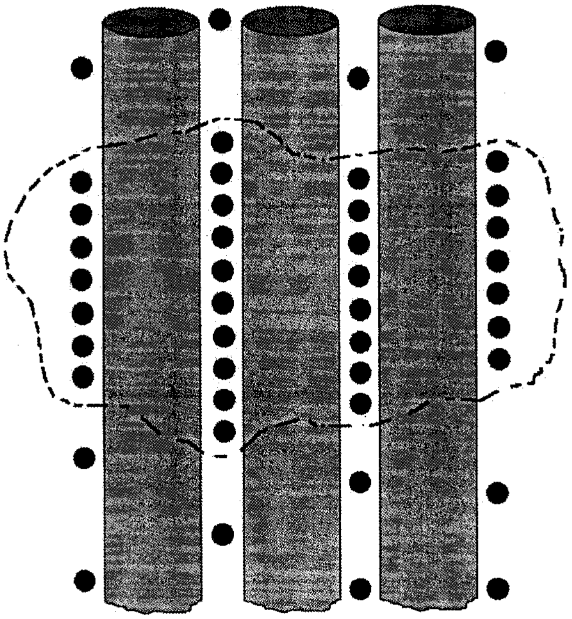

Figure 2.7: Depiction of condensation due to interchannel interactions. Figure from Calbi and Cole [15].

unlikely that our experimental temperature range is low enough to see any effect of these interactions, with the predictions all having negligible effects above ~20 mK.

2.5 Dimensional Crossover

There are many ways for our lines of atoms to escape strictly 1-D behavior, with some of the 'phases' already mentioned being 'quasi'-1-D. When the system can be more or less 1-D, as a smooth function of some experimental parameter, this gives us yet another tool to characterize the 1-D behavior. Helium in a small tube is found to have such a crossover as a function of temperature [15, 14]. The interchannel interactions above are another example, with the resulting BEC behaving as a 4-D gas [2]. If the zig-zag phase exists, and if there is a solid phase in the 1-line system, it suggests that the 1-line solid phase may have transverse modes available, If these have a much different dispersion from the longitudinal modes, this

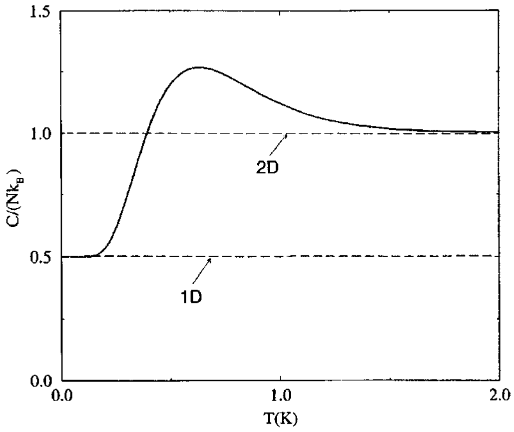

Figure 2.8: Depiction of the specific heat of helium in a tube of radius 5 Å as it crosses over from one- to two-dimensional behavior. Figure from Calbi and Cole [15].

system may also crossover as a function of temperature.

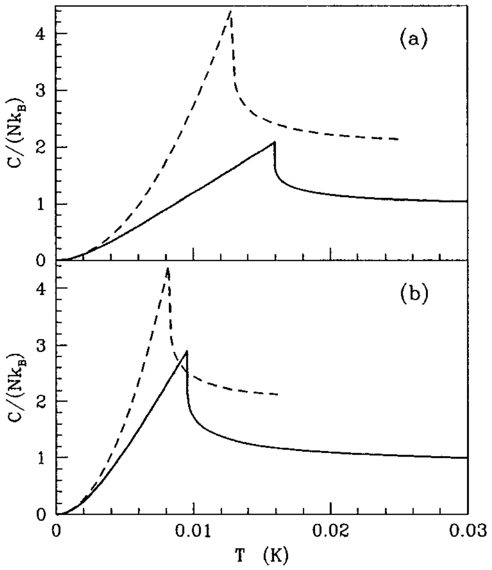

Figure 2.9: Schematic of the heat capacity of a predicted Bose-Einstein transition for helium and hydrogen in the interstitial channels. Panel (a) is hydrogen and panel (b) is helium. The solid lines are the prediction for adsorbed films and the dotted lines are for an ideal 4-D gas. Figure from Ancilotto, *et al.* [2].

Chapter 3

REVIEW OF RELEVANT EXPERIMENTAL RESULTS

Many experiments by other groups, and a few by our own, have produced results which aid and complement the interpretation of the research presented here. Many of these are vapor pressure isotherm measurements, as reported here, but for other adsorbates. There are also scattering experiments, temperature-programmed desorption experiments, and another independent measurement of the heat capacity of helium on SWCNs. This chapter will hardly do justice to the work that has been done in this field. It is not intended to be a comprehensive review, but simply to introduce the existing evidence for film properties that seem to be manifest in our experiments, and to point the interested reader to some of the relevant literature.

3.1 Vapor Pressure Isotherms

Volumetric adsorption isotherms on nanotube bundles for all the usual adsorbate gasses, except CO_2, show the same well defined features for the first layer, that correspond to two main regimes of adsorption: a) For the lowest coverages up to about 1/4 to 1/3 of the first layer, "high" energy binding sites are occupied, with $q_{st} > q_{st}(gr)$, where $q_{st}(gr)$ is the isosteric heat of adsorption for the same adsorbate at similar densities on graphite, and b) For the rest of the first layer q_{st} is somewhat lower and follows the trend of $q_{st}(gr)$. These two regions are associated with a) adsorption in irregular interstitials, external grooves, defects, and perhaps some open tubes, and b) adsorption on the graphene external surface of the bundle.

With our collaborators in Marseille, we have measured vapor pressure isotherms for a variety of adsorbates [8]. These all have a similar behavior, see Figure 3.1, except CO_2,

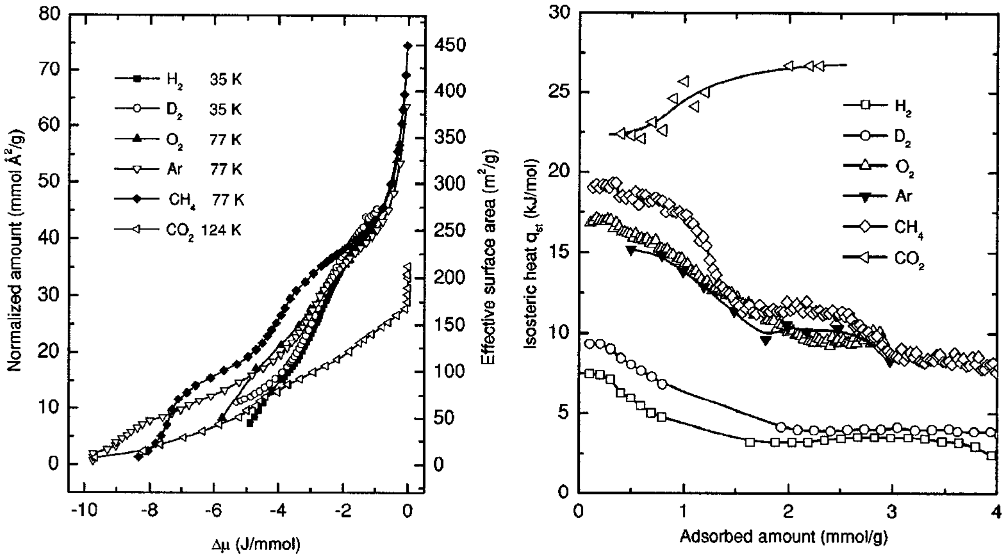

Figure 3.1: Comparison of vapor pressure isotherms and isosteric heat for several different adsorbates on nanotube bundles. They all have a similar form except for CO_2, which is the only one of these which does not wet planar graphite. Figure from Bienfait *et al.* [8].

which is the only one of these which does not wet planar graphite. They display the typical form for adsorption on nanotubes: there are two steps in the isotherm, and correspondingly two plateaus in the isosteric heat of adsorption. The lower plateau in q_{st} is always similar to that on planar graphite, leading to the assignment of both isotherm steps to different sites within the first layer.

We have previously published isotherm results for hydrogen, shown in Figure 3.1, and for helium [84]. The helium data here is for Montpellier tubes and doesn't fully agree with our current HiPco result, for reasons discussed in Section 5.3.

Aldo Migone's group have published a large number of vapor pressure isotherm results for a large number of adsorbates on nanotubes. They have reported variously evidence for many of the predicted behaviors including the one-dimensionality of the adsorbed films [73], the 3-line phase [73], and the 2nd layer 1-line phase [45, 72]. They also compared the specific area available to many different adsorbates, including some which are predicted to not fit in the ICs, in order to conclude that nothing goes in the ICs [74]. This has been explained elsewhere in terms of dirty samples.

3.2 Neutron Scattering

Most of the information on the cahracterisation of the bundles comes from neutron diffraction of the bundles themselves. Rols *et al.* have published a very extensive ananlysis of the effects of the variations of chirality and other properties of the tubes on the diffraction [63].

Bienfait *et al.* [8] used the realistic bundle (variation of tube sizes) and scattering results to argue *for* adsorption in ICs, though at a much smaller level than predicted for perfect bundles. This work also uses isotherm measurements and a molecular dynamics model to compare many adsorbates, H_2, D_2, methane, argon, oxygen, and CO_2, to search for universal behavior. Bienfait's group also were the ones to report, and then re-explain the result which looked like swelling of the bundles (dilation) [9, 8].

Muris, et al. first predicted the zig-zag phase, discussed in the previous chapter, to explain the exceptionally high densities seen in the scattering data [56].

3.3 Desorption

Teizer *et al.* have measured temperature programmed desorption of ^{4}He from bundles of nanotubes prepared by laser ablation [75, 76]. They have concluded that the helium desorbs from 1-D sites, with a binding energy of 230 K. They have suggested that this adsorption may take place either in the interstitial channnels, but with a much lower binding energy than the predicted 340 K, or inside of individual open tubes, where the prediction is $E_b = 210$ K. They have ruled out an explanation of their data based on adsorption on the outer surface of the bundles, but seem not to have considered the grooves as a distinct site, separate from the rest of the outer surface and with a higher binding energy. The binding energy they report is in remarkable agreement with our isosteric heat, on the plateau that we have assigned to the 3-line phase in the groove. Part of their objection to the outer surface as the binding site is that the area available there is much to small for the quantity they see adsorbed. This suggests that we should check our results for consistency. The ratios of adsorption in the groove and the rest of the surface is fine, but perhaps we are assuming far to much surface area overall.

A. C. Dillon *et al.* [23] reported temperature programmed desorption for hydrogen, as part of their work on hydrogen storage. There is an expected low temperature (~150 K) peak similar to that for porous 'acitivated carbon', but with much greater capacity. There is a much higher temperature peak as well, at about 290 K. This peak shifts with coverage in a way which can be explained by heterogeneity of the adsorption site. These sites yield a desorption activation energy (equivalent to the heat of adsorption, in the case of physisorption) of 19.6 kJ mol^{-1}, almost 5 times that for planar graphite. We see nothing even approaching this in our experiment, but the difference may be due to the conditions during dosing. The much higher temperature during dosing in the desorption experiments may make more adsorption sites accessible. There is also an interesting discussion in this paper of how the H_2 in their samples is denser than expected given some reasonable assumptions about the H_2-H_2 spacing and closest approach to the tubes.

3.4 Heat Capacity

Measurements of the heat capacity of helium on nanotube bundles have been reported [47, 48, 35]. In both cases these were experiments to measure the heat capacity of the bundles themselves. Helium was used as an exchange gas, to cool the sample prior to measurement. It was found that this helium must be carefully removed, or a film remains and contributes a large signal to the heat capacity.

J. Hone *et al.* report only one measured helium film, see Figure 3.2, with no attempt to determine the coverage or otherwise further analyse the data. By rough comparison to our data, it looks as if they had roughly half a monolayer. This measurement is helpful to us because it looks as though their film is fully desorbed by 20 K, reassuring us that our annealing temperature of 30 K is sufficient. We were not able to measure to temperatures

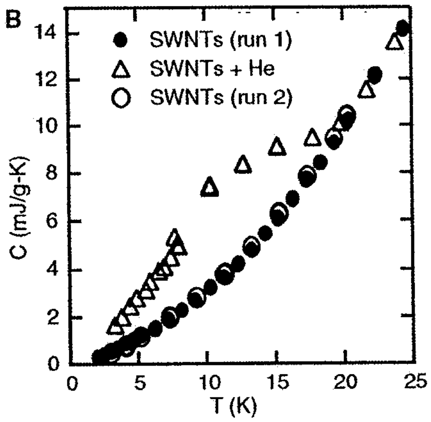

Figure 3.2: Heat capacity of bundles and helium film from J. Hone, *et al.* [35], showing a non-constant heat capacity (coverage unknown) and a peak due to desorption. Note the higher temperature range than the data of Lasjaunias *et al.*.

this high ourselves.

Lasjaunias *et al.* performed considerably more analysis on the 'spurious' helium signal in their data. They have extracted estimates of the coverages from from the dosing and desorption conditions, and have fit and subtracted the background heat capacity. The results are shown in Figure 3.3 for two helium coverages. There is some uncertainty in the coverages, and therefore also in the value of 1/2 for the specific heat of the lower coverage film. What is very clear however is that the heat capacity is constant over a large temperature range, which includes the temperature range of our experiments. We have not seen this in our measurements for any coverage. It is again possible that the difference is due to the conditions under which the films are adsorbed. Because they use the helium as an exchange gas, it is admitted to the sample at relatively high temperatures. This may make different adsorption sites available than in our samples, where the helium is always admitted at lower than 30 K.

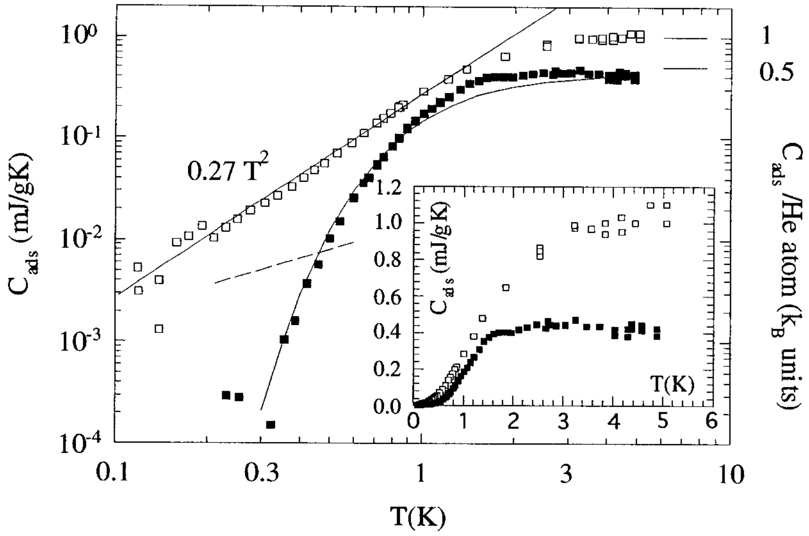

Figure 3.3: Heat capacity of helium films from Lasjaunias *et al.* [48], showing the 1-D and 2-D gasses at different coverages. This data sets the dividing line between regions I and II in Figure 1.8 to 1.5K.

3.5 Other

Yano *et al.* have studied helium adsorbed in FSM-16, a porous substrate with straight 18 Å pores [86]. As mentioned in Chapter 2, this substrate, like the nanotubes, has sparked interest as a candidate for a 1-D experimental system. Using a torsional oscillator, the existence of a superfluid transition for this quasi-one-dimensional system has been verified. Previously no superfluid has been observed in pores smaller than 50 Å. The superfluid onset temperature is coverage dependent and ranges from ~0.7 to ~0.8 K, much higher that T_{KT} for 2-D. The pores are smaller that the estimated vortex core diameter for superfluid in larger pores in glass, ~25 Å. In larger pores the transition temperature is seen to increase with decreasing pore diameter.

Chapter 4

EXPERIMENTAL DETAILS

In this chapter the experimental apparatus is described as well as the specific quantities that are actually measured and how they are related to physical quantities of interest. In the first two sections I'll describe the quantities to be measured in order to introduce the capabilities that the apparatus must have. Then I'll describe the apparatus itself and how it is designed to meet these requirements. Finally, I'll present the tedious details which are essential to make the system actually work.

4.1 Volumetric Adsorption Isotherms

We can take advantage of the fact that the film in a physisorbed system always coexists with a three dimensional vapor of the same species. If we allow the two to be in equilibrium, they have the same chemical potential. The chemical potential of the vapor, and therefore of the film, is easily measured. At fixed temperature, and in the approximation that the vapor is an ideal gas, the chemical potential is just proportional to the log of the pressure. Therefore a plot of the amount of gas adsorbed vs. the log of the pressure of the vapor, is a plot of the density of the film[1] vs. its own chemical potential. The use of this information is explained in detail in Chapter 5, where the analysis of our isotherm data is presented.

We want to measure the quantity of adsorbate bound to the surface and the equilibrium pressure of the 3-D phase simultaneously. The latter is trivial, we simply use a pressure gauge and measure it. There are many ways to measure the adsorbed quantity. The simplest, if one has the luxury of a substrate sample with large surface area and small

---

[1] The substrate is effectively a fixed volume system (fixed surface area), so the number of adsorbed particles is proportional to the *average* density the film. This doesn't take into account that the film may be condensed or localised within a subset of the available surface area.

volume, and strong binding compared to the container it is held in, is the volumetric method. Using the same pressure gauge that determines the equilibrium pressure, we measure the initial and final pressures in a 'dosing' volume of known size, V_D. This pressure difference gives us the number of molecules that passed the dosing valve, N_p as

$$N_p = N_f - N_i = \frac{V_D}{k_B T}(P_f - P_i) \tag{4.1}$$

where the subscripts f and i refer to the final and initial values, respectively[2].

N_p is the number of molecules that passed the valve, but not all of them adsorbed. It is easy to find out how many did if we know the total volume, V_{eff} on the cell side of the valve. Then N_p minus the number left in the 3-D gas phase, N_g, is the number adsorbed, N_a

$$N_a = N_p - N_g = N_p - \frac{P_f V_{eff}}{k_B T} \tag{4.2}$$

We would like to map out this dependence of P_f on N_a quasi-continuously. We do this by taking small additive steps, allowing the system to reach a new equilibrium each time. Then at each step J, the final pressure is P_{Jf}, and the number adsorbed is

$$N_a = \frac{V_D}{k_B T}\sum_{j=0}^{J}(P_{jf} - P_{ji}) - \frac{P_{Jf} V_{eff}}{k_B T} \tag{4.3}$$

Effective Volume

Once we have the initial and final pressure for each dosing step, the equation 4.3 is used to find the number of particles adsorbed on the surface. This equation is not simple to apply due to two purely experimental complications. The dead volume (V_{eff}) correction is very important here because it can't be trivially measured like it usually is for other experiments. To measure it we usually use a gas which does not adsorb appreciably on the substrate at the temperature of interest. This is not true for *any* gas on nanotubes at low temperatures.

---

[2] The use of the ideal gas law here is a convenience only. This calculation can also be carried out for more realistic formulations. For typical adsorbate gasses at room temperature and low pressure, we can ignore the discrepancy.

Thermal Transpiration

The final complication is that P_f is not the actual equilibrium pressure of the 3-D vapor in the cell. Due to an effect called thermal transpiration the pressure measured at room temperature is not the same as the pressure at the cold end of the cell fill-line, if the tube is narrow and the pressure is low. This effect arises due to the very narrow fill line with a temperature gradient along it. If the mean free path of the molecules in the tube is larger or about equal to the diameter of the tube, then molecules are more likely to collide with the walls than with other molecules. Those molecules which are moving 'up' the tube (toward higher temperatures) encounter increasingly warm walls as they move along, while those moving down bounce off increasingly cold walls. This leads to an enhancement of the velocity of a particle if it was moving up the tube and a decrease in velocity if it was moving down. The pressure will therefore be higher in a vessel attached to the warm end of the tube than it will be for one attached to the cold end. For many gasses, this pressure difference is accurately given by an empirical formula due to Takaishi and Sensui [71]. The pressure in the cell at low temperature, (P_1 and T_1), are related to the pressure in the dosing volume at room temperature, (P_2 and T_2), by

$$\frac{(P_1/P_2)-1}{\sqrt{T_1/T_2}-1} = \frac{1}{A^*X^{*2}+B^*X^*+C^*\sqrt{X^*}+1}, \tag{4.4}$$

$$\text{for} \qquad T_2 > T_1 \qquad \text{and} \qquad X^* = 2\,P_2\,d/(T_1+T_2).$$

Quantities measured at room temperature have a subscript 2 and d is the diameter of the tube in mm. A*, B*, and C* are gas specific constants, measured empirically. The values for ^{4}He and H_2 are listed in Table 4.1.

This pressure correction doesn't enter into Equation 4.3 for the number of adsorbed molecules. All of those pressures are correctly the values measured at room temperature, and the effective volume takes into account this effect as well as the density gradient in the system. When the isotherm is plotted however, or when other quantities are extracted from it, it is the corrected pressure in the cell that we use, as this is the one which has a direct relation to the chemical potential of the film.

Table 4.1: The constants used in calculating the thermal transpiration effect for helium and hydrogen, from Takaishi and Sensui [71].

	A* 10^5 K^2 $torr^{-2}$ mm^{-2}	B* 10^2 K $torr^{-1}$ mm^{-1}	C* $K^{1/2}$ $torr^{-1/2}$ $mm^{-1/2}$
helium	1.5	1.15	19
hydrogen	1.24	8.00	10.6

4.2 Calorimetry

To measure the heat capacity, we must add heat to the cell, and measure the change in temperature. The cell reaches equilibrium internally in some finite amount of time, and during this time some of the heat leaks from the cell to the surroundings. We wish to minimize this leak, but we cannot make it zero or we would not be able to control the temperature of the cell. This 'leak' of heat from the cell turns out to be an essential ingredient of the AC technique we use, see Appendix A, but it must be carefully controlled by choice of materials and geometry of the cell, fill-line, and electrical leads. The trade-offs involved in these choices are discussed in the Appendix.

Just as we can't heat the cell and not allow any of that heat to escape, we also can't heat the film and not heat the substrate. We are interested in the properties of the film as an independent entity, so we must measure the properties of the whole system, with and without the film, and assign the difference to the film (see References [21] and [13] for discussions of the approximations involved in making this assignment). Because the film makes a small contribution to the total measured heat capacity of the cell, we use an AC technique to improve our sensitivity to very small changes in the signal.

4.3 Cryostat

These experiments were done in a simple ^{4}He cryostat, with a pumping stage, or 'pot', to achieve temperatures as low as ~1.2 K. The cryostat consists of two nested glass vacuum dewars, the inner dewar containing liquid ^{4}He and the outer containing liquid N_2 to further insulate the helium. Inside the liquid helium is a brass can suspended from stainless steel tubes. The tubes house the cell fill-line, the electrical leads, and pumping lines for the vacuum can, inner can, and the helium pot. There is also a valve on the outside of the can, manually operated from outside the cryostat, which allows ^{4}He from the bath into the pot.

The inner vacuum can is a heavy brass can, to provide a stable thermal reference for the cell. The can thermometer is attached to the top of this can on the outside, and a wound wire heater on the support for the can is used by the PCB-ATC temperature controller to set and stabilize the temperature of this can. The support of the inner can hangs directly from the pot, allowing cooling of the can to 1.2 K. All of the electrical leads entering the can are thermally anchored to the pot.

A commercial diffusion pump, Veeco model EP25W, is used to evacuate the outer vacuum can. A rotary vane pump, Welch Duo-Seal™, is used to pump on the pot. The glass diffusion pump on the dosing system is used to evacuate the inner can.

4.4 Gas Handling/Dosing System

We have a metal gas handling system, composed mostly of copper pipes and brass valves. There are several separate volumes enclosed by the valves to allow adjustment of dosing amounts by pressure, as well as calibration of the volumes themselves. The main dosing volume and the volume comprised of the cell and fill-line are attached to the pressure gauges. We use a glass diffusion pump, expertly maintained by Bob Morley, the department glass blower, for the cell and dosing system.

The pressures are measured using MKS Baratron capacitance pressure gauges, see Figure 4.2. There are three Baratrons on the system, one each of 10 torr and 1000 torr ranges on the dosing volume, and one 10 torr range on the cell fill-line. The Baratrons each put out 0 to 10 volts full range, and all three are read by one multi-channel Keithley 199 DMM/Scanner, which is in turn read by the computer on the GPIB bus.

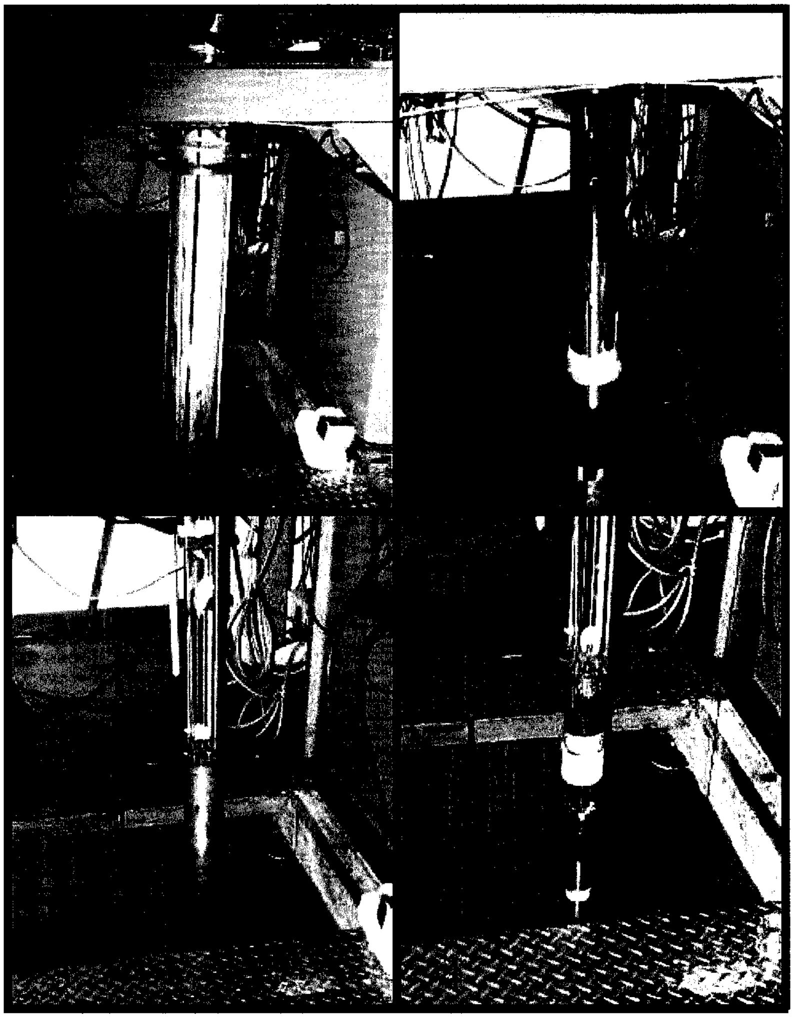

Figure 4.1: These photos show the nesting of the vacuum cans and dewars of the cryostat. Seen in the photos are: 1) the outer N2 dewar, 2) the inner dewar for liquid helium, 3) the outer vacuum can, and 4) the inner vacuum can. In photo 4 the helium pot can also be seen, above the brass inner can, and in 3 and 4 the stainless steel tubes that house wiring, pumping lines and the fill line are seen.

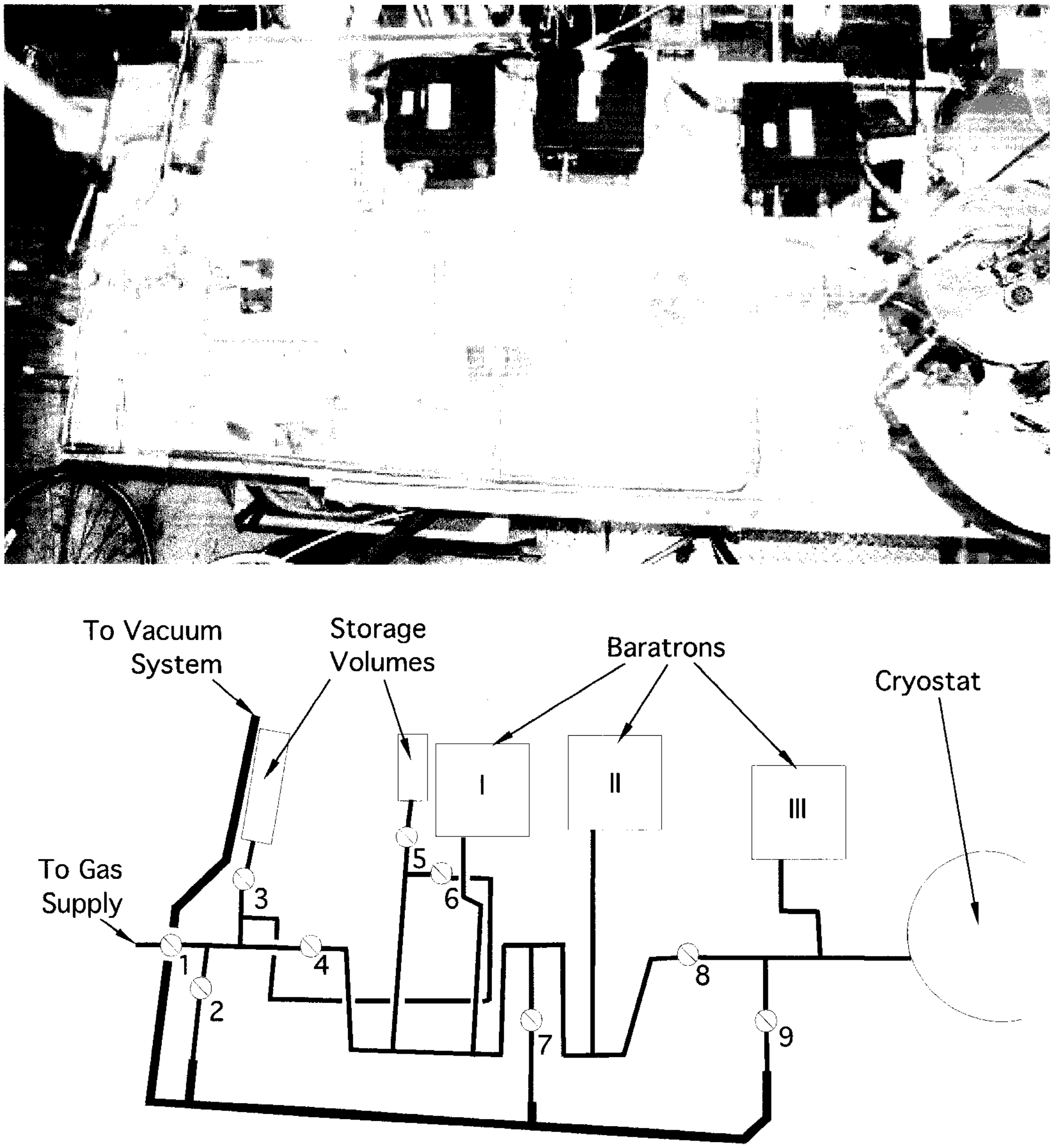

Figure 4.2: Top view of the cryostat, showing the gas handling system used to admit known amounts of adsorbate into the sample cell and measure the equilibrium pressure. Baratrons II and III are 10 torr full range, and I is 1000 torr full range. The dosing volume is the volume of pipes enclosed by valves 4, 5, 6, 7, and 8, and by Baratrons I and II. This volume is 60.2 cc STP.

4.5 Sample Cell

The cell is essentially a copper container to hold the substrate sample, with a thermometer and heater on the outside, which is connected to the reference temperature of the cryostat by a stainless steel tube which also serves as a fill-line to add doses of the adsorbate. The details of the construction of the cell are as follows.

Two disks were cut from 0.002 inch thick copper sheet. The disks were then press-formed into cylindrical cups 28 mm in diameter and 5 mm deep. These cups form the top and bottom of the cell, with the sides of the cups providing a large surface for soldering to seal the cell vacuum tight. A 3 inch long stainless steel tube 0.1 inches in outer diameter with 0.005 inch walls is soldered to a hole in the center of the cup forming the top of the cell. This tube is the heat link between the cell and bath and also allows the introduction of adsorbate gas into the sample. Next the cups are tinned with solder on the mating surfaces, pressed together with the nanotube sample between them, and heated to bond the two tinned surfaces. They are allowed to cool while still pressed in the hope that the copper disks will remain under tension and will squeeze the nanotube sample between them. This tension is the only thing providing a heat link between the nanotube sample and the rest of the cell. It is essential that the sample and the cell be in good thermal contact so that the internal relaxation time is small. This is always difficult to achieve with powder samples and we did not have great confidence that this cell would give good thermal contact, as indeed it did not (see the section on frequency scans below).

We used a Cernox$^{\text{TM}}$ resistance temperature sensor from Lakeshore Cryotronics Incorporated, model CX-1050-SD. The sensor was Indium soldered to the top surface of the cell and was measured in a four-wire, DC mode. The current for the thermometer was provided by a S.H.E. Corporation battery powered current source.

A heater was made from approximately 3 feet of 0.003 inch Manganin wire, coiled into a flat disk between two sheets of cigarette paper bonded together with Stycast$^{\text{TM}}$ epoxy. The disk was then bonded to the bottom of the cell, also with Stycast$^{\text{TM}}$ epoxy. The heater was also operated with four leads, to allow constant precise monitoring of the input power

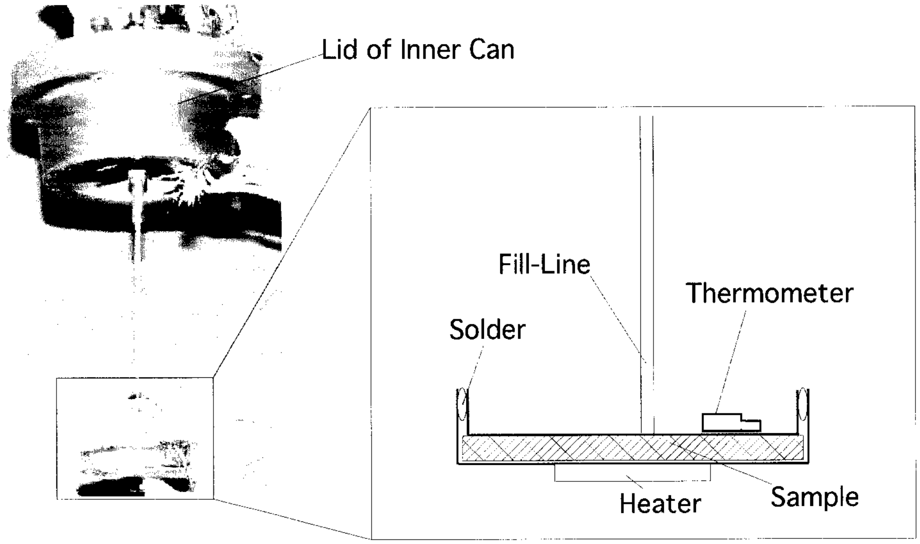

Figure 4.3: A diagram showing the basic construction of the cell.

regardless of changes in the resistance of the heater.

For the vapor pressure isotherms the cell need only have an inlet and be vacuum tight. The properties that a cell must have to be well suited to measurements of the heat capacity are more complicated and subtle. A detailed analysis of the suitability of this cell design for AC calorimetry can be found in Appendix A.

4.6 Data Acquisition

4.6.1 Vapor Pressure Isotherms

The cell fill-line can alternately be connected to the dosing volume, or directly to the diffusion pump. The dosing volume in turn can be alternately connected to the diffusion pump or to an adsorbate source, such as a pressure cylinder.

We measure the amount of gas adsorbed on the surface with the same pressure measurement that gives us the chemical potential. To do this the system is arranged as in Figure 4.2.

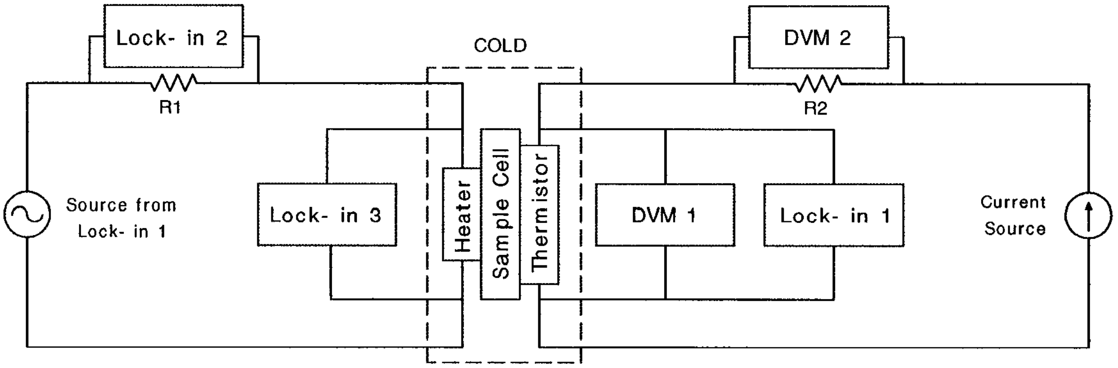

Figure 4.4: Schematic of the electronics used to measure the heat capacity (excluding the computer, and the PCB/ATC temperature controller used to maintain the base temperature).

4.6.2 Heat Capacity

The heat capacity data is acquired by a set of digital volt meters and lock-in amplifiers as shown in the schematic, Fig. 4.4. The DVMs are two Fluke 8840A digital multimeters and the three LIs are all Stanford Research SR830 digital lock-in amplifiers.

The power input to the cell is continually measured during the experiment. This monitoring was done with LI2 and LI3. LI2 monitors the voltage across a standard resistor in series with the heater and at room temperature, LI3 monitors the voltage across the heater itself, and both are slaved to the drive frequency of LI1, which provides the driving excitation and measures the response of the thermometer. The heater is driven at a frequency f and the detection on the cell thermometer is done at frequency $2f$, see Section 6.1 and Appendix A.

The DC current to the cell thermometer was measured by using DVM2 to measure the voltage across a standard resistor placed at room temperature and in series with the thermometer. Together with the DC voltage on the cell measured by DVM1, this gives us the resistance of the thermometer. The resistance is used in the fit function $T = F(R_\Theta)$ to determine the cell temperature.

The experimental instruments naturally measure only voltages, not temperature or heat. The computer collects the following values:

$\langle V_{HR}\rangle$	is the RMS voltage at frequency f on the resistor in series with the heater.
$\langle V_H\rangle$	is the RMS voltage at frequency f on the heater itself.
$\langle V_\Theta\rangle$	is the RMS voltage at frequency $2f$ on the cell thermometer.
$V_{\Theta dc}$	is the DC voltage on the cell thermometer.
$V_{\Theta R}$	is the DC voltage on the resistor in series with the cell thermometer.

These, together with the fixed values:

f is the driving frequency in Hz of LI1 (equal to half the power frequency),
$R1 = 620$ Ohms, is the resistor in series with the heater, and
$R2 = 80$ kOhms, is the resistor in series with the cell thermometer,

and the fit function $T = F(R_\Theta)$ for the cell thermometer described in section 4.8.1, allow us to calculate the quantities in equation 6.1 as follows:

$$\begin{aligned}
\omega &= 4\pi f, \\
P_0 &= \tfrac{\sqrt{2}\langle V_{HR}\rangle}{R1}\sqrt{2}\langle V_H\rangle, \\
|T_{ac}| &= \sqrt{2}\tfrac{dF(R_\Theta)}{dR_\Theta}\tfrac{\langle V_\Theta\rangle}{V_{\Theta R}/R2},
\end{aligned}$$

where,

$$R_\Theta = \tfrac{V_{\Theta dc}}{V_{\Theta R}/R2},$$

and finally,

$$C = \frac{\sqrt{2}\,\frac{\langle V_{HR}\rangle}{R1}\,\sqrt{2}\,\langle V_H\rangle}{2\,(4\pi f)\,\sqrt{2}\,\frac{d}{dR_\Theta}\left[F\left(\frac{V_{\Theta dc}}{V_{\Theta R}/R2}\right)\right]\frac{\langle V_\Theta\rangle}{V_{\Theta R}/R2}} = \frac{\langle V_{HR}\rangle\langle V_H\rangle\,V_{\Theta R}}{\sqrt{2}\,(4\pi f)\,R1\,R2\,\frac{dF(R_\Theta)}{dR_\Theta}\,\langle V_\Theta\rangle}. \tag{4.5}$$

4.7 Computer Data Automation and Logging

All the measurement devices (except for the PCB/ATC temperature controller) are GPIB enabled and are controlled and read by a computer using a National Instruments card, model

PCI-GPIB. The computer is a GIC PC, with an 804 MHz Pentium III processor. The computer was equiped with the GPIB card, as well as a DAQ card from National Instruments, model PCI-6035E. The program was written using National Instruments' LabWindows CVI. For the complete program and discussion of how to use it see Appendix C. Here I will just discuss how the computer was used to bring all the values together, take various averages, record the data when equilibrium is reached, and update the base temperature and applied power.

The DMMs and Lock-In amplifiers were all connected to the computer on the GPIB bus. The PCB temperature controller was modified to take an analog input from the DAQ card, instead of from a dial on the front face, for its temperature set-point. This allowed automated updating of the base temperature by the computer. The current source for the cell thermometer was not connected to the computer and could not be changed automatically, but we never need to change the current during the experiment, and prefer not to once the calibration of the thermometer is done.

The computer collects the raw data from each instrument once every ten seconds. It computes various time averages of these data, and uses the standard deviation of one of the averages (the 10-minute average of the AC voltage on the cell thermometer) to decide when the system is in equilibrium. The experimenter sets the threshold for this deviation when beginning the experiment, and can change it at any point during. When the criteria is met, the computer writes the data point to a file and updates for the next point. Typically the base temperature and AC power applied to the cell are both incremented by a fixed amount at this time. Again, both of these increments are set by the experimenter at the beginning, and can be changed at any time during.

The gas handling/dosing system has manual valves and cannot be automated, therefore the vapor pressure isotherms and dosing for heat capacity runs were all done manually. The DMM used to read the Baratron pressure gauges was connected to the computer, however, and a program was written to display the pressure continuously to the computer screen on a strip chart. Being able to see the recent history of the pressure, rather than just the current value, greatly assists the experimenter in judging when equilibrium is reached.

4.8 Calibrating, Testing and Diagnostics

4.8.1 Thermometer Calibration

The Cernox$^{\text{TM}}$ resistor thermometer was chosen for this cell due to its low thermal mass and high sensitivity in the range of 1 to 4 Kelvin. It was not commercially calibrated, so a calibration was made in-situ on the calorimeter. With the inner vacuum can of the cryostat filled with exchange gas (see Figure 4.1) we can be reasonably certain that the cell and the can will be at the same temperature. The thermometer on the outside of the inner can (hereafter referred to as the 'can thermometer'), used to balance the base temperature for the experiment, is a Lakeshore germanium resistor, commercially calibrated from 4 to 40 Kelvin. This thermometer is very sensitive below 4 Kelvin, but had unfortunately never been calibrated in this range. We were able to calibrate the cell thermometer by direct comparison to the can thermometer from 4 to 20 Kelvin.

Before starting the experiment, in order to be able to reduce the data as it was gathered, we obtained 3 more data points for calibration near 2 Kelvin, by comparison of the cell thermometer to the vapor pressure of the helium in the pot used to cool the apparatus below 4 Kelvin (see Figure 4.1). This was unlikely to be very accurate due to the large separation of the pot and the cell within the cryostat, and the impossibility of using exchange gas or some other means to link the two temperatures better. These points were indeed shown later to be significantly wrong. All the data presented in this thesis were reduced using the more complete and robust calibration done after the experiment was finished. Therefore the vapor pressure points and the initial calibration which resulted are not included here.

When it was clear that we would not take further data with the cell, another commercially calibrated Lakeshore germanium thermometer (hereafter referred to as 'Roberto's thermometer') was attached directly to the cell in order to complete the calibration. This of course adds thermal mass to the cell, some of which cannot be accurately removed again (such as varnish).

The actual calibrations used for the various thermometers

- Can thermometer:

  The inner vacuum can of the cryostat serves as the temperature bath for the cell, so its temperature needs to be controlled and very stable. The thermometer used for this purpose was a Lakeshore Cryotronics germanium resistor thermometer, model GR-200A-1500, serial number 26323. This thermometer was commercially calibrated between 4 and 40 K by Lakeshore Cryotronics. They use an 11th order Chebychev polynomial to fit the calibration points to a smooth curve. The polynomial is defined by

  $$T = \sum_{i=0}^{7} A_i t_i(x), \tag{4.6}$$

  where the A_i are adjustable parameters and $t_i(x)$ is the ith Chebychev polynomial, satisfying the recursion relations:

  $$t_0(x) = 1 \qquad t_1(x) = x \qquad t_{n+1} = 2xt_n(x) - t_{n-1}, \tag{4.7}$$

  where the argument x is given by

  $$x = \frac{(Z - ZL) - (ZU - Z)}{(ZU - ZL)}, \qquad Z = log_{10}(R). \tag{4.8}$$

  ZL and ZU are the lower and upper limits, of the log of the resistance in Ohms, used in computing the Chebychev coefficients. The coefficients for this thermometer are:

  $$ZL = 1.02764854624$$
  $$ZU = 3.38415138422$$
  $$A_0 = 18.215067$$
  $$A_1 = \text{-}19.275605$$
  $$A_2 = 5.736554$$

$$A_3 = \text{-}1.367368$$
$$A_4 = 0.357428$$
$$A_5 = \text{-}0.096822$$
$$A_6 = 0.062228$$
$$A_7 = \text{-}0.026894$$
$$A_8 = \text{-}0.002592$$
$$A_9 = 0.002344$$
$$A_{10} = 0.001443$$
$$A_{11} = \text{-}0.001185$$

- Roberto's thermometer:

  This was a thermometer used by Roberto Ramos, among others, for other experiments in the dilution refrigerator in our lab. Like the can thermometer, it is a Lakeshore, commercially calibrated, germanium resistor - model GR-200A-50, serial number 26087. Its calibration was fit using Chebychev polynomials, as for the can thermometer, but using only 8 terms. The calibration was also given two fits, corresponding to different temperature ranges. One of the fits was for temperatures less than 1.05 K, lower than the cryostat used in this experiment can go. The coefficients relevant to this experiment are, for 1.05 K < T < 6.00 K:

$$ZL = 1.27320234793$$
$$ZU = 1.98177331863$$
$$A_0 = 3.035568$$
$$A_1 = \text{-}2.902901$$
$$A_2 = 0.865913$$
$$A_3 = \text{-}0.146281$$
$$A_4 = \text{-}0.003540$$

$$A_5 = 0.007139$$
$$A_6 = -0.000275$$
$$A_7 = -0.001822$$

- The cell thermometer:

  The data comparing this thermometer to the two commercially calibrated thermometers is in Table 4.2. The first series is the data comparing the cell thermometer to the germanium resistor on the inner can. The rest compare the cell thermometer to the germanium resistor that was attached directly to the cell when the experiment was finished. All of this data was used to arrive at the final fit function, $T = F(R_\Theta)$, used to reduce the data in its final form.

  These data are fit as an ordinary 3rd order polynomial for $1/T$ as a function of $Log(R)$, or $1/T = \sum_0^3 A_i(Log(R))^i$. The coefficients of this fit are:

$$A_0 = 1.966111$$
$$A_1 = -1.713324$$
$$A_2 = 0.4435658$$
$$A_3 = -0.0268892$$

  The data and fit are shown together in Figure 4.5.

4.8.2 Frequency Scan

The cell and heat bath system of an AC calorimeter form a network of capacitors and resistors of heat, much like an electric circuit. The response of the system to a heat input can be predicted and analysed in much the same way as the response of an equivalent electric circuit to a voltage input. A complete accounting of the details of the AC method

Table 4.2: The calibration data for the cell thermometer, as described in the text. R cell is the resistance of the cell thermometer in Ohms. T can and T Rob. are temperatures in Kelvin, as measured by the can thermometer and Roberto's thermometer, respectively.

R cell	T can	R cell	T Rob.	R cell	T Rob.	R cell	T Rob.
3716.69	3.605	22600.6	1.439	12383.2	1.856	8139.66	2.254
3425.49	3.804	22165.2	1.442	12375.0	1.856	7951.45	2.312
3181.37	4.00	22075.1	1.452	11993.2	1.866	7950.93	2.312
2965.89	4.20	21540.1	1.463	11915.9	1.869	7368.91	2.374
2801.62	4.40	20868.5	1.482	11303.4	1.919	6700.45	2.496
2659.05	4.60	20000.0	1.508	11257.8	1.924	6122.31	2.624
2657.70	4.60	19137.7	1.535	11382.0	1.934	5694.91	2.771
2473.19	4.80	18399.0	1.560	11375.8	1.934	5181.07	2.882
2349.77	5.00	18403.8	1.560	10641.4	1.976	5016.39	2.952
2236.48	5.20	18188.9	1.567	10501.1	2.008	4466.95	3.151
2136.25	5.40	17224.4	1.603	10501.2	2.008	3916.96	3.420
2045.55	5.60	16250.3	1.641	10035.3	2.030	3254.33	3.874
1961.23	5.80	15730.0	1.668	9794.67	2.076	2944.13	4.153
1885.15	6.00	15720.0	1.668	9792.10	2.076	2652.09	4.464
1722.59	6.50	15336.4	1.683	9517.90	2.083	2411.41	4.783
1589.69	7.00	14367.1	1.730	9304.25	2.132	2211.12	5.109
1477.48	7.50	13836.6	1.766	9311.22	2.132	2078.24	5.365
1379.85	8.00	13835.9	1.766	9027.97	2.142	1972.31	5.596
1090.60	10.0	13497.9	1.770	8790.15	2.193		
553.362	20.0	12760.4	1.815	8791.10	2.193		

is given in Appendix A. The equation used to go from the oscillations in temperature of the cell to the heat capacity has two time constants, which represent the behaviour of the cell as that of two frequency filters in series. That equation, slightly simplified from the one in the seminal work of Sullivan and Seidel [70], is

$$T_{ac} = \frac{P}{2\omega C}[1 + (\omega\tau_1)^{-2} + (\omega\tau_2)^2]^{-1/2}, \tag{4.9}$$

where T_{ac} and P are the peak values of the sinusoidal temperature and applied power at frequency ω, and C is the total heat capacity of the cell and sample system. The two terms with ω inside the square brackets represent the effect of a high-pass and low-pass filter, in series, with time constants τ_1 and τ_2 respectively. If the cell is well designed, the cutoff

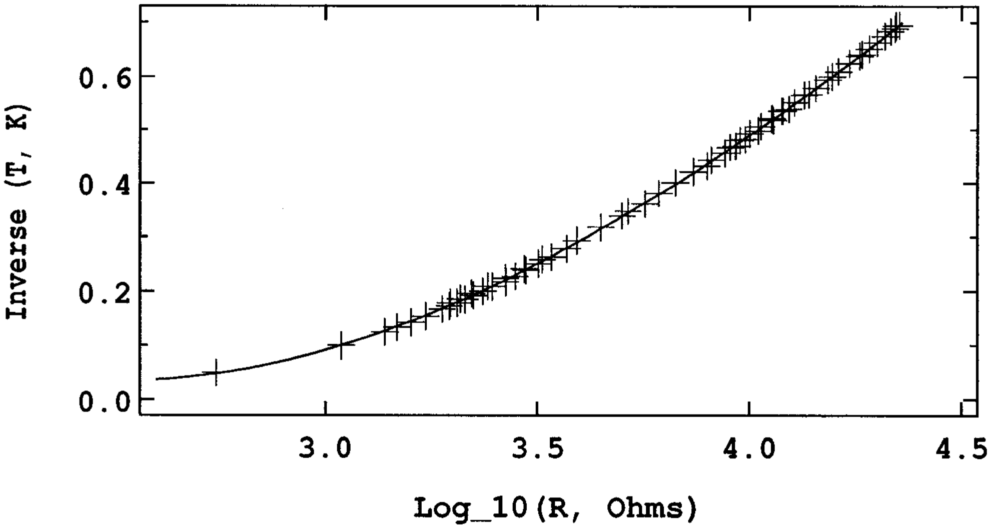

Figure 4.5: The data used to fit the cell thermometer. The fit function is also shown.

frequency for the low-pass filter, ω_2, will be significantly higher than that of the high-pass filter, ω_1, so that for some frequency range the entire signal is passed unattenuated. Once the cell is built, it is difficult to change the parameters that go into the two time constants, but it is easy to check if they are good. To do this one just measures the response of the system to a fixed magnitude excitation at various frequencies. The result of this test for our cell is shown in Figure 4.6.

The frequency response of an ideal AC calorimeter looks like the plateaus in Figure 4.7. With the 2 cutoff frequencies well separated, there is a range of frequency for which the signal is not significantly attenuated. If instead the frequency filters overlap, the frequency scan shows a rounded peak, with the response being attenuated to some degree at all frequencies. In this case the best one can do is to measure at the top of the peak.

Because the heat capacity goes as the inverse of the AC temperature response, the measured magnitude of the heat capacity is always too large in the ideal AC calorimeter. If the measurement is done on a nice plateau in the the frequency scan, this discrepancy is

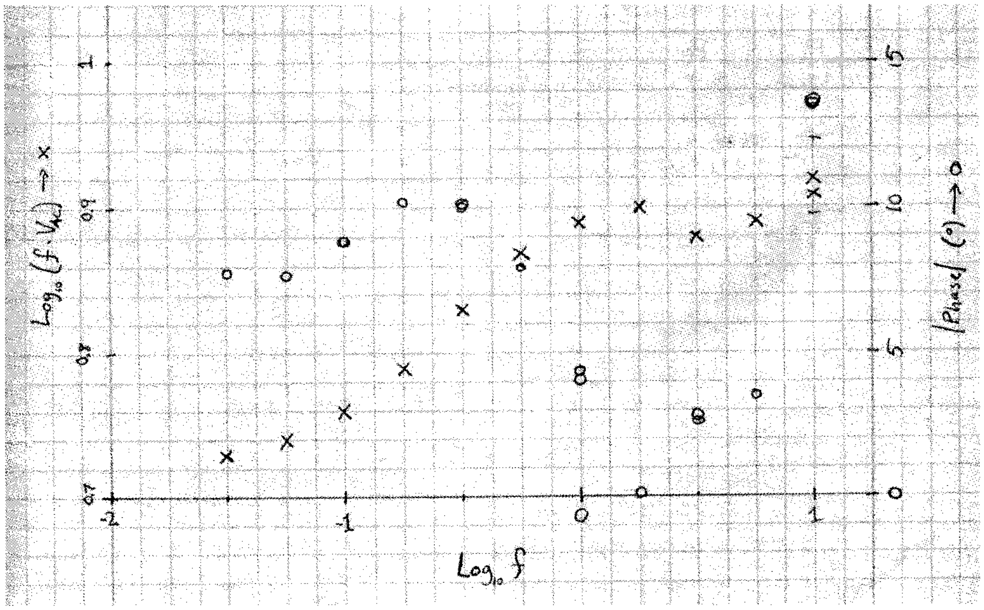

Figure 4.6: The original frequency scan. Also plotted is the phase of the response. The x-axis is $Log_{10}(f)$, where f is the driving frequency in Hertz. The phase is plotted in magnitude; the phase is negative for frequencies higher than 2 Hz.

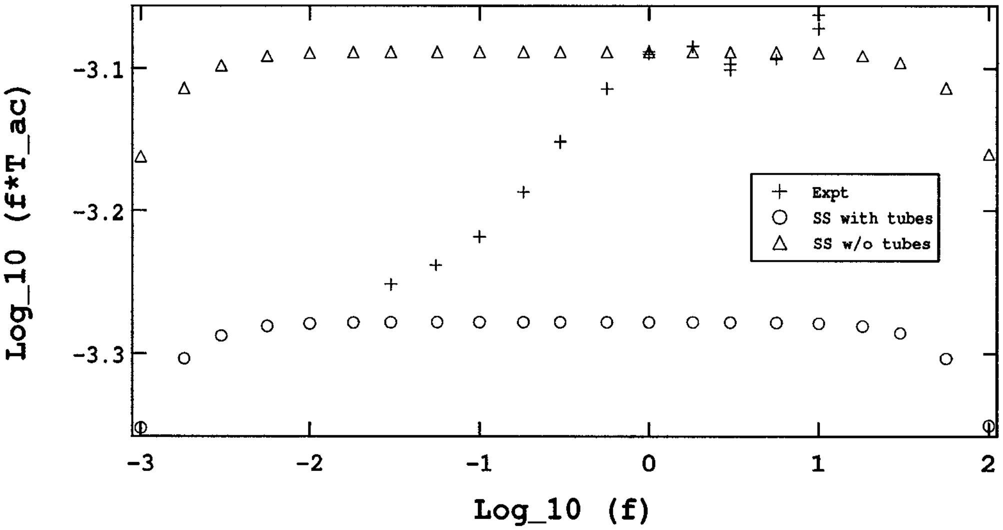

Figure 4.7: Ideal Sullivan and Seidel frequency scans, shown with the measured data. The upper S&S f-scan is calculated using the same cell heat capacity as that measured at 1 Hz and the lower one uses the cell heat capacity measured at DC. The time constants are the same for both, and are chosen so that both cut-offs are just out of the range of the measured data.

minimal. It is larger the further one moves from down the slope of the filter's attenuation. If the calorimter's response is a peak with no plateau, the correct magnitude cannot be measured.

We believe that our calorimeter measures heat capacities smaller than the correct magnitude, because the measured Debye temperatures near monolayer completion are much too high. We believe the frequency scan for this cell is limited to a range of frequencies smaller than that of the heat filters for the following systematic reasons. If on the plateau, $\omega * T_{ac}$ should be constant. Then as ω is increased, T_{ac} decreases. There is a fixed amount of intrinsic noise in T_{ac} due to the sensitivity of the thermometer, the sensitivity of the lock-in amplifiers, the stability of the current source, etc.. At about 10 Hz the signal is too small to reliably pick out of the noise. Going the other direction, to lower frequency, we have problems with the long time stability of the cryostat itself. The lowest frequency we were able to measure reliably was about 0.02 Hz. At this frequency the period of T_{ac} is 25 seconds. If we think of the lock-in measurement like a statistical measurement, we need to average at least 100 cycles to get just 10% accuracy. This means we need the cryostat to remain 'quiet' for almost an hour to get one data point. Not only is our system not that stable, the experiments take much too long this way.

Within the frequency scan for our cell we did not see a high frequency cut-off. We did see a drop in the response going to lower frequencies, and we initially assumed that this was the low frequency cut-off. We originally interpreted this frequency scan as having ω_1 at about 1 Hz, and ω_2 at higher frequencies than we were able to measure. We then decided to take data at 1 Hz, attempting to compromise between wanting a lower frequency to get larger signals, and wanting higher frequency to stay on the plateau. We did not at the time attempt to explain the positive curvature of the scan for frequencies of 0.1 Hz and lower.

After collecting a great deal of data at 1 Hz, and many attempts to explain why the heat capacity was so small, we decided to test the cell by DC calorimetry as described in the next section and Appendix B. These measurements, together with a reanalysis of the low frequency part of the frequency scan, and a reassessment of the quality of thermal contact which might be obtained simply by pressing the copper against the SWCNs, convinced us that a better operating frequency was 0.1 Hz. There was again a compromise, in that even lower frequencies would likely give a slightly better result, but the system is not stable enough over long enough time periods for the lock-ins to properly average the signal at very low frequencies. For this reason the rest of the data was taken at 0.1 Hz, even though we believe that the magnitude of the heat capacity is still slightly under-measured.

In the time constant τ_2 in Equation 4.9 there are really many properties of the cell lumped together. This is often referred to as the 'internal time constant', and describes how fast the cell itself reaches equilibrium internally. The other, τ_1, describes how long it takes for the cell to reach equilibrium with the bath. The problem is that the cell may easily have multiple 'internal' time constants. In our cell it is very likely that the heater, casing, and thermometer distribute heat amongst themselves much faster than heat is transferred into the sample itself.

We have reinterpreted the frequency scan of the cell and now believe that the system response is as follows: There is an 'underlying' plateau in the frequency scan, which covers the entire range we were able to measure. The low frequency cutoff is below 0.03 Hz and the high frequency cutoff is above 10 Hz. This plateau represents the 'good' frequency range for the calorimeter shell alone (the copper cups, solder, heater, thermometer, and portion of the fill-line).

Within this frequency range there is a 'crossover' behavior, due to the poor coupling to the nanotube sample itself. For high frequencies, the sample is effectively decoupled; the sample reaches the average temperature of the cell, but does not respond to the AC signal. At low frequencies the sample and cell oscillate as one and the total heat capacity is measured. At intermediate frequencies the behavior crosses over smoothly between the two.

Figure 4.7 shows the frequency scan again, this time with two plots of the response of a perfect Sullivan and Seidel calorimeter. The frequency cutoffs of the perfect calorimeters have been set to just above and below our measuring range, leaving only the total heat capacity as an adjustable parameter. For the higher plateau we us the heat capacity measured at 10Hz and for the lower we use the result from our DC measurement (Section 4.8.3). The two Sullivan and Seidel plateaus clearly make a good envelope for the measured frequency scan, but the difference in the heat capacity needed to generate them is larger than the expected heat capacity of the nanotube sample, based on 3 published measurements of the heat capacity of bundles [54, 47, 35]. The sample in this cell is 106 mg of HiPco™ tubes, which should have a heat capacity of ~0.05 mJ/K at 2K. The difference in heat capacity needed to generate the curves was 0.17 mJ/K, leaving 0.12 mJ/K to be explained another way. This could be explained if the measured heat capacity of the cell also changes due to the fill-line and electrical leads, which may contribute to the measured heat capacity in a proportion which is frequency dependent. The fill-line is 1.1 gram of stainless steel with a total heat capacity of 1 mJ/K at 2K. If the portion of the fill-line measured by the calorimeter changes by 10% over our frequency range this could explain the rest of the frequency scan plateau shift.

4.8.3 DC Calorimetry

AC calorimetry is a very sensitive method to measure small changes in heat capacity, but it is notoriously bad at measuring correct overall magnitudes. In other words, it is precise, but not accurate. This is because the frequency filters in the cell are lossy, and even if you have a nice plateau in the frequency response, there will be some attenuation of the signal there.

DC[3] Calorimetry can be more accurate, in a well designed experiment. While all the necessary components to make DC measurements are present in our AC system, the system is not well designed for such measurements. Still, it is helpful to have a non-frequency dependent measurement to compare to the AC as a double check on the frequency scan, to

---

[3] DC, in this context, is only meant to differentiate from AC, in that the measured response of the cell is not to an excitation at a given frequency, but rather to an excitation which is turned on or off only once. There are at least two ways to make non-frequency dependent heat capacity measurements, see Section 4.2.

see if we are getting even close to the correct magnitude.

We used the time constant calorimetry method described in Appendix B. The result, shown in Figure B.2, is in reasonable agreement with the data we took at 0.1 Hz, reinforcing our interpretation of the unusual frequency response of the cell.

4.9 Other Experiments

All of the data presented in this thesis was taken in the same calorimeter cell, with the exception of the hydrogen vapor pressure isotherms. We used a glass cells in another cryostat for these measurements. This cell contained 63 mg of HiPco™ nanotubes.

Mike Groves made SEM images of our two kinds of samples, Montpellier AD tubes and HiPco™ tubes, at the UW nanotechnology center. In Figure 4.8 the top two images are AD tubes and the bottom two are HiPco™ tubes. It is readily apparant that the AD tubes have a great deal more 'junk' in them. We attribute this to a greater amount of catalyst, and also likely a greater amount of amorphous carbon.

In comparing isotherms on the two samples, the AD tubes are seen to have a far smaller specific area, as expected, but also show somewhat sharper features than the HiPco™ tubes. It seems that, disregarding the junk in the samples, the AD tubes are more uniform and the bundles are less heterogeneous.

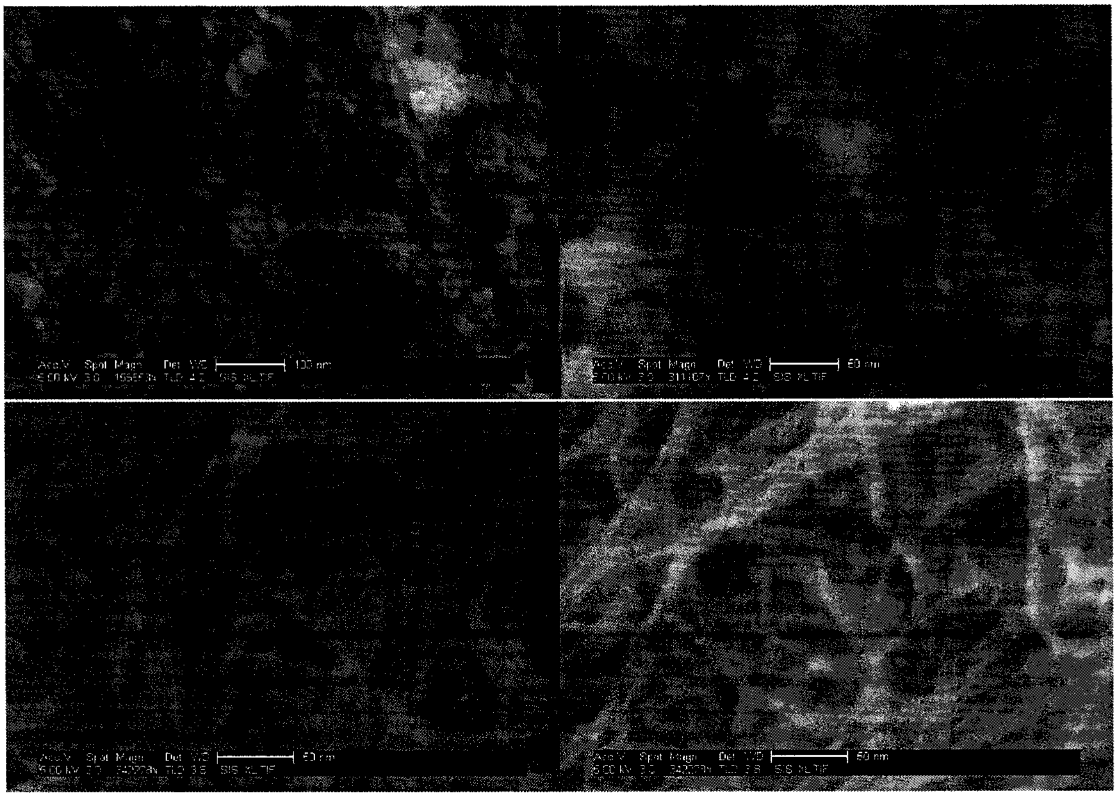

Figure 4.8: Scanning Electron Microscope images of our samples of AD nanotubes from Montpellier and HiPco™ nanotubes from Carbon Nanotechnologies Incorporated. These images courtesy of Mike Groves at the University of Washington.

Chapter 5

VAPOR PRESSURE ISOTHERMS

The canonical experiment of physisorption studies is the volumetric vapor pressure isotherm. As described in Section 4.1, we use such measurements to create a map of the chemical potential of the film as a function of both the density and the temperature. The map contains qualitative information about the film which is readily apparent, for example layering of the film appears as 'steps' in the isotherms. Coexistence of phases with different densities can also appear as steps in the isotherm.

Deeper analysis brings out a wealth of quantitative information. The slope of the chemical potential vs. density (at fixed temperature) can be related to the compressibility of the film, which in turn helps to infer the structure, and the slope of the chemical potential vs inverse temperature (at constant density) can be related to the heat of adsorption, which in turn helps to infer the binding energy.

We have only a small number of isotherms of helium taken on the same sample as the heat capacity measurements. These isotherms show some striking features, and the relationship between the isosteric heat of adsorption and the heat capacity forms the basis for some of the main conclusions of this work.

5.1 Isotherms

The isotherms as measured on the heat capacity cell are shown in Figure 5.1. They give us the usual two step pattern typical of these tubes, one to $\sim$ 9 cc and the next to $\sim$ 25 cc, indicating that there are at least two distinct binding 'regions'.

Isotherms are an important first characterisation of the cell because the coverages at which all other data is measured is referred to the complete monolayer as determined here.

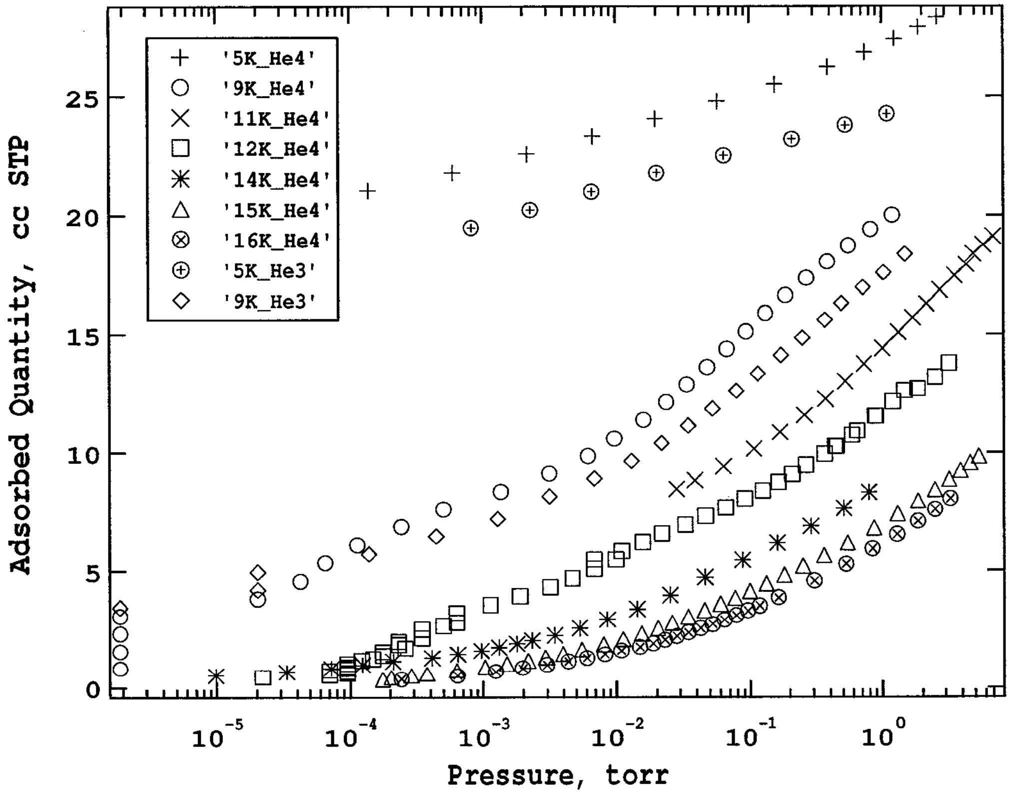

Figure 5.1: Vapor pressure isotherms of helium on HiPco SWCN bundles. For comparison, two isotherms for ^{3}He are also shown. These are the only two ^{3}He isotherms which were measured on the same sample as the heat capacity cell. The 12 K isotherm was taken hastily (intended only for diagnostic purposes) and equilibrium was not reached for most of the low pressure points. We do not believe that points below P$\sim$ 10^{-4} torr are in equilibrium for any of the isotherms.

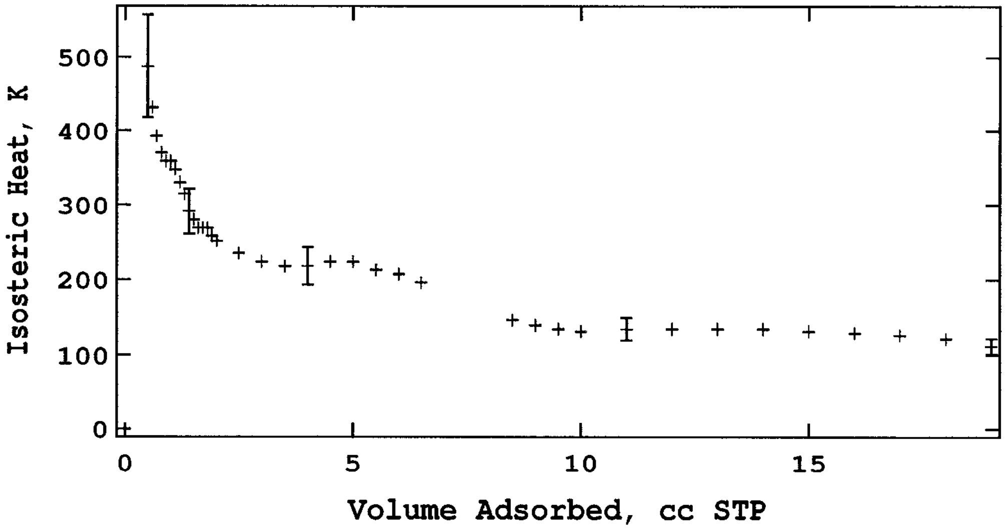

Figure 5.2: Isosteric heat of ^{4}He films. The data below 7 cc is from the 14 K and 16 K isotherms, and above 7 cc from the 9 K and 11 K isotherms.

We have identified monolayer completion for helium on this sample at ~27 cc. This is determined by the B-point of our 5 K isotherm. It also agrees well with scaling of a nitrogen isotherm on this cell, and with a scaling of the isosteric heat of this cell to that on a Montpellier sample. The compressibility of the 5 K isotherm shows a small dip at 25 cc.

5.2 *Isosteric Heat*

In physisorbed systems, the film on the surface always coexists with the remnant of the 3-D vapor from which it formed. If we think of the film as a condensed phase in equilibrium with a vapor, the situation is analogous to the coexistence of a liquid with its vapor. In the spirit of this analogy, we define a quantity to parallel the latent heat of vaporization of the liquid.

$$q_{st} = \left[\frac{\partial \mu}{\partial \beta}\right]_{N_a} = k_B \left[\frac{\partial \ln P}{\partial (1/T)}\right]_{N_a}, \tag{5.1}$$

where μ is the chemical potential of the film and N_a is the number of adsorbed particles.

The isosteric heat of adsorption (q_{st}) is somewhat more complicated than the latent heat of vaporization, because it includes contributions from the binding energy to the substrate and from the internal energy of the film. Nevertheless it is a very valuable tool for understanding the film, especially for examing trends in the growth of the film, or when comparing films of the same adsorbate on different surfaces. Because q_{st} involves the internal energy of the film, it is in general a function of temperature. To extract it from isotherm measurements, one must use neighboring isotherms of different temperature and calculate the finite differential, $\Delta \ln P/\Delta(1/T)$, and thus obtain the *average* of q_{st} over the temperature range spanned by the isotherms. Typically, one has a number of different isotherms, all at different temperatures, and uses all the pairs to obtain many such averages. We have few isotherms to work with here, and have used just one pair (9 K and 11 K) for high coverages, and one pair (14 K and 16 K) for low coverages. This limited amount of data enhances possible errors due to small deviations in one isotherm. It also limits our ability to track changes in q_{st} as a function of temperature. In particular, we cannot track q_{st} back to $T = 0$, where it would be equal to the binding energy.

To make isotherm measurements the pressure of the vapor must naturally be large enough to measure. For this reason the measurements are usually made at temperatures above or near the boiling point of the bulk adsorbate at atmospheric pressure. This also ensures that condensation of the gas in parts of the apparatus other than the sample substrate will be negligible. Heat capacity measurements, on the other hand, are typically made at much lower temperatures, where desorption of the film and thermal conductivity of the vapor can be neglected. This, together with the dependence of q_{st} on T, makes it difficult to make quantitative comparisons of q_{st} with the heat capacity. Trends of q_{st} with coverage have a much weaker dependence on temperature than q_{st} itself, and we are confident that qualitative comparisons of these trends with those of the heat capacity measured at lower temperatures are meaningful.

Our measured q_{st}, Figure 5.2, has the usual 2 plateaus, with the lower one corresponding to adsorption on the curved outer surface of individual tubes, and the higher corresponding, presumably, to adsorption in some higher binding energy site with a fair degree of homogeneity (else the plateau would not be flat). We assign this higher plateau to the high coverage regime in the grooves, which should be a 3-line phase. It is also typical of isotherms on bundles that q_{st} rises steeply going to zero coverage, indicating adsorption on heterogeneous strong-binding sites, probably due in part to large irregular interstitial channels, but also to amorphous carbon, catalyst particles, and other junk in the sample.

Unlike the other adsorbates we've studied, this lowest coverage regime extends to a relatively high coverage (~0.11 monolayers) and, except for the very lowest coverages (less than 0.02 monolayers), it is not as steep. In fact, this low coverage portion looks like another plateau, albeit not a very flat one. We tentatively assign this lowest coverage feature to adsorption of 1-line in the groove, though we should point out that q_{st} here rises to ~350 K, in good agreement with the predicted binding energy for adsorption in the interstitial channels.

It is sensible that the 1-line phase should be very heterogeneous, because the spread in tube size leads to each groove having a different shape and overall depth, and the spread in tube chiralities leads to each groove having a very different corrugation. The 3-line phase, on the other hand, should be more homogeneous. Each atom adsorbed is on only one tube and is next to a fixed line of other adsorbate atoms. The orientation and curvature of the graphene sheet should have some effect, but much less than in the groove.

5.3 Isotherms on Montpellier Nanotubes

We have previously published results of vapor pressure isotherms of ^{4}He on Montepellier, AD SWCNs [84]. We see markedly different behavior for helium adsorption on this particular sample. In particular, the low coverage plateau in q_{st} seen for the LA sample (see Section 5.2) is not seen for the AD sample we used. This was a surprise, because it was our experience with other adsorbates that the behavior of the two substrates is very similar. This AD sample was previously used in a cell in which we attempted a heat capacity measurement using a PVDF pyroelectric detector as a bolometer to measure the power

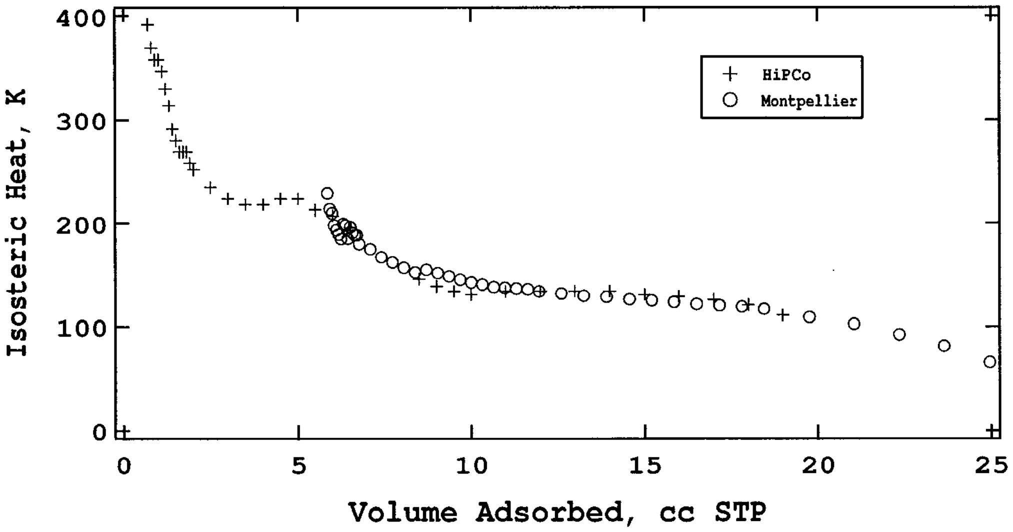

Figure 5.3: The isosteric heat as measured on Montpellier tubes, shifted as discussed in the text to match the HiPco™ result.

transmitted through the sample. In one round of 'baking' the sample, the pyroelectric film melted. We believe that some of the polymer molecules of the PVDF adsorbed on the SWCN sample and were never completely removed by subsequent baking, thus permanently blocking the highest energy adsorption sites. Attempts to scale the isotherms and isosteric heat based on this presumption gave very good agreement, see Figure 5.3.

In other experiments where we have compared HiPco™ and Montpellier tubes (samples other than the one mentioned above) the agreement has always been much better.

Chapter 6

OVERVIEW OF HEAT CAPACITY DATA

Because the discussion of the heat capacity data is long and complex, I have broken it into two chapters. In this chapter I will explain the initial reduction of the raw data, as well as the fitting and subtraction of the background heat capacity. Then I will present the full set of final data and discuss the features which are immediately apparent with the data in this form. All analyses which depend upon further mathematical reduction of the data will be presented in the next chapter.

Because the cell's frequency response was not ideal, as discussed in section 4.6, we have data for helium films taken at 1 Hz and at 0.1 Hz. The data in these two sets are in very good qualitative agreement, but differ greatly in magnitude. In order to have one unified data set, we have shifted the 1 Hz data, as described in Section 6.3.

6.1 Reduction of Data

We assume when reducing the data that the system was operating in an ideal frequency range, and that we can therefore ignore the terms related to the time constants of the cell. In this approximation the heat capacity C is just

$$C = \frac{P_0}{2\omega|T_{ac}|}, \tag{6.1}$$

where P_0 and $|T_{ac}|$ are the peak values of the applied power and the temperature response at frequency ω, see Equation A.3. This is not a good approximation in our case , due to the complicated frequency response of the cell, but we have chosen to first reduce the data this way, and then make adjustments to it based on the 0.1 Hz and DC results. The relation between the quantities in Equation 6.1 and those actually measured by the experimental apparatus is explained in Section 4.6.2.

6.2 Background and Fitting

Because the properties of the bare cell are to be subtracted from the bare cell plus film measurements, we must have a particularly good measurement of the background heat capacity. We then fit this background measurement with a functional form, in this case simply a polynomial, and use the function to subtract from the film data. Because we took the heat capacity data both at 1 Hz and at 0.1 Hz, we needed background fits at both of these frequencies.

6.2.1 1 Hz Background

The data for the 1 Hz background is presented in Appendix D, and is shown, together with the fit in Figure 6.1. The background data was taken at several different times. Whenever the cryostat was warmed to room temperature and cooled back down, new background data was acquired to verify that no calibrations had changed, and that no long-time systematic drifts were at play. These re-takes were always in good agreement with the original result.

In principle, all of the materials that make up the cell, with the exception of the nanotube sample itself are well understood, three dimensional solids (mostly metals). The background heat capacity should be well fit by a 3rd order polynomial in temperature, with contributions coming from the conduction electrons and the 3-D phonons in each of the constituents. The actual agreement with this fit is very poor. This may be due to the fact that the thermal conductivity of the fill-line changes with temperature, so we measure different amounts of the heat capacity of the stainless steel of the line at different temperatures. If we had measured frequency scans at different temperatures, this effect might have shown up as a shifting of the frequency plateau with temperature. The agreement of the DC measurement with the 0.1 Hz data over a large temperature range suggests this is not the case. It is also possible that the heat capacity of the various cell constituents, particularly the thermometer and the nanotube sample, is simply more complicated in this temperature range.

At any rate, we fit the background with what I would call a 'brute-force' method. With a

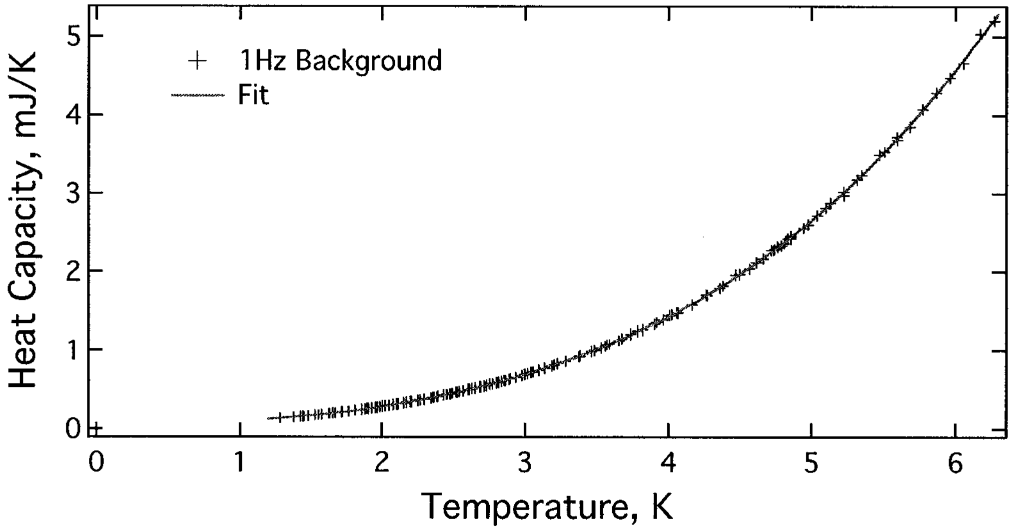

Figure 6.1: The background heat capacity measured at one Hertz, shown with the fit.

third order polynomial giving poor results, we simply up the order. An 8th order polynomial gives fair agreement. This was fine for an initial rough reduction of the data, but it was eventually found that some of the lower coverage films had such a small difference with the background that small deviations of the fit would produce noticeable 'trends' in the film data. We determined to correct this by applying what we call a 'nested' or 'layered' fit.

We took all of the 1 Hz background data and subtracted the original 8th order fit from it. We smoothed the result using the "smooth" function in WaveMetrics Incorporated's IGOR software. This function is basically a weighted, running average. In a sense we had already weighted the data for averaging by subtracting the first fit from it. We then fit the resulting data, over 2 overlapping sub-ranges, again with an 8th order polynomial. Finally, we identified by graphical inspection a point in the overlap region in which the fits meet smoothly (i.e. have the same value and nearly the same slope). This point defines the boundary of the region where each fit is applied to the film data.

We note that, except for the smoothing between fits, this method simply approximates a common piece-wise curve fitting algorithm [85].

The coefficients are listed here such that $C = A_0 + A_1T + A_2T^2 + \ldots + A_8T^8$. The coefficients are, for the first fit:

Coeff.	All T
A_0	-4.662554E-01
A_1	1.360149E+00
A_2	-1.415713E+00
A_3	8.397450E-01
A_4	-2.803966E-01
A_5	5.869974E-02
A_6	-7.566755E-03
A_7	5.668416E-04
A_8	-1.919528E-05

And for the nested fits:

Coeff.	0 to 3.8 K	3.8 K up
A_0	-2.375328E+00	8.809523E+01
A_1	8.236206E+00	-1.854828E+02
A_2	-1.198643E+01	1.614826E+02
A_3	9.562724E+00	-7.705668E+01
A_4	-4.575916E+00	2.223615E+01
A_5	1.345812E+00	-3.995966E+00
A_6	-2.377909E-01	4.384246E-01
A_7	2.309972E-02	-2.692819E-02
A_8	-9.453478E-04	7.104508E-04

6.2.2 0.1 Hz Background

The 0.1 Hz background was fit in much the same way as the 1 Hz background, except that the first 'nested' fit has more regions, because the 0.1 Hz data covered a much larger temperature range.

When attempting to reduce the hydrogen data, an anomaly in the background became apparent, possibly due to a superconducting transition in the solder in the cell, or to some other unaccounted for feature. This left a small peak in the background which was not adequately fit, even with the nesting procedure described above. this required yet a third round of fits, or a second set of 'nested' fits. This time one of the ranges is centered right over the anomalous 'peak' in order to ensure that it was fit well, and one more fit is made to either side of this.

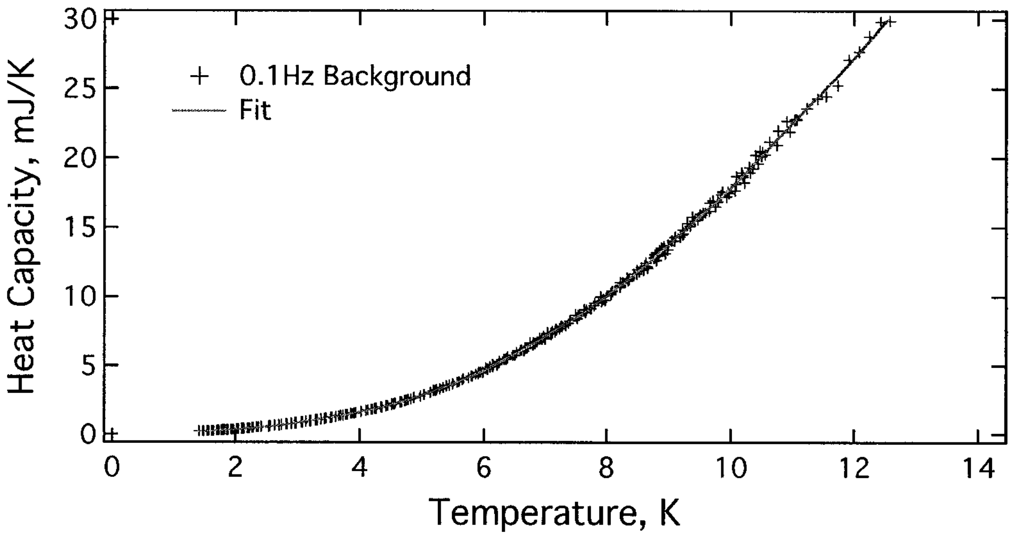

Figure 6.2: The background heat capacity measured at 0.1 Hertz, shown with the fit function.

The coefficients are, for the first fit:

Coeff.	All T
A_0	-4.036289218
A_1	7.167049411
A_2	-4.894279225
A_3	1.795742102
A_4	-0.373719994
A_5	0.047036005
A_6	-0.003480586
A_7	0.00013874
A_8	-2.29292E-06

And for the first nested fit:

Coeff.	0 to 4.5 K	4.5 to 6.1 K	6.1 to 7.5 K	7.5 K Up
A_0	0.922658165	-8765.678874	296585.6965	-6055.243456
A_1	2.301286408	9930.379379	-270501.6339	5370.629866
A_2	-7.00946868	-4483.92435	98012.18542	-2052.570121
A_3	6.625814718	955.7736723	-16514.53203	441.9417816
A_4	-3.236306322	-63.95771918	749.0393762	-58.67743596
A_5	0.922142712	-12.72449249	182.2537768	4.922303293
A_6	-0.155536632	3.112802291	-33.27583861	-0.254893237
A_7	0.01443951	-0.259799618	2.228519916	0.007452332
A_8	-0.000569082	0.008030865	-0.056061327	-9.42188E-05

And for the final fit:

Coeff.	0 to 5 K	5 to 8.5 K	8.5 K Up
A_0	4.326146957	1133.363496	154279.2113
A_1	-12.76345447	-1453.689282	-113849.4605
A_2	15.99684198	811.6659754	36551.75299
A_3	-11.12753941	-257.7227475	-6668.378202
A_4	4.702265194	50.90839265	756.1183859
A_5	-1.237550215	-6.406865692	-54.5668702
A_6	0.198380759	0.501717556	2.447695109
A_7	-0.017738126	-0.022352488	-0.062399709
A_8	0.000678482	0.00043376	0.000692234

6.3 Shifting the 1 Hz Data

Given the unusual frequency response of the cell, both the 1 Hz and 0.1 Hz data measure less than the true heat capacity, but the 0.1 Hz data are much closer to the correct magnitude. Lacking enough data to model the system response to low enough frequencies to find the correct overall magnitude, we have chosen to use the 0.1 Hz data as the best we can do. We then would like to shift the 1 Hz data to match the 0.1 Hz data and have one complete, unified set. If the errant time constant, τ_1 does not depend on the heat capacity of the sample, this shift should be just a constant multiplier at all coverages and temperatures. This is probably not the case for our cell, but we haven't enough information to model the frequency response exactly. We have therefore introduced the only shift which can't have an arbitrary subjective influence on the data, a constant multiplier. This constant was chosen by taking the ratio of heat capacity at a median coverage and temperature, for which we have data at both frequencies. This ratio for the 11.74 cc run at 1 Hz and the 11.96 run at 0.1 Hz is 3.9 . There is no spread in this ratio, beyond the scatter of the data, at any temperature. But these are not the same coverage, and they should not be shifted to have exactly the same heat capacity. We can find what the difference should be quantitatively from the slope of the heat capacity isotherms near these coverages. Adjusting the scaling factor in this way we arrive at 3.8 for the final factor. Applying this scaling to the entire 1 Hz data set brings the two sets to good agreement over most of the coverage range, see Figure 6.6. The agreement is worst at the lowest coverages, where the 1 Hz data is very bad anyway, because the signal is very small and the noise dominates. The coverage dependence of the agreement of the shift may also be due to the fact that a constant shift is not likely to be the correct form. The correct shift should most likely depend on the magnitude of the heat capacity of the sample, and therefore on the coverage. Lacking the correct functional form for the shift, we use a constant only in order to not introduce a false bias into the data. Quantitatively, a much better adjustment can be made by multiplying the 1 Hz data by a line, $(C = 5 - 0.7\,V_{ads})$, rather than by the constant 3.8, but we have no justification for such a shift.

The data presented in Appendix D has been shifted in the same way. Because the shift is due to systematics of the calorimeter, the shift is considered part of the 'as taken' data, and not part of the analysis. In the rest of the thesis, whenever the 1 Hz data is presented it has been shifted by 3.8. One can easily determine what the result of any of the analyses would be without this shift, by simply dividing the C-dependence by 3.8. For example, the Debye temperature in 2D is $\Theta_D = \sqrt{28.848 N k_B T^2 \delta T/\delta C}$. Our results for the 2D Debye temperature would be $\sqrt{3.8}$, or 1.9 times larger without the shift. None of the conclusions in Chapter 9 depends essentially on the shift.

6.4 Heat Capacity Isotherms

The heat capacity of all the helium films is shown in Figures 6.3, 6.4, and 6.5. One sees in the data so presented that the heat capacity is linear at low coverages, becoming slightly more 'curved' at high coverages. Some of the highest coverages show desorption. The heat

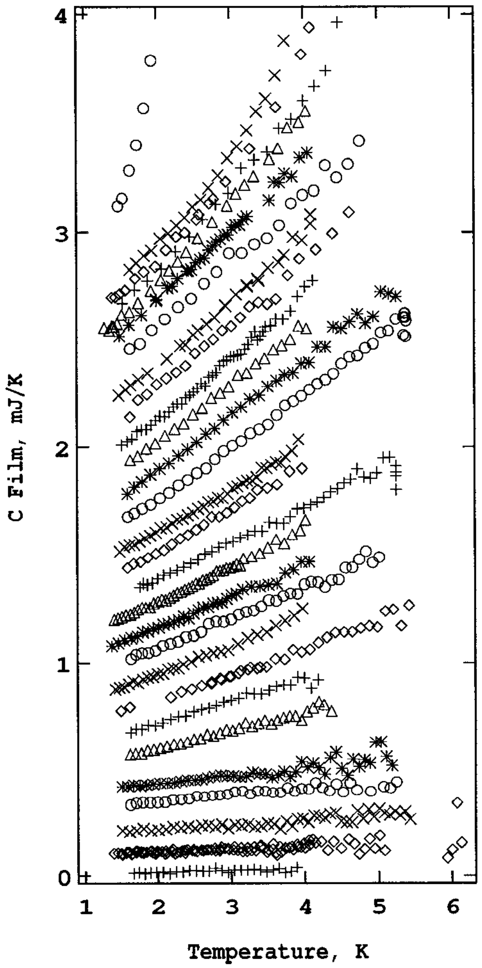

Figure 6.3: This figure shows all of the 1 Hz ^{4}He heat capacity data together. Each run (coverage) is offset by 0.1 mJ/K higher than the run before, in order to not overlap. This format has been used extensively in our lab, and proves very useful when there is some feature in the heat capacity which changes as a function of coverage. The traces are, from bottom to top, 0.465 cc, 0.763 cc (all 4 runs together), 1.134 cc, 1.186 cc, 2.534 cc, 3.212 cc, 4.02 cc, 4.07 cc, 4.75 cc, 5.477 cc, 6.32 cc, 7.32 cc, 8.32 cc, 9.13 cc, 10.35 cc, 11.05 cc, 11.45 cc, 11.74 cc, 12.92 cc, 12.96 cc, 15.07 cc, 15.81 cc, 18.86 cc, 20.06 cc, 21.8 cc, 23.01 cc, and 30.18 cc.

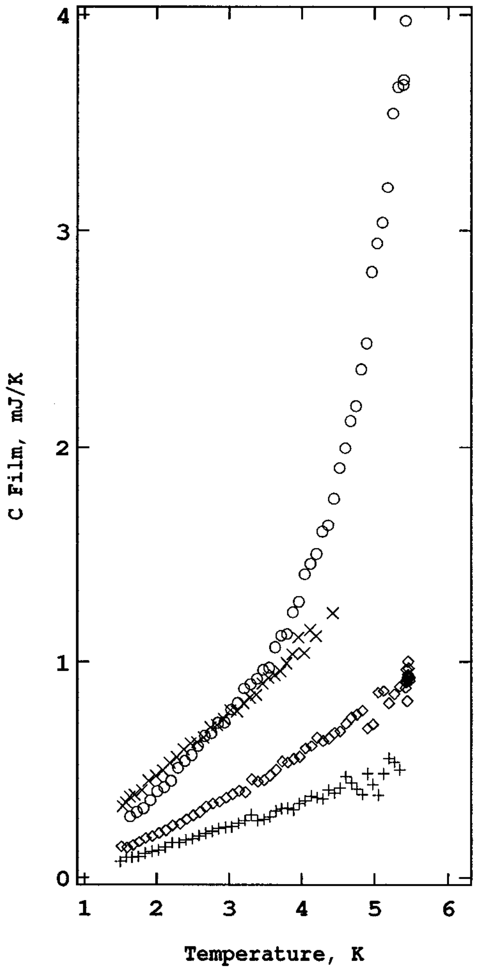

Figure 6.4: The heat capacity runs for ^{3}He at 1 Hz. Each run is offset by 0.1mJ/K higher than the run before, in increasing coverage. The traces are, from bottom to top, 3.46 cc, 8.15 cc, 15.68 cc, and 19.49 cc.

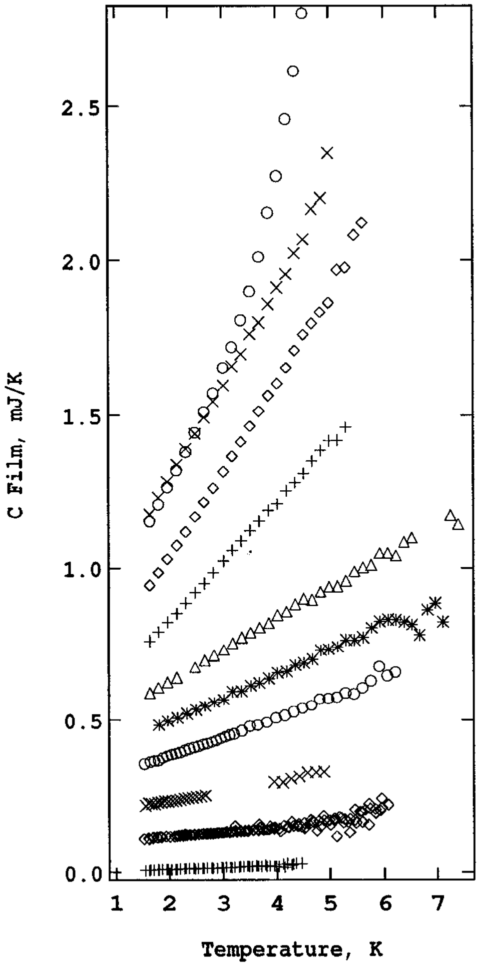

Figure 6.5: The heat capacity runs for ^{4}He at 0.1 Hz. Each run is offset by 0.1mJ/K higher than the run before, in increasing coverage. The traces are, from bottom to top, 0.0955 cc, 0.22 cc, 0.441 cc, 1.11 cc, 1.6 cc, 2.34 cc, 8.45 cc, 11.96 cc, 16.19 cc, and 21.8 cc.

capacity also becomes steeper with coverage, naturally.

We have a very large amount of data and, as one can see from Figures 6.3, 6.4, and 6.5, looking at it all at once is not a clear way to see trends in it. In order to extract information explicitly about the growth of the films we take constant temperature cuts through the data and plot the heat capacity vs coverage for a given temperature. These heat capacity isotherms are shown in Figure 6.6.

The first feature that immediately stands out is the break at ~9cc. A second look reveals that there are four regions of behavior with increasing coverage: a steep rise to ~3 to 5 cc, a plateau to 9 cc, another steep rise to ~16 cc, and then a decrease beyond that (except at the higher temperatures, which will be discussed). It is the correspondence between the two lower coverage regions here with features in the isosteric heat which best supports a 1-line→3-line→monolayer model of the growth.

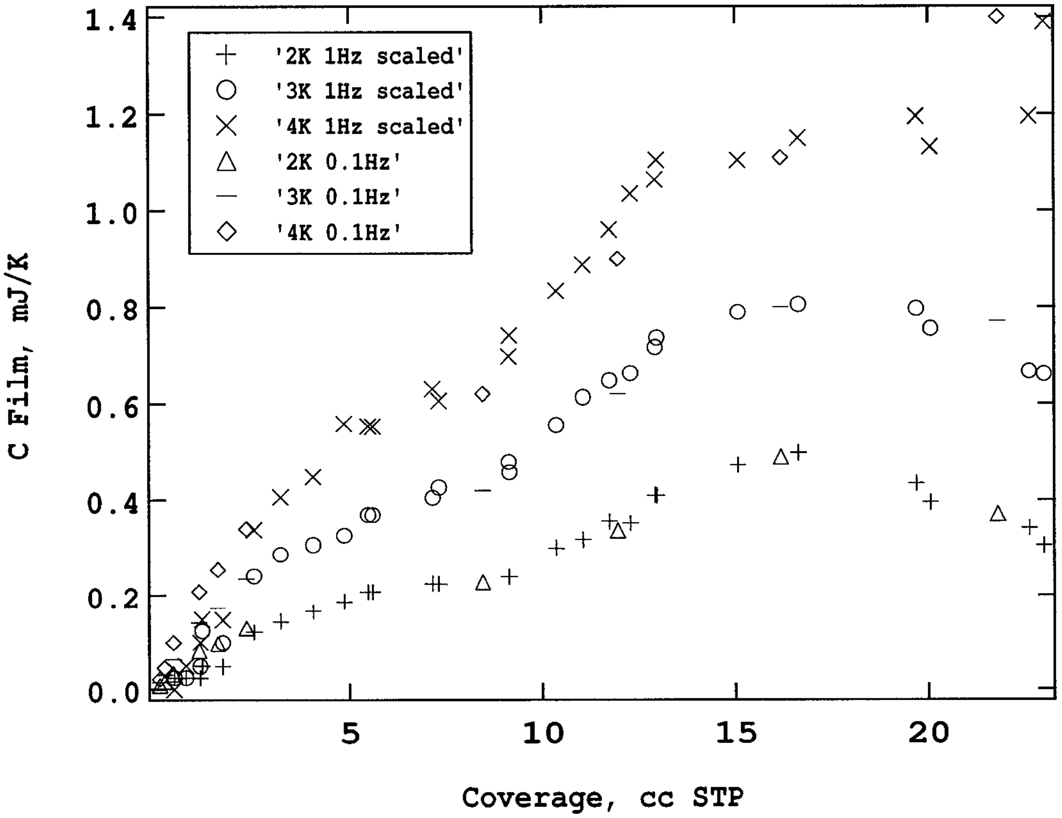

Figure 6.6: Helium heat capacity isotherms. The 1 Hz data is presented here scaled as described in the text, in order to facilitate comparison to the 0.1 Hz data.

Chapter 7

ANALYSIS OF HEAT CAPACITY DATA

The heat capacity presented as in Chapter 6, Figure 6.3, shows some qualitative trends. This type of view of the data is much more useful when there is a phase transition which gives a peak in the heat capacity. Then it easy in this view to see how the temperature of the peak depends on coverage.

While our data shows no such stark feature, there is a great deal more quantitative information we can extract with a little more reduction.

7.1 Dimension of Films

We began these experiments expecting to see a gas-like behavior in the films, particularly at higher temperatures. In this case 'gas-like' means that the system displays a heat capacity which is constant as a function of temperature. Were this the case for our system we would infer the dimensionality of the film directly from the magnitude of the heat capacity. For an ideal gas the classical specific heat in units of k_B is simply 1/2 times the number of degrees of freedom of the particles, or in the case of simple particles with no internal degrees of freedom, 1/2 times the number of dimensions.

We did not see a constant heat capacity for any coverage in any temperature range. Instead, the fact that the heat capacity is small and increases with temperature suggests that the film may be solid. This is not the only possible explanation, see Section 7.5 for a discussion. If the film is solid, and if the heat capacity is dominated by phonon modes (as it must be for a van der Waals solid), then the heat capacity should be proportional to the temperature to a power which is the number of independent degrees of freedom of the phonons. In particular, for a 2-D solid $C \propto T^2$ and for 1-D $C \propto T^1$. We will assume for the moment that the film is solid and follow this line of reasoning to determine the film properties which follow from it.

7.1.1 Quadratic Fits

One obvious way to see how linear or how quadratic the data is, is to fit it to a quadratic function. The result is a bit difficult to interpret however, because the magnitude of the coefficients does not have a simple relationship to the dimensionality. In particular, even if the system were in fact strictly 1-D, so that the data should represent a straight line, if the data have some scatter and a quadratic fit is forced, the coefficient of the squared term will not be zero. Then there is the question of whether to force the fit to go through zero. The answer becomes rather elusive if one believes that the functional form of the heat capacity may be different at even lower temperatures than what was measured. It gets even worse if one assumes that the heat capacity of the substrate was significantly altered by the film.

Still, something can be gleaned from this type of fitting, particularly for changes as a function of coverage, because we can do the fit for every coverage we studied and see how the coefficients evolve. If the dimensionality is not changing as the film density increases (and if the effect on the substrate is not too large), the coefficients should track the magnitude of the heat capacity (plus some scatter due to the scatter in the actual data). To see this, just picture that the heat capacity is strictly linear. If one film has twice the heat capacity of another, the fit to its heat capacity is twice as steep, so the coefficient of the linear term should be twice as large, while the coefficient of the quadratic term is just random. If the trends in the exponents versus coverage do not track the magnitude of the heat capacity, we may be able to infer something about the dimensionality of the film.

For the data sets presented here the linear coefficient (Figure 7.1) tracks the magnitude of the heat capacity until about 15 cc. Then it drops, as does the heat capacity, but the drop of α is much more drastic. The quadratic coefficient does not track the heat capacity at all (Figure 7.2). β is increasing for coverages above 15 cc STP, where the magnitude of the heat capacity is decreasing. This is as expected, that the film should become 'more two

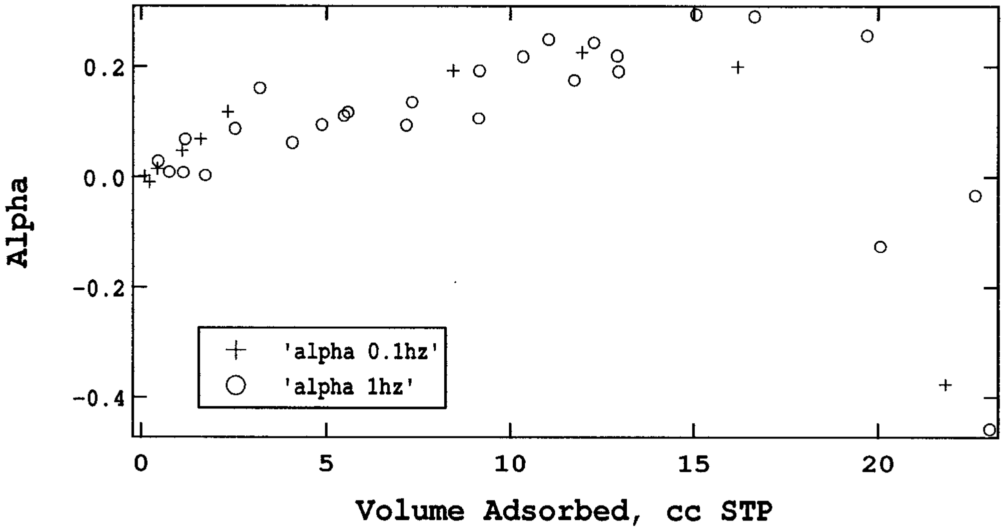

Figure 7.1: Linear coefficient of quadratic fits to the heat capacity of the helium films.

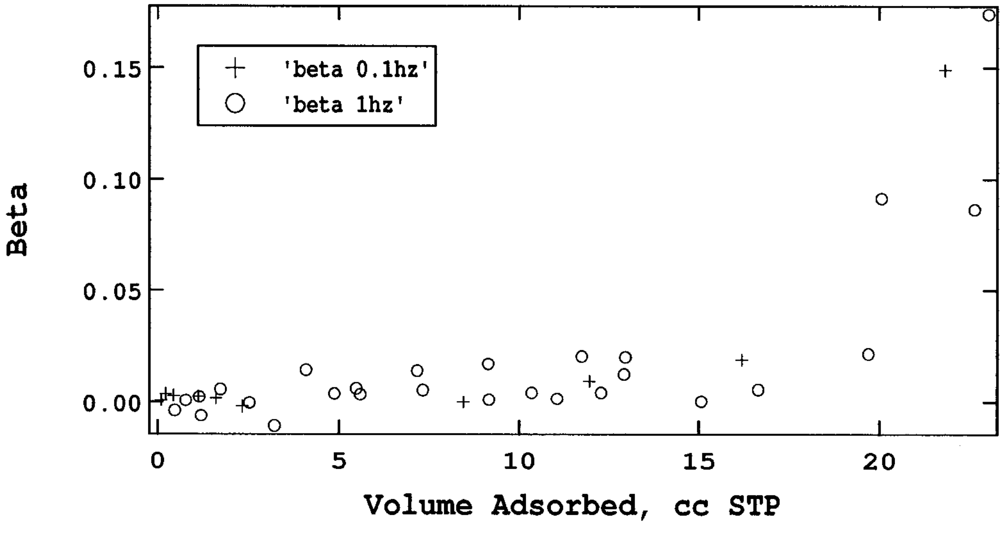

Figure 7.2: Quadratic coefficient of quadratic fits to the heat capacity of the helium films.

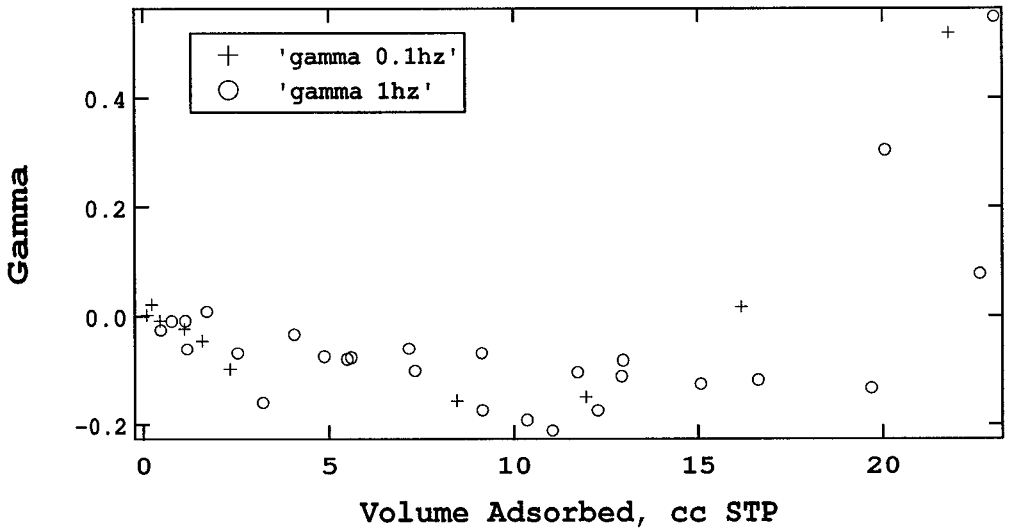

Figure 7.3: Constant from quadratic fits to the heat capacity of the helium films.

dimensional' as the outer surface of the bundle is covered. What is more surprising (and somewhat less convincing in this particular analysis) is the apparent drop in the quadratic coefficient for coverages approaching 15 cc STP, where the magnitude of the heat capacity is increasing. This suggests that the film may be becoming more one dimensional in this high coverage range.

7.1.2 Log-Log Fits

Another natural approach to find the power dependence of data is to find the slope of a log-log plot. If the data really depended only on T or T^2, or some combination of these, this would work well. Instead our data has a real, non-zero offset at T=0, which cannot be due to these temperature dependences. Log-log fits cannot be used without first removing the offsets, but the offsets cannot be found without making an assumption about the form of the temperature dependence. We arrive at a different set of offsets when the data is fit with linear or quadratic forms (the offset for quadratic fits is shown in Figure 7.3). Because we have to pick a form for the temperature dependence before making the log-log fit, there is no extra information to be gained this way.

7.2 Debye Temperature

7.2.1 Debye's Model in One Dimension

It is easily shown that the contribution to the heat capacity from phonon modes in a solid is

$$C_V = k_B \int_0^\infty \frac{e^{\beta\hbar\omega}}{(e^{\beta\hbar\omega} - 1)^2} (\beta\hbar\omega)^2 \sigma(\omega)\, d\omega \tag{7.1}$$

where $\sigma(\omega)$ is the density of phonon modes [61]. The heat capacity of solids is in general quite complicated, due to the non-triviality of this density of modes. In a useful approximation by Debye, one uses instead the density of modes of a continuous elastic medium with a uniform speed of sound for all frequencies and polarizations. The discreet particles making up the solid require that this density of modes have an upper cutoff frequency, ω_D, so that the total number of modes is correct. In 1-D this condition is

$$\int_0^\infty \sigma(\omega)\, d\omega = \int_0^{\omega_D} \sigma(\omega)\, d\omega = N \tag{7.2}$$

where N is number of particles in the solid. In a continuous elastic solid in 1-D the dispersion relation $\omega = c\kappa$, where c is the speed of sound, leads to the particularly simple density of modes

$$\sigma(\omega) d\omega = \frac{L}{2\pi} d\kappa = \frac{L}{2\pi c} d\omega \tag{7.3}$$

Inserting this in eqn 7.2, we have

$$\frac{L}{2\pi c} \int_0^{\omega_D} d\omega = \frac{L\omega_D}{2\pi c} = N \tag{7.4}$$

or

$$\omega_D = 2\pi c \frac{N}{L} \tag{7.5}$$

We are interested in the low temperature limit[1] of the heat capacity. While the continuum solid approximation is in general very poor, it is best for long wavelength, low frequency modes, where the displacement of any one atom in the solid is not very different from that of its neighbors, and the details of the interatomic forces are therefore less important. At low temperatures, the exponential factors in Equation 7.1 ensure that only these low frequency modes will contribute to the integral. This not only ensures that the approximations will be valid, it also allows us to set the limit of integration back to ∞ instead of ω_D, as frequencies higher than this will not contribute significantly to the integrand anyway.

We are now ready to evaluate the integral. We just introduce some notation to keep things neat. Let $x = \beta\hbar\omega$ and $\Theta_D = \beta\hbar\omega_D$ is the 'Debye temperature'. With these assignments, and substituting eqn 7.5 and eqn 7.3 in eqn 7.1, we have

$$C_L = \frac{Nk_B}{\Theta_D}\int_0^\infty \frac{e^x x^2}{(e^x-1)^2}\,dx = \frac{\pi^2}{3}nk_B\frac{T}{\Theta_D} \tag{7.6}$$

We can use this equation to fit our heat capacity data and extract values for Θ_D. This will be useful for comparisons to the known solid phases for helium and hydrogen adsorption on graphite.

We expect that for some coverages the system will be one dimensional, but for others it will be more two dimensional. We fit all of the data for Debye temperatures assuming 1-D solids, and again assuming 2-D solids. Both the quality of the fit and the value of Θ_D can help us determine the dimensionality of the film. The similarity of this substrate to graphite encourages us to look for 2-D phases similar to those on graphite. The possible 1-D solid must likewise have properties which make sense, i.e., it must have a speed of sound comparable to that for longitudinal modes in 2-D and 3-D helium at similar densities.

Following the steps above, with proper substitution of 2-D quantities where needed, we

---

[1] If there is a solid in the films we study, it is not to be taken for granted that the temperature range of the experiment is 'low'. Still, we can extract a Debye temperature from the data we have, and then worry about what the range of validity may be.

arrive at the expression[2]

$$C_A = 28.848\, N k_B \left(\frac{T}{\Theta_D}\right)^2 \tag{7.7}$$

7.2.2 Our Data

Forcing Zero

The Debye model is expected to fit data better and better as T → 0, because the approximations made get better and better there. In particular, the Debye model should be an excellent fit to the data at T=0. For this reason, experimental data is usually fit by preferentially weighting the lowest temperature data, and forcing the fit to go to zero. Our data has a large zero temperature offset, the cause of which we can speculate about, but we haven't adequately explained yet. Many of the lowest coverage runs are clearly linear, but a linear fit forced through zero is very poor.

For 2-D Debye temperatures we have used only the traditional fit through zero method. It is more complicated to remove the offset from these fits, and we only expect the film to be 2-D for a few of the highest coverages anyway. For 1-D Debye temperatures, we have fit our data both using the traditional fit through zero, and using a best fit to the actual slope of the data. One possible explanation for the offset makes this unforced fitting sensible, see Section 7.4 for a speculative model of the low T behavior.

Results

Figures 7.4, 7.5, and 7.6 show the results of these three types of fits. The poor agreement of the two frequency data sets at very low coverages is due to the poor quality of the 1 Hz data at these low coverages. We have a great deal more confidence in the 0.1 Hz data at these coverages.

We would add our Debye temperatures to a plot that has data for bulk and 2-D ^{4}He solids as well, Figure 1.4, but the densities are difficult to estimate, and can only be guessed. We

---

[2] The final integral that one arrives at for the 2-D case cannot be solved analytically and must be evaluated numerically, which is why the result is expressed here as a decimal number

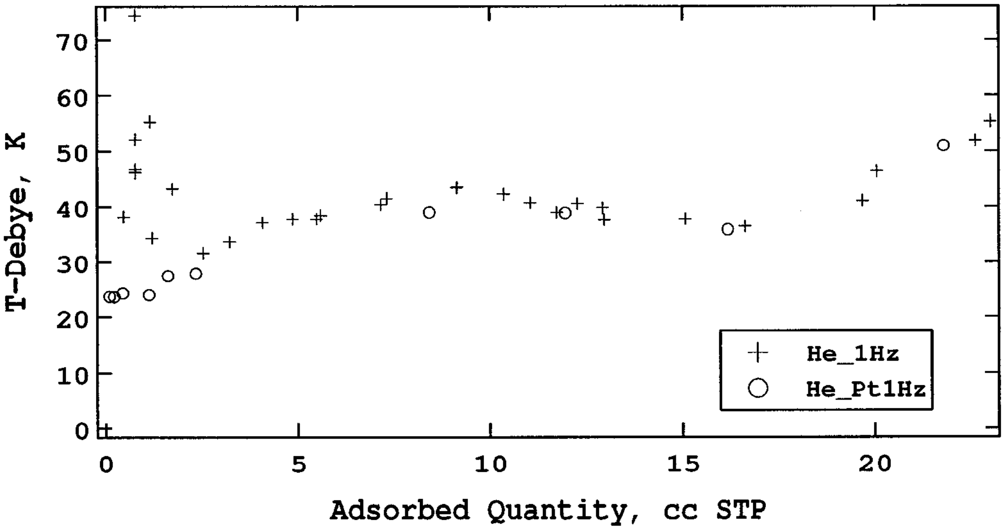

Figure 7.4: The 2-D Debye temperatures found from linear fits to C vs T^2, from zero through the lowest temperature data.

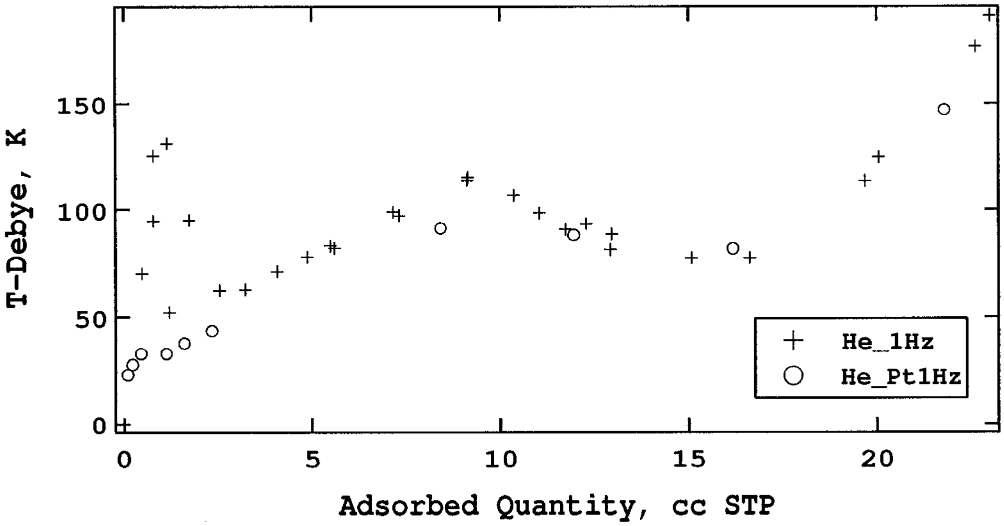

Figure 7.5: The 1-D Debye temperatures found from linear fits from zero through the lowest temperature data.

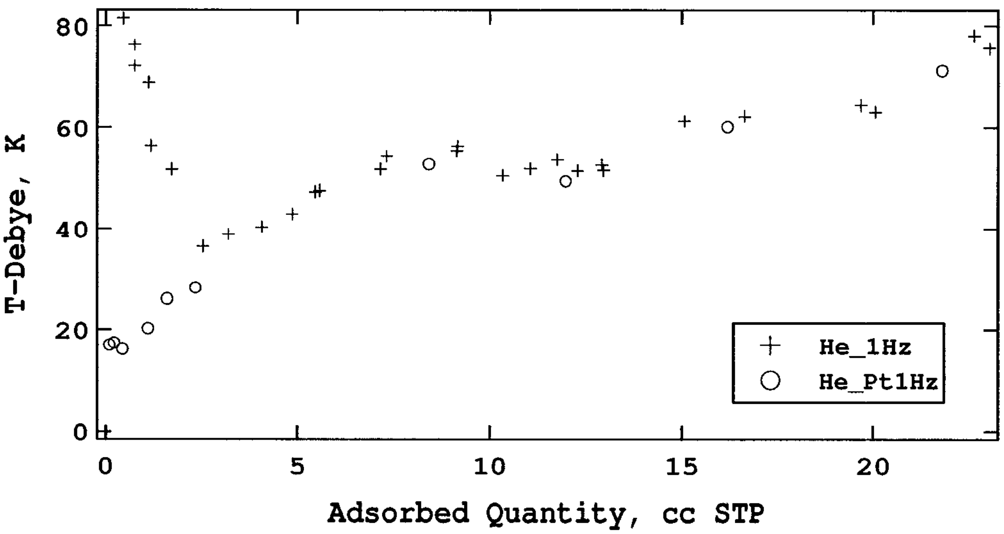

Figure 7.6: The 1-D Debye temperatures found from linear fits to the data, not forced to go through zero.

have already concluded that the monolayer completion is at ~27 cc, with the 1-line phase full at 3 cc and the 3-line full at 9 cc. If these assumptions hold, the nearest neighbor distance at 3 cc adsorbed should be similar to that for the tightest packing in 2-D and 3-D solids, or ~3.2 Å. We have data for one run at 3.2 cc adsorbed, so we could put one point on the plot with some confidence. At other coverages, it is unlikely that the 'true' density is equal to the average density. More likely the film is condensed in regions within the grooves with the highest binding energy, and substantial areas of the weaker grooves are empty. We therefore overestimate the nearest neighbor spacing when we use the average density, but it is the only information we have. We hope to resolve this issue soon, using neutron scattering data just taken with our collaborators in France. If we can extract the real nearest neighbor from this data we will be able to add the 1-D solid Debye temperatures to the plot.

While we don't yet know the density, it is clear that the Debye temperatures are in the correct range for helium solids. The lowest coverage 1-D temperatures range from 18 to about 40 K (from the unforced fits) and the highest coverage 2-D fits give just over 50 K.

There are densities for which this data would fit on the plot in Figure 1.4, such that it would agree exactly in 2-D, and the 1-D data would make a line somewhat lower than the 2-D, just as the 2-D lies somewhat below the 3-D. At this point this is pure speculation.

7.3 Separation of 1-D and 2-D Systems

One assumption which flows through all of the above analyses (with the partial exception of the quadratic fits) is that the the film is one homogeneous system, with one set of extensive properties applying to all the constituent particles. This is almost certainly a poor assumption at high coverages. As we can see from the isosteric heat, which has two plateaus within the coverage range of the first layer, the atoms find a very different environment for adsorption depending on the coverage already adsorbed. It is natural to think of the film as adsorbed in two different systems, one in the grooves and one on the rest of the surface. To separate the actual quantitative properties of the two systems is not trivial, because they certainly will have a non-negligible effect on each other. Nevertheless, we have attempted such a separation.

The heat capacity isotherms have a 'break' at ~9 cc, which we have interpreted as the end of the filling of the 3-line phase. Any adsorption beyond this should be on the outer surface, well away from the groove, and should behave more like planar graphite than the lower coverages. Though it is entirely unlikely that the properties of the 9.15 cc film are unchanged by further adsorption, we have used this film as a background, and subtracted it from the higher coverage films. We hoped that, if there was a gas phase of the atoms adsorbed beyond this coverage, we would be able to see it in spite of the poor background approximation. The heat capacity of the resulting 'partial' films is shown in Figure 7.7. It is once again small and linearly increasing. It seems that in this higher coverage range the atoms are still immobile. Perhaps this is due to a kind of nucleation by the fixed lines already in the grooves, or perhaps the narrowness of the strips of graphene surface available to the atoms leads to this unexpected behavior.

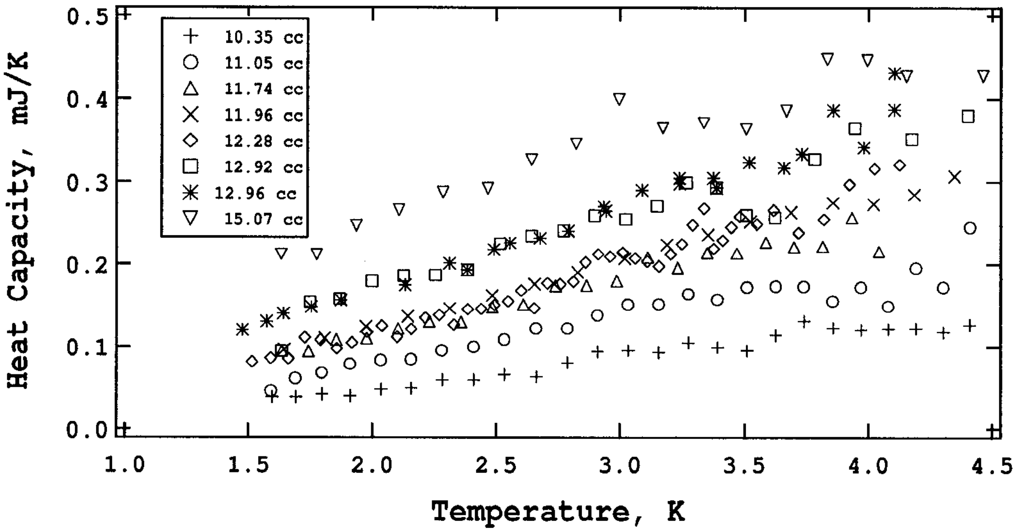

Figure 7.7: Heat capacity of partial helium films, with the 9.15 cc film used as background.

7.4 Possible Explanations of the Zero Offset

We need to explain (or at least attempt it) why the data, extrapolated to T=0, either linearly or using a quadratic fit, does not intercept at C=0.

- Low Temperature Behavior

Perhaps there is some low temperature behavior which is only significant below our temperature range. We have attempted to 'model' this in the following way. One possibility that wouldn't seem too surprising is that the heat capacity would be exponential for low T. We have simply added this dependence to the Debye model, so that the heat capacity becomes

$$C = e^{T^*/T}\frac{\pi^2}{3}nk_B\frac{T}{\Theta_D} \; ,$$

(compare to Equation 7.6). All of our low coverage data is well fit by this equation, using the Debye temperatures already reported and $T^* = 1.6$ K. To emphasize that this is not a real model, but only an empirical fitting, we will not even speculate as to the physical meaning of T^*, except to point out that it would be some type of 'activation energy', below which many of the atoms do not participate in the phonon modes, and that energies of similar magnitude exist on planar graphite due to the corrugation.

- Frequency Response of the Calorimeter

  We have frequency-scan data only at 2 K, so we can't rule out a shift of the plateau with temperature. However, we have DC measurements from 1.5 to 5 K, which suggests that such a shift isn't a large concern.

- Possible Modification of the Bundle Heat Capacity

  Perhaps the assumption that the substrate is relatively unaffected by the adsorbate is unjustified. There have been many measurements of the heat capacity of the bundles, and attempts to explain why it is smaller than a collection of the same number of tubes not associated in bundles [54, 64, 87, 57]. The model in the paper of Hone *et al.* leads to a very weak tube-tube binding, with a Debye energy of 1.2 meV. This is enough, however to substantial alter the bundle heat capacity below 4 K. Adsorbed atoms in the grooves and interstitial channels should alter this tube-tube interaction. For helium the binding energy to the surface is comparable to the tube-tube energy, and for hydrogen it is much greater. If this effect is causing our zero offset, it should then be greater for hydrogen than for helium, but the result is just the opposite.

  It need not be the binding energy of the adsorbate that alters the bundle heat capacity. I first began to consider a modification of the bundle after a paper from Cole's group [16], where they discuss the enhanced adsorption in the ICs if the bundle is allowed to expand. If the bundle lattice is altered, regardless of the binding energy of the adsorbate, the tube-tube interaction in the bundle will be significantly altered. The authors must have realised this, as they claim a change in the 'breathing mode' frequencies of the tubes of about 3%. They have suggested that this effect may lead to an experiment to verify the dilation. The tube-tube binding energy from Hone *et al.* is used in this study.

7.5 Alternative Explanations of the Linear Heat Capacity

To this point I have assumed that linearity of the heat capacity would indicate one-dimensionality (as well as solidity) of the film. There are several other possible explanantions for the linearity of the heat capacity, consistent with the conditions of our experiment.

- Heterogeneity of the substrate.

  Singleton and Halsey found that the heat capacity of a film on a highly heterogeneous substrate is linear at low temperature. Dash also explained this in his book [21].

  This can be easily understood by analogy. Suppose that at a given temperature a great many of the particles are fixed in sites on the surface and these sites have a large and widely varying binding energy. There are also a few particles with enough energy to be 'free' or mobile on the surface. The situation is similar to electrons in the valance band and conduction bands of a metal. By far the largest contribution to the heat capacity comes from the free particles, and their contribution (per particle) doesn't change with temperature. The heat capacity of the system then depends only on the number of particles in these free states. For a metal (at low T) this number is linear in temperature. For an adsorbed film, the linearity of this relationship is, in some sense, a measure of the heterogeneity. If there are no two sites on the surface with the same binding energy, and there are no large gaps in binding energy for which there are no sites (in other words, if the the film is perfectly heterogeneous), the number of free particles and hence the heat capacity will be linear in temperature.

- Clustering.

The Monte Carlo simulations of Dash and Phillips [58] found that helium clusters at low temperature in one-dimension. Krotsheck and Miller [43] found that at zero temperature the ground state of helium is a self-bound fluid, but also that dimerization is an important prerequisite for this condensed state to occur. The Monte Carlo simulations of Gordillo *et al.* [32] and Cole *et al.* [20] confirmed the calculations of Krotsheck and Miller.

- Bundle Modification.

  To achieve the offsets observed in the heat capacity, the possible modification of the heat capacity of the bundles due to the presence of the adsorbate (see Section 7.4) must be at least of order T^2. If this is the case, it means that any possible quadratic term in the film heat capacity can also be modified by the change in the bundle heat capacity. This is unlikely, because in the model of Hone *et al.* the modification due the tube interaction itself is linear in T.

- System response.

  Again, the poorly characterized frequency response of the cell discussed elswhere could be the gremlin.

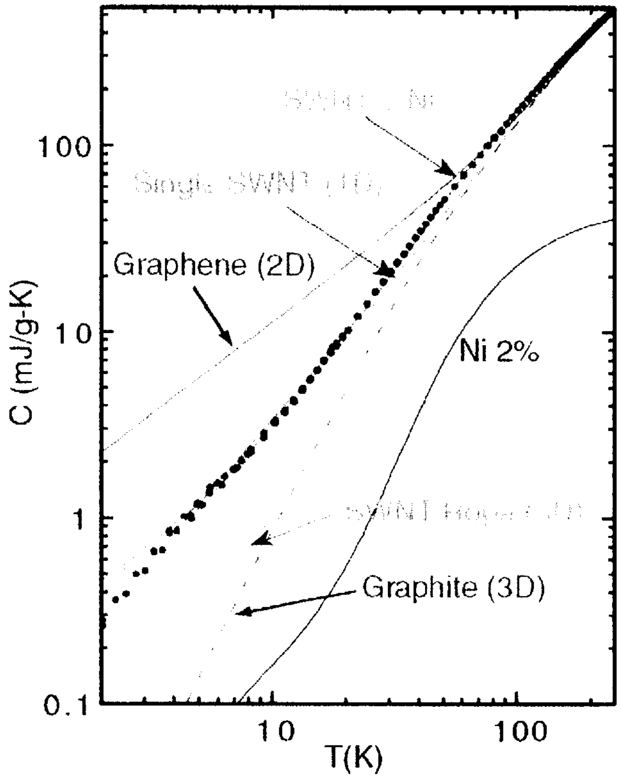

Figure 7.8: Data and models of the heat capacity of the bundles, from J. Hone *et al.* [35].

Chapter 8

HYDROGEN

In this chapter I will present all of the same analysis that was done for Helium, but this time with Hydrogen as the adsorbate. I will not repeat the details of how and why each step is taken, but just present the results and make comparisons to the Helium results.

8.1 Vapor Pressure Isotherms

All of our vapor pressure isotherm data for hydrogen was taken in a different cell from the calorimeter, as described in Section 4.9. With this data being taken on different cell in a different cryostat, it was subject to different systematic errors than on the heat capacity cell. For this reason the isosteric heat data does not go as low in coverage and has increasing error at higher coverages. We have previously published isotherms on Montpellier tubes [83], and the heat capacity measurements reported here [59].

8.1.1 Isosteric Heat

The isosteric heat is shown in Figure 8.1, together with the heat capacity isotherms. Here we see the two plateau pattern typical of adsorption on nanotubes. We don't see the low coverage feature that is present for our helium measurement.

8.2 Heat Capacity

This data was taken at 0.1 Hz on the same cell used for all the measurements reported here, so the background heat capacity is the same as that used for the 0.1 Hz helium data. The hydrogen heat capacity runs are shown all together in Figure 8.2. Many of the films were measured to much higher temperature than shown here (see Appendix D for the complete

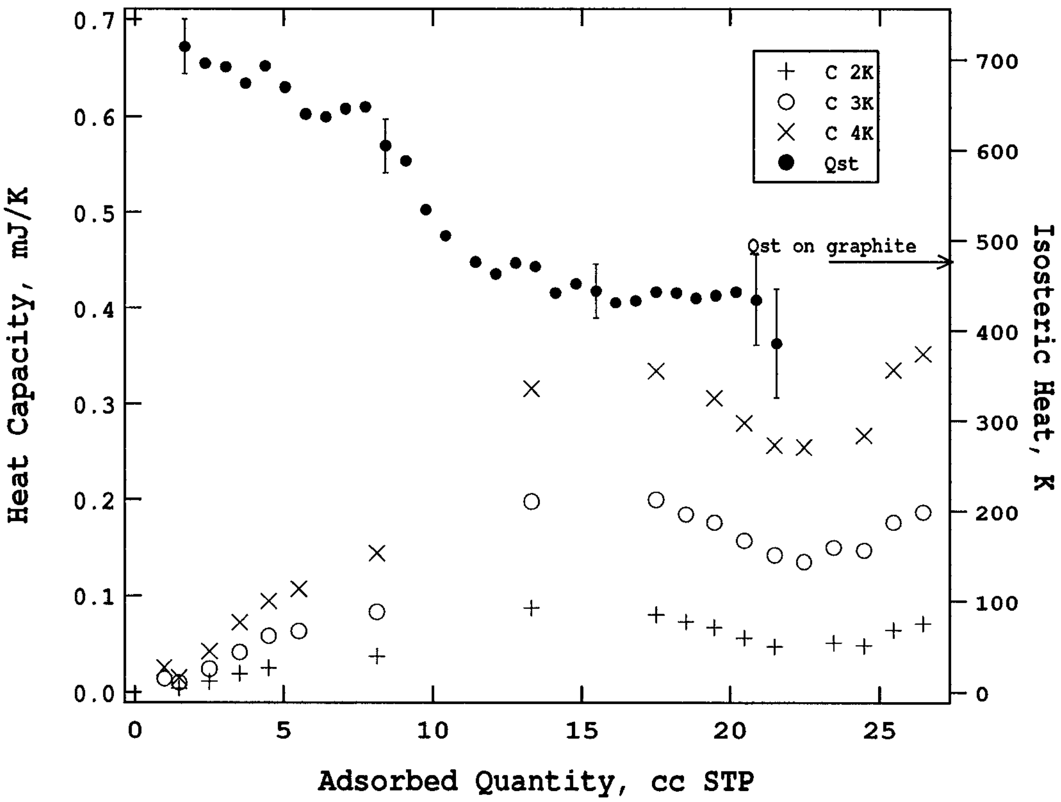

Figure 8.1: Here they are, shown together. The q_{st} data was taken in another cell with 63 mg HiPco™ tubes. It has been scaled in coverage by the ratios of the masses of tubes in the two cells.

data set). Due to poorly understood systematic problems with the cell, the data above 8K is very noisy and of little utility except to try to discern qualitative trends.

8.2.1 Heat Capacity Isotherms

The heat capacity isotherms for Helium ended just before one monolayer coverage because desorption made the heat capacity difficult to measure at high coverages in the available temperature range. With Hydrogen we were able to go higher in coverage, and significant desorption did not set in until coverages greater than a monolayer. This allows us to constuct the heat capacity isotherm that goes through the monolayer completion, Figure 8.1. We see clearly a minimum at monolayer completion, with a steep rise following. Also visible, though less convincing, is a small jog in the slope just above the monolayer. This could be due to the filling of grooves in the second layer, as predicted by Cole's group and measured by Migone's for other adsorbates.

8.2.2 Dimensionality

Quadratic fits to the hydrogen data are radically different than for helium, see Figure 8.3. While β is linearly increasing over most of the coverage range, α remains small or even negative at all coverages, except 13.33 cc. The films appear for this reason to be more two-dimensional than the helium films. This is reinforced by the Debye analysis.

8.2.3 Debye Temperature

Two dimensional fits to the Debye temperature fit our data very well over the entire coverage range, though the data is quite noisy for the lowest two or three coverages. The temperatures extracted this way are in good agreement with hydrogen on graphite, though again we don't know the densities. The one dimensional fits are poor, whether forced to zero or not, and give values for Θ_D which are much larger than for 2-D, which is the wrong trend. From this we again conclude that the hydrogen films are much more two-dimensional than the helium.

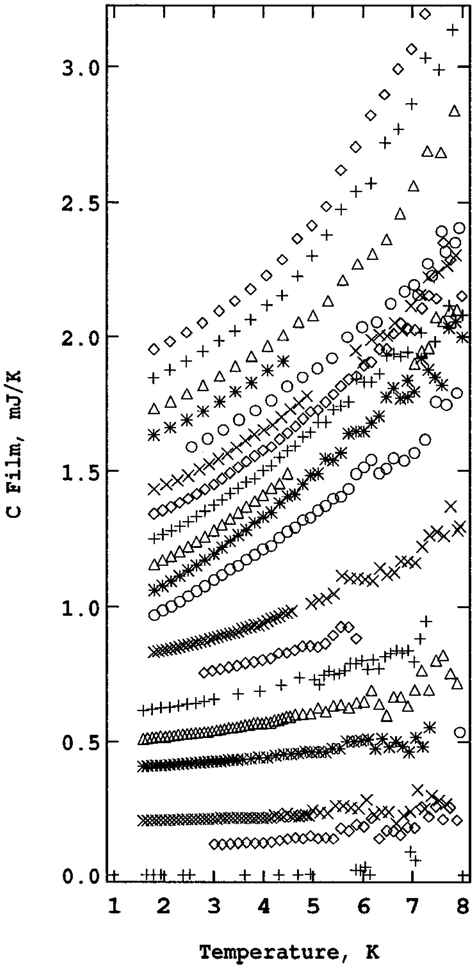

Figure 8.2: The heat capacity of hydrogen films at 0.1 Hz, shown for all of the coverages measured. For clarity, each run is offset by 0.1 mJ/K higher than the run before, in increasing coverage. The traces are, from bottom to top, 0.5 cc, 1.0 cc, 1.5 cc, 2.5 cc (only one point for this run appears, at high T), 2.5036 cc, 3.5 cc, 4.5 cc, 5.5 cc, 8.13 cc, 13.33 cc, 17.5 cc, 18.5 cc, 19.47 cc, 20.47 cc, 21.47 cc, 22.47 cc, 23.47 cc, 24.47 cc, 25.47 cc, and 26.47 cc.

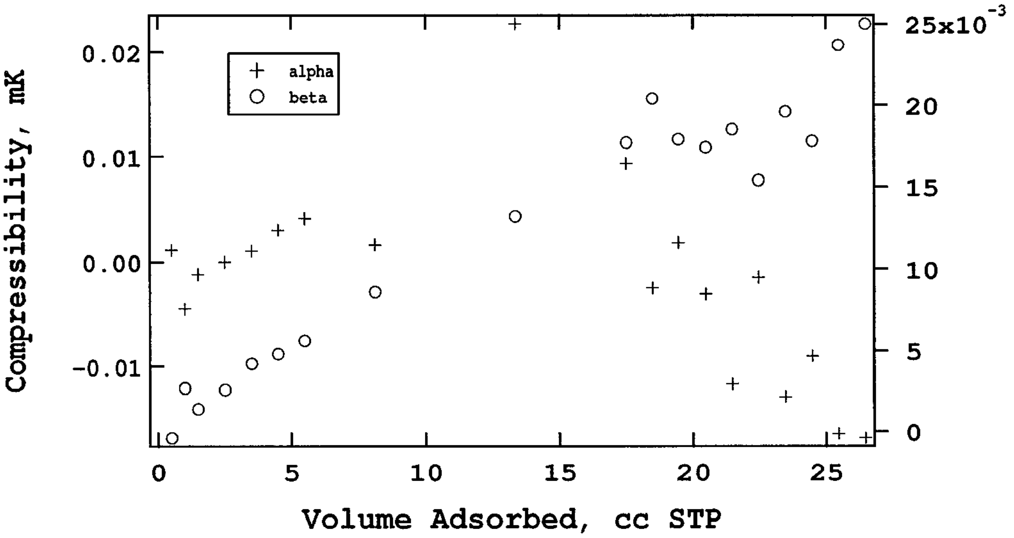

Figure 8.3: Coefficients of quadratic fits to the heat capacity of hydrogen films.

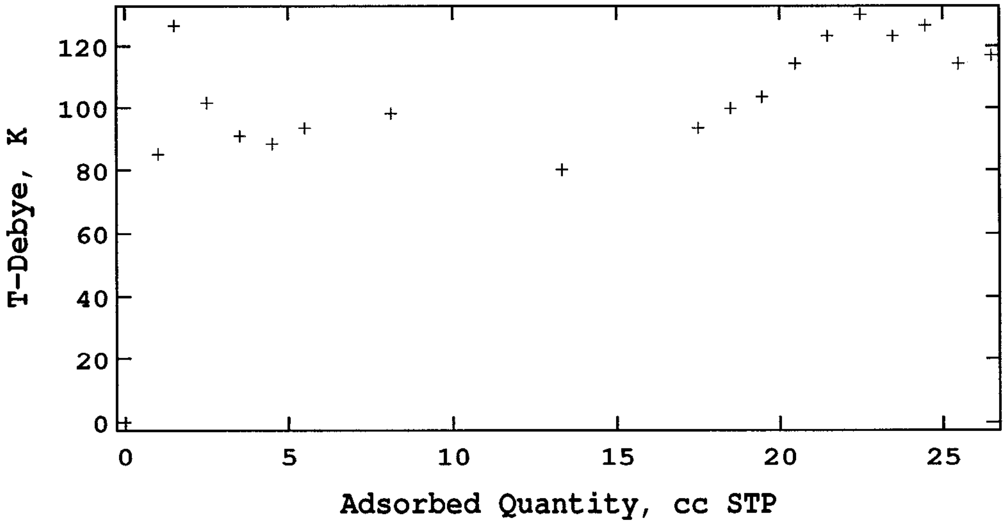

Figure 8.4: The 2-D Debye temperatures found from linear fits to C vs T^2, from zero through the lowest temperature data.

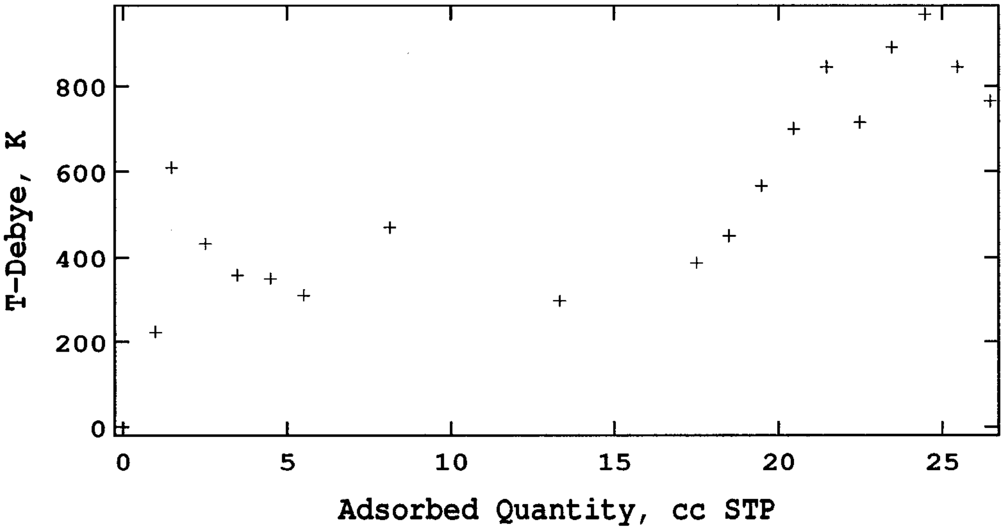

Figure 8.5: The 1-D Debye temperatures found from linear fits from zero through the lowest temperature data.

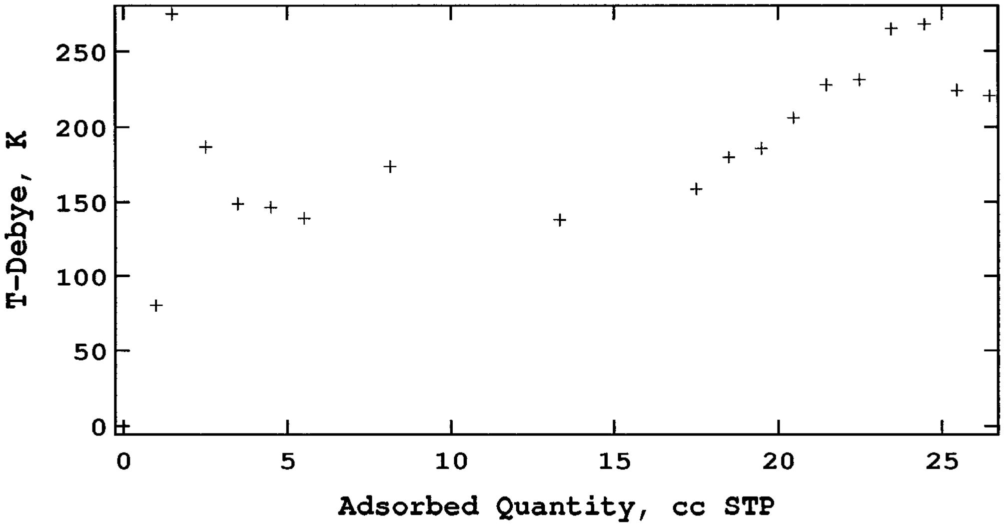

Figure 8.6: The 1-D Debye temperatures found from linear fits to the data, not forced to go through zero.

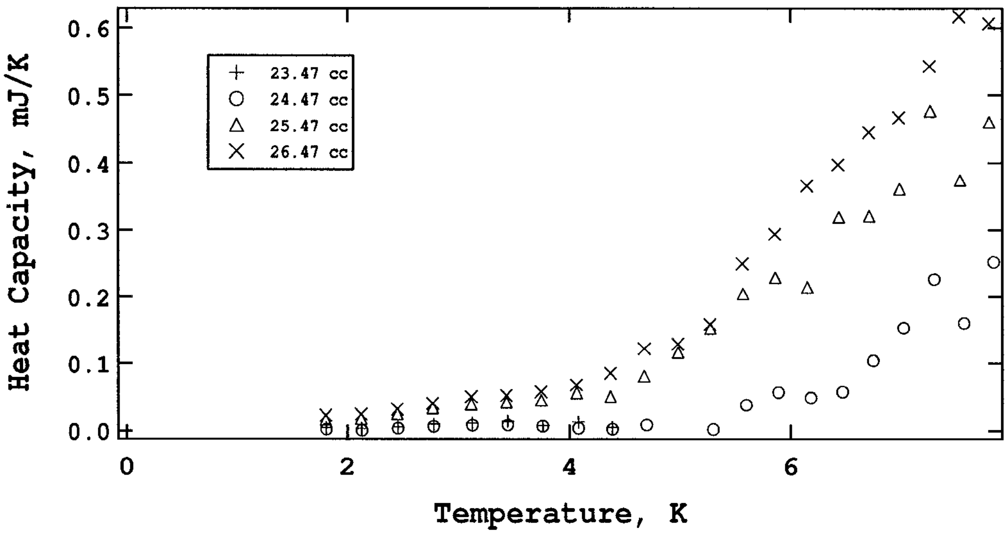

Figure 8.7: Heat capacity of the second layer hydrogen films, using the 22.5cc coverage for a background.

8.3 Second Layer

We took data for several coverages past the monolayer completion at ∼ 22cc. Migone's group has also seen the one line phase on the second layer from adsorption isotherms. Here we hoped there finally should be a gas, and we should see its constant heat capacity, and hopefully it will even be 1-D. We used the 22.5 cc data as a background for the films at higher coverage, in a 'partial film' analysis as we did for the helium films above 9 cc. The heat capacity of the high coverage films is shown in Figure 8.7. It is again very small, too small for a gas phase, though the lowest two coverages seem to be constant from about 3 to 5 K. The specific heat here is less than 0.1. The steep rise in each film at higher temperatures is due to desorption, as verified by monitoring the pressure in the cell during the measurements.

Chapter 9

CONCLUSIONS

We have made systematic meaurements of the thermodynamic properties of ^{4}He and H_2 films adsorbed on bundles of single-walled carbon nanotubes, both as a function of coverage and of temperature, by the techniques of calorimetry and vapor pressure isotherms. These measurements are complemented by similar experiments on different adsorbates and different experiments on the same and different adsorbates, some of which were done by our own group and many by others. From this wealth of experimental data a unified picture is emerging of the growth of the films, but contradictions persist about the structure.

In these experiments there are two 'regimes' we wanted to examine: trends vs. coverage, and trends vs. temperature. Though there are 'surprises' in both, the temperature regime is by far the more unexpected. In coverage we see the expected 3-line phase, and what we interpret to be the 1-line phase at low coverages. At higher coverage we expect to see 2-D behavior. The temperature behavior is entirely unexpected, with seemingly a dense solid structure of the film at all temperatures and coverages, in contradiction to a previous experiment [48] as well as to our intuition.

The major points we can conclude from these experiments are:

- Growth of films.

  After a small amount of high energy, inhomogeneous binding, the growth of the film begins in the grooves, and proceeds in three steps: 1-line → 3-line → monolayer.

- Structure of films.

  We see no gas phase anywhere. All the films at any coverage have too small a heat capacity to indicate a gas phase. Furthermore the heat capacity is not constant with temperature anywhere, but rather increasing roughly linearly. Attempting to divide out a portion of the film which is at low density on the outer surface of the tubes from the portion which remains fixed in the grooves, still doesn't yield gas-like behavior. Even in the second layer of H_2 we don't see gas-like behavior.

- Dimensionality of films.

  Although the film appears to be solid everywhere, the behavior of this solid may be one dimensional, in contrast to the possibility that it would be an 'Einstein solid', in which the individual particles do not interact significantly. There are many other possibilities to explain the linearity we see in the heat capacity. The hydrogen films are significantly more two dimensional than helium.

- Comparison of ^{4}He and H_2.

  We have compared the behavior of ^{4}He and H_2 on this substrate, and related this to the same comparison on graphite. The coverages scale much like on graphite, with the bundles having a specific area for adsorption approximately 1.2 times higher for ^{4}He than for H_2. The magnitude of the heat capacity is much lower for H_2 than for ^{4}He at the same temperature, as it is for graphite, but the ratio is somewhat different.

- Quality of the substrate.

  The substrate needs to be better characterized, and the effects of different preparations better understood. The effect of the adsorbate on the substrate needs to be better understood.

I'll address each of these points in turn.

9.1 Growth of Films

The samples are quite impure and heterogeneous. Even excluding the catalyst and amorphous carbon in the sample, a rope of carbon nanotubes is almost certainly a messy tangle, with only a vague resemblance to the idealised cartoon we usually use to represent them. It is likely that some of the junk in the cell, and rare adsorption sites such as the end of the bundle of tubes, have the strongest potential for adsorption, and are the first to fill at very low coverages. It is possible that the filling of such sites is responsible for the very high and steep (with coverage) isosteric heat observed for the lowest coverages (Section 5.2). However, the portion of the vapor pressure isotherms used to deduce this q_{st} are measured from the lowest range of our baratron pressure gauges, and it seems as likely that this extremely low coverage data is simply too inaccurate to draw conclusions from. Once the isoteric heat levels out on a first plateau (as a function of increasing coverage) we can assume that the adsorbate is filling sites homogeneous at least in binding energy, if not in detailed geometry.

9.1.1 Calculated Order of Binding Energies

Calculations suggest that the highest energy binding is in the interstitial channels, for adsorbates that fit inside these channels. In our interpretation of our data we have assumed that helium and hydrogen fit only into the largest of the interstitial channels (of the realistic bundle, see Figure 2.4) and that we can lump this adsorption into the inhomogeneous binding. In this case the first plateau should correspond to the filling of a single line of atoms in the outer grooves of the bundles. These grooves should also not be homogeneous.

9.1.2 Interpretation of Isotherms and Isosteric Heat Plateaus

The first plateau begins when the single line is full and ends when the 3-line phase is full. This makes it appear the isosteric heat in the 1-line phase is a strong function of density. This is sensible, because the 1-line phase should be the most sensitive to the heterogeneity of the substrate. In different grooves the corrugation may be radically different depending on the orientation and type of neighboring tubes. If the tubes are tangled, the places where tubes cross are also grooves, but very different ones from the grooves between straight, parallel tubes. Once the lines are full however, the situation is much different. The atoms that adsorb into the 3-line phase are always on the curved surface of just one tube, and adjacent to a fixed line of other adsorbate atoms. It matters very little what the orientation or type of the tube is and even less what the neighboring tube is like. The binding surface for the 3-line phase is therefore much more homogeneous than for the 1-line phase, even though they are on the same substrate. The situation is somewhat analogous to the use of plating to achieve more uniform surfaces, such as in the adsorption of helium on one or more layers of hydrogen on graphite. The hydrogen film fills irregularities in the surface and presents the helium with a much smoother surface than the bare graphite, in addition to lowering the overall binding energy and 'floating' the helium, effectively reducing the corrugation.

Somewhere in the middle of the graphite like plateau the behaviour of the film changes dramatically from 1-D to 2-D. This appears in q_{st} as the beginning of the drop-off from the graphite-like plateau.

9.1.3 Comparison with Heat Capacity Isotherms

For helium, the trends with coverage in the isosteric heat and the heat capacity are in remarkable coincidence. For hydrogen, though we don't see the same low coverage feature in the isosteric heat, the rest of the coverage dependence is again in good correspondence with the heat capacity.

9.2 Structure of the Films

It has long been known that there can be no phase equilibrium in one dimension. This is equivalent to saying that the behaviour of the one dimensional system must be gas-like at all temperatures, pressures and densities. In particular the specific heat of a classical one dimensional gas of particles with no internal degrees of freedom is 1/2[1] (in units of Boltzmann's constant). Nowhere within the range of our experiments did we see a constant

---

[1] 1/2 is the specific heat of an *ideal* 1-D gas. There is no fundamental principle implying that a real 1-D system should be ideal, and in fact it almost certainly will not be. Still, for some large range of the thermodynamic variables of the system the heat capacity should be constant and nearly $1/2Nk_B$. In 2-D helium on graphite the behavior is well described by an ideal gas, for some range of the parameters.

heat capacity. Instead the heat capacity of every film coverage measured was small and increasing, more or less linearly, at all temperatures.

We have applied several analyses to the data which have meaning only in the case that the film is solid, or at least immobile. This does not represent our unequivocal advocacy of this interpretation, but rather it is one necessary course of action when faced with data which calls for it. It is also possible that the film is as inhomogeneous as the surface it is adsorbed on, with some portions of the film fixed and immobile while others are more gas like. It may be impossible to apply such a 'two-film' interpretation quantitavely to our data without more information, because the separation of the films' properties will be a very poor approximation. We already suspect that separating the properties of the film from the substrate may be a poor approximation in the case of adsorption on SWCNs, because the film may have a non-negligible effect on the properties of the substrate. The effect of one film on another of the same species on the same substrate will certainly be very large.

9.3 Dimensionality of the Films

The films at low coverage are one dimensional. This conclusion results from the linearity of the heat capacity and the good agreement of the 1-D Debye temperatures with those for 2-D and 3-D helium, though that assumes that the film is a solid and the heat capacity is phonon dominated. We're also assuming that we measured in a good temperature range for the Debye fit. For two dimensional fits to helium on planar graphite the fit is sometimes only good to just above 1K.

sectionComparison of Helium and Hydrogen

They scale in coverage like on graphite. I still have to figure out how their scaling in heat capacity compares with that on graphite. Also see if the comparison can let us push back the lower temp. of helium to the point where it goes negative. This lets us say that the offset is not due only to low T behaviour that we don't see.

We have hydrogen data for the second layer, unlike for helium. What does it tell us? It is not the 1-D gas, though it has been shown that it forms a line phase on the second layer and these grooves should be very smooth.

9.4 Quality of the Substrate

9.4.1 Heterogeneity and Junk in the Samples

Our experiments are well understood without considering adsorption in the interstitial channels as a significant contribution. This appears to contradict the predictions that for both ^{4}He and H_2 adsorption in the ICs is favorable, and the specific area for adsorption there is large. Rather than pointing out problems with the calculations, these measurements more likely expose complications with the substrate itself. As an example, it is possible that the ICs are blocked with amorphous carbon, or catalyst particles, or some unknown junk. It is also possible that the ICs are full of something else that adsorbed after their creation, and that is not removed during our outgassing procedures. Much of the rest of the surface is blocked by such junk, as is seen by the dramatic change in available surface area for adsorption depending on substrate preparations such as temperature of 'baking' in vacuum or chemical purification prior to adsorption experiments.

9.4.2 Heat Capacity of the Bundles

It is possible that the heat capacity of the substrate is significantly modified by the presence of the adsorbate, as discussed in Section 7.4. This has not been seen to be a difficulty in previous studies of adsorption on graphite, the substrate most similar to nanotube bundles. High surface area graphite preparations such as Grafoil™ have up to 30 m^2/gram of uniform surface area for adsorption, compared with 700 m^2/gram for purified HiPco™ nanotube bundles.

BIBLIOGRAPHY

[1] K. N. Altmann, J. N. Crain, A. Kirakosian, J. L. Lin, D. Y. Petrovykh, and F. J. Himpsel. Electronic structure of atomic chains on vicinal Si(111)-Au. *Physical Review B*, 64:035406, 2001.

[2] F. Ancilotto, M. M. Calbi, S. M. Gatica, and M. W. Cole. Bose-Einstein condensation of helium and hydrogen inside bundles of carbon nanotubes. *submitted to the proceedings of QFS 2004*, 2004.

[3] Francesco Ancilotto, M. Mercedes Calbi, Silvina M. Gatica, and Milton W. Cole. Bose-Einstein condensation of molecular hydrogen in nanotube bundles. *preprint*, 2003.

[4] R. A. Aziz, V. P. S. Nain, J. C. Carley, W. J. Taylor, and G. T. McConville. *Journal of Chemical Physics*, 70:4330, 1979.

[5] A. Bachtold, M. S. Fuhrer, S. Plyasunov, M. Forero, Erik H. Anderson, A. Zettl, and Paul L. McEuen. Scanned probe microscopy of electronic transport in carbon nanotubes. *Physical Review Letters*, 84(26):6082, 2000.

[6] J. J. M. Beenakker, V. D. Borman, and S. Yu. Krylov. *Chemical Physics Letters*, 232:379, 1995.

[7] D. S. Bethune, C. H. Kiang, M. S. de Vries, G. Gorman, R. Savoy, J. Vazquez, and R. Beyers. Cobalt-catalysed growth of carbon nanotubes with single-atomic-layer walls. *Nature*, 363:605, 1993.

[8] M. Bienfait, P. Zeppenfeld, N. Dupont-Pavlovsky, M. Muris, M. R. Johnson, T. Wilson, M. DePies, and O. E. Vilches. Thermodynamics and structure of H2, Methane, Ar, O2, and CO2 adsorbed on SWCNTBs. *Physical Review B*, 70:035410, 2004.

[9] M. Bienfait, P. Zeppenfeld, N. Dupont-Pavlovsky, J. -P. Palmari, M. R. Johnson, T. Wilson, M. DePies, and O. E. Vilches. Adsorption of argon on carbon nanotube bundles and its influence on the bundle lattice parameter. *Physical Review Letters*, 91(3):035503, 2003.

[10] Marc Bockrath, Wenjie Liang, Dolores Bozovic, Jason H. Hafner, Charles M. Lieber, M. Tinkham, and Hongkun Park. Resonant electron scattering by defects in single-walled carbon nanotubes. *Science*, 291:283, 2001.

[11] Lawrence J. Bovie and Oscar E. Vilches. Melting and evaporation of monolayer H_2-D_2 mixtures adsorbed on D_2-plated graphite. *Journal of Low Temperature Physics*, 110(1/2):621, 1998.

[12] J. Breton, J. Gonzalez-Platas, and C. Girardet. Endohedral adsorption in graphitic nanotubules. *Journal of Chemical Physics*, 101(4):3334, 1994.

[13] L. W. Bruch, Milton W. Cole, and Eugene Zaremba. *Physical Adsorption: Forces and Phenomena.* Oxford University Press, 1997.

[14] M. Mercedes Calbi and Milton W. Cole. Dimensional crossover and quantum effects of gases adsorbed on nanotube bundles. *Physical Review B*, 66:115413, 2002.

[15] M. Mercedes Calbi, Milton W. Cole, Silvina M. Gatica, Mary J. Bojan, and George Stan. Colloquium: Condensed phases of gases inside nanotube bundles. *Reviews of Modern Physics*, 73(4):857, 2001.

[16] M. Mercedes Calbi, Flavio Toigo, and Milton W. Cole. Dilation-induced phases of gases adsorbed within a bundle of carbon nanotubes. *Physical Review Letters*, 86(22):5062, 2001.

[17] P. M. Chaiken and T. C. Lubensky. *Principles of Condensed Matter Physics.* Cambridge University Press, 1995.

[18] Siu-Pang Chan, Gang Chen, X. G. Gong, and Zhi-Feng Liu. Chemisorption of hydrogen molecules on carbon nanotubes under high pressure. *Physical Review Letters*, 87(20):205502, 2001.

[19] I. W. Chiang, B. E. Brinson, A. Y. Huang, P. A. Willis, M. J. Bronicowski, J. L. Margrave, R. E. Smalley, and R. H. Hauge. Purification and characterization of single-wall carbon nanotubes (swnts) obtained from the gas-phase decomposition of CO (HiPco process). *Journal of Physical Chemistry B*, 105:8297, 2001.

[20] M. W. Cole, V. H. Crespi, G. Stan, J. M. Hartman, S. Moroni, and M. Boninsegni. Condensation on helium in nanotube bundles. *Physical Review Letters*, 84(17):3883, 2000.

[21] J. G. Dash. *Films on Solid Surfaces.* Academic Press, Inc., 1975.

[22] J. G. Dash. Two-dimensional matter. *Endeavor, New Series*, 6(1):15, 1982.

[23] A. C. Dillon, K. M. Jones, T. A. Bekkedahl, C. H. Kiang, D. S. Bethune, and M. J. Heben. Storage of hydrogen in single-walled carbon nanotubes. *Nature*, 386(27):377, 1997.

[24] J. A. Duffy, N. J. Wilkinson, H. M. Fretwell, M. A. Alam, and R. Evans. Phase transitions of CO_2 confined in nanometer pores as revealed by positronium annihilation. *Journal of Physics: Condensed Matter*, 7:L713, 1995.

[25] Robert Elgin. *The Thermodynamics of the ^{4}He Submonolayer Film Adsorbed on Grafoil.* PhD thesis, California Institute of Technology, 1973.

[26] V. J. Emery and J. D. Axe. One-dimensional fluctuations and the chain-ordering transformation in $Hg_{3-\delta}AsF_6$. *Physical Review Letters*, 40(23):1507, 1978.

[27] R. Evans. Fluids adsorbed in narrow pores: phase equilibria and structure. *Journal of Physics: Condensed Matter*, 2:8989, 1990.

[28] Lucyna Firlej and Bogdan Kuchta. Helium adsorption in single wall carbon nanotubes - grand canonical monte carlo study. *preprint*, 2003.

[29] S. M. Gatica, M. J. Bojan, G. Stan, and M. W. Cole. Quasi-one- and two-dimensional transitions of gases adsorbed on nanotube bundles. *Journal of Chemical Physics*, 114(8):3765, 2001.

[30] Martin P. Gelfand and Reinhard Lipowsky. Wetting on cylinders and spheres. *Physical Review B*, 36(16):8725, 1987.

[31] M. C. Gordillo, J. Boronat, and J. Casulleras. Quasi-one-dimensional ^{4}He inside carbon nanotubes. *Physical Review B*, 61(2):R878, 2000.

[32] M. C. Gordillo, J. Boronat, and J. Casulleras. Zero-temperature equation of state of quasi-one-dimensional H_2. *Physical Review Letters*, 85(11):2348, 2000.

[33] M. C. Gordillo, J. Boronat, and J. Casulleras. Isotopic effects of hydrogen adsorption in carbon nanotubes. *Journal of Low Temperature Physics*, 126:199, 2002.

[34] F. J. Himpsel, K. N. Altmann, R. Bennewitz, J. N. Crain, A. Kirakosian, J. L. Lin, and J. L. McChesney. One-dimensional electronic states at surfaces. *Journal of Physics: Condensed Matter*, 13:11097, 2001.

[35] J. Hone, B. Batlogg, Z. Benes, A. T. Johnson, and J. E. Fischer. Quantized phonon spectrum of single-wall carbon nanotubes. *Science*, 289:1730, 2000.

[36] J. Hone, M. C. Llaguno, N. M. Nemes, A. T. Johnson, J. E. Fischer, D. A. Walters, M. J. Casavant, J. Schmidt, and R. E. Smalley. Electrical and thermal transport properties of magnetically aligned single wall carbon nanotube films. *Applied Physics Letters*, 77(5):666, 2000.

[37] Sumio Iijima. Helical microtubules of graphitic carbon. *Nature*, 354:56, 1991.

[38] Sumio Iijima and Toshinari Ichihashi. Single-shell carbon nanotubes of 1-nm diameter. *Nature*, 363:603, 1993.

[39] M. R. Johnson, S. Rols, P. Wass, M. Muris, M. Bienfait, P. Zeppenfeld, and N. Dupont-Pavlovsky. Neutron diffraction and numerical modelling investigation of methane adsorption on bundles of carbon nanotubes. *Chemical Physics*, 293:217, 2003.

[40] M. K. Kostov, H. Cheng, R. M. Herman, M. W. Cole, and J. C. Lewis. Hindered rotation of H_2 adsorbed interstitially in nanotube bundles. *Journal of Chemical Physics*, 116(4):1720, 2002.

[41] M. K. Kostov, M. W. Cole, G. D. Mahan, C. Carraro, and M. L. Glasser. Enhanced cohesion of matter on a cylindrical surface. *Physical Review B*, 67(7):75403, 2003.

[42] Milen K. Kostov, Milton W. Cole, and John Courtenay Lewis. Many-body interactions among adsorbed atoms and molecules within carbon nanotubes and in free space. *Chemical Physics Letters*, 332(1/2):26, 2000.

[43] E. Krotscheck and M. D. Miller. Properties of ^{4}He in one dimension. *Physical Review B*, 60:13038, 1999.

[44] E. Krotscheck, M. D. Miller, and J. Wojdylo. *Physical Review B*, page 13028, 1999.

[45] Vaiva Krungleviciute, Luke Heroux, Saikat Talapatra, and Aldo D. Migone. Gas adsorption on HiPco™ nanotubes: surface area determinations, and neon second layer data. *preprint*, 2004.

[46] L. D. Landau and E. M. Lifshitz. *Statistical Physics, Part 1.* Butterworth-Heinemann, 1951.

[47] J. C. Lasjaunias, K. Biljaković, Z. Benes, J. E. Fischer, and P. Monceau. Low-temperature specific heat of single-wall carbon nanotubes. *Physical Review B*, 65:113409, 2002.

[48] J. C. Lasjaunias, K. Biljaković, J. L. Sauvojol, and P. Monceau. Evidence of 1D behaviour of He^4 confined within carbon-nanotube bundles. *Physical Review Letters*, 91:025901, 2003.

[49] R. S. Lee, H. J. Kim, J. E. Fischer, J. Lefebvre, M. Radosavljevió, J. Hone, and A. T. Johnson. Transport properties of a potassium-doped single-wall carbon nanotube rope. *Physical Review B*, 61(7):4526, 2000.

[50] J. E. Lennard-Jones. *Transcripts of the Farraday Society*, 28:333, 1932.

[51] Fritz London. *Zeitschrift für Physik*, 63:245, 1930.

[52] Daniel C. Mattis. *Statistical Mechanics made Simple.* World Scientific, 2003.

[53] E. V. Mello, J. J. Rehr, and O. E. Vilches. Virial calculations for $H_{\downarrow}$ in two and three dimensions. *Physical Review B*, 28(7):3759, 1983.

[54] Ari Mizel, Lorin X. Benedict, Marvin L. Cohen, Steven G. Louie, A. Zettle, Nasser K. Budraa, and W. P. Beyermann. Analysis of the low-temperature specific heat of multi-walled carbon nanotubes and carbon nanotube ropes. *Physical Review B*, 60(5):3264, 1999.

[55] Frederick C. Motteler. *A Heat Capacity Study of p-H_2 Monolayers on Graphite.* PhD thesis, University of Washington, 1986.

[56] M. Muris, M. Bienfait, P. Zeppenfeld, N. Dupont-Pavlovsky, M. Johnson, O. E. Vilches, and T. Wilson. Diffraction study of CD_4 and D_2 adsorbed on carbon nanotubes. *Applied Physics A*, 74[Suppl.]:S1293, 2002.

[57] R. Nicklow, N. Wakabayashi, and H. G. Smith. Lattice dynamics of pyrolytic graphite. *Physical Review B*, 5(12):4951, 1972.

[58] James M. Phillips and J. G. Dash. Thermal disorder, fluctuations, growth and fragmentation of finite one-dimensional atomic chains. *in preparation*, 2004.

[59] S. Ramachandran, T. A. Wilson, D. Vandervelde, D. K. Holmes, and O. E. Vilches. Heat capacity of H_2 adsorbed on carbon nanotube bundles. *Journal of Low Temperature Physics*, 134(1/2):115, 2004.

[60] Roberto Canaban Ramos, Jr. *Liquid-Vapor Coexistence in Two-Dimensional ^3He-^4He Mixtures.* PhD thesis, University of Washington, 1999.

[61] F. Reif. *Fundamentals of statistical and thermal physics.* McGraw-Hill, Inc., 1965.

[62] A. W. Rempel, E. D. Waddington, J. S. Wettlaufer, and M. G. Worster. Possible displacement of the climate signal in ancient ice by premelting and anomalous diffusion. *Nature*, 411:568, 2001.

[63] S. Rols, R. Almairac, L. Henrard, E. Anglaret, and J. L. Sauvojol. Diffraction by finite-size crystalline bundles of single wall nanotubes. *The European Physical Journal B*, 10:263, 1999.

[64] R. Saito, T. Takeya, and T. Kimura. Raman intensity of single-wall carbon nanotubes. *Physical Review B*, 57(7):4145, 1998.

[65] Wei Shi and J. Karl Johnson. Gas adsorption on heterogeneous single-walled carbon nanotube bundles. *Physical Review Letters*, 91(1):1015504, 2003.

[66] R. L. Siddon and M. Schick. Low-density helium monolayers as two-dimensional imperfect gases: An analysis employing the second virial coefficient. *Physical Review A*, 9(2):907, 1974.

[67] R. Spal, C. E. Chen, T. Egami, P. J. Nigrey, and A. J. Heeger. X-ray scattering study of one-dimensional lattice dynamics in $Hg_{3-\delta}AsF_6$. *Physical Review B*, 21(8):3110, 1980.

[68] George Stan and Milton W. Cole. Low coverage adsorption in cylindrical pores. *Surface Science*, 395:280, 1997.

[69] George Stan, Vincent H. Crespi, Milton W. Cole, and Massimo Boninsegni. Interstitial He and Ne in nanotube bundles. *Journal of Low Temperature Physics*, 113(3/4):447, 1998.

[70] Paul F. Sullivan and G. Seidel. Steady-state, ac-temperature calorimetry. *Physical Review*, 173(3):679, 1968.

[71] T. Takaishi and Y. Sensui. Thermal transiration effect of hydrogen, rare gases and methane. *Transcripts of the Farraday Society*, 59:2503, 1963.

[72] S. Talapatra, V. Krugleviciute, and A. D. Migone. Higher coverage gas adsorption on the surface of carbon nanotubes: Evidence for a possible new phase in the second layer. *Physical Review Letters*, 89(24):246106–1, 2002.

[73] S. Talapatra and A. D. Migone. Existence of novel quasi-one-dimensional phases of atoms adsorbed on the exterior surface of close-ended single wall nanotube bundles. *Physical Review Letters*, 87(20):206106–1, 2001.

[74] S. Talapatra, A. Z. Zambano, S. E. Weber, and A. D. Migone. Gases do not adsorb on the interstitial channels of close-ended single-walled carbon nanotube bundles. *Physical Review Letters*, 85(1):138, 2000.

[75] W. Teizer, R. B. Hallock, E. Dujardin, and T. W. Ebbesen. ^{4}He desorption from single wall carbon nanotube bundles: A one-dimensional adsorbate. *Physical Review Letters*, 82(26):5305, 1999.

[76] W. Teizer, R. B. Hallock, E. Dujardin, and T. W. Ebbesen. Erratum: ^{4}He desorption from single wall carbon nanotube bundles: A one-dimensional adsorbate. *Physical Review Letters*, 84(8):1844, 2000.

[77] Andreas Thess, Roland Lee, Pavel Nikolaev, Hongjie Dai, Pierre Petit, Jerome Robert, Chunhui Xu, Young Hee Lee, Seong Gon Kim, Daniel T. Colbert, Gustavo Scuseria, David Tománek, John E. Fischer, and Richard E. Smalley. Crystalline ropes of metallic carbon nanotubes. *Science*, 273:483, 1996.

[78] O. E. Vilches. I am indebted to Oscar Vilches for making this drawing by hand, for use in my general exam., 2002.

[79] Antonio Šiber. Adsorption of He atoms in external grooves of single-wall carbon nanotube bundles. *Physical Review B*, 66:205406, 2002.

[80] Antonio Šiber. Phonons and specific heat of linear dense phases of atoms physisorbed in the grooves of carbon nanotube bundles. *Physical Review B*, 66:235414, 2002.

[81] Qinyu Wang, Sivakumar R. Challa, David S. Sholl, and J. Karl Johnson. Quantum sieving in carbon nanotubes and zeolites. *Physical Review Letters*, 82(5):956, 1999.

[82] John Wettlaufer. private communication, 2001.

[83] T. Wilson, A. Tyburski, M. R. DePies, O. E. Vilches, D. Becquet, and M. Bienfait. Adsorption of H_2 and D_2 on carbon nanotube bundles. *Journal of Low Temperature Physics*, 126(1/2):403, 2002.

[84] Tate Wilson and Oscar E. Vilches. Adsorption of ^{4}He on carbon nanotube bundles. *Physica B*, 2003.

[85] Zheng Yan. Piecewise cubic curve fitting algorithm. *Mathematics of Computation*, 49:203, 1987.

[86] H. Yano, S. Yoshizaki, S. Inagaki, Y. Fukushima, and N. Wada. Observation of superfluid ^{4}He adsorbed in one-dimensional mesopores. *Journal of Low Temperature Physics*, 110(1/2):573, 1998.

[87] Jin Yu, Rajiv K. Kalia, and Priya Vashishta. Phonons in graphitic tubules: a tight-binding molecular dynamics study. *Journal of Chemical Physics*, 103(15):6697, 1995.

Appendix A

AC CALORIMETRY

In this Appendix I'll just review Sullivan and Seidel's AC calorimetry theory, and direct the reader there [70] for greater detail. Then I'll describe the choices that have to go into the cell design, to meet the requirements of a good AC calorimeter.

A.1 Theory

Consider a thin slab, with cross sectional area A, thickness L, thermal conductivity κ, specific heat c, and density ρ. We will also need the thermal diffusivity $n = \kappa/\rho c$, the characteristic length $l_0 = (2n/\omega)^{1/2}$, and its reciprocal $k = 1/l_0$. The slab is connected on one face to a temperature bath through a thermal conductance K_b, and has a heater on the other side. This heater supplies a sinusoidal heat flux $\dot{q}(t) = (\dot{Q}_0/2A)e^{i\omega t}$. The temperature on the opposite face is found to be

$$T_{ac}(t) = \dot{q}(t)\frac{A/K_b}{\cosh\theta + (\kappa K_b \theta/AL)\sinh\theta}\ , \tag{A.1}$$

where $\theta = kL(1+i)$. After some approximations and expanding the cosh and sinh, this is approximately

$$T_{ac}(t) = \frac{-i\dot{Q}_0 e^{i\omega t}}{2A\omega\rho c L}\left[1 + \left(\frac{K_b}{\omega\rho c L A}\right)^2 + \omega^2\left(\frac{L^2}{(90)^{1/2}n}\right)^2 + \frac{2LK_b}{3A\kappa}\right]^{-1/2} . \tag{A.2}$$

Written in this form the equation looks complicated, but it sometimes nicer for understanding the effect of certain properties of the cell design. For example, notice that the second term in the square brackets goes as the conductance to the bath squared. This leads to choices of the cell stem which minimize the conductance. On the other hand, the third term depends inversely on the sample diffusivity, which prompts us to try to maximize this quantity.

The equation is usually written in a much simpler form in the following way. First we note that $AL\rho c$ is just C, the total heat capacity, then we note that we are only interested in the magnitude of T_{ac} (the time dependence is trivial), and finally we lump a few constants together and rename them, to arrive at

$$|T_{ac}| = \frac{\dot{Q}_0}{2\omega C}\left[1 + \frac{1}{\omega^2\tau_1^2} + \omega^2\tau_2^2 + \frac{2K_b}{3K_s}\right]^{-1/2} . \tag{A.3}$$

This is the canonical equation of AC calorimetry. It is, however, normally only used in designing the cell. If we have done a good job of setting the time constants and conductivities, we assume that we can ignore the terms in the square brackets, and reduce the experimental data according to

$$T_{ac} = \frac{\dot{Q}}{2\omega C} . \tag{A.4}$$

A.2 Practical Considerations

The mechanical design of the cell and materials used are described in Section 4.5. The choices of materials and geometry are meant to satisfy the following requirements, necessary for effective AC calorimetry:

1. The cell should reach internal thermal equilibrium quickly, so that the temperature of the thermometer is really the temperature of all of the sample.

2. The cell must also reach thermal equilibrium with a temperature bath, but this must be a considerably slower process. This is a point of compromise in the cell design - the external time constant can be *too* long, leading to large DC offsets of the cell temperature during data acquisition.

3. Finally, the overall heat capacity of the cell should not be enormously larger than that of the system to be measured, as it must eventually be subtracted, and this is more accurate if the difference is large.

Requirements 1 and 3 compete subtly. We make our cells from copper because its high thermal conductivity aids in achieving low internal time constants. On the other hand copper, like most metals, has a large and rapidly increasing heat capacity at low temperature. This prompts us to use as little of the material as possible. However, we need mechanical strength of the copper container walls for two reasons. It must withstand any pressures generated in the cell during dosing, annealing, or from desorption on warming up after a run. Also the thermal contact to the sample is provided only by the mechanical contact of the copper pressing against the nanotubes. The copper must be stiff to maximize this pressure.

Requirement 2 likewise presents a troublesome compromise. The ideal thermal conductivity between the cell and bath depends on the desired input power, which is chosen based on the sample heat capacity, to achieve a minimum AC temperature oscillation. Since the sample heat capacity increases with temperature, the desired power also goes up with temperature. If the thermal contact to the bath were constant, this would mean that the DC offset would increase with temperature as well, which may be undesirable if it gets too large. This would be helped if the thermal conductivity to the bath decreased with increasing temperature. Most materials' thermal conductivity increases with temperature, so it is usually only possible to choose this to be ideal for a given calorimeter at one temperature, and hope it doesn't get too bad for nearby temperatures.

Appendix B

RELAXATION TIME CONSTANT CALORIMETRY IN THE AC CALORIMETER

We have made DC, relaxation time constant heat capacity measurements of our AC calorimetry cell in order to improve our understanding of the absolute magnitude of the heat capacity as measured by the AC technique. The measurement technique is described here, as well as the comparison of the AC and DC results for the bare calorimeter and with a helium coverage of ~ 0.83 monolayers.

The basic principle is that the cell has heat capacity C, and the link from the cell to the temperature bath has thermal resistance R. Then if there is initially a temperature T on the cell, which is higher than the temperature of the bath T_0, the temperature of the cell will decrease exponentially toward T_0 with a time constant RC. Or mathematically,

$$T(t) = T_0 \, e^{-t/RC}, \tag{B.1}$$

analogous to an electric RC circuit.

B.1 The AC System

We use essentially the same system as the AC calorimeter to measure the DC values. The parts of the AC system used are shown in Figure B.1. As in the AC system, the current source biases the thermometer and a standard resistor at room temperature, DVM1 reads the voltage on the standard resistor, to verify the current, and DVM2 reads the voltage on the thermometer, which can then be converted to $R(T)$ from which the temperature is derived. LI1 drives the cell heater and a standard resistor at room temperature, and provides the frequency reference for the other two lock-ins. LI2 and LI3 measure the excitation

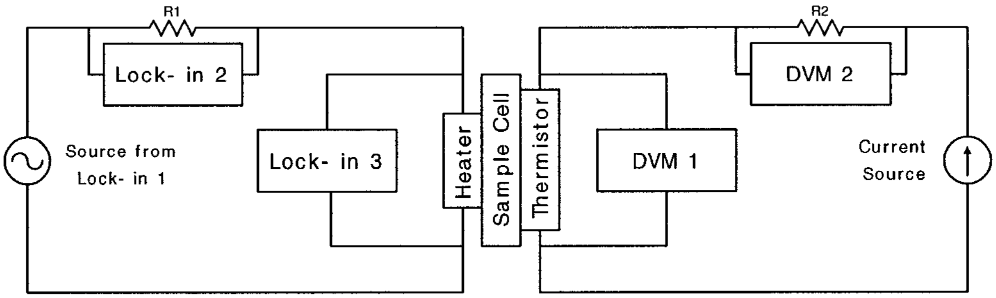

Figure B.1: Schematic of the DC System. The parts of the AC system which are not used are not shown.

at $1f$ on the standard resistor and the cell heater respectively, in order to establish the power to the cell heater. All of these instruments are queried by the computer every ten seconds and the values are stored, processed and averaged in various ways. Separate from the measurement apparatus is a potentiometric conductance bridge (PCB) and automatic temperature controller (ATC) which maintain a constant reference temperature of the heat bath (inner can) to which the cell is thermally linked via the thin walled stainless steel fill-line tube.

Because the signal applied to the heater is a sinusoidal voltage $V = V_0 \sin \omega t$, the power goes as $\sin^2 \omega t$:

$$P(t) = \frac{V_0^2}{R} \sin^2 \omega t = V_0 I_0 \left(\frac{1}{2} + \frac{1}{2} \cos 2\omega t \right). \tag{B.2}$$

Lock-ins 2 and 3 measure the RMS values of V_0 and I_0 ($I_0 = V_R / R$, where R is the standard resistor in series with the heater) and the computer calculates the RMS AC power as:

$$\langle P \rangle = \langle V_0 \rangle \langle I_0 \rangle \tag{B.3}$$

This is the value used by the AC calorimetry program to calculate the heat capacity. Because the DC calorimetry program was pieced together from the AC one, it is also the value for the power given by the DC calorimetry program, and in a happy coincidence, also happens to be equal to the average DC power P_{DC}. We need this power to calculate the thermal resistance of the link between the cell and the temperature bath.

B.2 Modifying the AC Program

The AC calorimetry program uses the values that come every 10 seconds only to calculate averages and deviations, and it waits for a steady state situation to actually record the data. To make DC measurements the AC system was modified to use all of the 10 second readings, and no averages, in order to find the time constant of the system as it relaxes to the base temperature. We fix the base temperature, apply power to the cell and allow everything to reach a steady state. We then start the computer program and allow it to collect a few points. This program now writes all of the values that it collects every 10 seconds to a data file. With the high temperature T_{high} established, we disconnect the cell heater and allow the cell temperature to drift down to the base temperature, logging the temperature vs. time until it stops changing. When the temperature no longer changes from point to point more than the resolution we have, we stop the program and record the final temperature as T_{low}. $\triangle T$ is the difference between the starting temperature of the cell (T_{high}) and the final temperature (T_{low}). From $\triangle T$ and the applied power we can get the heat conductance to the bath (κ) as

$$\kappa = \frac{P_{DC}}{\triangle T}. \tag{B.4}$$

In the approximation that the cell is a capacitor and the fill-line is a resistor and they are in series, the time dependence of the drop in the cell temperature is

$$T_{cell}(t) = T_{low} + \triangle T e^{-t/\tau}, \tag{B.5}$$

where $\tau = C/\kappa$ and C is the heat capacity of the cell. Finally, we extract τ from the slope (m) of a semi-log plot of $T_{cell}(t)$ and use the known value of κ to get C:

$$C = \kappa\tau = \frac{\sqrt{2}\langle P\rangle}{\triangle T m}. \tag{B.6}$$

The measured parameters and calculated C are shown in Table B.1 and compared to the AC values taken at 1 Hz and 0.1 Hz in Figure B.2.

Table B.1: The DC background data, after analysis as described in the text.

T_{high} (K)	T_{low} (K)	$\langle P \rangle$ (μW)	Slope (s^{-1})	C (mJ/K)
1.2218	1.1899	0.1506	0.01926	0.3466
1.2759	1.241	0.1506	0.01889	0.3230
1.3732	1.346	0.1506	0.01946	0.4024
1.4018	1.347	0.3389	0.02139	0.4089
1.7267	1.594	0.9412	0.02145	0.4676
2.0488	1.822	2.1127	0.02093	0.6294
2.4551	2.142	3.7563	0.02090	0.8118
2.6882	2.407	3.7578	0.01994	0.9478
3.1259	2.912	3.7571	0.01885	1.3178
3.5256	3.357	3.7581	0.01824	1.7282
3.9059	3.762	3.7569	0.01852	1.9936
4.3966	4.132	8.4551	0.01628	2.7758
4.7129	4.480	8.4551	0.01523	3.3710
5.1006	4.807	12.1713	0.01441	4.0685

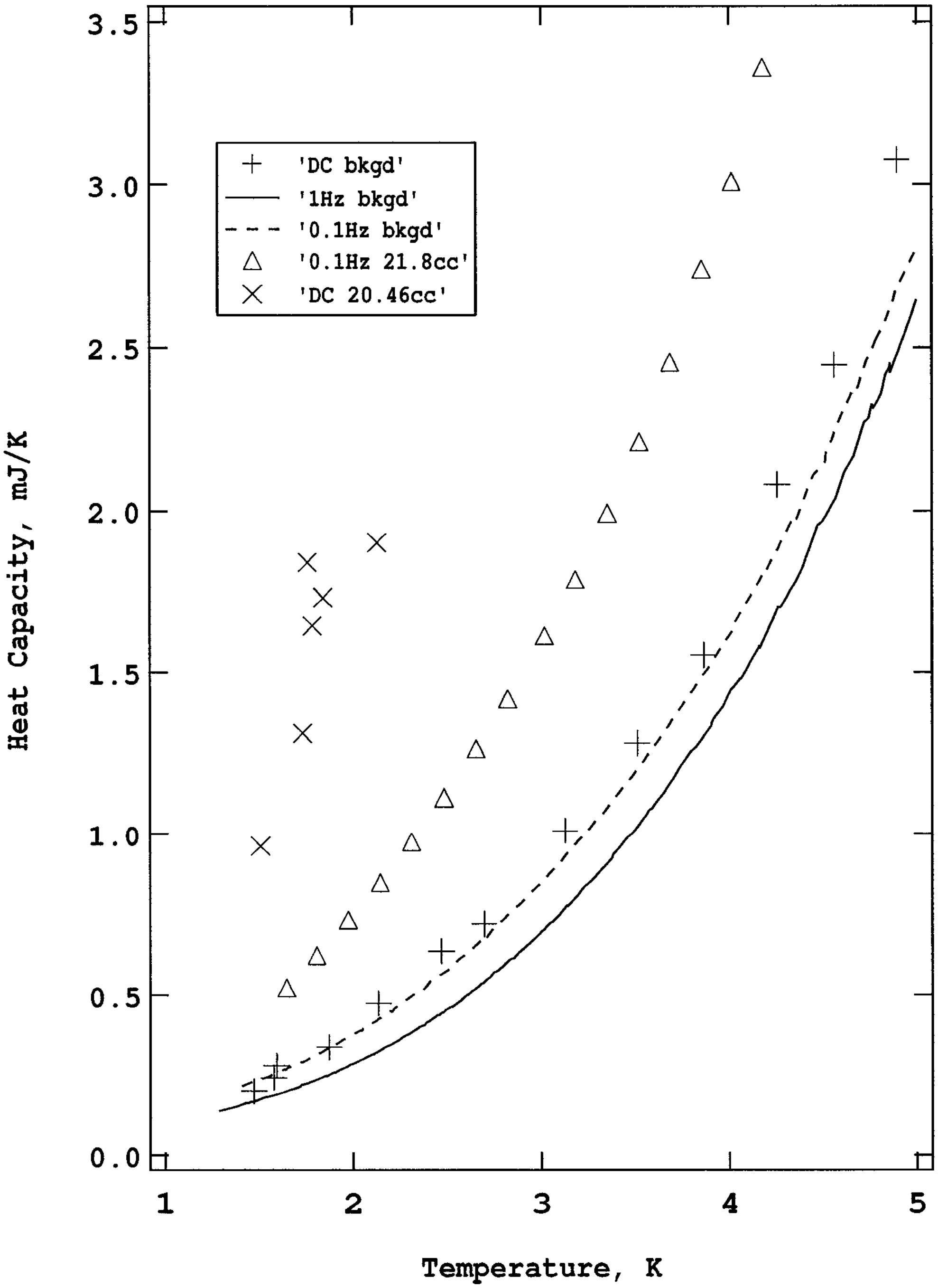

Figure B.2: Comparing the DC heat capacity to two AC frequencies. Also included is the DC and 0.1 Hz measurements for a high coverage film.

B.3 Problems

Several simplifying assumptions were made in analyzing this measurement. The result becomes more difficult to interpret if the following are taken into consideration.

B.3.1 Steady State

The relaxation data is started when the 'steady state' temperature has been reached, but the power to the cell heater is oscillating, as is the temperature, around the equilibrium value. It is known from the AC experiments that the AC deviations in temperature from the DC value are never more than 1 part in 1000 of the temperature difference $\triangle T$, and are usually less than half of that. This introduces an error of less than 0.05% in our estimate of κ. Furthermore, in our measurement of the time constant, if we disconnect the heater exactly when the temperature of the cell is the average value there is no error at all, but if we do make an error it only affects the constants in temperature vs time, not the slope. Therefore we conclude that using AC heating in place of DC introduces an error in C of at most 0.05%, or much less than the intrinsic noise in the measurement.

B.3.2 Multiple Internal Time Constants

The simplifying assumption behind the canonical equation of AC calorimetry is that the temperature response of the system can be described in terms of two time constants, one for the internal relaxation to equilibrium within the cell, and one for the external relaxation of the cell to the reference temperature of the bath. We expect that one of the complications of our nanotube cell is that it has at least two internal time constants: τ_1 describes the relaxation of the copper, solder, epoxy, heater, and thermometer, and τ_2 involves the link between those and the nanotube plus helium sample that is inside. τ_1 is small by design, in accordance with the principle for designing an AC cell, that the internal relaxation must be orders of magnitude faster than the link to the bath, with the inverse of the desired operating frequency lying somewhere between. τ_2, on the other hand, is too large to be conveniently included in τ_1, and may even be of the order of the external time constant τ_{ext}. This is precisely the flaw in the cell design that we hope to understand by using DC calorimetry to determine the absolute magnitude of C, but if τ_2 is of the order of τ_{ext}, the DC analysis is complicated. Different parts of the cell can be cooling at different rates.

Appendix C

COMPUTER PROGRAM FOR AC CALORIMETRY DATA ACQUISITION

In this Appendix I am including the computer code that was used to aquire and automate the data. This code is written in C, but it is not stand-alone and cannot be run in this form. It makes use of National Instruments' Lab Windows CVI to write header files, provide libraries, and create the graphical user interface. However, anyone with an understanding of C can see here how the code functions: how the averages were made, how the criteria for various operations were implemented, etc. In part I also include it here only to preserve it. The experiment grows and changes with each new student who works on it, and in a year or two the code running on the same experiment will barely resemble this one.

```
#include <stdlib.h>
#include <stdio.h>
#include <analysis.h>
#include <utility.h>
#include <dataacq.h>
#include <userint.h>
#include <math.h>
#include <ansi_c.h>
#include <gpib.h>
#include "AC_CAL.h"
#definePI  3.141592654
#define LI1 7   /* SRS 830: Provides the heater signal and measures T_ac   */
#define LI2 8      /* SRS 830: Measures heater current using series resistor  */
#define LI3 6      /* SRS 830: Measures heater voltage                       */
#define DMM1    03     /* Fluke 8840A: standard resistor voltage=>current         */
#define DMM2    01   /* Fluke 8840A: cell resistor voltage                        */

int Init_Set (void);
int ProcessLoop (int panel, int control, int event, void *callbackData, int eventData1, int
eventData2);
void getsamples (double*, double*, double*, double*, double*, short int*);
void writefile (void);
void main (void);
double Temp (double);
double dTemp (double, double);
```

```
FILE *raw001, *calc001;
unsigned short GPIB_LIST[6] ;
int handle1, handle2, handle3, handle4, handle5;
int confirm, flag_save, auto_index = 1;
int m, n;
static short int M, M_a = 12, M_b = 30, M_c = 60,  N_store = 10;
double R_ths, scale, PCB;
double freq, V_appl, I_heater, V_heater, V_offset, t_aquire, t, dt;
double I_avg, Vac_avg, Vdc_avg, phase_avg, Tac_avg, Tdc_avg, Q_avg, C_avg;
double I_15, Vac_15, Vdc_15, Tac_15, Tdc_15, phase_15, Q_15;
double I_30, Vac_30, Vdc_30, Tac_30, Tdc_30, phase_30, Q_30;
double dVdc_30, dVac_30, dphase_30, dQ_30, dI_30;
double C_B, C_C, tdc, dvac, di, dR_ac, dvdc, dQ, dvac_30;
double dI_avg, dVac_avg, dVdc_avg, dphase_avg, dTac_avg, dTdc_avg, dQ_avg;
double I_plot[4] , Tac_plot[4] , Tdc_plot[4] , Q_plot[4] ;
double C[200] , T[200] , C_15[200] , T_15[200] , C_30[200] , T_30[200] ;
static double pcb_incr, v_incr, err_max;
static double I[120] , Vac[120] , phase[120] , Vdc[120] , Q[120] ;
short int count, count_15, flag_go, flag_more, M_max, N_aquire;
static char FREQ[15] , SLVL[12] , IHEAT[15] , VHEAT[15] , VAPP[20] ;

void main (void)
{
R_ths = 80000; scale = .125; flag_save = 0;
InstallMainCallback (ProcessLoop, 0, 1) ;
SetIdleEventRate (250) ;
handle1 = LoadPanel (0, "AC_CAL.uir", SET_PANEL) ;
handle2 = LoadPanel (0, "AC_CAL.uir", MONITOR) ;
handle4 = LoadPanel (0, "AC_CAL.uir", RESULT) ;
DisplayPanel (handle4) ;
DisplayPanel (handle2) ;
DisplayPanel (handle1) ;
Init_Set() ;
SetActivePanel (handle1) ;
RunUserInterface () ;
}

int Init_Set (void)
{
SendIFC (0) ;
GPIB_LIST[0] = LI1;
GPIB_LIST[1] = DMM1;
GPIB_LIST[2] = DMM2;
GPIB_LIST[3] = LI2;
GPIB_LIST[4] = LI3;
GPIB_LIST[5] = NOADDR;
DevClearList (0, GPIB_LIST) ;
EnableRemote (0, GPIB_LIST) ;

Send (0, LI1, "OVRM1", 5L, 1) ;
Send (0, LI1, "FREQ?", 5L, 1) ; Receive (0, LI1, FREQ, 12L, 256) ;
```

```
freq = strtod (FREQ, NULL); SetCtrlVal (handle1, SET_PANEL_FREQ, freq);
Send (0, LI1, "SLVL?", 5L, 1); Receive (0, LI1, SLVL, 12L, 256);
V_appl = strtod (SLVL, NULL);SetCtrlVal (handle1, SET_PANEL_V_APPLIED, V_appl);
Send (0, LI2, "OUTP?3", 6L, 1);Receive (0, LI2, IHEAT, 15L, 1);
*(IHEAT + 14) = '\0';I_heater = atof(IHEAT);
Send (0, LI3, "OUTP?3", 6L, 1);Receive (0, LI3, VHEAT, 15L, 1);
*(VHEAT + 14) = '\0';V_heater = atof(VHEAT);

return (0);
}

int ProcessLoop (int panel, int control, int event, void *callbackData, int eventData1, int
eventData2)
{
if (event == EVENT_IDLE && flag_go == 1)
{
getsamples (Vac, phase, Vdc, I, Q, &M);

if (M && flag_more)
{
Tac_plot[0] = dTemp (Vdc[M-1] / I[M-1], Vac[M-1] / I[M-1]);
Tdc_plot[0] = Temp (Vdc[M-1] / I[M-1]);
if (M >= M_a)
{
StdDev (I + M - M_a, M_a, &I_avg, &dI_avg);
StdDev (Vdc + M - M_a, M_a, &Vdc_avg, &dVdc_avg);
StdDev (Vac + M - M_a, M_a, &Vac_avg, &dVac_avg);
StdDev (phase + M - M_a, M_a, &phase_avg, &dphase_avg);
StdDev (Q + M - M_a, M_a, &Q_avg, &dQ_avg);
}
else
{
StdDev (I, M, &I_avg, &dI_avg);
StdDev (Vdc, M, &Vdc_avg, &dVdc_avg);
StdDev (Vac, M, &Vac_avg, &dVac_avg);
StdDev (phase, M, &phase_avg, &dphase_avg);
StdDev (Q, M, &Q_avg, &dQ_avg);
}

if (M >= M_b)
{
Mean (I + M - M_b, M_b, &I_15);
Mean (Vdc + M - M_b, M_b, &Vdc_15);
Mean (Vac + M - M_b, M_b, &Vac_15);
Mean (phase + M - M_b, M_b, &phase_15);
Mean (Q + M - M_b, M_b, &Q_15);
}
else
{
    Mean (I, M, &I_15);
    Mean (Vdc, M, &Vdc_15);
Mean (Vac, M, &Vac_15);
Mean (phase, M, &phase_15);
Mean (Q, M, &Q_15);
}
if (M >= M_c)
{
```

```
StdDev (I + M - M_c, M_c, &I_30, &dI_30);
StdDev (Vdc + M - M_c, M_c, &Vdc_30, &dVdc_30);
StdDev (Vac + M - M_c, M_c, &Vac_30, &dVac_30);
StdDev (phase + M - M_c, M_c, &phase_30, &dphase_30);
StdDev (Q + M - M_c, M_c, &Q_30, &dQ_30);
}
else
{
StdDev (I, M, &I_30, &dI_30);
StdDev (Vdc, M, &Vdc_30, &dVdc_30);
StdDev (Vac, M, &Vac_30, &dVac_30);
StdDev (phase, M, &phase_30, &dphase_30);
StdDev (Q, M, &Q_30, &dQ_30);
}

dvac = 100 * dVac_avg / Vac_avg;
dvdc = 100 * dVdc_avg / Vdc_avg;
di = 100 * dI_avg / I_avg;
dQ = 100 * dQ_avg / Q_avg;
dvac_30 = 100 * dVac_30 / Vac_30;

Tac_avg = dTemp (Vdc_avg / I_avg, Vac_avg / I_avg);
Tac_15  = dTemp (Vdc_15 / I_avg, Vac_15 / I_avg);
Tac_30  = dTemp (Vdc_30 / I_avg, Vac_30 / I_avg);

Tdc_avg = Temp (Vdc_avg / I_avg);
Tdc_15  = Temp (Vdc_15 / I_avg);
Tdc_30  = Temp (Vdc_30 / I_avg);

Q_plot[0] = Q[M-1];
Q_plot[1] = Q_avg;
Q_plot[2] = Q_15;
Q_plot[3] = Q_30;

I_plot[0] = (1.0E+6) * I[M-1];
I_plot[1] = (1.0E+6) * I_avg;
I_plot[2] = (1.0E+6) * I_15;
I_plot[3] = (1.0E+6) * I_30;

 Tdc_plot[1] = Tdc_avg;
 Tdc_plot[2] = Tdc_15;
Tdc_plot[3] = Tdc_30;

Tac_plot[1] = Tac_avg;
Tac_plot[2] = Tac_15;
Tac_plot[3] = Tac_30;

C_avg = 1E+3 * Q_avg / (4 * sqrt(2) * PI * freq * Tac_avg);
C_B   = 1E+3 * Q_15  / (4 * sqrt(2) * PI * freq * Tac_15);
C_C   = 1E+3 * Q_30  / (4 * sqrt(2) * PI * freq * Tac_30);

PlotStripChart (handle2, MONITOR_TDC_CHART, Tdc_plot, 4, 0, 0, VAL_DOUBLE);
PlotStripChart (handle2, MONITOR_TAC_CHART, Tac_plot, 4, 0, 0, VAL_DOUBLE);
PlotStripChart (handle2, MONITOR_I_CHART, I_plot, 4, 0, 0, VAL_DOUBLE);
PlotStripChart (handle2, MONITOR_Q_CHART, Q_plot, 4, 0, 0, VAL_DOUBLE);

SetCtrlVal (handle2, MONITOR_I_OUT, (1.0E+6) * I_avg);
SetCtrlVal (handle2, MONITOR_TDC_OUT, Tdc_avg);
SetCtrlVal (handle2, MONITOR_TAC_OUT, 1000 * Tac_avg);
SetCtrlVal (handle2, MONITOR_VAC_OUT, Vac_avg);
SetCtrlVal (handle2, MONITOR_VAC_ERR, dvac);
SetCtrlVal (handle2, MONITOR_VAC_ERR_30, dvac_30);
```

```
SetCtrlVal (handle2, MONITOR_VDC_OUT, Vdc_avg);
SetCtrlVal (handle2, MONITOR_VDC_ERR, dvdc);
SetCtrlVal (handle2, MONITOR_Q_OUT, Q_avg);
SetCtrlVal (handle2, MONITOR_Q_ERR, dQ);
SetCtrlVal (handle2, MONITOR_I_ERR, di);
SetCtrlVal (handle2, MONITOR_C_OUT, C_avg);
SetCtrlVal (handle2, MONITOR_C_B, C_B);
SetCtrlVal (handle2, MONITOR_C_C, C_C);
auto_index ++;
}
if (auto_index > 100)
{
GetCtrlVal (handle1, SET_PANEL_ERR_MAX, &err_max);
if (dvac_30 < err_max)
{
writefile ();
GetCtrlVal (handle1, SET_PANEL_V_APPLIED, &V_appl);
GetCtrlVal (handle1, SET_PANEL_V_INCR, &v_incr);
GetCtrlVal (handle1, SET_PANEL_PCB_INCR, &pcb_incr);
PCB = PCB + pcb_incr;
V_appl= V_appl + v_incr;
sprintf (VAPP, ”SLVL%E”, V_appl);
SetCtrlVal (handle1, SET_PANEL_V_APPLIED, V_appl);
AO_VWrite (1, 0, PCB);
Send (0, LI1, VAPP, 20L, 1);

auto_index = 1;
}
}
}
return (0);
}

void getsamples (double Vac[120], double phase[120], double Vdc[120],
  double I[100], double Q[120], short int *pM)
{
static double Vac_temp[100], phase_temp[100], Vdc_temp[100], I_temp[100];
static double Q_temp[100];
double Vac_hld, Vdc_hld, phase_hld, I_hld, Q_hld;
double Vdc_offset, Vst_offset;
short int n, M = *pM;

char VDC[13], VAC[15], PHASE[15], VCST[13], VHEAT[15], IHEAT[15];
Send (0, LI1, ”OUTP?3”, 6L, 1);Receive (0, LI1, VAC, 15L, 1);
*(VAC+14) = ’\0’;
Send (0, DMM1, ”?”, 1L, 2);Receive (0, DMM1, VCST, 13L, 2);
*(VCST+12) = ’\0’;
Send (0, DMM2, ”?”, 1L, 2);Receive (0, DMM2, VDC, 13L, 2);
*(VDC+12) = ’\0’;
Send (0, LI1, ”OUTP?4”, 6L, 1);Receive (0, LI1, PHASE, 15L, 1);
*(PHASE+14) = ’\0’;
Send (0, LI2, ”OUTP?3”, 6L, 1);Receive (0, LI2, IHEAT, 15L, 1);
*(IHEAT + 14) = ’\0’;
```

```
Send (0, LI3, "OUTP?3", 6L, 1);Receive (0, LI3, VHEAT, 15L, 1);
*(VHEAT + 14) = '\0';

Vac_temp[N_aquire] = atof (VAC) ;
phase_temp[N_aquire] = atof (PHASE);
Vdc_temp[N_aquire] = atof (VDC);
I_temp[N_aquire] = atof (VCST) / R_ths;
Q_temp[N_aquire]= (atof (IHEAT)) * (atof (VHEAT)) / 392;/*620 ohm resistor
replaced with a 392 ohm*/

N_aquire++;
t = Timer();
dt = t - t_aquire;
if (dt >= 10)
{
 Mean (Vac_temp, N_aquire, &Vac_hld);
 Mean (phase_temp, N_aquire, &phase_hld);
 Mean (Vdc_temp, N_aquire, &Vdc_hld);
Mean (I_temp, N_aquire, &I_hld);
Mean (Q_temp, N_aquire, &Q_hld);
 N_aquire = 0;
 if (M == 120)
 {
  for(n = 0; n < 119; n++)
  {
  Vac[n] = Vac[n+1];
 phase[n] = phase[n+1];
 Vdc[n]= Vdc[n+1];
 I[n]= I[n+1];
 Q[n]  = Q[n+1];
 }

 M = 119;
 *pM = 119;
 }
 Vac[M]   = Vac_hld;
 phase[M] = phase_hld;
 Vdc[M]   = Vdc_hld;
I[M]      = I_hld;
Q[M]  = Q_hld;
 (*pM)++;
 t_aquire = Timer();

 flag_more = 1;
}
else
{
flag_more = 0;
}
}

double Temp (double R)
{
static double A[3], log_R, log_T, T;
int n = 1;
A[0] =  5.769811;
A[1] = -2.183763;
```

```
A[2] =  0.20188;
log_R = log10(R);
log_T = A[0];
for (n=1; n<3; n++)
{
log_T = log_T + A[n] * pow(log_R, n);
}
T = pow(10, log_T);
return(T);
}

double dTemp (double R, double dR)
{
static double A[3], dT, T;
int n = 0;
A[0] =  5.769811;
A[1] = -2.183763;
A[2] =  0.20188;
T = Temp(R);
/*For a better understanding of the following algorithm
  see the notebook for March '02 */
dT =  -dR * T * ((A[1] / R) + (2 * A[2] * log(R)) / (R * log(10)));
return (dT);
}

int  GO (int panel, int control, int event, void *callbackData, int eventData1,
int eventData2)
{
int size, size_len;
char SIZE[7];
char *date, *dte = ”XXXX”, *fle1;
if (event == EVENT_COMMIT)
{
flag_go = 1;
DisplayPanel (handle2);
GetCtrlVal (handle1, SET_PANEL_PCB, &PCB);
AO_VWrite (1, 0, PCB);
t_aquire = Timer();
N_aquire = 0;
SetCtrlAttribute (handle1, SET_PANEL_GO, ATTR_DIMMED, 1);
date = DateStr();
strncpy (dte, date, 2);strncpy(dte+2, date+3, 2);
fle1 = ”ac_calXXXX.dat";
strncpy (fle1+6, dte, 4);
raw001 = fopen (fle1, ”a”);
fprintf (raw001, ”%s \n”, date);
fprintf (raw001, ”Vdc (V) \t Vac (V) \t I (A)     \t P (W) \t phase (deg) \t freq (Hz) \t
time \n”);
fclose (raw001);
}
return (0);
```

```
}

int FREQ_SETTING (int panel, int control, int event, void *callbackData,
int eventData1, int eventData2)
{
char FREQ[20];
if (event == EVENT_COMMIT)
{
GetCtrlVal (handle1, SET_PANEL_FREQ, &freq);
sprintf (FREQ, "FREQ%E", freq);
Send (0, LI1, FREQ, 20L, 1);
Send (0, LI1, "FREQ?", 5L, 1);Receive (0, LI1, FREQ, 20L, 1);
freq = atof(FREQ);
SetCtrlVal (handle1, SET_PANEL_FREQ, freq);
}
return (0);
}

int IDLE_RATE (int panel, int control, int event, void *callbackData, int eventData1,
int eventData2)
{
int rate;
if (event == EVENT_COMMIT)
{
GetCtrlVal (handle1, SET_PANEL_IDLE_RATE, &rate);
SetIdleEventRate(rate);
}
return (0);
}

void writefile (void)
{
char *time;
char *date, *dte = "XXXX", *file1;
time = TimeStr();
date = DateStr();
strncpy (dte, date, 2);
strncpy (dte+2, date+3, 2);
file1 = "ac_calXXXX.dat";
strncpy (file1+6, dte, 4);
raw001 = fopen (file1, "a");
fprintf (raw001, "%E  \t %E \t %E \t %E \t %f \t %Lf \t %s \n",
Vdc_15, Vac_15,  I_15, Q_15, phase_15, freq, time);
fclose (raw001);
}

int STORE15 (int panel, int control, int event, void *callbackData, int eventData1,
int eventData2)
{
if (event == EVENT_COMMIT)
{
writefile ();
}
return (0);
```

```
}

int  PLOT15 (int panel, int control, int event, void *callbackData, int eventData1,
int eventData2)
{
if (event == EVENT_COMMIT)
{
GetCtrlVal (handle4, RESULT_COUNT_B, &count_15);
C_15[count_15] = C_avg * Tac_avg / Tac_15;
T_15[count_15] = Tdc_15;
count_15++;
SetCtrlVal (handle4, RESULT_COUNT_B, count_15);
PlotXY (handle4, RESULT_HEAT, T_15, C_15, count_15, VAL_DOUBLE,
VAL_DOUBLE,
VAL_SCATTER, VAL_SOLID_DIAMOND, VAL_SOLID, 1, VAL_DK_BLUE);
}
return (0);
}

int  PLOT30 (int panel, int control, int event, void *callbackData, int eventData1,
int eventData2)
{
static short int count_30=0;
if (event == EVENT_COMMIT)
{
GetCtrlVal (handle4, RESULT_COUNT_C, &count_30);
C_30[count_30] = C_avg * Tac_avg / Tac_30;
T_30[count_30] = Tdc_30;
count_30++;
SetCtrlVal (handle4, RESULT_COUNT_C, count_30);
SetCtrlVal (handle4, RESULT_C_TOTAL, C_30[ count_30 - 1 ]);
SetCtrlVal (handle4, RESULT_TDC_OUT, Tdc_avg);
PlotXY (handle4, RESULT_HEAT, T_30, C_30, count_30, VAL_DOUBLE,
VAL_DOUBLE,
VAL_SCATTER, VAL_SOLID_DIAMOND, VAL_SOLID, 1, VAL_DK_GREEN);
}
return (0);
}

int  TAC_CHART (int panel, int control, int event, void *callbackData, int eventData1,
int eventData2)
{
 double Ymin, Ymax, scale;
if (event == EVENT_LEFT_CLICK)
{
GetCtrlVal (handle2, MONITOR_TAC_SCALE, &scale);
Ymin = (1 - (scale / 20)) * Tac_plot[0];
Ymax = (1 + (scale / 20)) * Tac_plot[0];
SetAxisRange (handle2, MONITOR_TAC_CHART, VAL_NO_CHANGE , 0.0, 1.0,
   VAL_MANUAL, Ymin, Ymax);
}
return (0);
}
```

```
int  TDC_CHART (int panel, int control, int event, void *callbackData, int eventData1,
int eventData2)
{
double Ymin, Ymax, scale;
if (event == EVENT_LEFT_CLICK)
{
GetCtrlVal (handle2, MONITOR_TDC_SCALE, &scale);
Ymin = (1 - (scale / 20)) * Tdc_plot[0];
Ymax = (1 + (scale / 20)) * Tdc_plot[0];
SetAxisRange (handle2, MONITOR_TDC_CHART, VAL_NO_CHANGE , 0.0, 1.0,
   VAL_MANUAL, Ymin, Ymax);
}
return (0);
}

int  Q_CHART (int panel, int control, int event,
void *callbackData, int eventData1, int eventData2)
{
double Ymin, Ymax, scale;
if (event == EVENT_LEFT_CLICK)
{
GetCtrlVal (handle2, MONITOR_Q_SCALE, &scale);
Ymin = (1 - (scale / 20)) * Q_plot[0];
Ymax = (1 + (scale / 20)) * Q_plot[0];
SetAxisRange (handle2, MONITOR_Q_CHART, VAL_NO_CHANGE , 0.0, 1.0,
   VAL_MANUAL, Ymin, Ymax);
}
return 0;
}

int  I_CHART (int panel, int control, int event, void *callbackData, int eventData1,
int eventData2)
{
double Ymin, Ymax, scale;
if (event == EVENT_LEFT_CLICK)
{
GetCtrlVal (handle2, MONITOR_I_SCALE, &scale);
Ymin = (1 - (scale / 20)) * I_plot[0];
Ymax = (1 + (scale / 20)) * I_plot[0];
SetAxisRange (handle2, MONITOR_I_CHART, VAL_NO_CHANGE , 0.0, 1.0,
   VAL_MANUAL, Ymin, Ymax);
}
return (0);
}

int  SCALE (int panel, int control, int event, void *callbackData, int eventData1,
int eventData2)
{
double T_max, T_min, C_max, C_min;
if (event == EVENT_COMMIT)
{
GetCtrlVal (handle4, RESULT_T_HI, &T_max);
GetCtrlVal (handle4, RESULT_T_LO, &T_min);
GetCtrlVal (handle4, RESULT_C_HI, &C_max);
GetCtrlVal (handle4, RESULT_C_LO, &C_min);
SetAxisRange (handle4, RESULT_HEAT, VAL_MANUAL, T_min, T_max,
```

```
        VAL_MANUAL, C_min, C_max);
}
return (0);
}

int  SET (int panel, int control, int event, void *callbackData, int eventData1,
int eventData2)
{
if (event == EVENT_COMMIT)
{
SetActivePanel (handle1);
}
return (0);
}

int  C_GRAPH (int panel, int control, int event, void *callbackData, int eventData1,
int eventData2)
{
if (event == EVENT_COMMIT)
{
SetActivePanel (handle4);
}
return (0);
}

int  BACK (int panel, int control, int event, void *callbackData, int eventData1,
int eventData2)
{
if (event == EVENT_COMMIT)
{
SetActivePanel (handle2);
}
return (0);
}

int  HEAT (int panel, int control, int event, void *callbackData, int eventData1,
 int eventData2)
{
double Cmin, Cmax, Tmin, Tmax,Cmin_15, Cmax_15, Tmin_15, Tmax_15;
int Ncmax, Ncmin,Ntmin,Ntmax;
short int count_a;
if (event == EVENT_LEFT_CLICK)
{
GetCtrlVal (handle4, RESULT_COUNT_B, &count_a);
MaxMin1D (C, count_a, &Cmax_15, &Ncmax, &Cmin_15, &Ncmin);
MaxMin1D (T, count_a, &Tmax_15, &Ntmax, &Tmin_15, &Ntmin);
Cmin = 0.99 * Cmin_15;Cmax = 1.01 * Cmax_15;
Tmin = 0.99 * Tmin_15;Tmax = 1.01 * Tmax_15;
SetAxisRange (handle4, RESULT_HEAT, VAL_MANUAL, Tmin, Tmax,
  VAL_MANUAL, Cmin, Cmax);
}
return (0);
}

int  PAUSE (int panel, int control, int event, void *callbackData, int eventData1,
int eventData2)
{
```

```
if (event == EVENT_COMMIT)
{
if (flag_go)
{
flag_go = 0;
}
else
{
flag_go = 1;
}
}
return (0);
}

int  STOP (int panel, int control, int event, void *callbackData, int eventData1,
int eventData2)
{
if (event == EVENT_COMMIT)
{
QuitUserInterface(0);
EnableLocal (0, GPIB_LIST);
}
return (0);
}
```

Appendix D

DATA

This appendix contains all of the raw data used in the analyses in preceeding chapters.

First I will include here a chronology of the experiment, mostly for the benefit of my lab mates who may one day need to locate the raw data files. When the computer program that runs the experiment creates the data files, it names them according to the current date. When it continues to take data past midnight, it starts a new data file with the new date in the title, so some data sets are not even in one file. Further, the data was not always taken in an order which later makes much sense, and it was convenient, when the experiment was finished, to organize all of the data according to increasing coverage of a particular adsorbate.

The heat capacity cell used in these experiments was built in March, 2002. Most of the frequency tests and the early thermometer calibration (compared to the can thermometer, as described in the text), and a small amount of 1.0 Hz background data were taken in March, 2002. Film data taking at 1.0 Hz began in April 2002. At the end of April we began using the dosing for heat capacity films to take vapor pressure isotherms. In early May we took the DC diagnostic data, as well as more 1.0 Hz background data. The ^{3}He data was also taken in May. In June 2002 we began the second set of 1Hz heat capacity data, taking vapor pressure isotherms along the way. On July 11th the DC data with a film of 20.456 cc STP ^{4}He was measured. In August 2002 we remeasured a vapor pressure isotherm on the previous Montpellier tubes cell (in which the isotherms and isosteric heat reported in [84] were taken) in order to verify the hypothesis that the tubes in that cell were 'dirty'. In September the final set of 1.0 Hz data was taken.

Table D.1: Chronology of the vapor pressure isotherm measurements made in the calorimeter cell.

Isotherm #	Adsorbate	T (K)	Starting Date
1	^{4}He	5.00	05/13/02
2	^{4}He	9.00	05/09/02
3	^{4}He	11.0	07/09/02
4	^{4}He	12.0	09/01/02
5	^{4}He	14.0	07/02/02
6	^{4}He	15.0	12/05/02
7	^{4}He	16.0	06/19/02
8	^{3}He	5.00	05/27/02
9	^{3}He	5.00	05/17/02

Table D.2: Chronology of the heat capacity data runs.

Run #	Adsorbate	Coverage, cc STP	f, Hz	Dosing Date
1	^{4}He	0.465	1.0 Hz	09/01/02
2	^{4}He	0.763	1.0 Hz	03/16/02
3	^{4}He	0.763	1.0 Hz	04/01/02
4	^{4}He	0.764	1.0 Hz	04/25/02
5	^{4}He	0.764	1.0 Hz	04/25/02
6	^{4}He	1.134	1.0 Hz	04/27/02
7	^{4}He	1.186	1.0 Hz	09/03/02
8	^{4}He	1.725	1.0 Hz	04/28/02
9	^{4}He	2.534	1.0 Hz	09/05/02
10	^{4}He	3.212	1.0 Hz	09/06/02
11	^{4}He	4.07	1.0 Hz	04/30/02
12	^{4}He	4.87	1.0 Hz	04/16/02
13	^{4}He	5.477	1.0 Hz	09/07/02
14	^{4}He	5.59	1.0 Hz	04/15/02
15	^{4}He	7.16	1.0 Hz	04/14/02
16	^{4}He	7.32	1.0 Hz	09/10/02
17	^{4}He	9.13	1.0 Hz	09/11/02
18	^{4}He	9.15	1.0 Hz	04/13/02
19	^{4}He	10.35	1.0 Hz	09/13/02
20	^{4}He	11.05	1.0 Hz	09/14/02
21	^{4}He	11.74	1.0 Hz	09/15/02
22	^{4}He	12.28	1.0 Hz	04/12/02
23	^{4}He	12.92	1.0 Hz	09/16/02
24	^{4}He	12.96	1.0 Hz	04/02/02
25	^{4}He	15.07	1.0 Hz	09/17/02
26	^{4}He	16.64	1.0 Hz	04/11/02
27	^{4}He	19.69	1.0 Hz	04/08/02

continued on next page

Table D.2: Chronology of the heat capacity data runs, continued.

Run #	Adsorbate	Coverage, cc STP	f, Hz	Dosing Date
28	^{4}He	20.06	1.0 Hz	09/18/02
29	^{4}He	22.62	1.0 Hz	04/04/02
30	^{4}He	23.01	1.0 Hz	09/20/02
31	^{4}He	31.03	1.0 Hz	04/17/02
32	^{3}He	3.46	1.0 Hz	05/17/02
33	^{3}He	8.15	1.0 Hz	05/20/02
34	^{3}He	15.68	1.0 Hz	05/22/02
35	^{3}He	19.49	1.0 Hz	05/24/02
36	^{4}He	0.0955	0.1 Hz	03/01/03
37	^{4}He	0.220	0.1 Hz	01/29/03
38	^{4}He	0.441	0.1 Hz	02/04/03
39	^{4}He	1.11	0.1 Hz	02/05/03
40	^{4}He	1.60	0.1 Hz	02/11/03
41	^{4}He	2.34	0.1 Hz	02/14/03
42	^{4}He	8.45	0.1 Hz	02/21/03
43	^{4}He	11.96	0.1 Hz	02/21/03
44	^{4}He	16.19	0.1 Hz	02/22/03
45	^{4}He	21.80	0.1 Hz	02/24/03
46	H_2	0.50	0.1 Hz	07/12/03
47	H_2	1.00	0.1 Hz	03/29/03
48	H_2	1.50	0.1 Hz	07/17/03
49	H_2	2.50	0.1 Hz	????
50	H_2	2.5036	0.1 Hz	07/18/03
51	H_2	3.50	0.1 Hz	07/19/03
52	H_2	4.50	0.1 Hz	07/23/03
53	H_2	5.50	0.1 Hz	07/25/03
54	H_2	8.13	0.1 Hz	04/01/03
55	H_2	13.33	0.1 Hz	04/04/03
56	H_2	17.50	0.1 Hz	04/07/03
57	H_2	18.50	0.1 Hz	04/10/03
58	H_2	19.47	0.1 Hz	04/12/03
59	H_2	20.47	0.1 Hz	04/14/03
60	H_2	21.47	0.1 Hz	04/17/03
61	H_2	22.47	0.1 Hz	04/19/03
62	H_2	23.47	0.1 Hz	04/21/03
63	H_2	24.47	0.1 Hz	04/23/03
64	H_2	25.47	0.1 Hz	04/25/03
65	H_2	26.47	0.1 Hz	04/27/03

Isotherm 1, 5 K ^{4}He

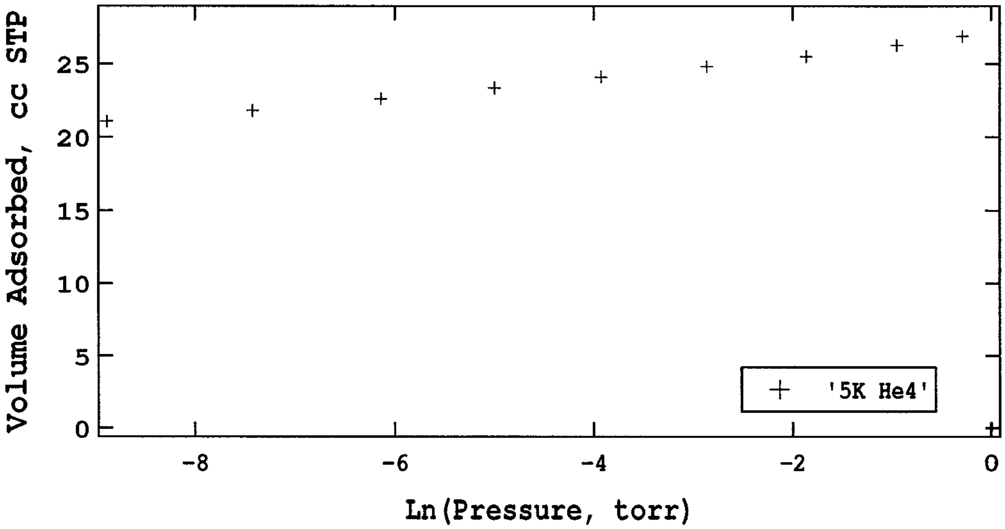

P (torr)	V_{ads} (cc STP)
0.0001	21.05
0.0006	21.79
0.0022	22.58
0.0068	23.32
0.0197	24.06
0.0573	24.80
0.1563	25.51
0.3875	26.25
0.7446	26.88
1.2429	27.45
1.8847	27.95
2.5965	28.38

Isotherm 2, 9 K ^{4}He

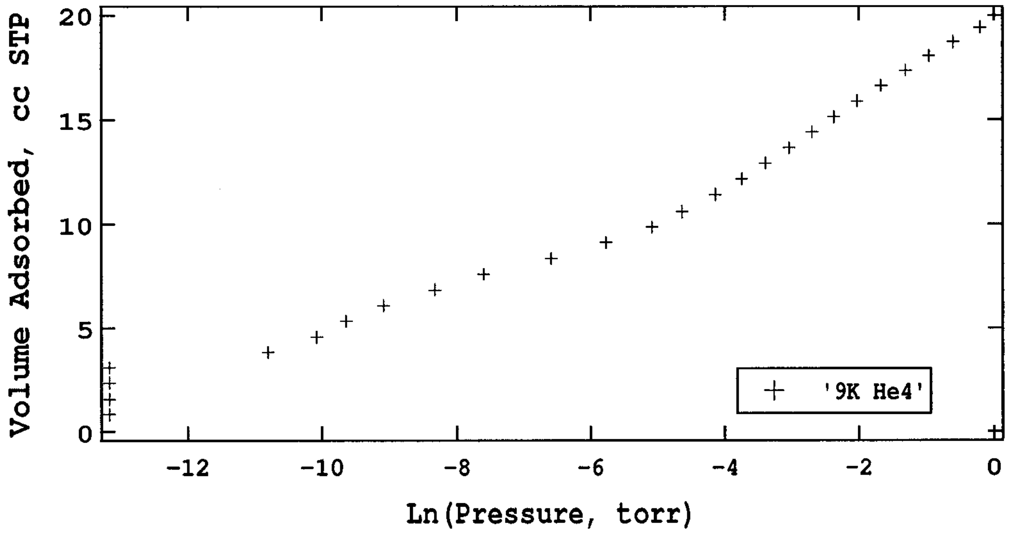

P (torr)	V_{ads} (cc STP)
0.0000	0.83
0.0000	1.57
0.0000	2.35
0.0000	3.09
0.0000	3.83
0.0000	4.57
0.0001	5.35
0.0001	6.10
0.0002	6.87
0.0005	7.61
0.0014	8.35
0.0031	9.12
0.0062	9.86
0.0097	10.60

P (torr)	V_{ads} (cc STP)
0.0158	11.41
0.0236	12.16
0.0340	12.90
0.0481	13.64
0.0670	14.39
0.0934	15.12
0.1320	15.87
0.1880	16.63
0.2681	17.36
0.3834	18.05
0.5525	18.73
0.8207	19.41
1.1943	20.01

Isotherm 3, 11 K ^{4}He

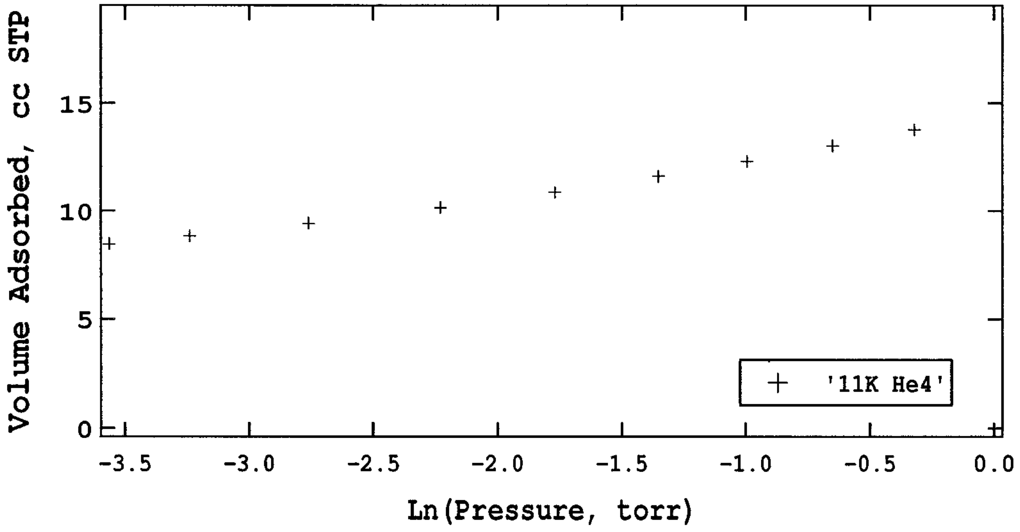

P (torr)	V_{ads} (cc STP)
0.0284	8.45
0.0392	8.82
0.0632	9.42
0.1076	10.15
0.1706	10.87
0.2587	11.59
0.3701	12.29
0.5233	13.03
0.7275	13.77
1.0087	14.42
1.3242	15.08
1.6904	15.69
2.1532	16.27
2.7351	16.85
3.5414	17.46
4.3415	17.93
4.8939	18.38
5.7935	18.75
6.8485	19.11

Isotherm 4, 12 K ^{4}He

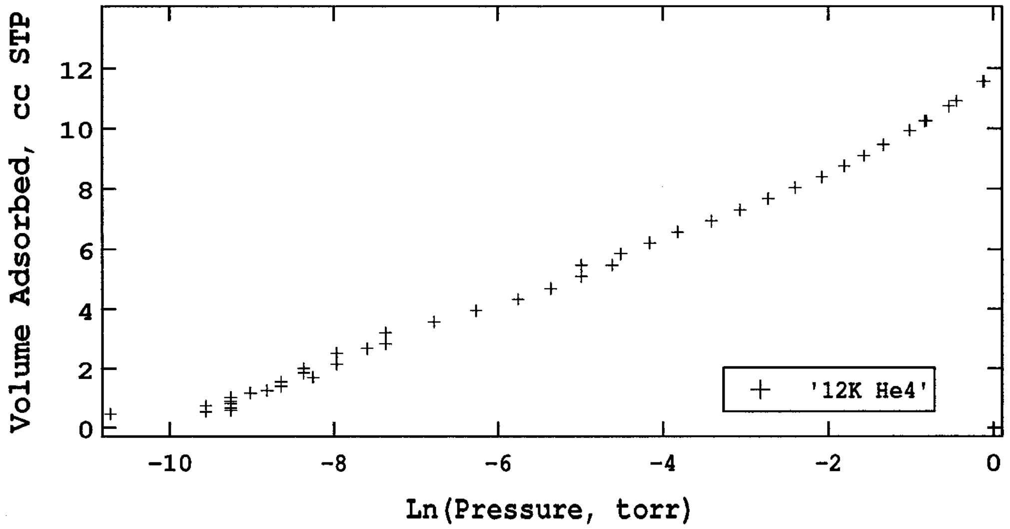

P (torr)	V_{ads} (cc STP)
0.0000	0.47
0.0001	0.54
0.0001	0.59
0.0001	0.67
0.0001	0.74
0.0001	0.81
0.0001	0.89
0.0001	1.04
0.0001	1.19
0.0001	1.26
0.0002	1.41
0.0002	1.57
0.0003	1.72
0.0002	1.87
0.0002	2.01
0.0003	2.16
0.0003	2.53
0.0005	2.69
0.0006	2.84
0.0006	3.21
0.0011	3.58
0.0019	3.95
0.0032	4.33
0.0047	4.69
0.0069	5.09
0.0099	5.47
0.0069	5.47
0.0109	5.84
0.0156	6.21
0.0219	6.57
0.0330	6.94
0.0466	7.31
0.0658	7.67
0.0911	8.03
0.1258	8.39
0.1655	8.74
0.2095	9.09
0.2644	9.46
0.3636	9.93
0.4476	10.26
0.4365	10.26
0.5860	10.75
0.6453	10.92
0.6467	10.92
0.8977	11.56
0.8819	11.57
1.2007	12.18
1.4665	12.64
1.8366	12.71
2.4961	13.22
3.1932	13.80

Isotherm 5, 14 K ^{4}He

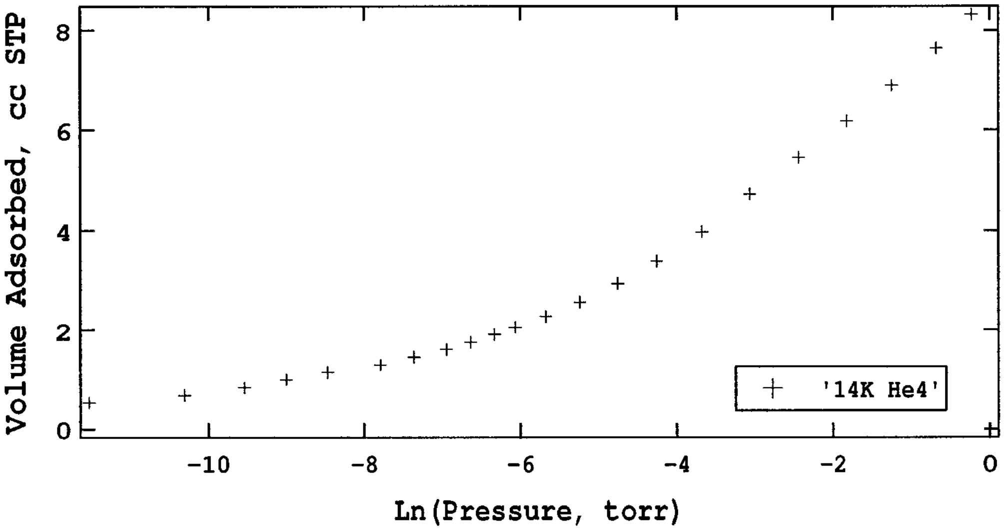

P (torr)	V_{ads} (cc STP)
0.0000	0.53
0.0000	0.68
0.0001	0.84
0.0001	1.00
0.0002	1.15
0.0004	1.30
0.0006	1.46
0.0010	1.61
0.0013	1.76
0.0018	1.91
0.0023	2.06
0.0034	2.28
0.0053	2.58
0.0086	2.95
0.0141	3.39
0.0252	3.98
0.0463	4.73
0.0873	5.45
0.1619	6.18
0.2872	6.88
0.5085	7.64
0.7950	8.32

Isotherm 6, 15 K ^{4}He

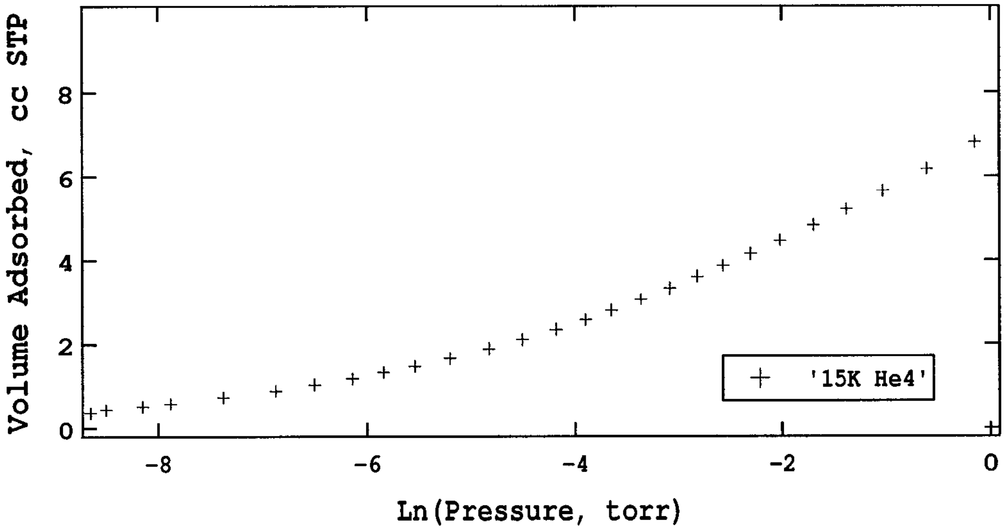

P (torr)	V_{ads} (cc STP)	P (torr)	V_{ads} (cc STP)
0.0002	0.37	0.0458	3.33
0.0002	0.44	0.0598	3.60
0.0003	0.52	0.0766	3.86
0.0004	0.59	0.0998	4.15
0.0006	0.74	0.1328	4.47
0.0010	0.89	0.1827	4.83
0.0015	1.04	0.2513	5.20
0.0022	1.18	0.3585	5.64
0.0029	1.33	0.5433	6.18
0.0039	1.48	0.8634	6.81
0.0055	1.66	1.3033	7.41
0.0080	1.88	1.8498	7.95
0.0111	2.11	2.4906	8.43
0.0153	2.35	3.1980	8.86
0.0203	2.58	3.9067	9.23
0.0261	2.80	4.6084	9.55
0.0346	3.06	5.3264	9.84

Isotherm 7, 16 K ^{4}He

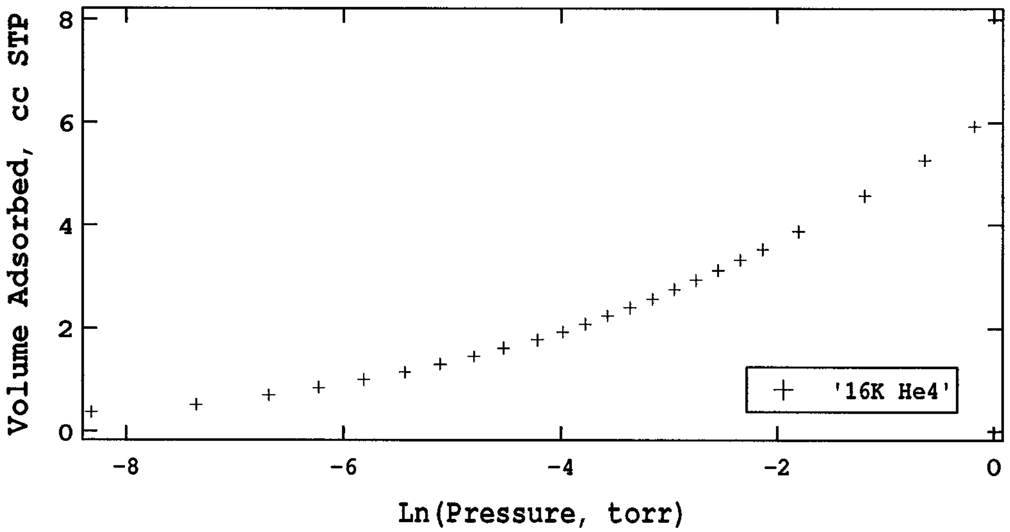

P (torr)	V_{ads} (cc STP)	P (torr)	V_{ads} (cc STP)
0.0002	0.37	0.0426	2.57
0.0006	0.52	0.0523	2.75
0.0012	0.70	0.0640	2.94
0.0020	0.85	0.0781	3.12
0.0030	1.00	0.0958	3.32
0.0043	1.15	0.1181	3.53
0.0060	1.30	0.1647	3.88
0.0082	1.46	0.3045	4.58
0.0108	1.62	0.5272	5.27
0.0148	1.78	0.8393	5.93
0.0186	1.93	1.2841	6.54
0.0230	2.08	1.8413	7.09
0.0283	2.24	2.4889	7.59
0.0347	2.40	3.2461	8.04

Isotherm 8, 5 K ^{3}He

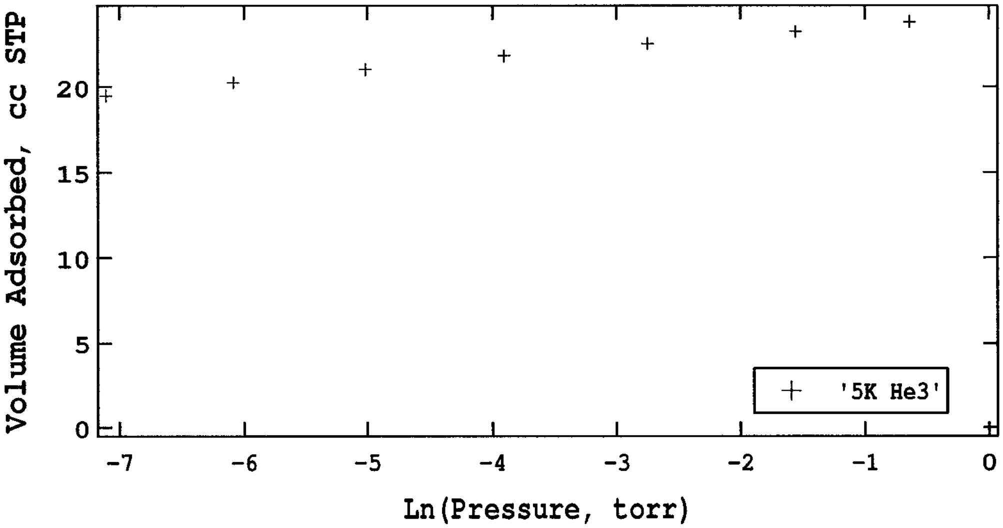

P (torr)	V_{ads} (cc STP)
0.0008	19.49
0.0023	20.24
0.0066	21.01
0.0201	21.78
0.0641	22.51
0.2107	23.20
0.5282	23.79
1.0960	24.26

Isotherm 9, 9 K ^{3}He

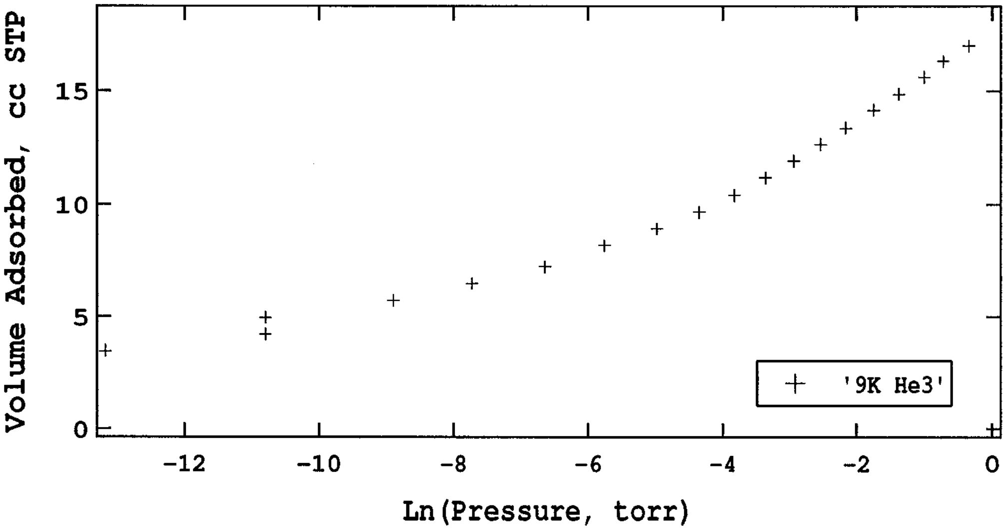

P (torr)	V_{ads} (cc STP)
0.0000	3.47
0.0000	4.21
0.0000	4.95
0.0001	5.71
0.0004	6.45
0.0013	7.20
0.0031	8.15
0.0069	8.91
0.0129	9.65
0.0219	10.40
0.0347	11.14
0.0527	11.88
0.0788	12.62
0.1156	13.35
0.1734	14.14
0.2499	14.86
0.3673	15.60
0.4901	16.30
0.7132	16.97
1.0265	17.59
1.4878	18.37

Run 1, 0.465 cc ^{4}He @ 1.0 Hz

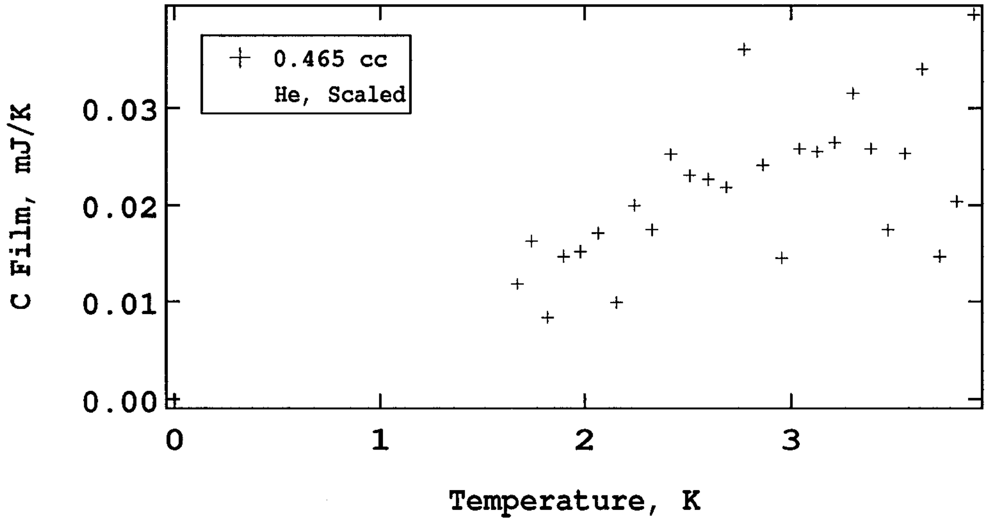

T (K)	C (mJ/K)
1.670	0.0119
1.739	0.0162
1.817	0.0083
1.896	0.0147
1.979	0.0152
2.063	0.0171
2.153	0.0099
2.240	0.0199
2.328	0.0175
2.418	0.0252
2.509	0.0230
2.598	0.0227
2.687	0.0218
2.776	0.0360

T (K)	C (mJ/K)
2.866	0.0241
2.954	0.0145
3.041	0.0258
3.128	0.0255
3.215	0.0264
3.302	0.0315
3.387	0.0258
3.472	0.0174
3.556	0.0253
3.640	0.0340
3.724	0.0147
3.806	0.0204
3.888	0.0395

Run 2, 0.763 cc ^{4}He @ 1.0 Hz

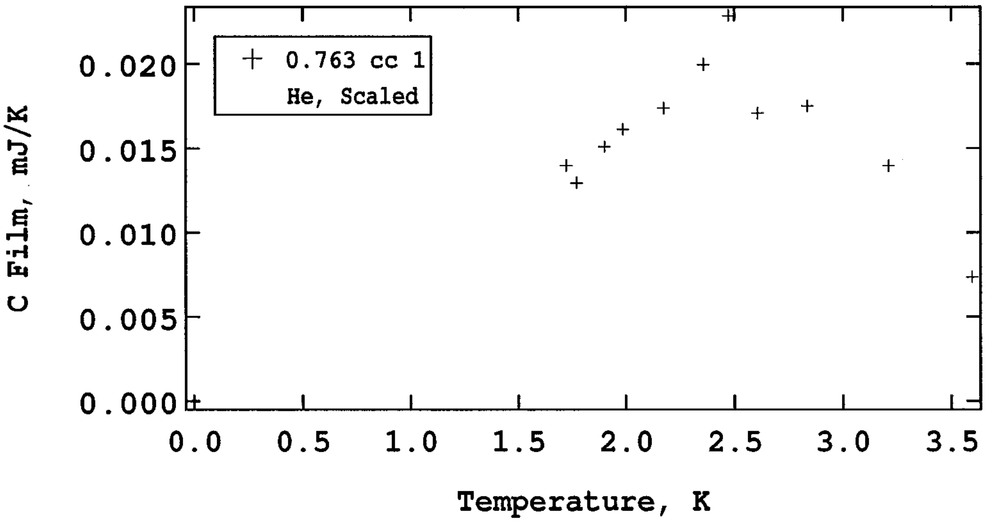

T (K)	C (mJ/K)
1.723	0.0140
1.769	0.0130
1.898	0.0151
1.986	0.0161
2.171	0.0174
2.356	0.0200
2.473	0.0228
2.605	0.0171
2.837	0.0175
3.211	0.0140
3.598	0.0073

Run 3, 0.763 cc ^{4}He @ 1.0 Hz

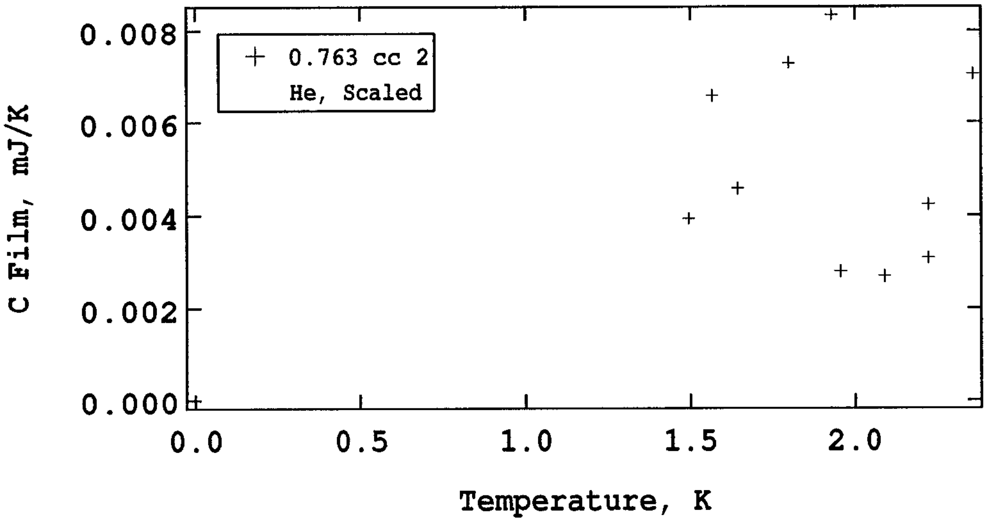

T (K)	C (mJ/K)
1.496	0.0039
1.568	0.0066
1.646	0.0046
1.801	0.0073
1.931	0.0083
1.957	0.0028
2.090	0.0027
2.223	0.0042
2.223	0.0031
2.358	0.0070

Run 4, 0.764 cc ^{4}He @ 1.0 Hz

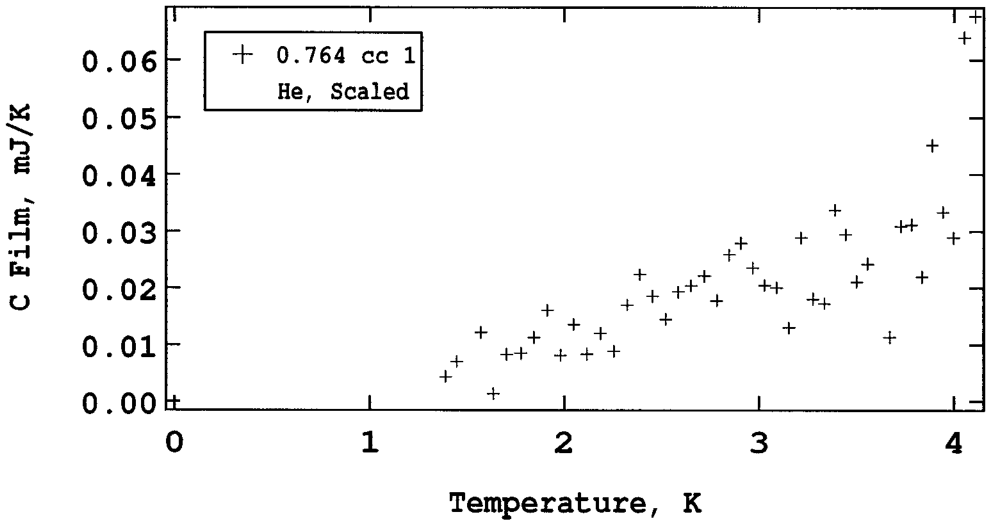

T (K)	C (mJ/K)	T (K)	C (mJ/K)	T (K)	C (mJ/K)
1.389	0.0044	2.386	0.0224	3.331	0.0172
1.448	0.0070	2.452	0.0185	3.388	0.0338
1.508	-0.0019	2.520	0.0145	3.444	0.0295
1.572	0.0122	2.586	0.0193	3.500	0.0211
1.637	0.0014	2.651	0.0204	3.557	0.0243
1.704	0.0083	2.715	0.0221	3.612	-0.0025
1.776	0.0085	2.779	0.0178	3.668	0.0113
1.844	0.0113	2.843	0.0260	3.724	0.0309
1.912	0.0161	2.905	0.0280	3.779	0.0311
1.980	0.0081	2.968	0.0236	3.834	0.0220
2.048	0.0135	3.029	0.0205	3.889	0.0452
2.116	0.0084	3.091	0.0201	3.944	0.0334
2.184	0.0120	3.153	0.0130	3.998	0.0289
2.252	0.0089	3.213	0.0289	4.053	0.0640
2.319	0.0170	3.273	0.0181	4.107	0.0678

Run 5, 0.764 cc ^{4}He @ 1.0 Hz

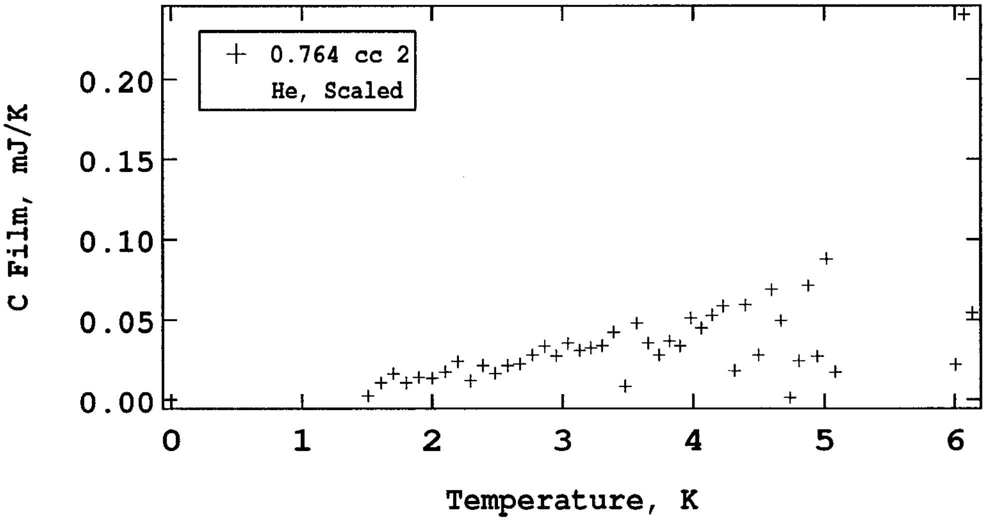

T (K)	C (mJ/K)	T (K)	C (mJ/K)	T (K)	C (mJ/K)
1.506	0.0026	3.042	0.0352	4.392	0.0592
1.605	0.0108	3.132	0.0310	4.496	0.0280
1.702	0.0164	3.220	0.0324	4.599	0.0687
1.799	0.0108	3.308	0.0338	4.670	0.0494
1.898	0.0144	3.394	0.0422	4.739	0.0014
2.000	0.0136	3.480	0.0086	4.808	0.0244
2.098	0.0176	3.566	0.0478	4.877	0.0711
2.194	0.0241	3.651	0.0353	4.946	0.0271
2.292	0.0121	3.734	0.0280	5.014	0.0879
2.390	0.0216	3.817	0.0365	5.083	0.0174
2.486	0.0167	3.900	0.0336	5.940	-0.0167
2.581	0.0216	3.982	0.0512	6.007	0.0221
2.674	0.0225	4.063	0.0447	6.073	0.2400
2.769	0.0281	4.143	0.0528	6.133	0.0544
2.861	0.0334	4.224	0.0585		
2.952	0.0276	4.312	0.0184		

Run 6, 1.134 cc ^{4}He @ 1.0 Hz

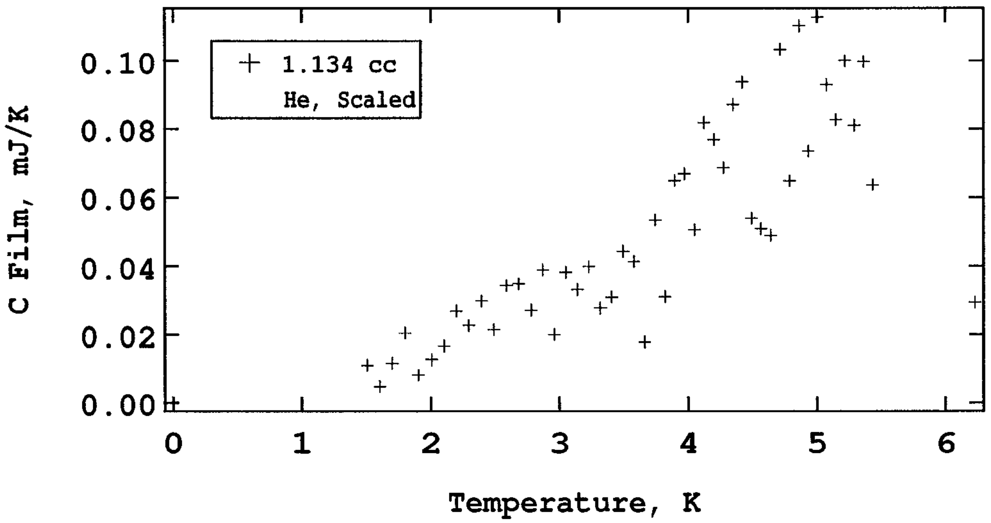

T (K)	C (mJ/K)
1.509	0.0111
1.608	0.0047
1.705	0.0116
1.803	0.0205
1.902	0.0082
2.004	0.0127
2.102	0.0167
2.201	0.0270
2.298	0.0226
2.397	0.0299
2.493	0.0214
2.588	0.0345
2.682	0.0349
2.777	0.0273
2.869	0.0390
2.960	0.0201
3.050	0.0382
3.141	0.0332
3.229	0.0399
3.317	0.0279
3.403	0.0311
3.490	0.0443
3.576	0.0414
3.661	0.0178
3.744	0.0534
3.821	0.0312
3.897	0.0649
3.973	0.0669
4.050	0.0506
4.124	0.0818
4.200	0.0768
4.274	0.0687
4.349	0.0871
4.423	0.0937
4.496	0.0539
4.570	0.0508
4.644	0.0489
4.717	0.1035
4.790	0.0648
4.863	0.1103
4.935	0.0735
5.007	0.1130
5.079	0.0929
5.151	0.0827
5.222	0.1000
5.293	0.0810
5.364	0.0997
5.434	0.0636
6.224	0.0296

Run 7, 1.186 cc ^{4}He @ 1.0 Hz

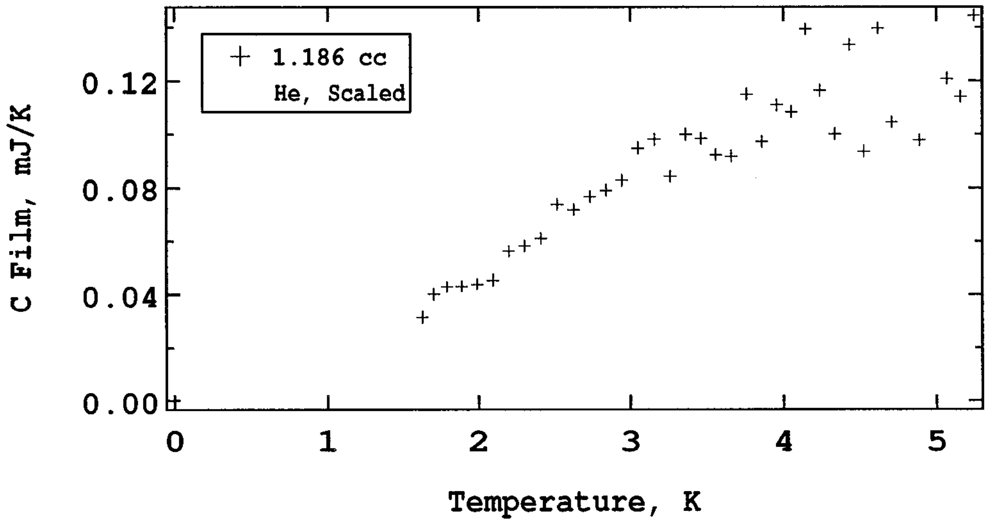

T (K)	C (mJ/K)	T (K)	C (mJ/K)
1.626	0.0316	3.459	0.0984
1.704	0.0402	3.560	0.0924
1.792	0.0430	3.661	0.0918
1.890	0.0432	3.759	0.1149
1.989	0.0441	3.857	0.0971
2.092	0.0456	3.954	0.1109
2.196	0.0562	4.052	0.1083
2.305	0.0582	4.148	0.1394
2.411	0.0611	4.243	0.1164
2.518	0.0739	4.337	0.1000
2.625	0.0718	4.431	0.1334
2.733	0.0767	4.524	0.0936
2.839	0.0791	4.617	0.1397
2.944	0.0828	4.708	0.1044
3.049	0.0948	4.890	0.0978
3.154	0.0980	5.069	0.1207
3.256	0.0843	5.159	0.1141
3.358	0.0999	5.247	0.1445

Run 8, 1.725 cc ^{4}He @ 1.0 Hz

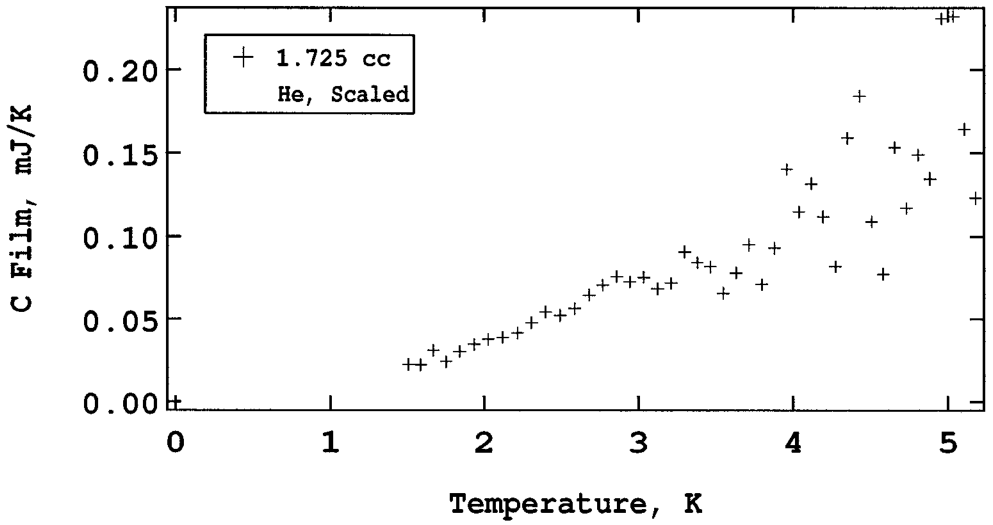

T (K)	C (mJ/K)
1.508	0.0225
1.589	0.0223
1.670	0.0312
1.755	0.0243
1.844	0.0304
1.935	0.0348
2.027	0.0379
2.119	0.0390
2.215	0.0418
2.308	0.0480
2.401	0.0543
2.493	0.0524
2.585	0.0563
2.676	0.0645
2.766	0.0704
2.858	0.0757
2.946	0.0726
3.035	0.0753
3.122	0.0684
3.209	0.0718
3.294	0.0909
3.380	0.0844
3.465	0.0818
3.549	0.0656
3.632	0.0780
3.714	0.0950
3.796	0.0710
3.877	0.0932
3.958	0.1402
4.039	0.1149
4.118	0.1318
4.196	0.1119
4.275	0.0819
4.353	0.1591
4.430	0.1840
4.507	0.1088
4.584	0.0771
4.660	0.1534
4.736	0.1172
4.811	0.1489
4.886	0.1345
4.960	0.2304
5.034	0.2316
5.109	0.1643
5.183	0.1231

Run 9, 2.534 cc ^{4}He @ 1.0 Hz

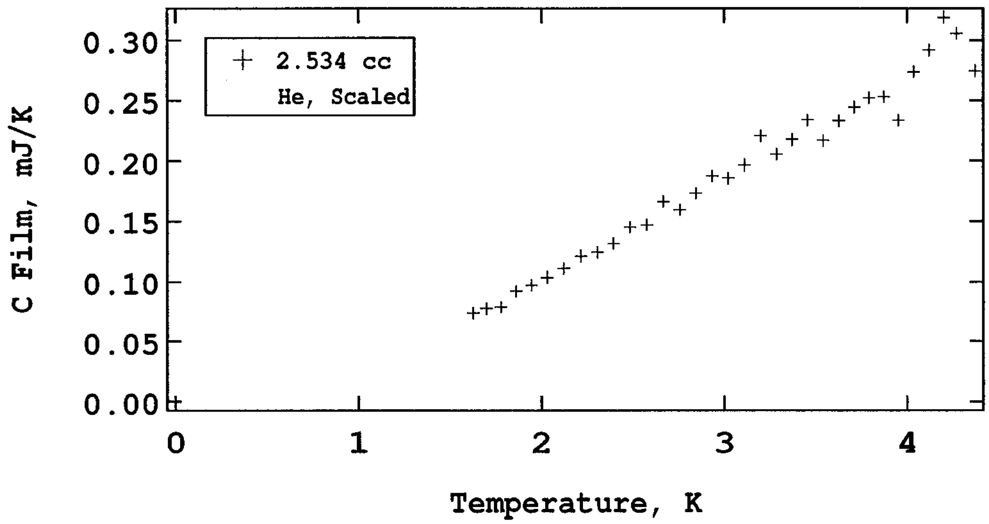

T (K)	C (mJ/K)
1.624	0.0737
1.696	0.0774
1.774	0.0787
1.859	0.0919
1.944	0.0970
2.031	0.1035
2.120	0.1108
2.212	0.1210
2.302	0.1240
2.393	0.1314
2.483	0.1450
2.576	0.1472
2.666	0.1666
2.756	0.1598
2.845	0.1735
2.935	0.1880
3.023	0.1862
3.110	0.1968
3.198	0.2209
3.284	0.2058
3.371	0.2180
3.456	0.2339
3.540	0.2171
3.624	0.2331
3.708	0.2445
3.791	0.2523
3.873	0.2532
3.955	0.2336
4.037	0.2739
4.117	0.2918
4.197	0.3193
4.267	0.3057
4.371	0.2748

Run 10, 3.212 cc ^{4}He @ 1.0 Hz

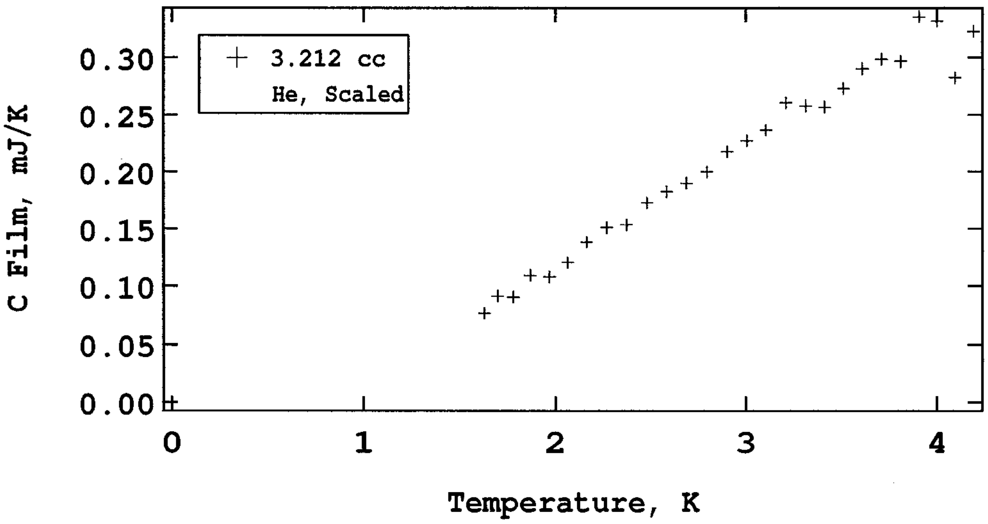

T (K)	C (mJ/K)	T (K)	C (mJ/K)
1.631	0.0770	3.005	0.2271
1.701	0.0916	3.108	0.2366
1.782	0.0908	3.210	0.2604
1.870	0.1093	3.311	0.2577
1.967	0.1081	3.412	0.2566
2.065	0.1206	3.513	0.2731
2.166	0.1386	3.612	0.2904
2.269	0.1512	3.711	0.2985
2.374	0.1535	3.808	0.2966
2.481	0.1728	3.905	0.3354
2.586	0.1827	4.002	0.3314
2.691	0.1900	4.097	0.2824
2.796	0.1997	4.192	0.3224
2.900	0.2174		

Run 11, 4.07 cc ^{4}He @ 1.0 Hz

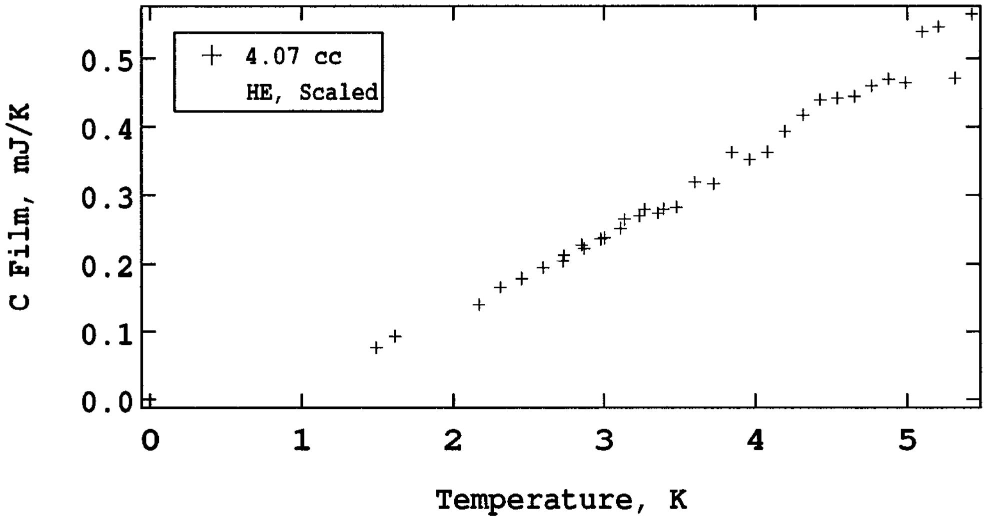

T (K)	C (mJ/K)	T (K)	C (mJ/K)
1.493	0.0766	3.479	0.2827
1.618	0.0932	3.601	0.3190
2.173	0.1403	3.723	0.3164
2.315	0.1656	3.843	0.3620
2.455	0.1789	3.962	0.3517
2.594	0.1943	4.080	0.3628
2.727	0.2040	4.197	0.3934
2.733	0.2123	4.313	0.4172
2.854	0.2277	4.428	0.4393
2.869	0.2226	4.542	0.4421
2.980	0.2364	4.655	0.4447
3.002	0.2378	4.767	0.4602
3.107	0.2519	4.878	0.4698
3.134	0.2648	4.990	0.4644
3.232	0.2695	5.100	0.5384
3.266	0.2797	5.209	0.5461
3.356	0.2739	5.318	0.4712
3.394	0.2801	5.426	0.5647

Run 12, 4.87 cc ^{4}He @ 1.0 Hz

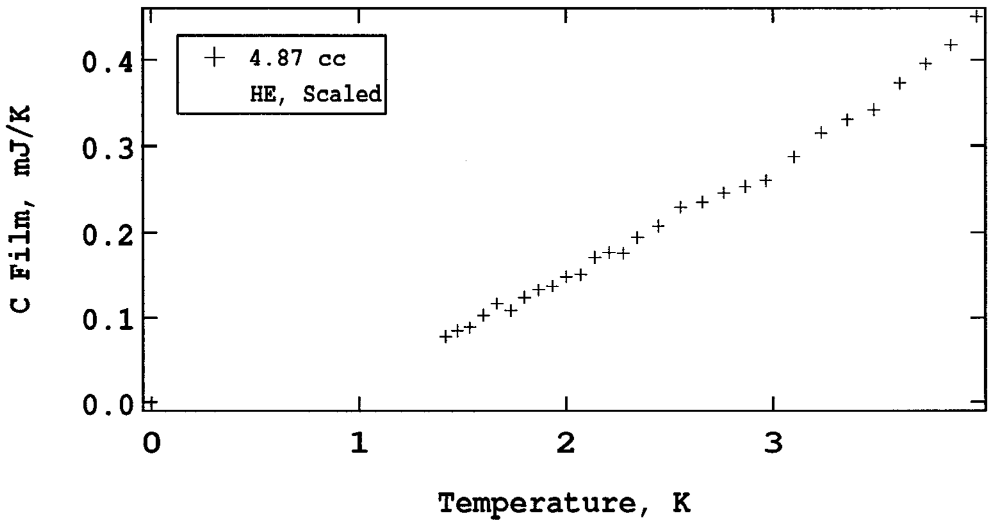

T (K)	C (mJ/K)
1.418	0.0777
1.475	0.0843
1.536	0.0882
1.603	0.1028
1.668	0.1165
1.733	0.1079
1.799	0.1237
1.866	0.1326
1.934	0.1369
2.001	0.1479
2.072	0.1510
2.140	0.1711
2.207	0.1767
2.274	0.1759
2.341	0.1945
2.446	0.2074
2.552	0.2294
2.657	0.2352
2.761	0.2462
2.864	0.2534
2.967	0.2606
3.099	0.2876
3.230	0.3148
3.358	0.3302
3.485	0.3417
3.610	0.3720
3.734	0.3949
3.856	0.4173
3.977	0.4506

Run 13, 5.477 cc ^{4}He @ 1.0 Hz

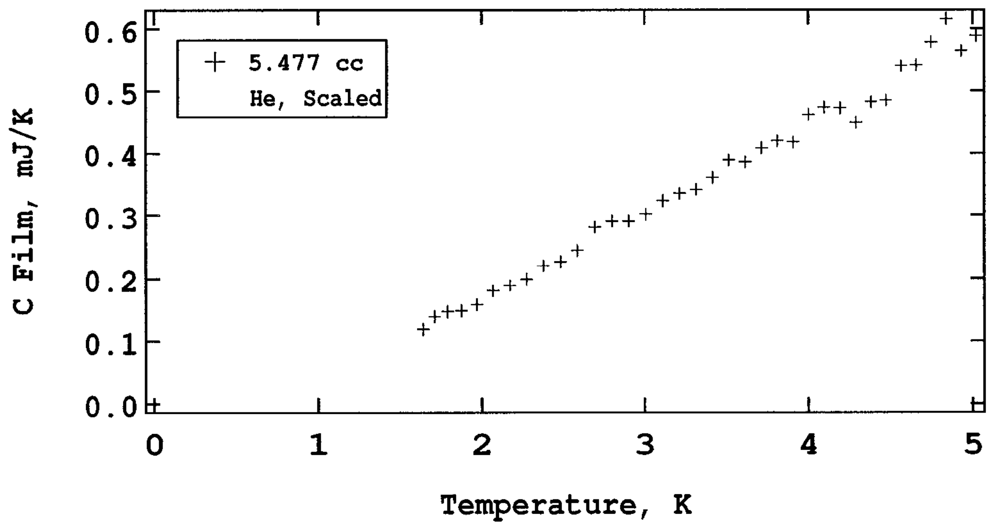

T (K)	C (mJ/K)	T (K)	C (mJ/K)
1.636	0.1190	3.413	0.3603
1.706	0.1394	3.514	0.3888
1.786	0.1466	3.613	0.3863
1.873	0.1478	3.712	0.4087
1.970	0.1581	3.809	0.4203
2.068	0.1803	3.906	0.4180
2.169	0.1891	4.003	0.4621
2.272	0.1986	4.098	0.4739
2.376	0.2200	4.193	0.4723
2.483	0.2264	4.287	0.4495
2.588	0.2439	4.379	0.4821
2.693	0.2814	4.472	0.4847
2.797	0.2906	4.565	0.5401
2.901	0.2905	4.657	0.5413
3.007	0.3014	4.748	0.5789
3.109	0.3235	4.838	0.6158
3.211	0.3356	4.928	0.5645
3.313	0.3415	5.018	0.5890

Run 14, 5.59 cc ^{4}He @ 1.0 Hz

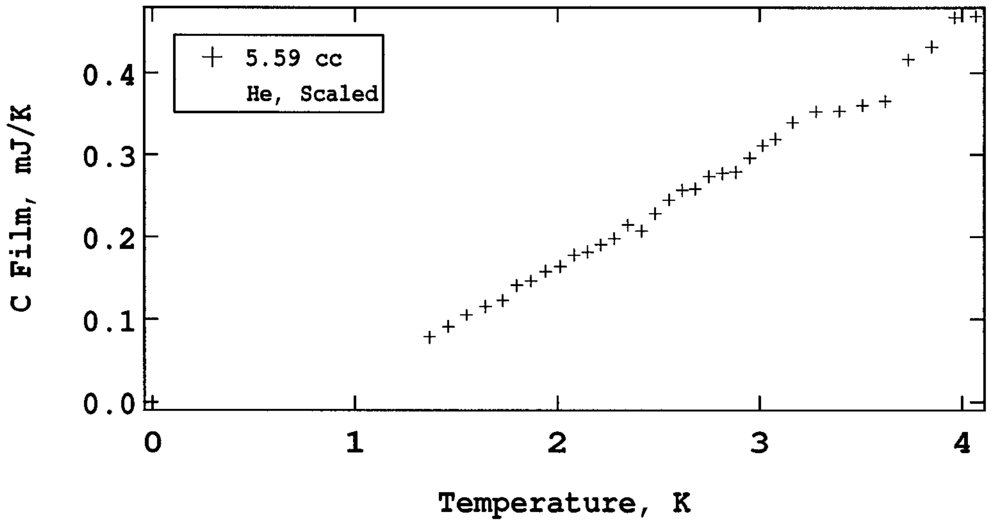

T (K)	C (mJ/K)	T (K)	C (mJ/K)
1.369	0.0786	2.618	0.2564
1.460	0.0912	2.685	0.2582
1.550	0.1056	2.753	0.2732
1.643	0.1156	2.819	0.2769
1.729	0.1228	2.884	0.2787
1.799	0.1413	2.950	0.2959
1.871	0.1464	3.015	0.3113
1.942	0.1582	3.080	0.3192
2.014	0.1641	3.168	0.3389
2.082	0.1780	3.282	0.3523
2.149	0.1815	3.396	0.3525
2.215	0.1901	3.510	0.3597
2.283	0.1978	3.624	0.3652
2.349	0.2141	3.737	0.4163
2.417	0.2065	3.850	0.4316
2.484	0.2281	3.963	0.4674
2.551	0.2447	4.069	0.4687

Run 15, 7.16 cc ^{4}He @ 1.0 Hz

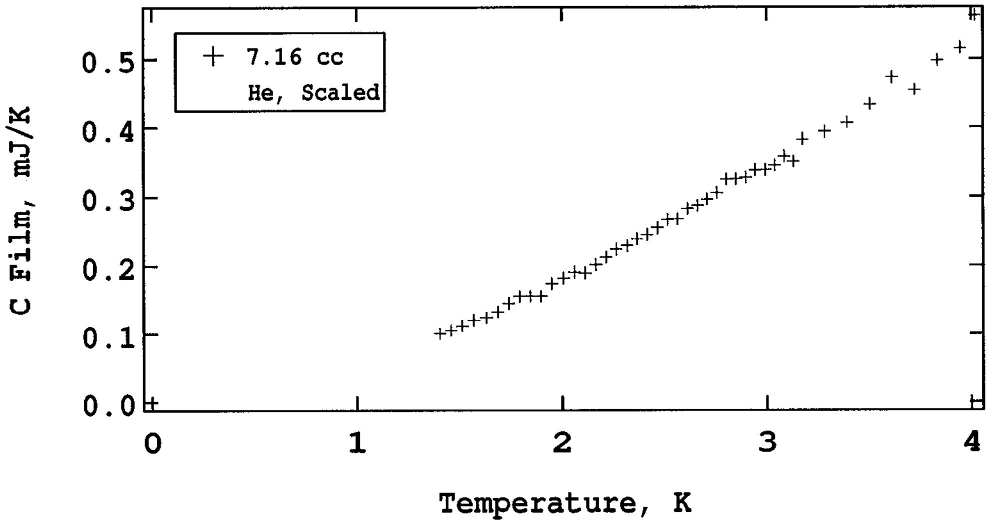

T (K)	C (mJ/K)	T (K)	C (mJ/K)	T (K)	C (mJ/K)
1.404	0.1006	2.212	0.2125	2.946	0.3384
1.458	0.1056	2.263	0.2241	2.994	0.3391
1.513	0.1121	2.316	0.2291	3.040	0.3455
1.568	0.1207	2.367	0.2387	3.085	0.3583
1.627	0.1243	2.416	0.2448	3.131	0.3514
1.682	0.1331	2.466	0.2545	3.176	0.3832
1.736	0.1452	2.515	0.2668	3.284	0.3939
1.790	0.1556	2.564	0.2671	3.393	0.4071
1.843	0.1558	2.612	0.2824	3.503	0.4339
1.897	0.1557	2.663	0.2872	3.614	0.4727
1.949	0.1747	2.711	0.2961	3.724	0.4545
2.005	0.1826	2.758	0.3057	3.835	0.4970
2.058	0.1911	2.806	0.3252	3.945	0.5157
2.110	0.1896	2.853	0.3258	4.017	0.5629
2.161	0.2012	2.899	0.3281		

Run 16, 7.32 cc ^{4}He @ 1.0 Hz

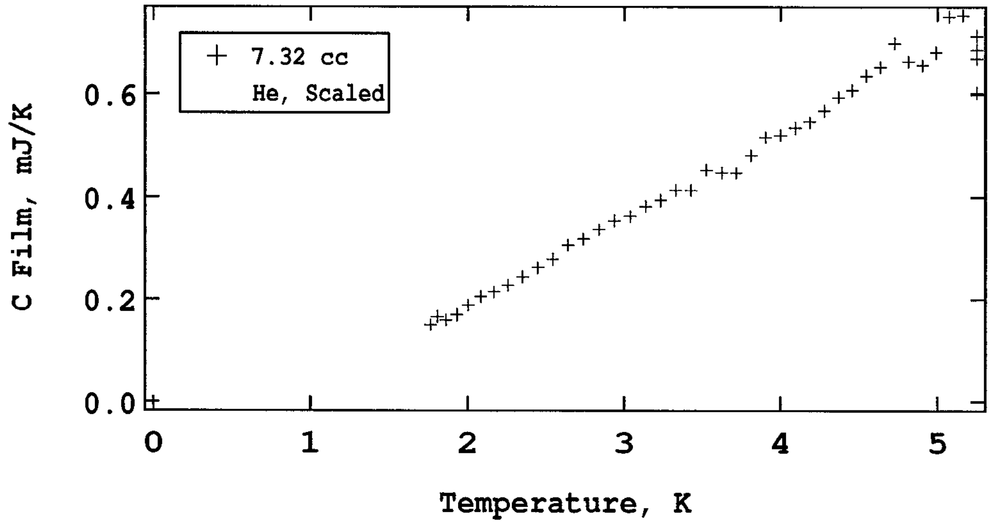

T (K)	C (mJ/K)
1.765	0.1504
1.808	0.1664
1.863	0.1601
1.929	0.1695
2.003	0.1885
2.084	0.2049
2.170	0.2147
2.260	0.2275
2.353	0.2438
2.448	0.2618
2.545	0.2782
2.642	0.3062
2.741	0.3180
2.840	0.3370
2.938	0.3542
3.037	0.3631
3.135	0.3824
3.233	0.3944
3.331	0.4135
3.428	0.4137
3.525	0.4525
3.621	0.4478
3.716	0.4472
3.811	0.4806
3.905	0.5153
3.999	0.5187
4.092	0.5332
4.184	0.5448
4.276	0.5674
4.367	0.5941
4.457	0.6077
4.547	0.6353
4.637	0.6516
4.726	0.6977
4.814	0.6624
4.902	0.6553
4.989	0.6803
5.078	0.7491
5.164	0.7519
5.251	0.6029
5.251	0.6850
5.251	0.7115
5.251	0.6684

Run 17, 9.13 cc ^{4}He @ 1.0 Hz

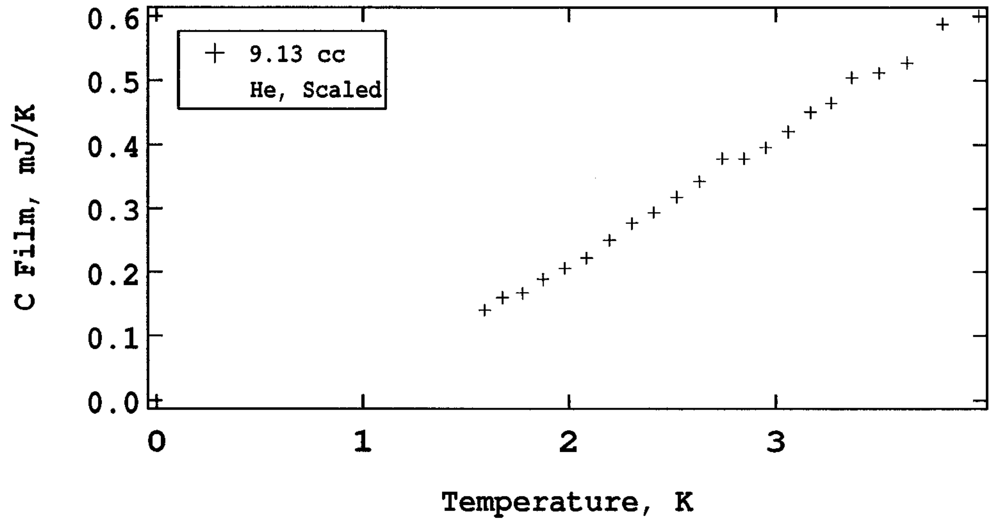

T (K)	C (mJ/K)	T (K)	C (mJ/K)
1.592	0.1401	2.739	0.3782
1.679	0.1598	2.846	0.3780
1.773	0.1668	2.952	0.3956
1.873	0.1892	3.058	0.4204
1.980	0.2060	3.163	0.4507
2.087	0.2226	3.266	0.4651
2.195	0.2509	3.368	0.5043
2.303	0.2766	3.499	0.5116
2.412	0.2939	3.631	0.5277
2.523	0.3180	3.805	0.5883
2.631	0.3422	3.977	0.6006

Run 18, 9.15 cc ^{4}He @ 1.0 Hz

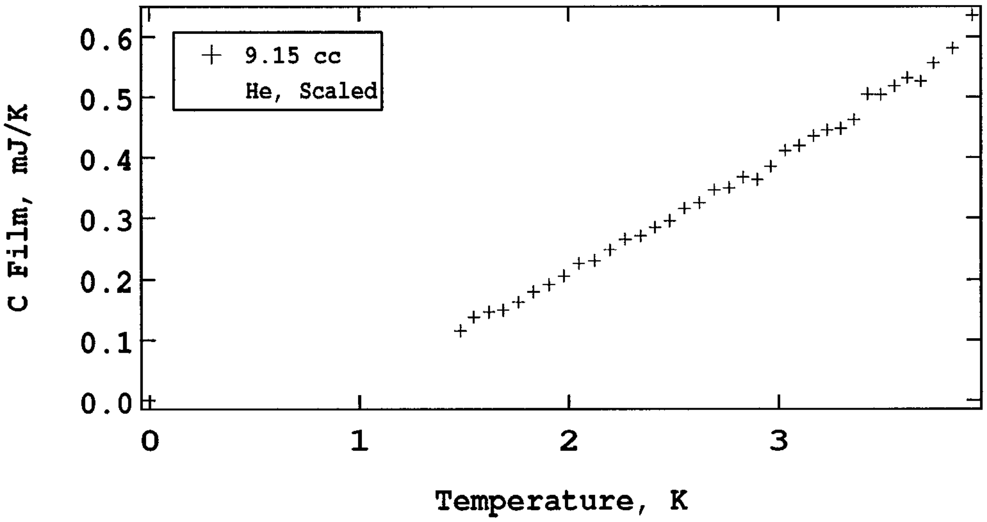

T (K)	C (mJ/K)	T (K)	C (mJ/K)
1.482	0.1156	2.762	0.3500
1.547	0.1380	2.830	0.3675
1.620	0.1465	2.898	0.3635
1.688	0.1493	2.965	0.3849
1.760	0.1630	3.032	0.4119
1.831	0.1796	3.100	0.4194
1.903	0.1913	3.166	0.4351
1.975	0.2056	3.231	0.4453
2.048	0.2257	3.297	0.4474
2.123	0.2303	3.360	0.4622
2.196	0.2481	3.425	0.5047
2.267	0.2656	3.488	0.5035
2.339	0.2704	3.554	0.5177
2.410	0.2849	3.616	0.5311
2.481	0.2955	3.679	0.5258
2.551	0.3157	3.741	0.5567
2.624	0.3248	3.833	0.5814
2.692	0.3465	3.925	0.6349

Run 19, 10.35 cc ^{4}He @ 1.0 Hz

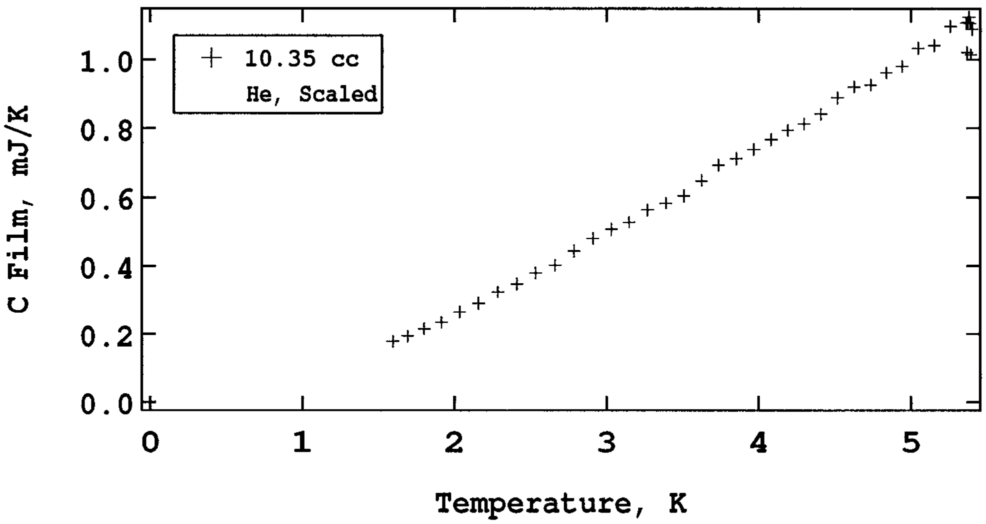

T (K)	C (mJ/K)	T (K)	C (mJ/K)	T (K)	C (mJ/K)
1.595	0.1783	3.275	0.5635	4.838	0.9612
1.690	0.1941	3.393	0.5824	4.943	0.9808
1.797	0.2158	3.511	0.6040	5.048	1.0335
1.913	0.2345	3.627	0.6488	5.152	1.0422
2.036	0.2654	3.742	0.6929	5.255	1.0966
2.159	0.2900	3.857	0.7127	5.358	1.1058
2.284	0.3247	3.970	0.7381	5.363	1.0223
2.410	0.3490	4.082	0.7666	5.369	1.1077
2.536	0.3802	4.193	0.7933	5.374	1.1238
2.663	0.4021	4.302	0.8123	5.380	1.1251
2.787	0.4436	4.411	0.8404	5.385	1.1055
2.910	0.4810	4.519	0.8878	5.391	1.0148
3.033	0.5060	4.627	0.9200	5.396	1.0887
3.154	0.5271	4.733	0.9255		

Run 20, 11.05 cc ^{4}He @ 1.0 Hz

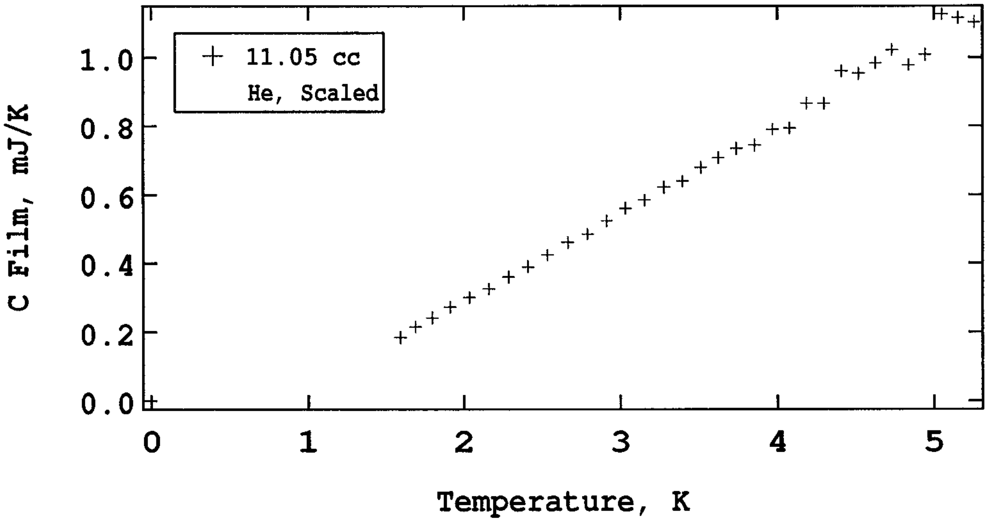

T (K)	C (mJ/K)	T (K)	C (mJ/K)
1.591	0.1846	3.626	0.7081
1.687	0.2158	3.741	0.7349
1.795	0.2412	3.856	0.7446
1.910	0.2729	3.969	0.7897
2.034	0.3005	4.080	0.7937
2.157	0.3253	4.191	0.8668
2.282	0.3603	4.302	0.8671
2.408	0.3893	4.411	0.9602
2.534	0.4226	4.520	0.9534
2.661	0.4608	4.627	0.9841
2.786	0.4847	4.734	1.0213
2.909	0.5246	4.840	0.9779
3.031	0.5613	4.944	1.0084
3.152	0.5853	5.050	1.1246
3.274	0.6224	5.154	1.1144
3.392	0.6403	5.257	1.1021
3.510	0.6808		

Run 21, 11.74 cc ^{4}He @ 1.0 Hz

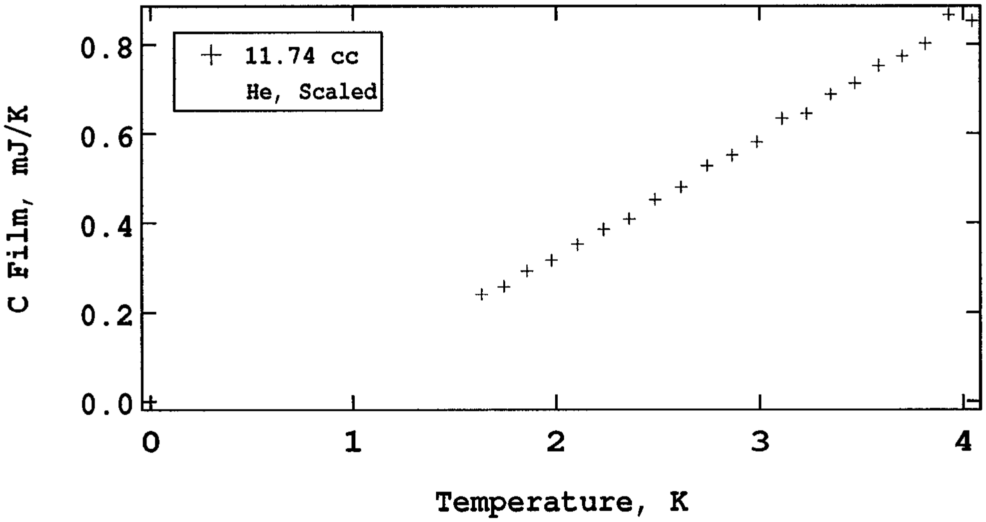

T (K)	C (mJ/K)	T (K)	C (mJ/K)
1.633	0.2402	2.988	0.5818
1.740	0.2582	3.110	0.6342
1.856	0.2925	3.230	0.6455
1.978	0.3164	3.351	0.6885
2.105	0.3524	3.469	0.7136
2.232	0.3852	3.586	0.7531
2.359	0.4090	3.702	0.7740
2.486	0.4524	3.817	0.8022
2.612	0.4803	3.931	0.8657
2.740	0.5280	4.044	0.8522
2.864	0.5521		

Run 22, 12.28 cc ^{4}He @ 1.0 Hz

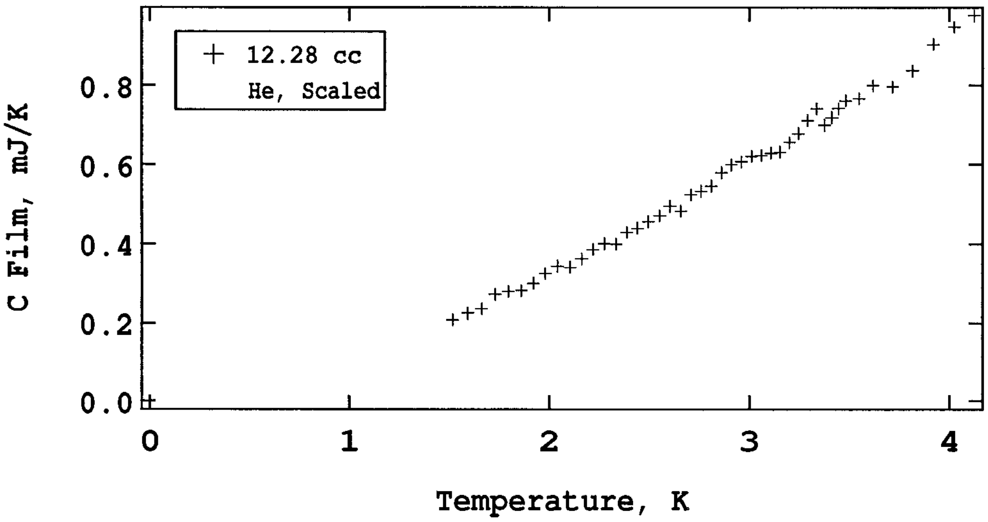

T (K)	C (mJ/K)	T (K)	C (mJ/K)	T (K)	C (mJ/K)
1.516	0.2084	2.440	0.4410	3.202	0.6563
1.591	0.2248	2.494	0.4567	3.248	0.6781
1.660	0.2358	2.550	0.4719	3.293	0.7108
1.726	0.2723	2.602	0.4958	3.339	0.7401
1.790	0.2804	2.655	0.4839	3.378	0.6997
1.857	0.2818	2.706	0.5244	3.413	0.7174
1.919	0.3006	2.758	0.5334	3.448	0.7405
1.980	0.3244	2.810	0.5464	3.481	0.7605
2.039	0.3433	2.861	0.5802	3.550	0.7666
2.101	0.3414	2.911	0.5995	3.619	0.7991
2.159	0.3620	2.961	0.6063	3.720	0.7959
2.216	0.3868	3.012	0.6210	3.821	0.8363
2.272	0.4009	3.060	0.6232	3.922	0.9032
2.331	0.4005	3.107	0.6288	4.025	0.9472
2.386	0.4302	3.154	0.6322	4.127	0.9774

Run 23, 12.92 cc ^{4}He @ 1.0 Hz

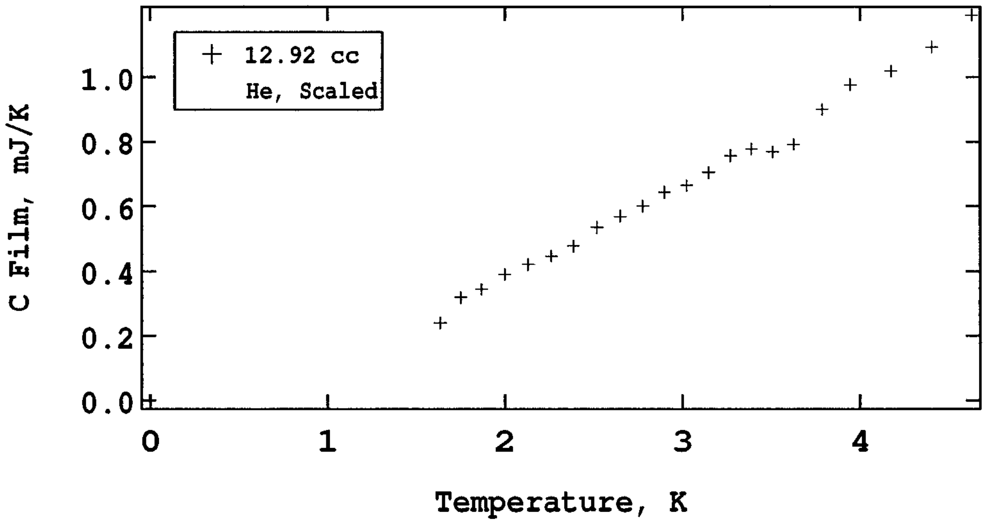

T (K)	C (mJ/K)	T (K)	C (mJ/K)
1.633	0.2402	3.023	0.6639
1.747	0.3190	3.146	0.7041
1.869	0.3448	3.267	0.7565
1.999	0.3907	3.387	0.7758
2.128	0.4208	3.507	0.7679
2.257	0.4472	3.624	0.7911
2.386	0.4787	3.785	0.9002
2.518	0.5364	3.944	0.9766
2.645	0.5707	4.175	1.0191
2.772	0.6018	4.402	1.0935
2.897	0.6435	4.626	1.1917

Run 24, 12.96 cc ^{4}He @ 1.0 Hz

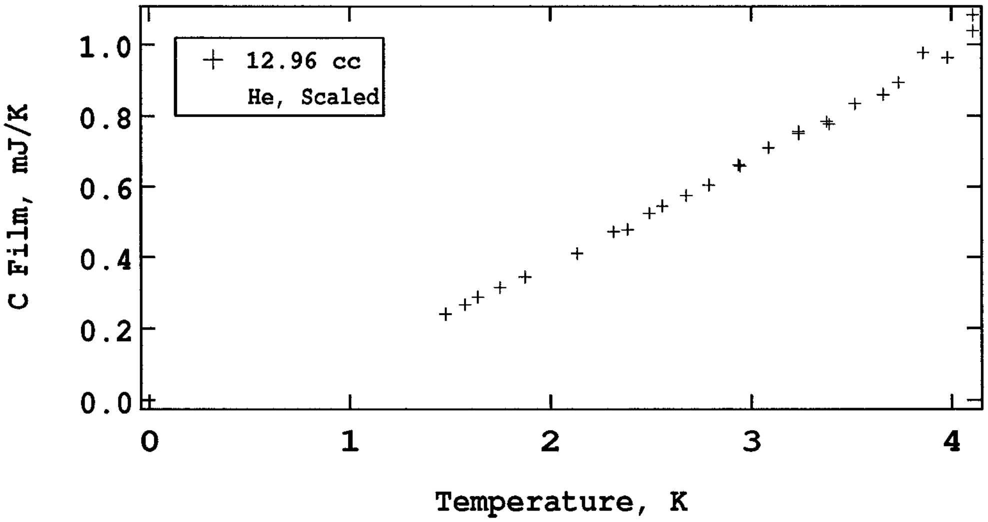

T (K)	C (mJ/K)	T (K)	C (mJ/K)
1.477	0.2404	2.944	0.6584
1.574	0.2660	3.087	0.7115
1.640	0.2868	3.237	0.7553
1.752	0.3142	3.238	0.7496
1.874	0.3438	3.377	0.7848
2.134	0.4110	3.389	0.7759
2.313	0.4722	3.518	0.8343
2.384	0.4782	3.661	0.8601
2.492	0.5242	3.734	0.8937
2.558	0.5452	3.858	0.9768
2.677	0.5742	3.981	0.9623
2.789	0.6046	4.105	1.0383
2.937	0.6618	4.105	1.0824

Run 25, 15.07 cc ^{4}He @ 1.0 Hz

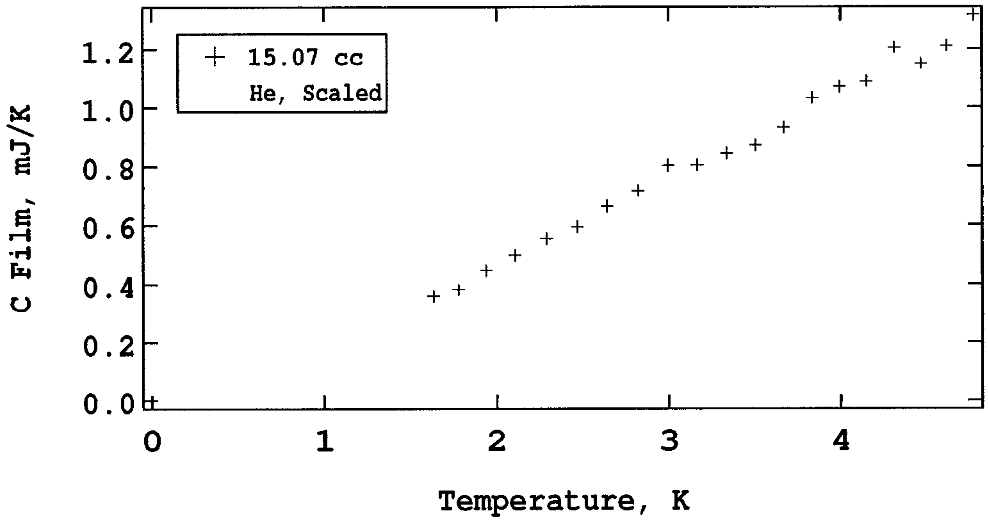

T (K)	C (mJ/K)
1.632	0.3579
1.774	0.3816
1.936	0.4463
2.108	0.4974
2.288	0.5540
2.466	0.5935
2.644	0.6625
2.821	0.7159
2.996	0.8026
3.169	0.8028
3.338	0.8434
3.506	0.8717
3.671	0.9312
3.833	1.0323
3.995	1.0711
4.153	1.0899
4.310	1.2050
4.463	1.1497
4.616	1.2106
4.768	1.3164

Run 26, 16.64 cc ^{4}He @ 1.0 Hz

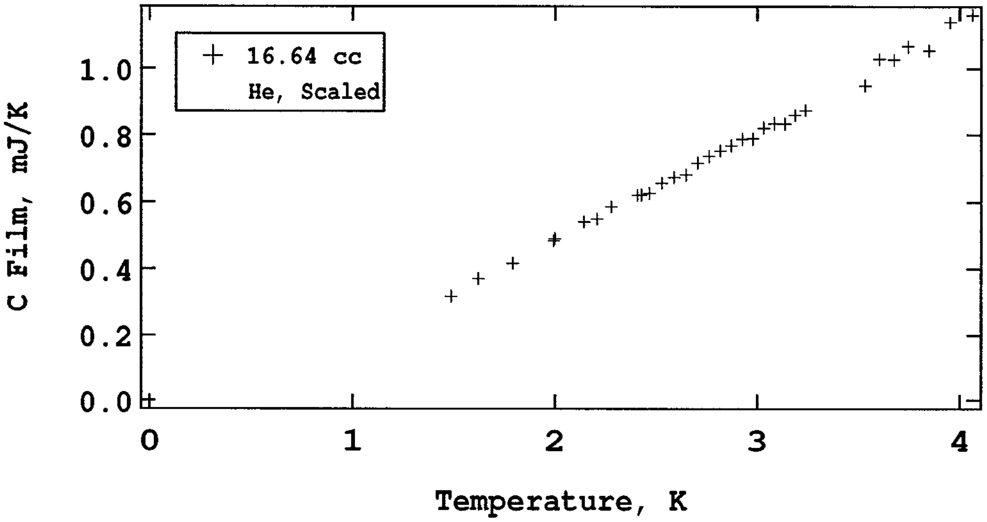

T (K)	C (mJ/K)	T (K)	C (mJ/K)
1.487	0.3168	2.818	0.7526
1.622	0.3704	2.872	0.7679
1.792	0.4155	2.926	0.7867
1.993	0.4829	2.979	0.7887
1.998	0.4894	3.033	0.8208
2.145	0.5411	3.085	0.8335
2.209	0.5494	3.136	0.8330
2.279	0.5853	3.187	0.8585
2.408	0.6197	3.237	0.8733
2.429	0.6215	3.533	0.9484
2.469	0.6259	3.603	1.0281
2.529	0.6570	3.673	1.0269
2.590	0.6742	3.743	1.0671
2.648	0.6811	3.849	1.0549
2.705	0.7168	3.955	1.1400
2.761	0.7364	4.061	1.1620

Run 27, 19.69 cc ^{4}He @ 1.0 Hz

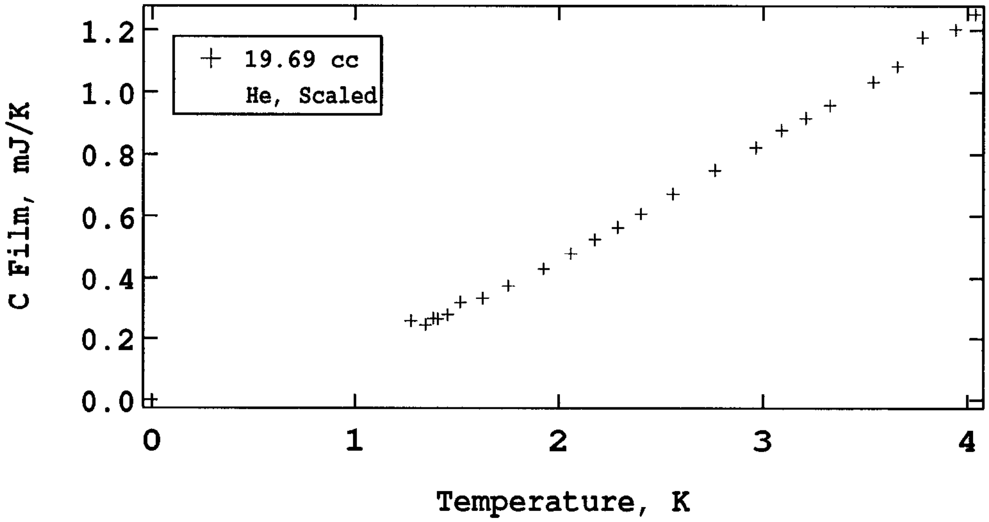

T (K)	C (mJ/K)	T (K)	C (mJ/K)
1.274	0.2569	2.400	0.6081
1.344	0.2435	2.557	0.6723
1.384	0.2639	2.762	0.7487
1.406	0.2623	2.965	0.8224
1.456	0.2763	3.089	0.8776
1.519	0.3177	3.209	0.9156
1.627	0.3316	3.329	0.9562
1.748	0.3735	3.538	1.0327
1.923	0.4292	3.658	1.0825
2.057	0.4786	3.783	1.1781
2.174	0.5245	3.942	1.2029
2.285	0.5632	4.038	1.2528

Run 28, 20.06 cc ^{4}He @ 1.0 Hz

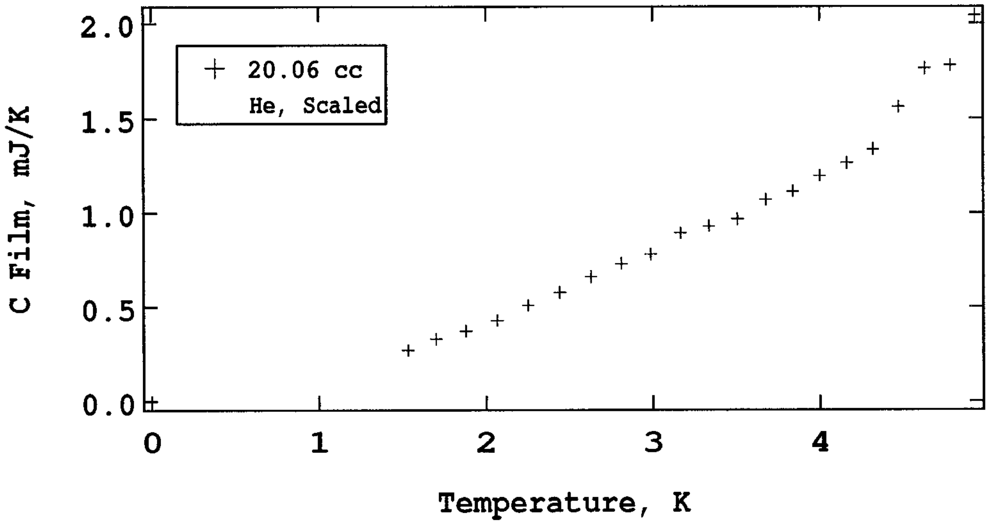

T (K)	C (mJ/K)
1.531	0.2710
1.701	0.3336
1.880	0.3738
2.066	0.4303
2.254	0.5117
2.443	0.5782
2.628	0.6604
2.810	0.7295
2.988	0.7802
3.166	0.8934
3.338	0.9310

T (K)	C (mJ/K)
3.508	0.9665
3.675	1.0732
3.840	1.1162
4.003	1.1994
4.162	1.2666
4.319	1.3380
4.475	1.5611
4.628	1.7625
4.780	1.7796
4.929	2.0412

Run 29, 22.62 cc ^{4}He @ 1.0 Hz

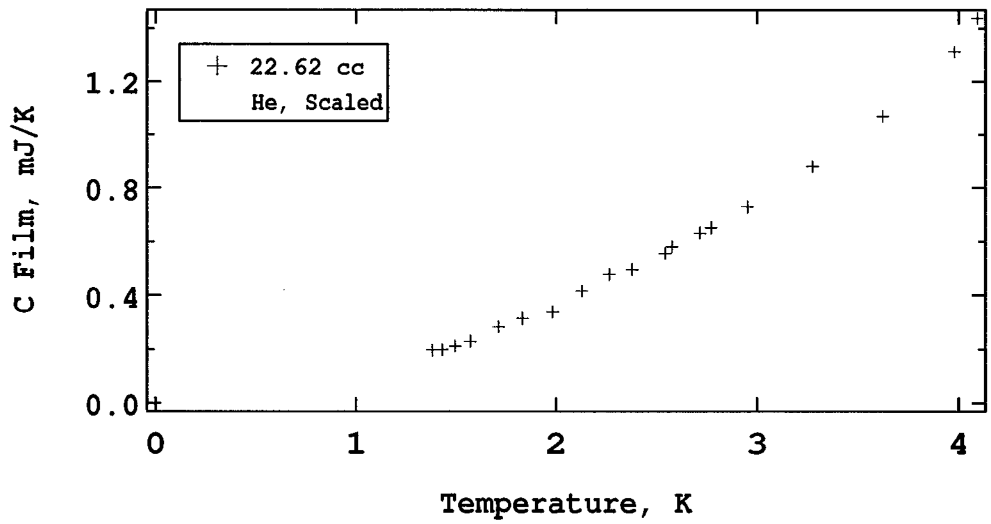

T (K)	C (mJ/K)
1.380	0.1986
1.380	0.1984
1.432	0.1999
1.495	0.2140
1.571	0.2316
1.709	0.2846
1.829	0.3158
1.983	0.3399
2.128	0.4175
2.265	0.4787
2.380	0.4969
2.542	0.5574
2.577	0.5823
2.718	0.6325
2.775	0.6535
2.953	0.7306
3.279	0.8803
3.626	1.0690
3.979	1.3130
4.095	1.4381

Run 30, 23.01 cc ^{4}He @ 1.0 Hz

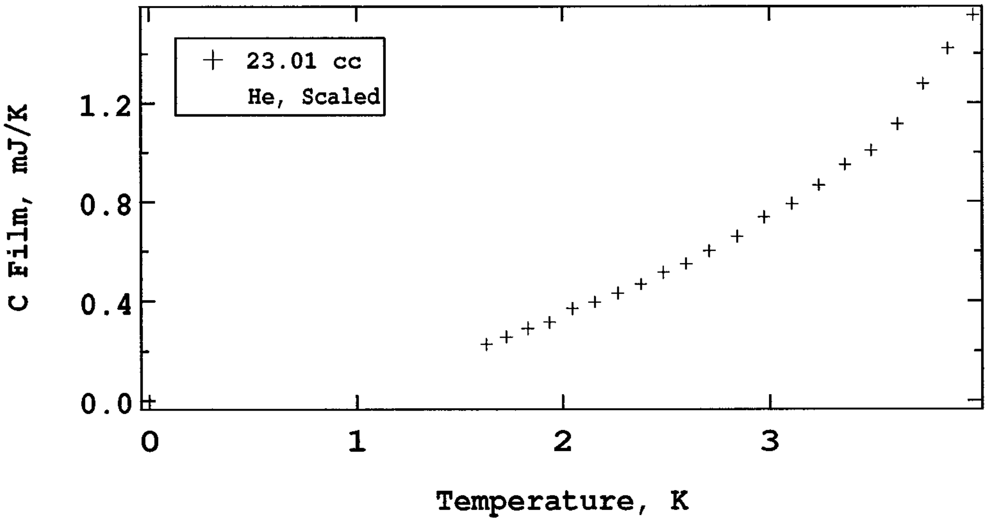

T (K)	C (mJ/K)	T (K)	C (mJ/K)
1.632	0.2271	2.841	0.6603
1.728	0.2567	2.974	0.7383
1.830	0.2905	3.108	0.7915
1.935	0.3147	3.238	0.8656
2.047	0.3692	3.366	0.9493
2.156	0.3953	3.493	1.0085
2.266	0.4308	3.619	1.1155
2.377	0.4678	3.743	1.2770
2.487	0.5159	3.866	1.4218
2.598	0.5506	3.987	1.5565
2.707	0.6019		

Run 31, 31.03 cc ^{4}He @ 1.0 Hz

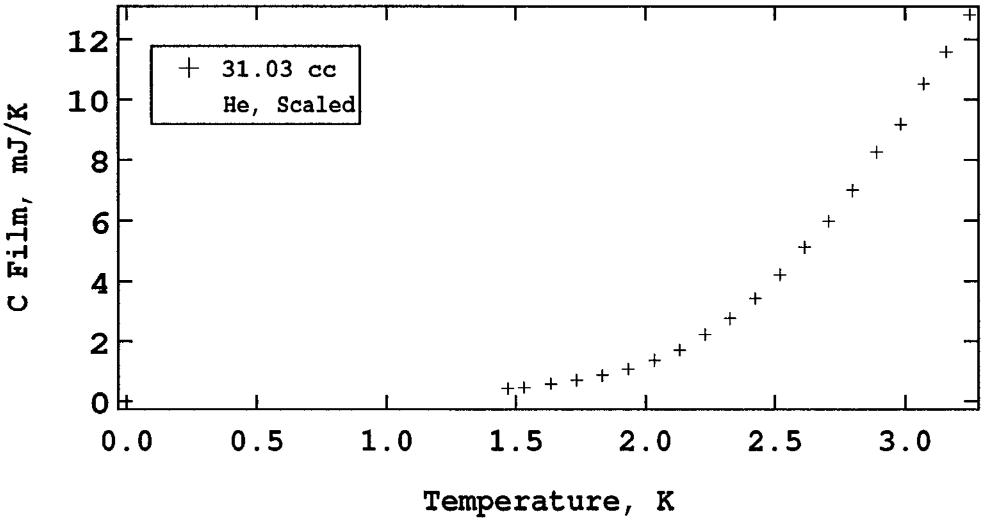

T (K)	C (mJ/K)
1.470	0.4199
1.532	0.4557
1.634	0.5828
1.734	0.6982
1.834	0.8649
1.933	1.0854
2.036	1.3763
2.134	1.7102
2.231	2.2293
2.326	2.7419
2.426	3.4211
2.520	4.2206
2.614	5.1303
2.708	5.9850
2.801	6.9951
2.893	8.2522
2.984	9.1704
3.073	10.5190
3.160	11.5822
3.250	12.8316

Run 32, 3.46 cc ^{3}He @ 1.0 Hz

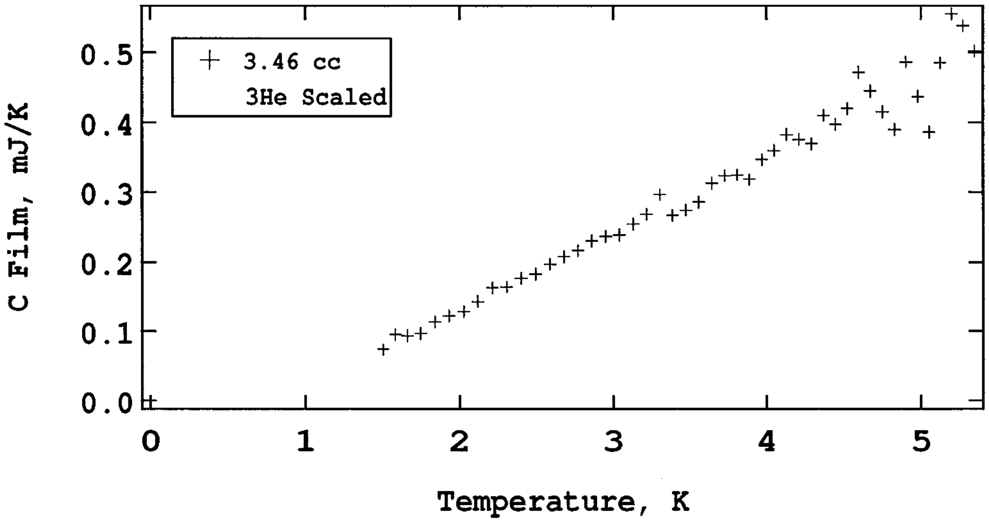

T (K)	C (mJ/K)	T (K)	C (mJ/K)	T (K)	C (mJ/K)
1.502	0.0737	2.952	0.2368	4.288	0.3697
1.583	0.0953	3.040	0.2385	4.366	0.4098
1.665	0.0942	3.128	0.2543	4.444	0.3968
1.751	0.0972	3.215	0.2682	4.522	0.4195
1.841	0.1142	3.301	0.2959	4.599	0.4712
1.932	0.1225	3.387	0.2669	4.676	0.4445
2.025	0.1291	3.474	0.2739	4.752	0.4148
2.118	0.1432	3.558	0.2857	4.828	0.3898
2.215	0.1630	3.641	0.3130	4.903	0.4858
2.309	0.1642	3.724	0.3237	4.978	0.4365
2.402	0.1772	3.806	0.3250	5.053	0.3865
2.495	0.1830	3.888	0.3183	5.127	0.4847
2.587	0.1972	3.969	0.3470	5.201	0.5554
2.679	0.2077	4.050	0.3602	5.275	0.5381
2.770	0.2167	4.130	0.3827	5.348	0.5017
2.862	0.2307	4.209	0.3758		

Run 33, 8.15 cc ^{3}He @ 1.0 Hz

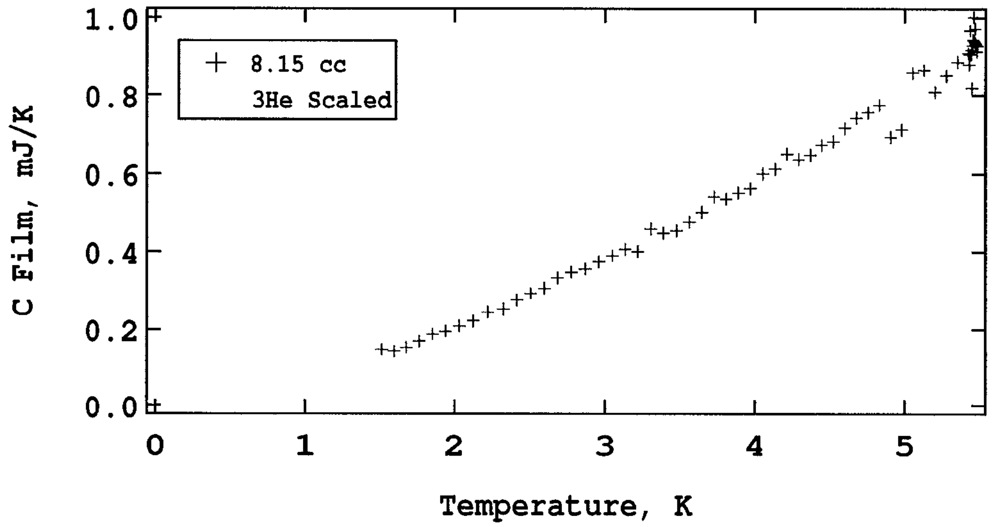

T (K)	C (mJ/K)	T (K)	C (mJ/K)	T (K)	C (mJ/K)
1.516	0.1464	3.392	0.4487	5.053	0.8572
1.596	0.1418	3.478	0.4547	5.128	0.8643
1.676	0.1521	3.562	0.4761	5.201	0.8081
1.762	0.1688	3.645	0.5015	5.275	0.8499
1.850	0.1867	3.728	0.5416	5.348	0.8853
1.941	0.1950	3.810	0.5356	5.421	0.9084
2.032	0.2089	3.891	0.5514	5.425	0.8792
2.125	0.2224	3.972	0.5623	5.429	0.9049
2.221	0.2446	4.054	0.6004	5.434	0.9673
2.323	0.2522	4.132	0.6117	5.437	0.9054
2.415	0.2748	4.212	0.6500	5.441	0.9179
2.507	0.2926	4.290	0.6357	5.445	0.8186
2.598	0.3062	4.369	0.6470	5.448	0.9285
2.689	0.3326	4.446	0.6728	5.452	0.9431
2.779	0.3471	4.524	0.6809	5.457	1.0022
2.871	0.3557	4.601	0.7146	5.461	0.9379
2.959	0.3743	4.677	0.7421	5.465	0.9720
3.048	0.3899	4.753	0.7560	5.469	0.9338
3.135	0.4062	4.829	0.7743	5.472	0.9294
3.221	0.4006	4.904	0.6929	5.476	0.9122
3.307	0.4585	4.979	0.7115	5.480	0.9268

Run 34, 15.68 cc ^{3}He @ 1.0 Hz

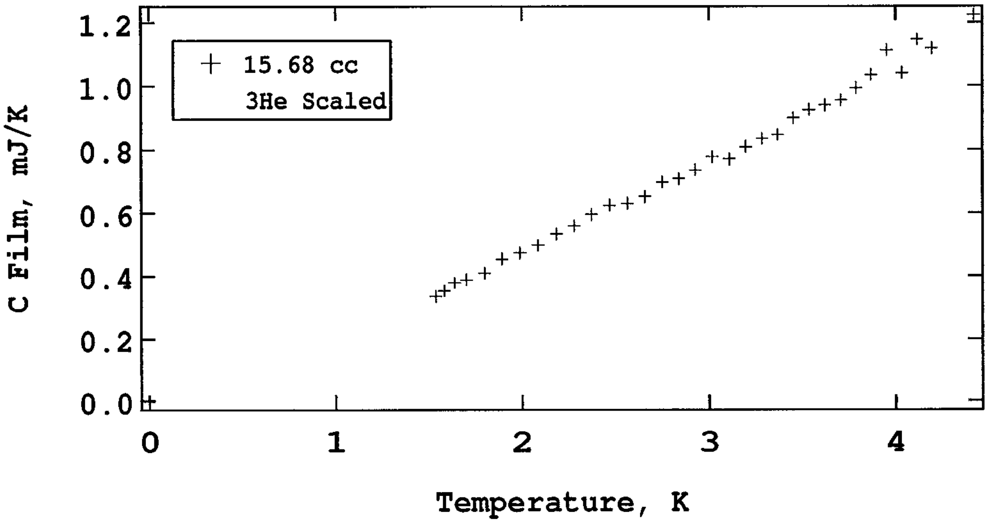

T (K)	C (mJ/K)	T (K)	C (mJ/K)
1.536	0.3343	3.019	0.7764
1.581	0.3521	3.108	0.7700
1.635	0.3789	3.196	0.8082
1.698	0.3876	3.283	0.8341
1.797	0.4095	3.370	0.8464
1.892	0.4542	3.455	0.8995
1.988	0.4750	3.539	0.9254
2.084	0.4985	3.623	0.9401
2.180	0.5347	3.707	0.9559
2.276	0.5602	3.790	0.9930
2.372	0.5961	3.872	1.0349
2.468	0.6248	3.954	1.1120
2.562	0.6296	4.035	1.0412
2.655	0.6514	4.115	1.1465
2.747	0.6976	4.194	1.1181
2.838	0.7088	4.420	1.2252
2.928	0.7351		

Run 35, 19.49 cc ^{3}He @ 1.0 Hz

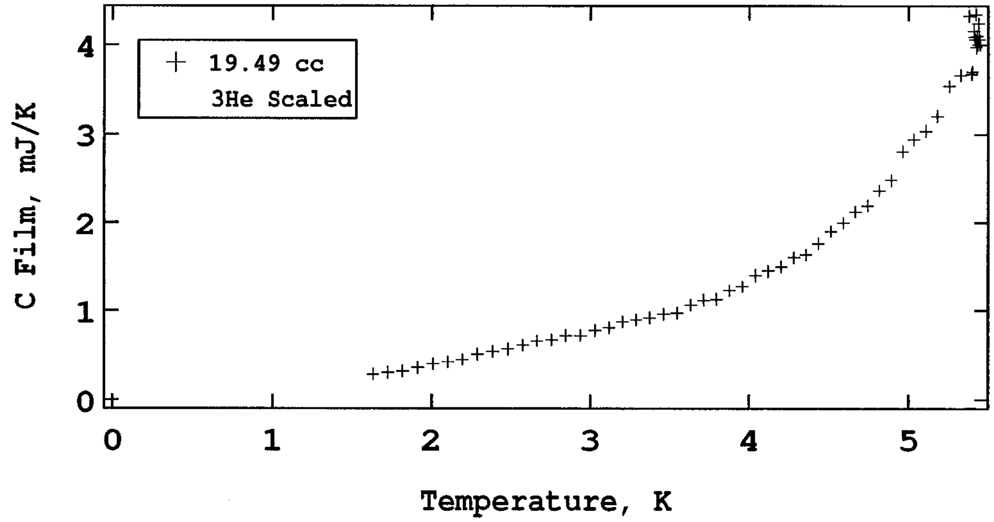

T (K)	C (mJ/K)
1.636	0.2865
1.729	0.3079
1.820	0.3250
1.914	0.3623
2.008	0.4047
2.102	0.4228
2.197	0.4516
2.292	0.5109
2.389	0.5428
2.482	0.5692
2.575	0.6107
2.667	0.6592
2.759	0.6723
2.849	0.7182
2.939	0.7204
3.030	0.7791
3.118	0.8085
3.205	0.8762
3.291	0.8965
3.377	0.9215
3.462	0.9637
3.547	0.9732
3.631	1.0675
3.714	1.1212
3.796	1.1281
3.878	1.2289
3.959	1.2772
4.040	1.4054
4.119	1.4549
4.199	1.5004
4.278	1.6040
4.356	1.6335
4.435	1.7594
4.513	1.9010
4.589	1.9956
4.663	2.1205
4.739	2.1909
4.813	2.3594
4.888	2.4794
4.962	2.8098
5.034	2.9415
5.108	3.0358
5.179	3.1985
5.252	3.5389
5.324	3.6619
5.392	3.6724
5.378	4.3284
5.396	3.6967
5.406	4.1568
5.410	4.0950
5.414	4.0612
5.418	4.3438
5.422	3.9716
5.426	4.1002
5.430	4.0050
5.434	4.2425
5.439	4.0685
5.443	4.0005

Run 36, 0.0955 cc ^{4}He @ 0.1 Hz

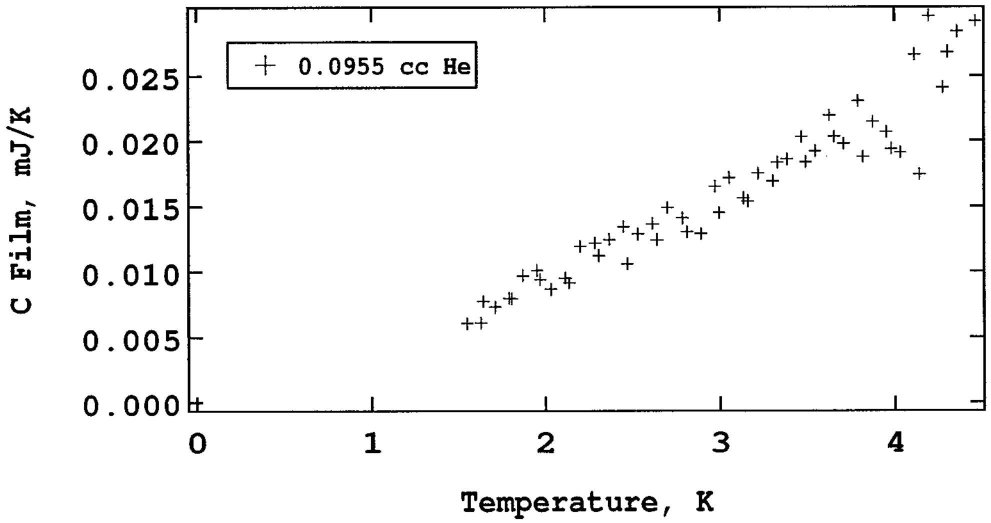

T (K)	C (mJ/K)
1.549	0.0061
1.628	0.0061
1.642	0.0077
1.708	0.0073
1.788	0.0080
1.804	0.0079
1.869	0.0097
1.950	0.0101
1.969	0.0094
2.033	0.0086
2.115	0.0095
2.136	0.0091
2.198	0.0119
2.281	0.0122
2.303	0.0112
2.364	0.0124
2.448	0.0134
2.471	0.0106
2.531	0.0129
2.615	0.0137
2.639	0.0124
2.699	0.0149
2.782	0.0141
2.807	0.0130
2.888	0.0129
2.970	0.0165
2.996	0.0145
3.053	0.0172
3.136	0.0156
3.161	0.0154
3.217	0.0175
3.300	0.0169
3.326	0.0183
3.383	0.0186
3.465	0.0203
3.491	0.0184
3.547	0.0192
3.628	0.0220
3.655	0.0203
3.710	0.0198
3.791	0.0231
3.819	0.0188
3.873	0.0215
3.954	0.0207
3.981	0.0194
4.035	0.0191
4.116	0.0266
4.143	0.0174
4.196	0.0296
4.276	0.0241
4.303	0.0268
4.356	0.0284
4.462	0.0291

Run 37, 0.22 cc ^{4}He @ 0.1 Hz

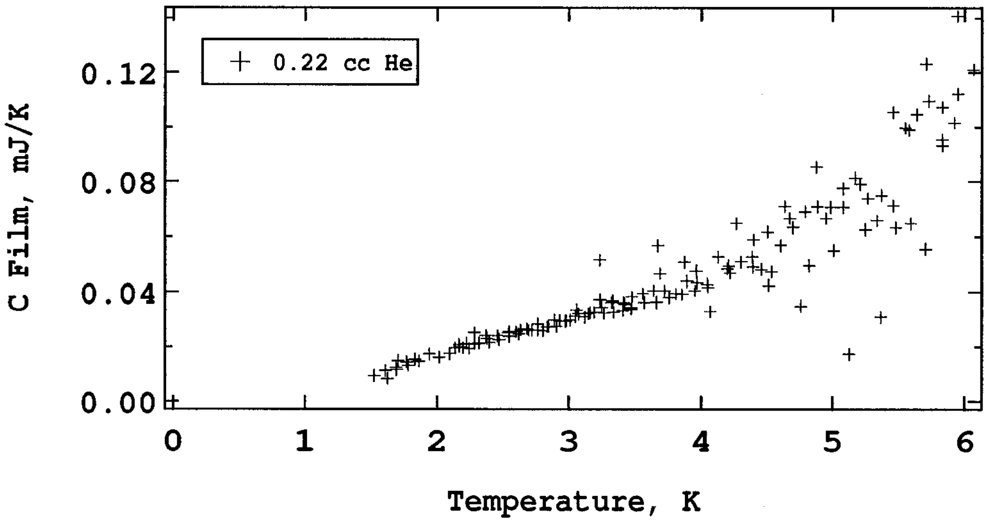

T (K)	C (mJ/K)
1.523	0.0093
1.609	0.0112
1.625	0.0083
1.690	0.0124
1.693	0.0115
1.706	0.0148
1.769	0.0143
1.779	0.0131
1.830	0.0153
1.858	0.0147
1.937	0.0173
2.014	0.0160
2.094	0.0174
2.137	0.0196
2.168	0.0209
2.170	0.0201
2.197	0.0196
2.226	0.0213
2.245	0.0193
2.285	0.0251
2.286	0.0211
2.316	0.0215
2.319	0.0212
2.370	0.0239
2.376	0.0230
2.396	0.0216
2.456	0.0239
2.457	0.0240
2.469	0.0227
2.539	0.0250
2.542	0.0237
2.542	0.0256
2.595	0.0255
2.615	0.0247
2.628	0.0262
2.678	0.0265
2.690	0.0260
2.715	0.0260
2.761	0.0284
2.762	0.0260
2.801	0.0259
2.834	0.0273
2.845	0.0272
2.888	0.0298
2.905	0.0275
2.928	0.0295
2.974	0.0293
2.978	0.0295
3.011	0.0298
3.049	0.0311
3.060	0.0335
3.074	0.0320
3.120	0.0309
3.146	0.0321
3.158	0.0324
3.190	0.0325
3.230	0.0516
3.233	0.0371
3.242	0.0344
3.263	0.0322

continued on next page

Run 37, 0.22 cc ^{4}He @ 0.1 Hz continued

T (K)	C (mJ/K)
3.318	0.0361
3.325	0.0367
3.334	0.0327
3.404	0.0332
3.409	0.0360
3.419	0.0355
3.467	0.0336
3.473	0.0344
3.476	0.0381
3.560	0.0393
3.568	0.0361
3.643	0.0405
3.665	0.0362
3.675	0.0567
3.691	0.0467
3.727	0.0405
3.761	0.0377
3.810	0.0393
3.856	0.0392
3.875	0.0507
3.893	0.0439
3.951	0.0405
3.961	0.0477
3.968	0.0435
4.044	0.0429
4.048	0.0419
4.068	0.0328
4.127	0.0527
4.199	0.0485
4.209	0.0495
4.218	0.0469
4.270	0.0648
4.305	0.0510
4.391	0.0527
4.396	0.0492
4.401	0.0588
4.460	0.0482
4.508	0.0617
4.514	0.0424
4.536	0.0474
4.602	0.0568
4.637	0.0709
4.673	0.0666
4.697	0.0634
4.757	0.0348
4.791	0.0691
4.821	0.0496
4.878	0.0852
4.885	0.0707
4.952	0.0666
4.990	0.0707
5.012	0.0549
5.082	0.0706
5.082	0.0775
5.129	0.0173
5.175	0.0814
5.210	0.0790
5.248	0.0626
5.268	0.0739
5.336	0.0657
5.365	0.0309
5.369	0.0749
5.460	0.1055
5.461	0.0712
5.480	0.0632
5.552	0.0998
5.583	0.0989
5.595	0.0648
5.644	0.1047
5.708	0.0555
5.714	0.1232
5.734	0.1096
5.832	0.0954
5.834	0.1074
5.834	0.0932
5.922	0.1016
5.947	0.1409
5.950	0.1121
6.067	0.1212

Run 38, 0.441 cc ^{4}He @ 0.1 Hz

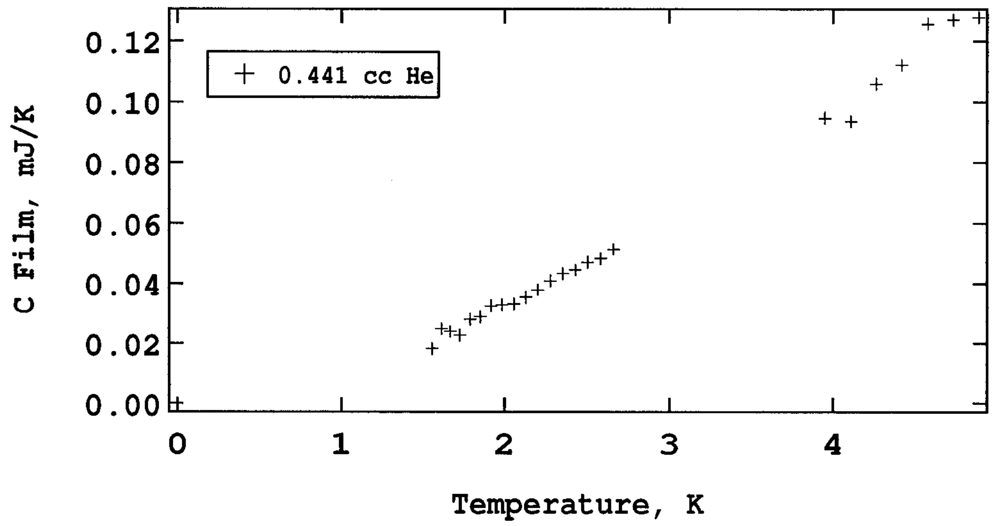

T (K)	C (mJ/K)	T (K)	C (mJ/K)
1.557	0.0182	2.352	0.0432
1.614	0.0249	2.429	0.0445
1.668	0.0240	2.506	0.0470
1.726	0.0227	2.587	0.0482
1.787	0.0280	2.666	0.0514
1.850	0.0289	3.953	0.0946
1.916	0.0325	4.109	0.0935
1.984	0.0329	4.266	0.1060
2.058	0.0332	4.422	0.1121
2.129	0.0354	4.578	0.1259
2.202	0.0379	4.734	0.1272
2.277	0.0410	4.889	0.1281

Run 39, 1.11 cc ^{4}He @ 0.1 Hz

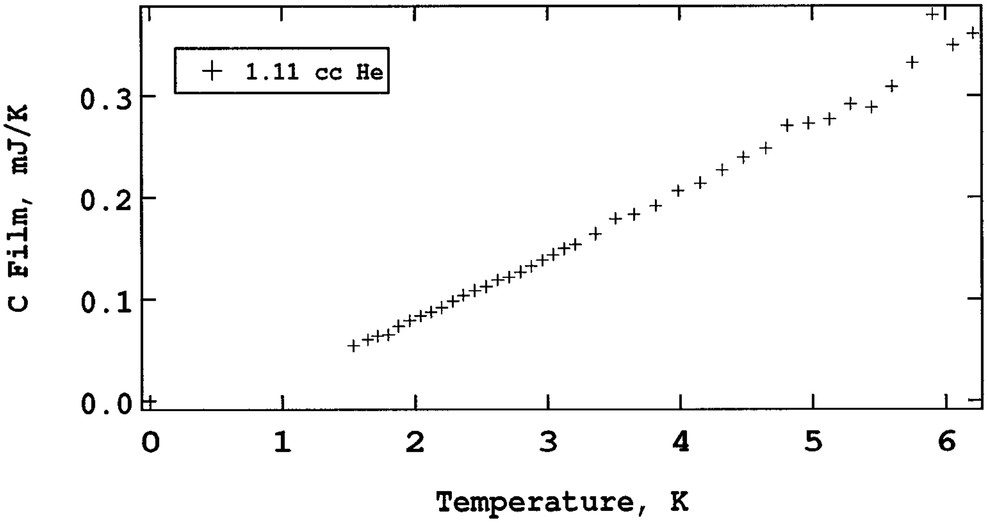

T (K)	C (mJ/K)	T (K)	C (mJ/K)
1.534	0.0545	3.209	0.1537
1.645	0.0606	3.358	0.1641
1.722	0.0643	3.508	0.1790
1.800	0.0654	3.651	0.1832
1.877	0.0738	3.817	0.1918
1.960	0.0793	3.985	0.2063
2.040	0.0841	4.151	0.2144
2.121	0.0875	4.316	0.2270
2.202	0.0922	4.480	0.2392
2.288	0.0983	4.648	0.2483
2.370	0.1039	4.810	0.2706
2.454	0.1087	4.972	0.2727
2.537	0.1125	5.131	0.2768
2.623	0.1186	5.288	0.2921
2.706	0.1216	5.444	0.2886
2.789	0.1267	5.598	0.3090
2.873	0.1320	5.753	0.3322
2.959	0.1384	5.905	0.3798
3.042	0.1436	6.056	0.3494
3.126	0.1496	6.207	0.3611

Run 40, 1.6 cc ^{4}He @ 0.1 Hz

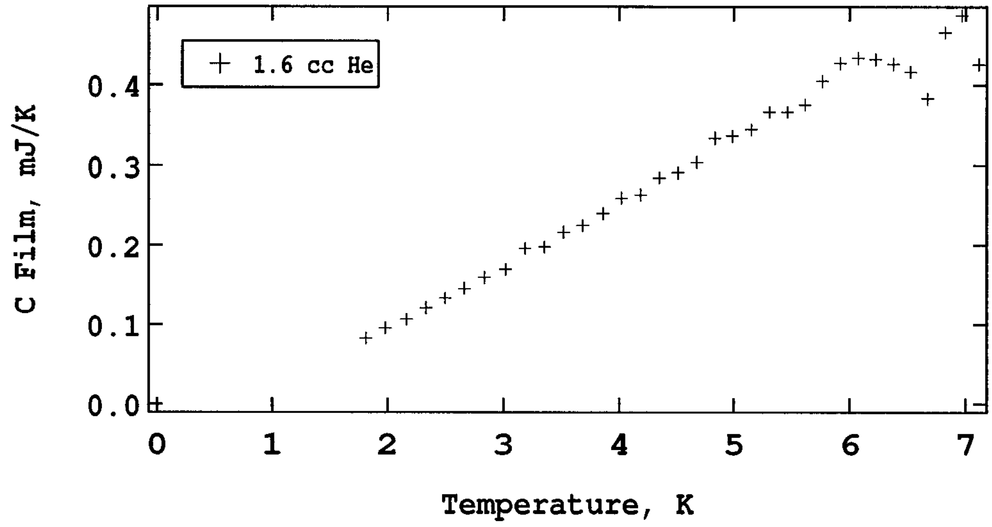

T (K)	C (mJ/K)	T (K)	C (mJ/K)
1.814	0.0824	4.674	0.3040
1.979	0.0956	4.834	0.3331
2.159	0.1065	4.987	0.3362
2.328	0.1208	5.150	0.3441
2.497	0.1330	5.306	0.3659
2.666	0.1458	5.461	0.3659
2.836	0.1592	5.615	0.3751
3.017	0.1690	5.767	0.4049
3.186	0.1963	5.921	0.4266
3.356	0.1979	6.073	0.4328
3.526	0.2163	6.224	0.4313
3.689	0.2251	6.381	0.4253
3.861	0.2400	6.529	0.4158
4.020	0.2593	6.676	0.3827
4.189	0.2632	6.822	0.4648
4.352	0.2846	6.966	0.4863
4.513	0.2913	7.111	0.4251

Run 41, 2.34 cc ^{4}He @ 0.1 Hz

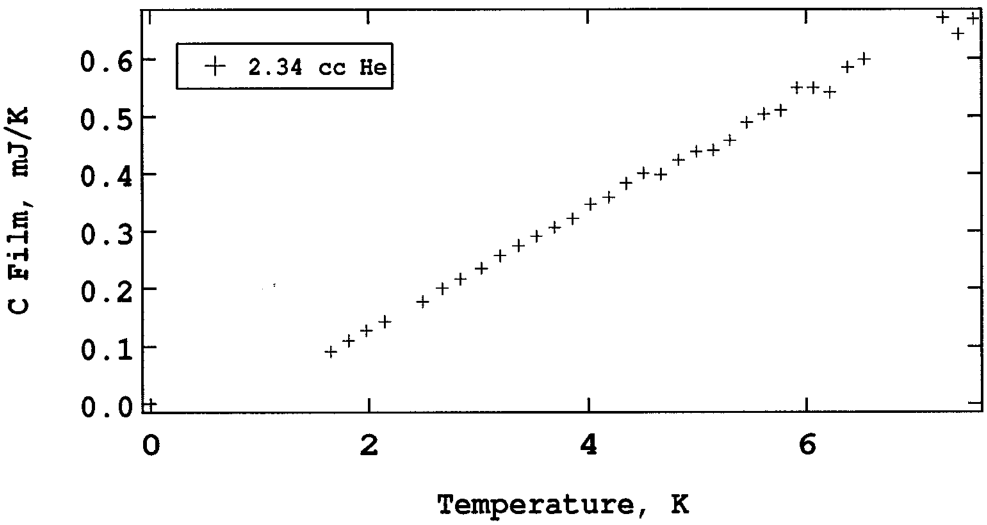

T (K)	C (mJ/K)	T (K)	C (mJ/K)
1.642	0.0913	4.671	0.3982
1.807	0.1099	4.831	0.4235
1.974	0.1275	4.993	0.4384
2.144	0.1434	5.151	0.4411
2.484	0.1775	5.306	0.4585
2.664	0.2000	5.460	0.4897
2.834	0.2165	5.614	0.5030
3.025	0.2350	5.766	0.5101
3.192	0.2568	5.918	0.5489
3.360	0.2745	6.069	0.5492
3.527	0.2906	6.222	0.5413
3.693	0.3060	6.380	0.5844
3.859	0.3211	6.528	0.5990
4.023	0.3472	7.249	0.6719
4.187	0.3585	7.387	0.6427
4.350	0.3830	7.525	0.6696
4.510	0.4004		

Run 42, 8.45 cc ^{4}He @ 0.1 Hz

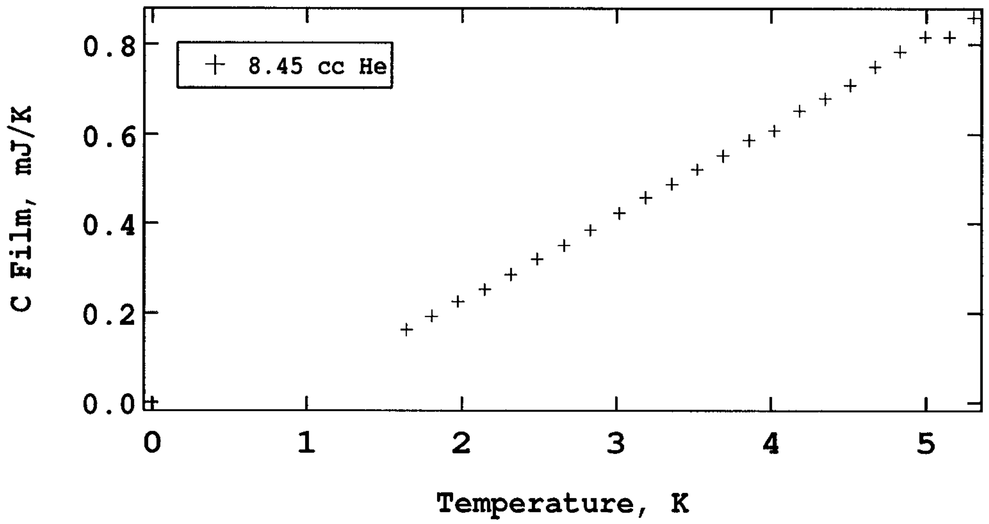

T (K)	C (mJ/K)
1.645	0.1625
1.809	0.1922
1.976	0.2250
2.146	0.2525
2.316	0.2862
2.486	0.3205
2.657	0.3505
2.828	0.3847
3.019	0.4231
3.188	0.4578
3.356	0.4881
3.524	0.5217

T (K)	C (mJ/K)
3.691	0.5527
3.857	0.5871
4.022	0.6087
4.187	0.6523
4.349	0.6793
4.511	0.7086
4.672	0.7486
4.833	0.7842
4.992	0.8163
5.150	0.8168
5.306	0.8602

Run 43, 11.96 cc ^{4}He @ 0.1 Hz

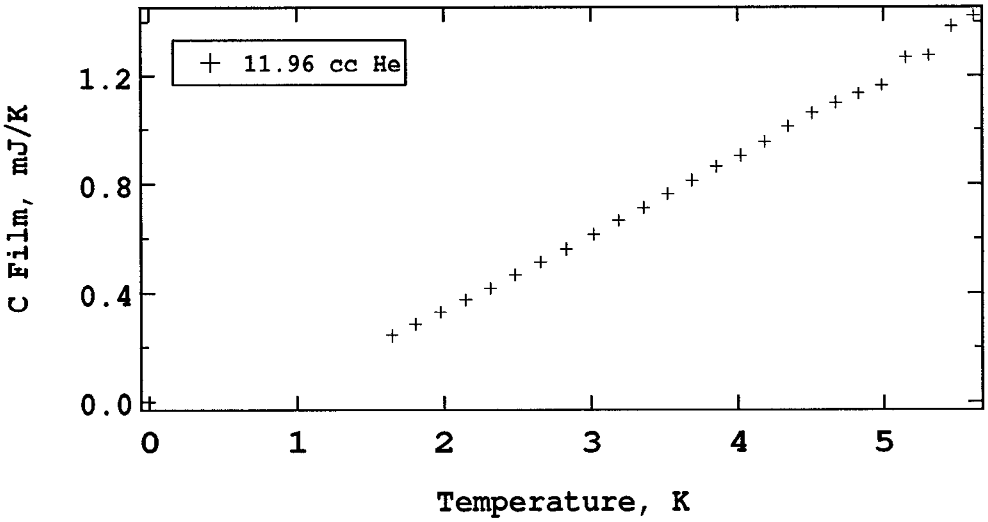

T (K)	C (mJ/K)
1.643	0.2439
1.807	0.2855
1.975	0.3299
2.145	0.3745
2.315	0.4172
2.485	0.4664
2.656	0.5137
2.827	0.5610
3.019	0.6147
3.187	0.6650
3.355	0.7118
3.523	0.7636
3.690	0.8130

T (K)	C (mJ/K)
3.856	0.8646
4.021	0.9038
4.185	0.9550
4.348	1.0110
4.510	1.0610
4.671	1.0979
4.831	1.1335
4.989	1.1645
5.148	1.2695
5.304	1.2763
5.461	1.3834
5.613	1.4227

Run 44, 16.19 cc ^{4}He @ 0.1 Hz

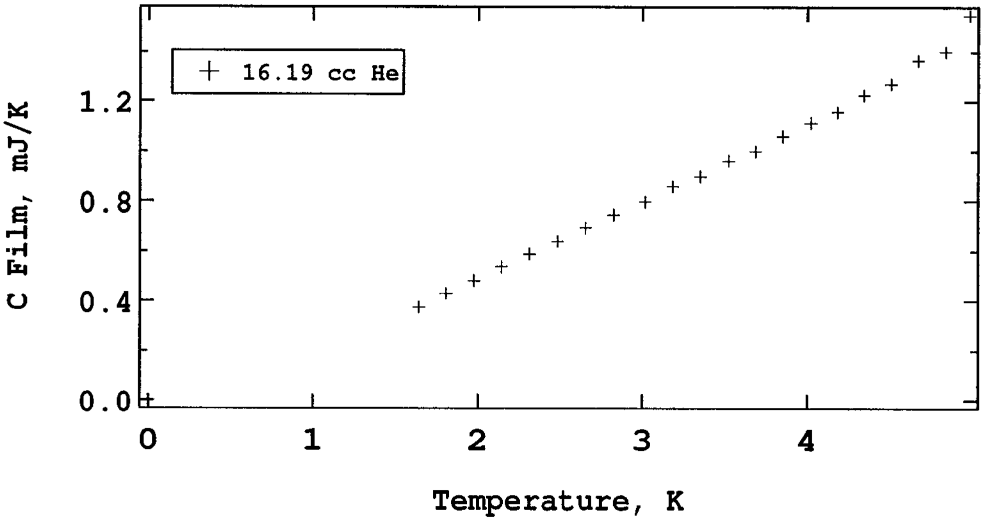

T (K)	C (mJ/K)
1.645	0.3743
1.808	0.4294
1.975	0.4822
2.145	0.5373
2.315	0.5887
2.486	0.6390
2.657	0.6929
2.828	0.7454
3.019	0.7974
3.187	0.8592
3.356	0.8984
3.524	0.9632
3.690	1.0003
3.857	1.0604
4.023	1.1136
4.186	1.1558
4.348	1.2242
4.511	1.2691
4.673	1.3657
4.842	1.4018
4.987	1.5473

Run 45, 21.8 cc ^{4}He @ 0.1 Hz

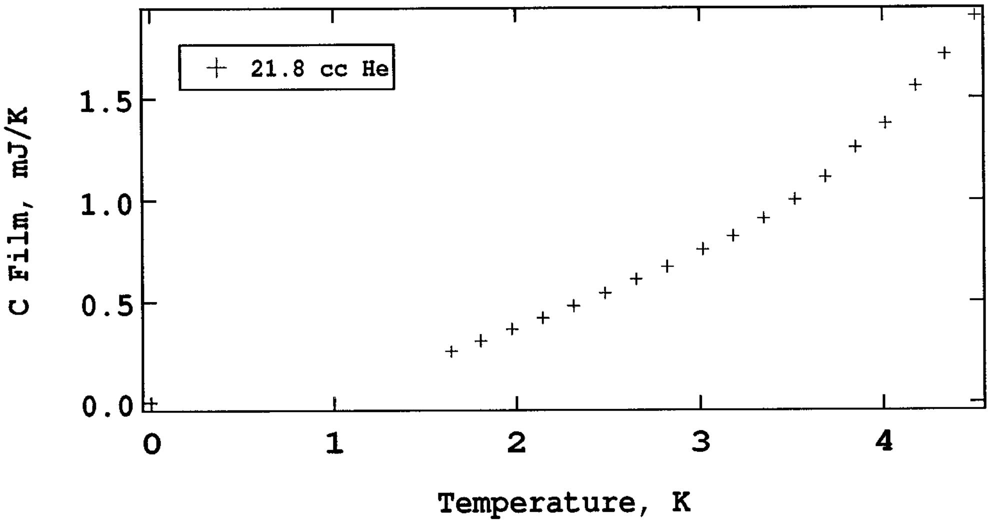

T (K)	C (mJ/K)
1.644	0.2519
1.807	0.3063
1.975	0.3634
2.144	0.4190
2.314	0.4787
2.484	0.5421
2.655	0.6100
2.826	0.6723
3.017	0.7551
3.184	0.8214
3.353	0.9080
3.521	1.0010
3.688	1.1116
3.854	1.2549
4.017	1.3725
4.182	1.5578
4.344	1.7146
4.505	1.9029

Run 46, 0.5 cc H_2 @ 0.1 Hz

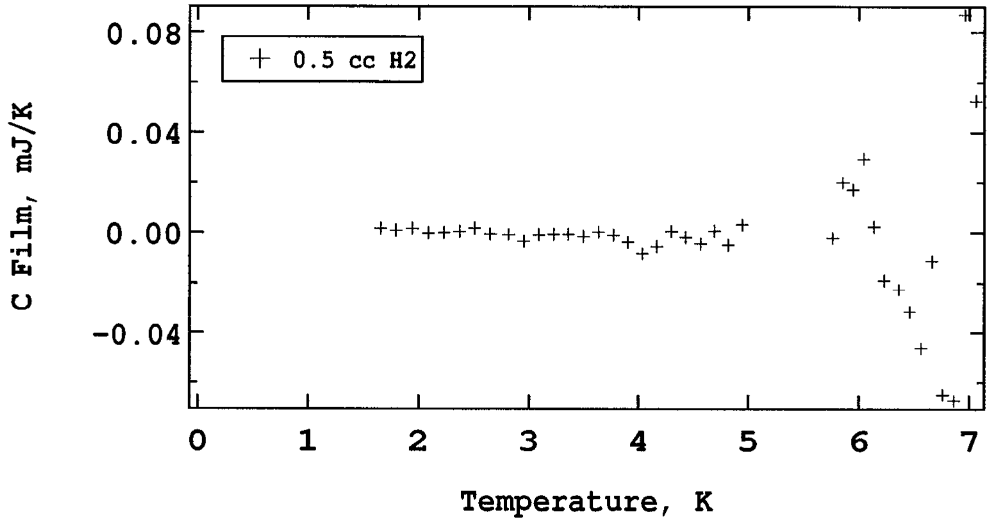

T (K)	C (mJ/K)	T (K)	C (mJ/K)
1.660	0.0015	4.431	-0.0020
1.797	0.0008	4.562	-0.0045
1.942	0.0016	4.691	0.0005
2.086	-0.0004	4.820	-0.0050
2.229	-0.0002	4.947	0.0029
2.372	0.0003	5.767	-0.0022
2.513	0.0016	5.860	0.0200
2.654	-0.0006	5.951	0.0171
2.817	-0.0009	6.043	0.0295
2.954	-0.0036	6.134	0.0022
3.092	-0.0010	6.229	-0.0188
3.229	-0.0008	6.362	-0.0225
3.365	-0.0008	6.461	-0.0316
3.501	-0.0017	6.565	-0.0462
3.636	0.0002	6.665	-0.0114
3.771	-0.0011	6.762	-0.0649
3.904	-0.0039	6.861	-0.0674
4.037	-0.0085	6.959	0.0870
4.169	-0.0056	7.058	0.0526
4.301	0.0004		

Run 47, 1.0 cc H_2 @ 0.1 Hz

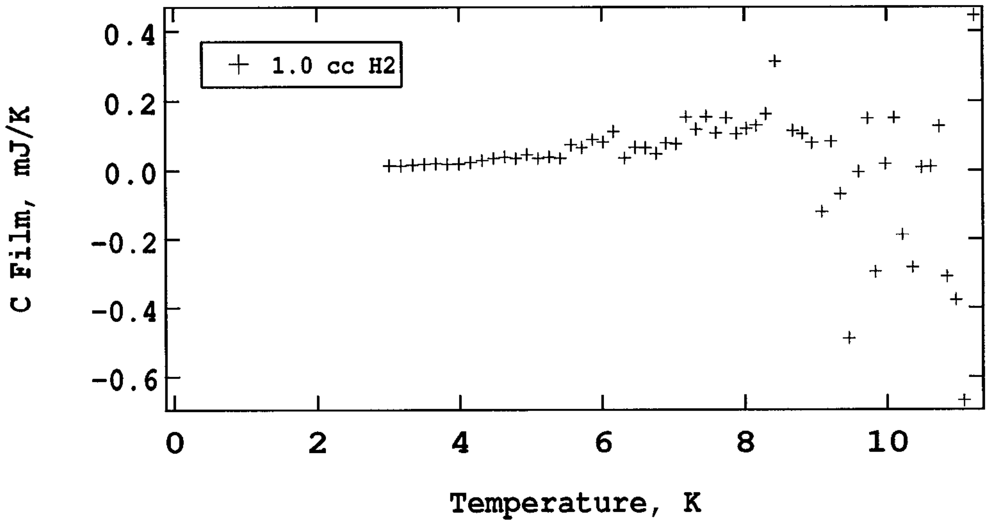

T (K)	C (mJ/K)
3.010	0.0150
3.175	0.0145
3.340	0.0164
3.505	0.0187
3.669	0.0207
3.833	0.0192
3.995	0.0200
4.157	0.0233
4.318	0.0287
4.477	0.0345
4.636	0.0389
4.794	0.0352
4.951	0.0458
5.106	0.0355
5.261	0.0386
5.414	0.0348
5.567	0.0736
5.718	0.0652
5.868	0.0876
6.018	0.0808
6.167	0.1113
6.323	0.0361
6.469	0.0660
6.614	0.0646
6.758	0.0486
6.900	0.0779
7.044	0.0759
7.186	0.1531
7.328	0.1179
7.468	0.1555
7.609	0.1074
7.747	0.1514
7.885	0.1047
8.023	0.1200
8.161	0.1293
8.298	0.1627
8.433	0.3132
8.687	0.1136
8.819	0.1047
8.952	0.0780
9.085	-0.1195
9.215	0.0824
9.343	-0.0676
9.456	-0.4878
9.599	-0.0049
9.726	0.1498
9.838	-0.2955
9.979	0.0186
10.104	0.1510
10.213	-0.1870
10.354	-0.2826
10.480	0.0085
10.603	0.0110
10.721	0.1261
10.828	-0.3098
10.956	-0.3765
11.068	-0.6690
11.218	0.4455

Run 48, 1.5 cc H_2 @ 0.1 Hz

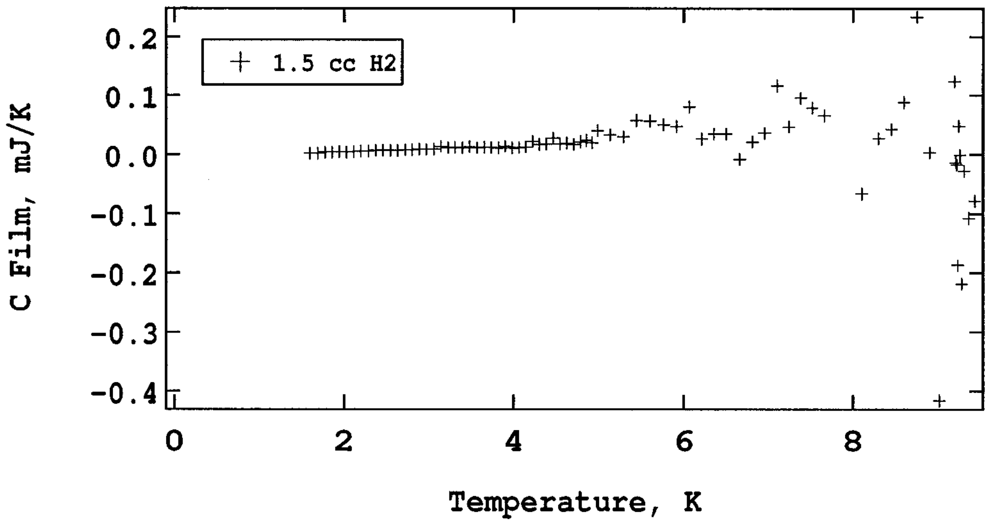

T (K)	C (mJ/K)
1.594	0.0022
1.684	0.0023
1.770	0.0038
1.855	0.0039
1.941	0.0045
2.030	0.0038
2.115	0.0045
2.201	0.0060
2.287	0.0059
2.375	0.0070
2.461	0.0072
2.546	0.0068
2.632	0.0072
2.720	0.0077
2.805	0.0084
2.890	0.0093
2.975	0.0088
3.062	0.0092
3.146	0.0138
3.231	0.0117
3.315	0.0123
3.399	0.0115
3.485	0.0133
3.568	0.0116
3.652	0.0124
3.735	0.0122
3.820	0.0112
3.902	0.0144
3.984	0.0113
4.066	0.0120
4.149	0.0131
4.230	0.0225
4.310	0.0175
4.390	0.0181
4.470	0.0282
4.549	0.0187
4.628	0.0194
4.707	0.0177
4.785	0.0219
4.856	0.0247
4.926	0.0202
4.992	0.0407
5.144	0.0337
5.302	0.0304
5.457	0.0579
5.611	0.0572
5.765	0.0508
5.917	0.0482
6.068	0.0805
6.219	0.0264
6.368	0.0352
6.515	0.0352
6.670	-0.0080
6.817	0.0216
6.959	0.0367
7.104	0.1167
7.247	0.0474
7.390	0.0952
7.532	0.0786
7.672	0.0658
8.104	-0.0662
8.304	0.0276
8.459	0.0430
8.610	0.0873
8.765	0.2353
8.910	0.0036
9.026	-0.4167
9.203	0.1236
9.219	-0.0133
9.232	-0.0168
9.244	-0.1870
9.256	0.0482
9.268	-0.0010
9.290	-0.2180
9.321	-0.0279
9.376	-0.1076
9.447	-0.0778

Run 49, 2.5 cc H_2 @ 0.1 Hz

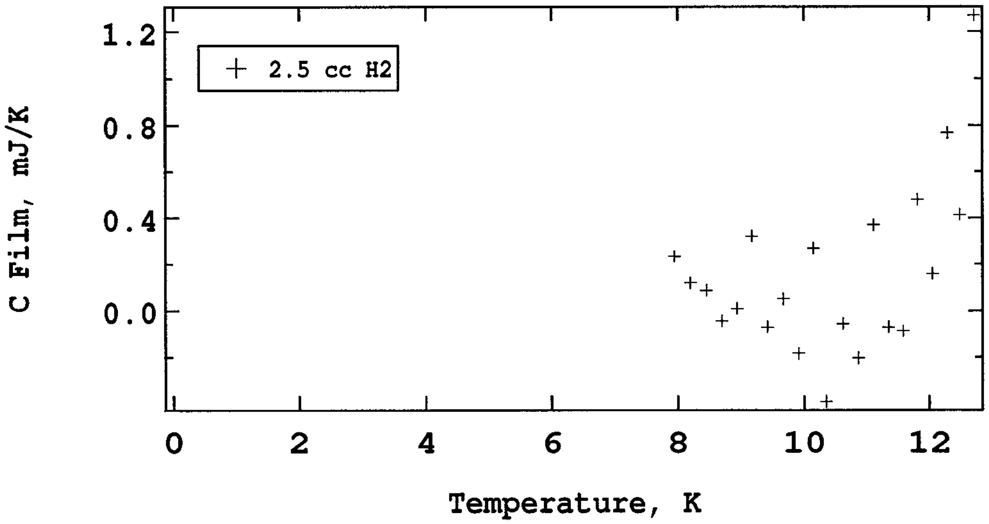

T (K)	C (mJ/K)
7.947	0.2350
8.195	0.1187
8.443	0.0864
8.688	-0.0451
8.934	0.0082
9.176	0.3222
9.421	-0.0727
9.671	0.0498
9.912	-0.1852
10.151	0.2701
10.357	-0.3885
10.624	-0.0571
10.866	-0.2042
11.105	0.3694
11.346	-0.0723
11.583	-0.0895
11.814	0.4796
12.045	0.1598
12.283	0.7675
12.471	0.4132
12.701	1.2690

Run 50, 2.5036 cc H_2 @ 0.1 Hz

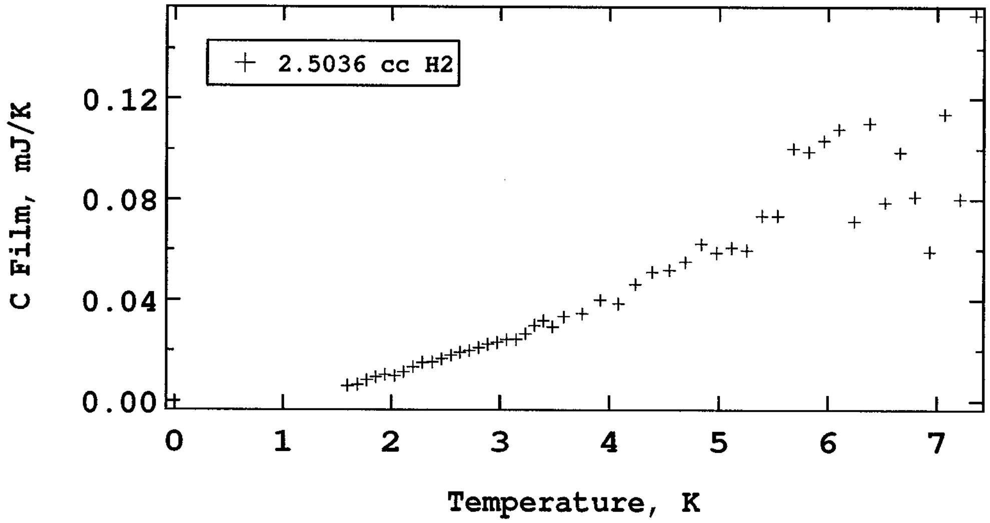

T (K)	C (mJ/K)
1.595	0.0060
1.685	0.0065
1.770	0.0082
1.855	0.0094
1.940	0.0104
2.029	0.0099
2.115	0.0114
2.200	0.0134
2.286	0.0151
2.374	0.0153
2.459	0.0167
2.545	0.0179
2.630	0.0192
2.718	0.0199
2.803	0.0212
2.888	0.0224
2.973	0.0231
3.060	0.0242
3.144	0.0244
3.228	0.0266
3.312	0.0299
3.397	0.0318
3.482	0.0294
3.588	0.0334
3.753	0.0347
3.917	0.0400
4.078	0.0386
4.238	0.0465
4.396	0.0515
4.553	0.0522
4.698	0.0553
4.839	0.0623
4.978	0.0590
5.119	0.0610
5.261	0.0600
5.400	0.0735
5.542	0.0735
5.683	0.1003
5.823	0.0991
5.964	0.1034
6.103	0.1081
6.244	0.0715
6.384	0.1104
6.522	0.0788
6.662	0.0987
6.800	0.0811
6.936	0.0594
7.073	0.1141
7.209	0.0802
7.346	0.1532

Run 51, 3.5 cc H_2 @ 0.1 Hz

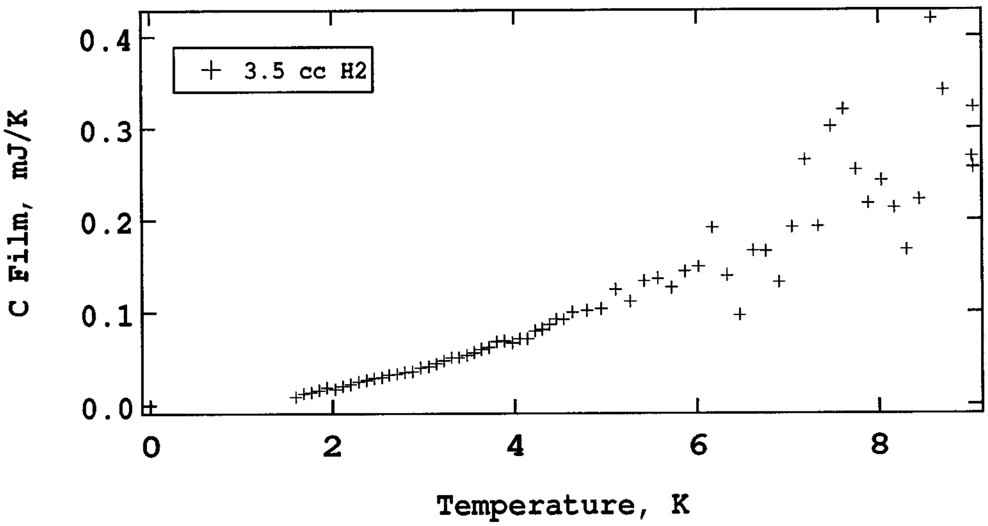

T (K)	C (mJ/K)	T (K)	C (mJ/K)	T (K)	C (mJ/K)
1.594	0.0091	3.559	0.0568	6.168	0.1906
1.684	0.0124	3.641	0.0605	6.323	0.1388
1.769	0.0138	3.724	0.0626	6.470	0.0965
1.854	0.0162	3.808	0.0680	6.616	0.1657
1.939	0.0189	3.891	0.0692	6.761	0.1654
2.028	0.0175	3.972	0.0670	6.905	0.1316
2.113	0.0205	4.054	0.0713	7.048	0.1916
2.198	0.0224	4.137	0.0714	7.191	0.2643
2.283	0.0250	4.217	0.0796	7.333	0.1923
2.371	0.0269	4.296	0.0813	7.474	0.3015
2.457	0.0290	4.376	0.0862	7.615	0.3198
2.542	0.0300	4.456	0.0924	7.754	0.2537
2.627	0.0329	4.534	0.0920	7.890	0.2174
2.714	0.0334	4.633	0.0998	8.030	0.2424
2.799	0.0357	4.791	0.1016	8.167	0.2125
2.884	0.0364	4.948	0.1036	8.302	0.1669
2.968	0.0405	5.105	0.1242	8.441	0.2215
3.055	0.0417	5.261	0.1112	8.577	0.4189
3.139	0.0448	5.416	0.1331	8.712	0.3404
3.223	0.0480	5.568	0.1360	9.019	0.2682
3.307	0.0513	5.719	0.1263	9.030	0.2567
3.391	0.0515	5.869	0.1432	9.032	0.2558
3.476	0.0538	6.019	0.1479	9.033	0.3220

Run 52, 4.5 cc H_2 @ 0.1 Hz

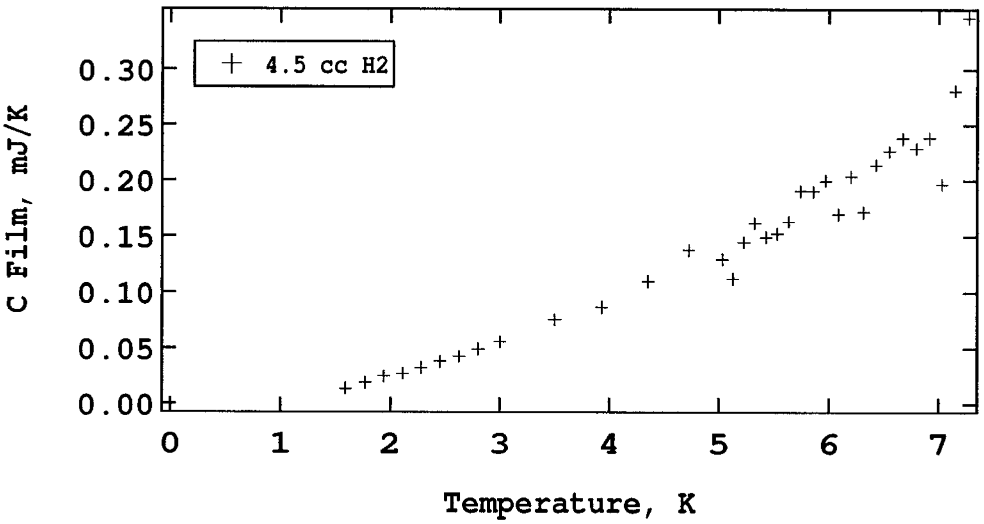

T (K)	C (mJ/K)	T (K)	C (mJ/K)
1.595	0.0135	5.430	0.1488
1.770	0.0188	5.535	0.1521
1.940	0.0247	5.641	0.1630
2.114	0.0269	5.752	0.1903
2.285	0.0321	5.863	0.1899
2.458	0.0378	5.974	0.1996
2.628	0.0424	6.090	0.1695
2.801	0.0490	6.205	0.2035
3.003	0.0556	6.320	0.1713
3.497	0.0757	6.438	0.2142
3.933	0.0865	6.557	0.2264
4.350	0.1096	6.675	0.2381
4.725	0.1372	6.796	0.2286
5.032	0.1294	6.915	0.2382
5.129	0.1122	7.033	0.1965
5.227	0.1447	7.156	0.2809
5.325	0.1615	7.277	0.3464

Run 53, 5.5 cc H_2 @ 0.1 Hz

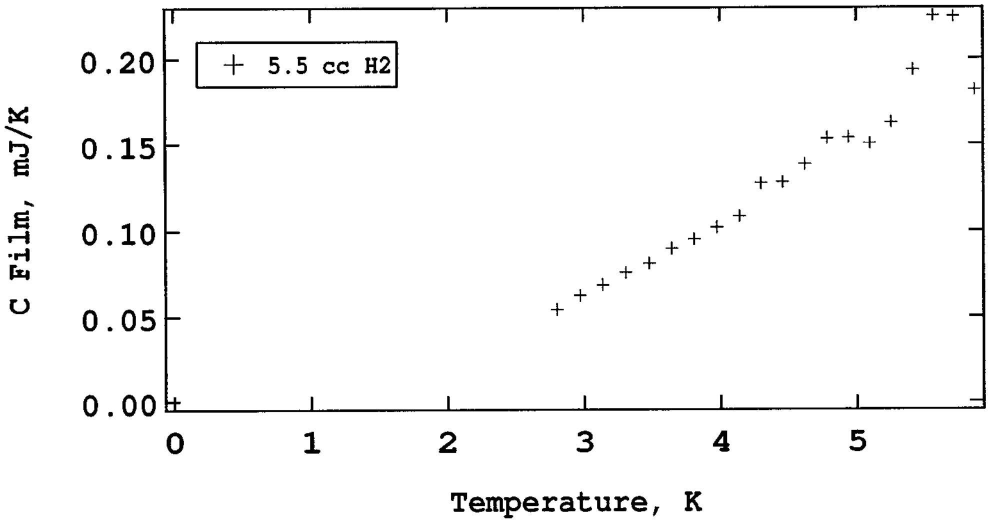

T (K)	C (mJ/K)
2.802	0.0542
2.971	0.0622
3.142	0.0684
3.310	0.0756
3.479	0.0809
3.645	0.0896
3.812	0.0951
3.976	0.1021
4.140	0.1083
4.302	0.1273
4.465	0.1279
4.624	0.1384
4.785	0.1535
4.943	0.1539
5.101	0.1504
5.257	0.1627
5.412	0.1934
5.564	0.2254
5.714	0.2249
5.867	0.1815

Run 54, 8.13 cc H_2 @ 0.1 Hz

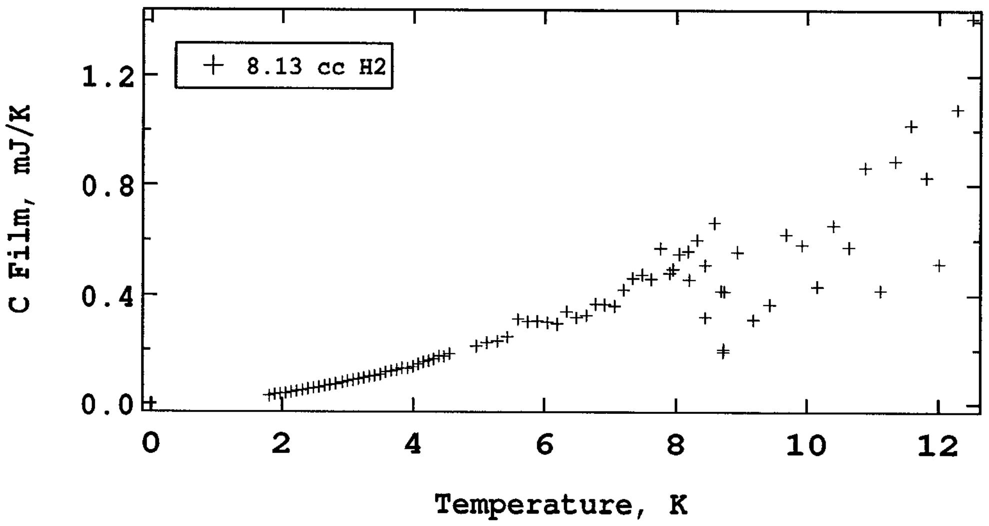

T (K)	C (mJ/K)	T (K)	C (mJ/K)	T (K)	C (mJ/K)	T (K)	C (mJ/K)
1.811	0.0294	3.584	0.1172	6.190	0.2946	8.692	0.4175
1.894	0.0341	3.666	0.1218	6.338	0.3411	8.718	0.1922
1.976	0.0370	3.748	0.1260	6.484	0.3179	8.729	0.2025
2.059	0.0386	3.830	0.1327	6.631	0.3267	8.741	0.4145
2.143	0.0423	3.912	0.1314	6.768	0.3689	8.939	0.5583
2.227	0.0466	3.994	0.1375	6.909	0.3664	9.184	0.3105
2.311	0.0503	4.075	0.1472	7.059	0.3618	9.430	0.3665
2.394	0.0544	4.156	0.1556	7.201	0.4209	9.680	0.6219
2.479	0.0574	4.236	0.1599	7.343	0.4641	9.921	0.5837
2.563	0.0612	4.316	0.1653	7.486	0.4760	10.160	0.4338
2.647	0.0664	4.397	0.1766	7.627	0.4608	10.404	0.6535
2.732	0.0691	4.476	0.1762	7.766	0.5712	10.639	0.5764
2.816	0.0737	4.556	0.1842	7.904	0.4821	10.880	0.8629
2.922	0.0789	4.964	0.2128	7.948	0.4963	11.115	0.4194
3.005	0.0840	5.121	0.2256	8.041	0.5508	11.348	0.8872
3.088	0.0881	5.276	0.2311	8.179	0.5610	11.585	1.0195
3.171	0.0921	5.428	0.2478	8.197	0.4591	11.820	0.8281
3.254	0.0956	5.590	0.3133	8.316	0.6012	12.007	0.5159
3.337	0.1009	5.742	0.3038	8.444	0.5102	12.281	1.0779
3.419	0.1033	5.893	0.3043	8.444	0.3204	12.514	1.4110
3.502	0.1083	6.042	0.3011	8.584	0.6629		

Run 55, 13.33 cc H_2 @ 0.1 Hz

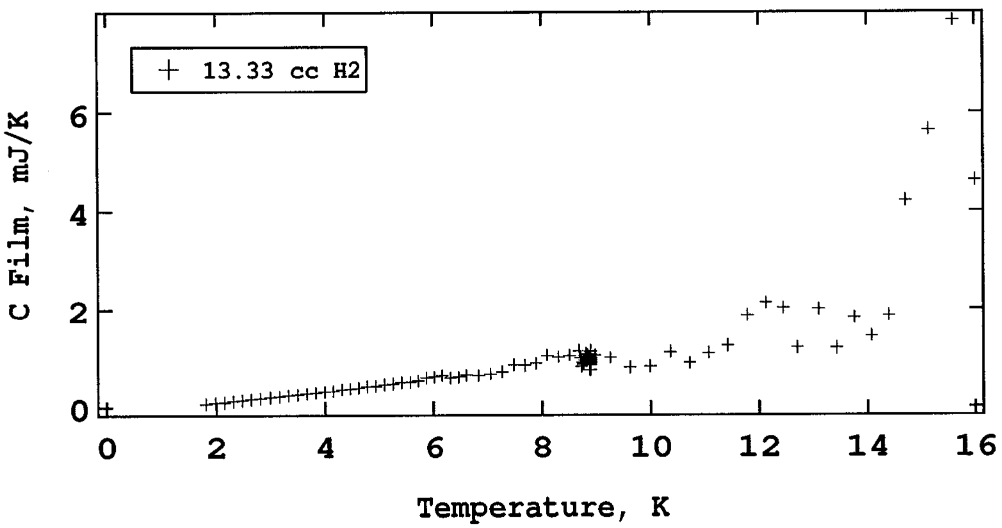

T (K)	C (mJ/K)	T (K)	C (mJ/K)	T (K)	C (mJ/K)
1.818	0.0687	5.102	0.4557	8.674	1.1487
1.981	0.0863	5.257	0.4713	8.706	0.9994
2.147	0.1012	5.412	0.4982	8.723	0.8224
2.314	0.1190	5.565	0.5055	8.737	0.8965
2.481	0.1391	5.716	0.5348	8.757	0.8631
2.649	0.1582	5.867	0.5899	8.774	0.9422
2.817	0.1762	6.017	0.6139	8.789	1.0020
3.005	0.1983	6.165	0.6416	8.804	1.0865
3.170	0.2166	6.321	0.5925	8.818	1.0274
3.335	0.2378	6.467	0.6091	8.832	1.0705
3.500	0.2516	6.613	0.6471	8.846	1.0358
3.665	0.2739	6.830	0.6383	8.861	1.0381
3.829	0.2917	7.043	0.6673	8.873	0.7512
3.991	0.3120	7.256	0.7167	8.873	0.8912
4.153	0.3247	7.469	0.8568	8.874	0.9493
4.313	0.3546	7.679	0.8460	8.875	0.8814
4.473	0.3773	7.887	0.8897	8.876	0.8820
4.632	0.3917	8.093	1.0536	8.877	0.9342
4.790	0.4198	8.296	1.0213	8.879	0.9878
4.946	0.4286	8.501	1.0538	8.880	1.0898

continued on next page

Run 55, 13.33 cc H_2 @ 0.1 Hz Continued

T (K)	C (mJ/K)
8.883	0.9010
8.883	1.0108
8.884	0.8830
8.884	0.8552
8.886	1.1456
8.887	0.9530
8.887	0.9997
8.888	0.9199
8.889	0.9103
8.890	0.7564
8.890	0.9571
8.890	0.9803
8.890	1.1521
8.891	0.8529
8.891	1.0613
8.891	0.9181
8.891	0.9540
8.968	1.0664
9.253	1.0060
9.621	0.8061
9.989	0.8232
10.355	1.1240
10.715	0.8957
11.071	1.1064
11.427	1.2485
11.785	1.8825
12.125	2.1316
12.447	2.0227
12.713	1.2080
13.112	1.9992
13.436	1.2038
13.761	1.8349
14.077	1.4413
14.398	1.8776
14.725	4.2248
15.141	5.6439
15.587	7.8699
15.987	4.6329

Run 56, 17.5 cc H_2 @ 0.1 Hz

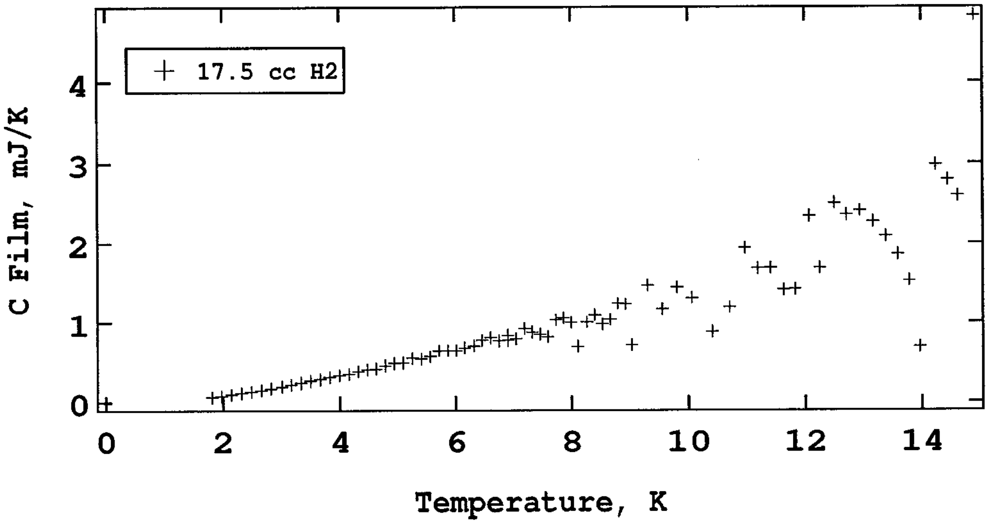

T (K)	C (mJ/K)	T (K)	C (mJ/K)	T (K)	C (mJ/K)	T (K)	C (mJ/K)
1.812	0.0611	4.946	0.4858	7.591	0.8195	10.976	1.9387
1.977	0.0775	5.102	0.4911	7.727	1.0328	11.197	1.6824
2.144	0.0938	5.257	0.5455	7.860	1.0540	11.414	1.6898
2.311	0.1128	5.411	0.5393	7.994	0.9983	11.638	1.4156
2.479	0.1336	5.564	0.5663	8.109	0.6979	11.831	1.4235
2.647	0.1518	5.715	0.6400	8.263	1.0019	12.069	2.3369
2.816	0.1727	5.865	0.6471	8.395	1.0897	12.256	1.6910
3.005	0.1944	6.015	0.6480	8.525	0.9766	12.513	2.4999
3.171	0.2185	6.163	0.6793	8.655	1.0336	12.726	2.3547
3.337	0.2422	6.318	0.7030	8.786	1.2410	12.952	2.4060
3.502	0.2646	6.465	0.7745	8.786	1.2410	13.170	2.2690
3.667	0.2829	6.611	0.8093	8.916	1.2306	13.384	2.0900
3.831	0.3103	6.755	0.7687	9.030	0.7115	13.587	1.8613
3.994	0.3303	6.898	0.8364	9.306	1.4694	13.783	1.5325
4.156	0.3480	6.906	0.7743	9.560	1.1660	13.971	0.6899
4.317	0.3818	7.043	0.7947	9.812	1.4442	14.249	2.9781
4.477	0.4071	7.182	0.9195	10.061	1.3121	14.450	2.7974
4.631	0.4148	7.318	0.8763	10.408	0.8787	14.623	2.5930
4.789	0.4517	7.454	0.8480	10.706	1.1913	14.902	4.8355

Run 57, 18.5 cc H_2 @ 0.1 Hz

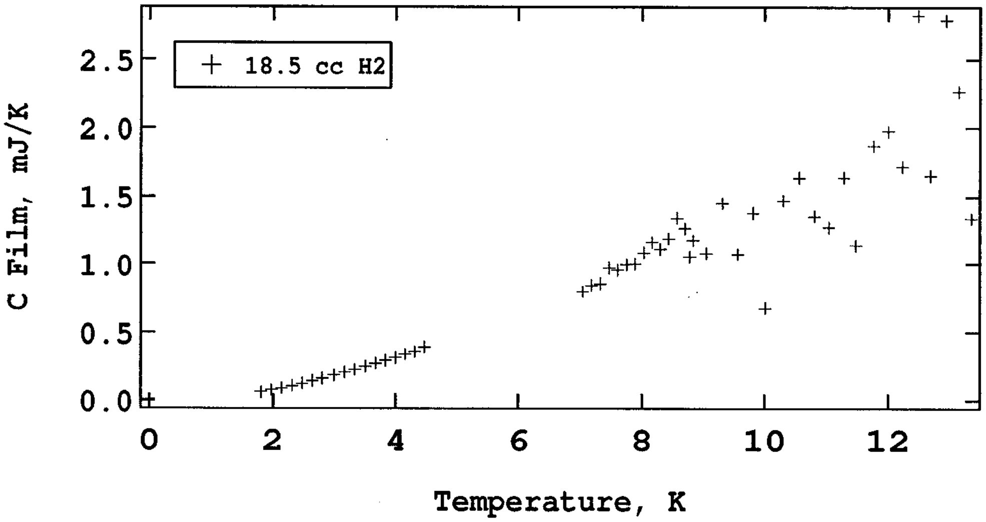

T (K)	C (mJ/K)	T (K)	C (mJ/K)	T (K)	C (mJ/K)
1.812	0.0566	7.046	0.8003	9.559	1.0723
1.977	0.0715	7.189	0.8468	9.812	1.3788
2.143	0.0857	7.332	0.8585	10.016	0.6777
2.310	0.1040	7.473	0.9733	10.305	1.4710
2.479	0.1208	7.612	0.9573	10.553	1.6388
2.647	0.1401	7.753	0.9968	10.797	1.3558
2.815	0.1590	7.886	0.9997	11.035	1.2715
3.004	0.1820	8.027	1.0838	11.289	1.6397
3.170	0.2029	8.166	1.1608	11.485	1.1378
3.335	0.2250	8.303	1.1106	11.773	1.8696
3.501	0.2473	8.438	1.1860	12.003	1.9753
3.665	0.2691	8.574	1.3395	12.229	1.7196
3.829	0.2897	8.708	1.2618	12.482	2.8217
3.993	0.3117	8.785	1.0543	12.690	1.6541
4.155	0.3381	8.840	1.1741	12.947	2.7852
4.316	0.3550	9.051	1.0774	13.152	2.2642
4.475	0.3922	9.307	1.4509	13.350	1.3366

Run 58, 19.47 cc H_2 @ 0.1 Hz

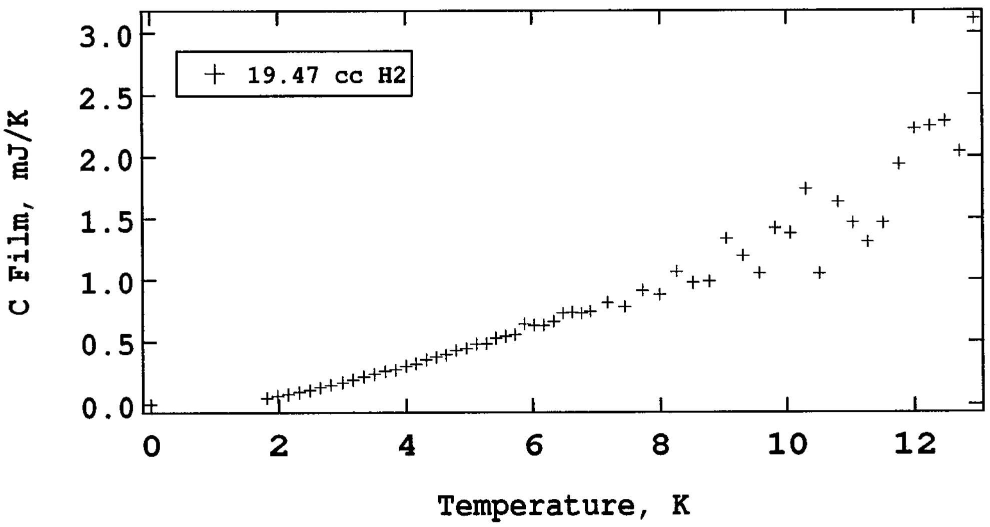

T (K)	C (mJ/K)
1.817	0.0508
1.981	0.0664
2.147	0.0799
2.314	0.0965
2.481	0.1127
2.649	0.1325
2.817	0.1523
3.005	0.1738
3.171	0.1931
3.337	0.2184
3.503	0.2377
3.667	0.2598
3.831	0.2739
3.994	0.3017
4.157	0.3202
4.317	0.3510
4.477	0.3749
4.636	0.3926
4.794	0.4275
4.951	0.4436
5.108	0.4807
5.263	0.4826
5.417	0.5275
5.570	0.5427
5.722	0.5561
5.871	0.6427
6.021	0.6312
6.169	0.6306
6.327	0.6621
6.473	0.7292
6.618	0.7355
6.762	0.7259
6.904	0.7405
6.906	0.7420
7.181	0.8150
7.455	0.7816
7.728	0.9136
7.996	0.8801
8.262	1.0657
8.525	0.9759
8.787	0.9861
9.053	1.3358
9.306	1.1948
9.562	1.0519
9.813	1.4205
10.063	1.3798
10.309	1.7368
10.512	1.0494
10.805	1.6295
11.037	1.4620
11.268	1.3071
11.519	1.4608
11.773	1.9385
12.006	2.2225
12.240	2.2456
12.475	2.2854
12.713	2.0384
12.940	3.1110

Run 59, 20.47 cc H_2 @ 0.1 Hz

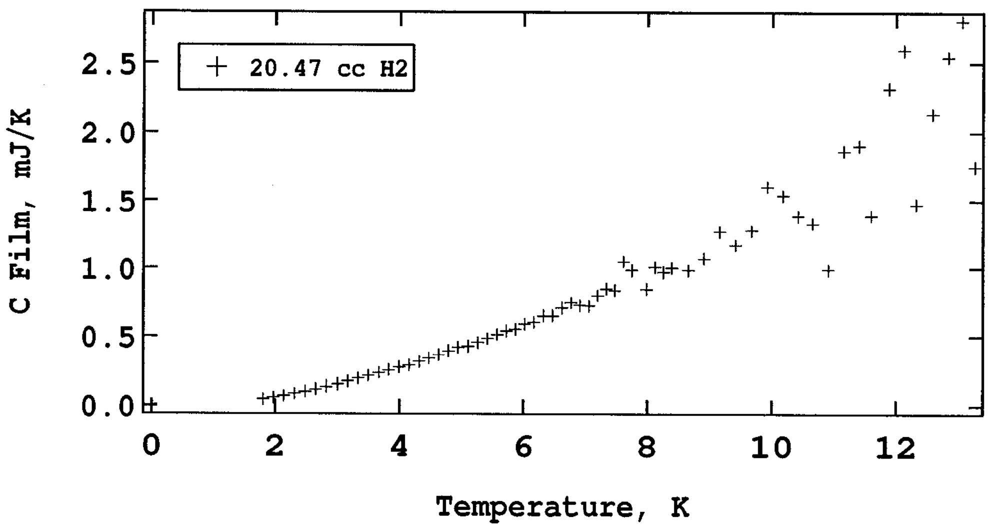

T (K)	C (mJ/K)	T (K)	C (mJ/K)	T (K)	C (mJ/K)
1.808	0.0421	5.262	0.4553	8.386	1.0033
1.974	0.0549	5.416	0.4846	8.646	0.9863
2.141	0.0670	5.569	0.5151	8.909	1.0725
2.309	0.0820	5.721	0.5421	9.170	1.2727
2.477	0.0969	5.869	0.5539	9.424	1.1721
2.646	0.1152	6.019	0.5933	9.676	1.2798
2.814	0.1337	6.168	0.6057	9.928	1.6050
3.004	0.1515	6.324	0.6533	10.176	1.5373
3.169	0.1727	6.471	0.6533	10.424	1.3876
3.336	0.1930	6.618	0.7108	10.666	1.3330
3.501	0.2141	6.767	0.7497	10.915	0.9916
3.666	0.2344	6.908	0.7295	11.158	1.8637
3.829	0.2557	7.051	0.7251	11.401	1.9023
3.992	0.2767	7.193	0.8047	11.597	1.3913
4.155	0.2903	7.335	0.8514	11.884	2.3209
4.316	0.3185	7.477	0.8410	12.126	2.5976
4.476	0.3415	7.617	1.0494	12.327	1.4736
4.636	0.3661	7.755	0.9856	12.590	2.1377
4.794	0.3937	7.989	0.8499	12.832	2.5465
4.951	0.4200	8.123	1.0073	13.055	2.8047
5.107	0.4274	8.255	0.9724	13.272	1.7529

Run 60, 21.47 cc H_2 @ 0.1 Hz

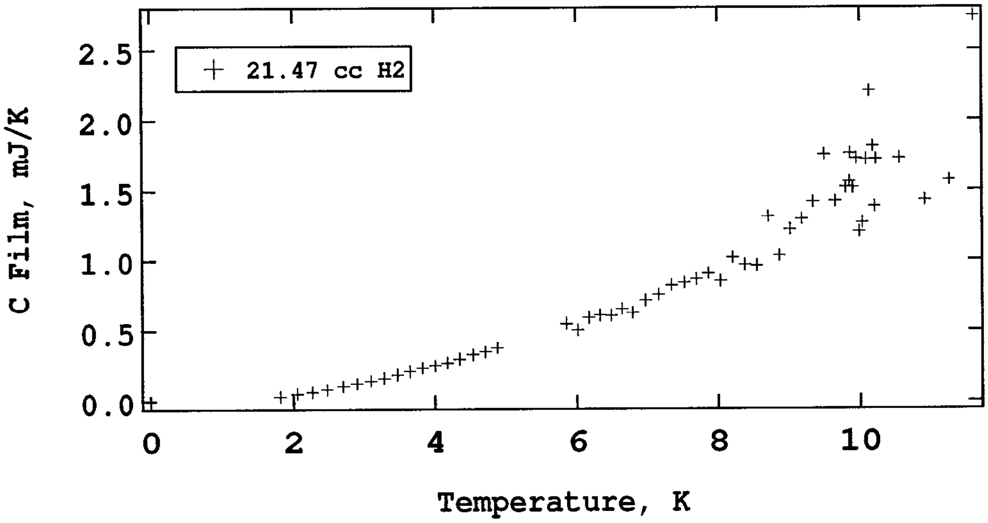

T (K)	C (mJ/K)
1.812	0.0335
2.049	0.0512
2.270	0.0656
2.480	0.0833
2.706	0.1059
2.901	0.1256
3.092	0.1447
3.280	0.1638
3.464	0.1882
3.646	0.2122
3.826	0.2355
4.004	0.2522
4.179	0.2728
4.353	0.3004
4.538	0.3291
4.707	0.3517
4.875	0.3792
5.853	0.5480
6.011	0.5046
6.167	0.5885
6.332	0.6073
6.487	0.6023
6.640	0.6494
6.791	0.6230
6.973	0.7134
7.154	0.7537
7.333	0.8203
7.518	0.8391
7.691	0.8642
7.863	0.9035
8.033	0.8509
8.202	1.0170
8.375	0.9639
8.540	0.9599
8.702	1.3102
8.862	1.0289
9.017	1.2180
9.181	1.2940
9.340	1.4166
9.497	1.7508
9.650	1.4223
9.801	1.5202
9.853	1.5599
9.857	1.7604
9.903	1.5180
9.950	1.7224
9.990	1.2044
10.037	1.2669
10.088	1.7162
10.141	2.2047
10.186	1.8129
10.211	1.3853
10.231	1.7192
10.562	1.7257
10.911	1.4290
11.257	1.5728
11.605	2.7388

Run 61, 22.47 cc H_2 @ 0.1 Hz

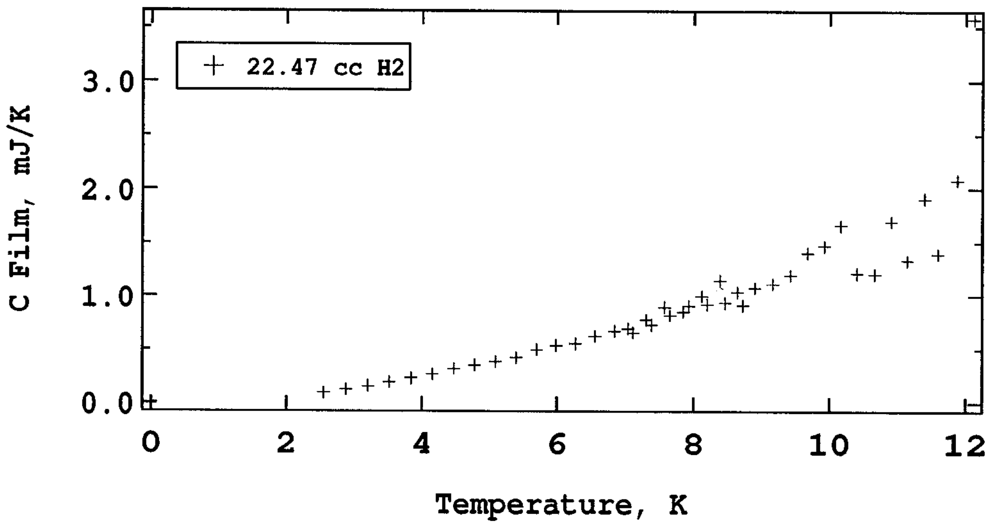

T (K)	C (mJ/K)	T (K)	C (mJ/K)	T (K)	C (mJ/K)
2.549	0.0897	7.036	0.6909	9.165	1.1117
2.872	0.1197	7.116	0.6540	9.421	1.1949
3.197	0.1531	7.311	0.7713	9.672	1.4059
3.520	0.1900	7.392	0.7261	9.922	1.4693
3.842	0.2247	7.584	0.8921	10.171	1.6623
4.156	0.2619	7.663	0.8161	10.409	1.2137
4.470	0.3147	7.851	0.8498	10.665	1.2035
4.785	0.3490	7.931	0.9053	10.909	1.6977
5.090	0.3817	8.119	0.9957	11.139	1.3327
5.391	0.4198	8.196	0.9185	11.397	1.9136
5.692	0.4975	8.383	1.1453	11.593	1.3946
5.985	0.5354	8.463	0.9326	11.880	2.0825
6.272	0.5537	8.644	1.0331	12.117	3.5761
6.557	0.6215	8.727	0.9099		
6.840	0.6669	8.905	1.0758		

Run 62, 23.47 cc H_2 @ 0.1 Hz

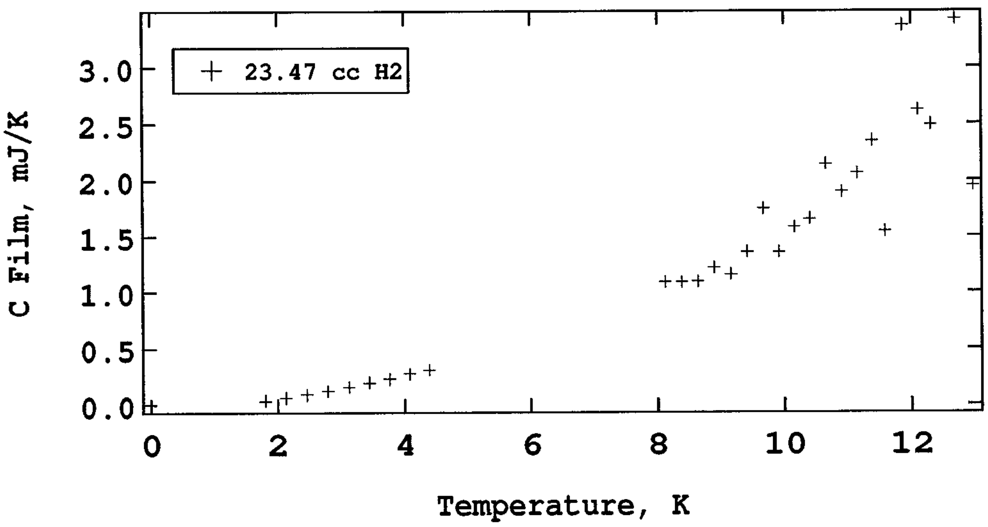

T (K)	C (mJ/K)
1.804	0.0342
2.127	0.0612
2.452	0.0894
2.779	0.1214
3.124	0.1569
3.445	0.1948
3.764	0.2276
4.080	0.2746
4.392	0.3089
8.117	1.0843
8.381	1.0847
8.641	1.0900
8.901	1.2143
9.161	1.1543
9.415	1.3541

T (K)	C (mJ/K)
9.667	1.7400
9.918	1.3550
10.166	1.5798
10.409	1.6536
10.663	2.1437
10.908	1.8926
11.149	2.0615
11.390	2.3461
11.588	1.5398
11.874	3.3617
12.111	2.6201
12.309	2.4880
12.698	3.4183
12.980	1.9504

Run 63, 24.47 cc H_2 @ 0.1 Hz

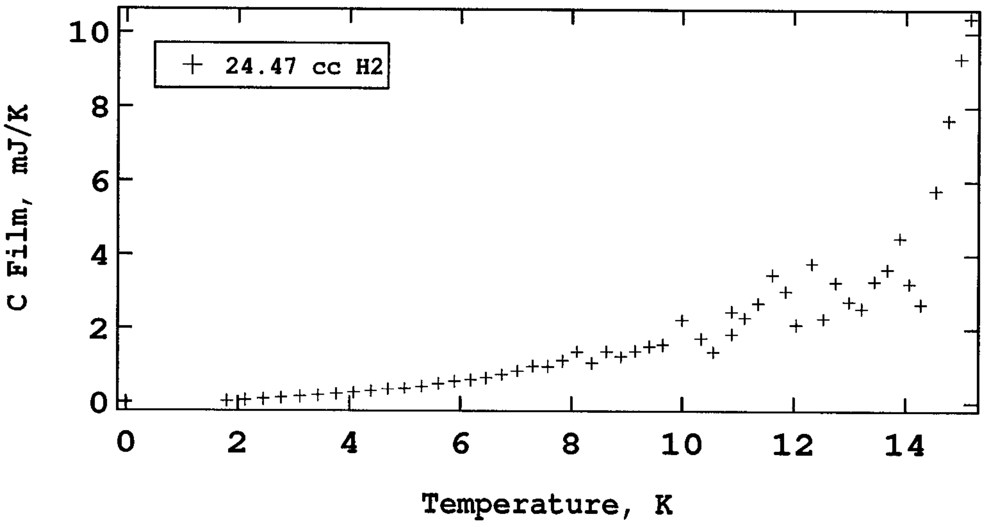

T (K)	C (mJ/K)
1.806	0.0322
2.128	0.0582
2.453	0.0875
2.779	0.1183
3.124	0.1538
3.445	0.1898
3.764	0.2271
4.080	0.2653
4.392	0.3063
4.700	0.3551
5.004	0.3789
5.306	0.4325
5.601	0.5100
5.892	0.5710
6.188	0.6079
6.471	0.6625
6.751	0.7582
7.026	0.8595
7.300	0.9888
7.571	0.9830
7.839	1.1371
8.105	1.3856
8.368	1.0709
8.630	1.3899
8.888	1.2530
9.151	1.4034
9.405	1.5263
9.653	1.5696
10.000	2.2350
10.339	1.7349
10.555	1.3780
10.888	1.8540
10.891	2.4640
11.133	2.2897
11.372	2.6867
11.616	3.4628
11.855	3.0187
12.042	2.1099
12.322	3.7723
12.533	2.2754
12.762	3.2661
12.997	2.7328
13.223	2.5550
13.449	3.2868
13.671	3.6084
13.896	4.4725
14.069	3.2260
14.276	2.6591
14.550	5.7445
14.776	7.6603
14.990	9.3124
15.152	10.3888

Run 64, 25.47 cc H_2 @ 0.1 Hz

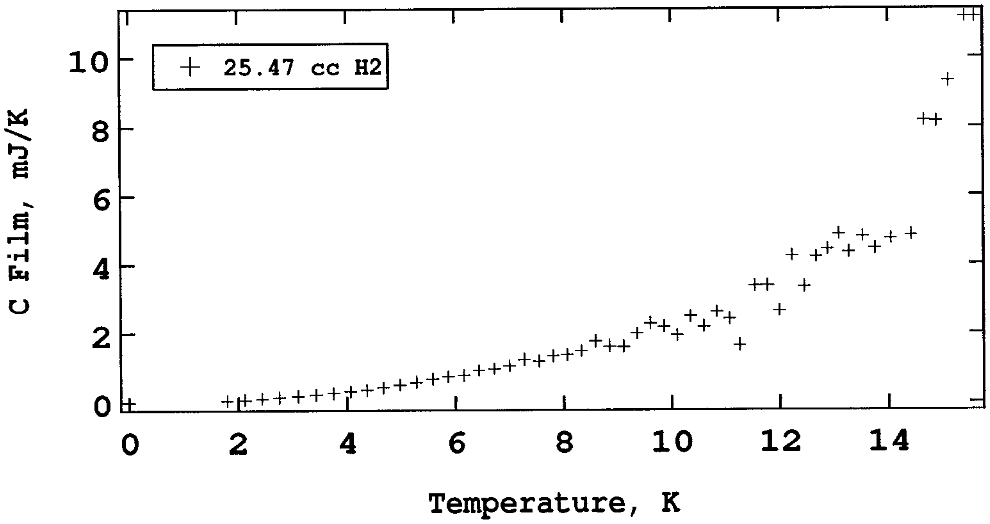

T (K)	C (mJ/K)
1.801	0.0456
2.121	0.0748
2.445	0.1083
2.770	0.1448
3.114	0.1836
3.433	0.2215
3.750	0.2631
4.064	0.3157
4.374	0.3518
4.680	0.4242
4.981	0.5018
5.279	0.5794
5.572	0.6726
5.861	0.7386
6.155	0.7685
6.438	0.9186
6.716	0.9688
6.990	1.0611
7.263	1.2325
7.533	1.1891
7.800	1.3371
8.064	1.3695
8.330	1.4844
8.589	1.7546
8.849	1.6202
9.108	1.6103
9.361	1.9810
9.613	2.2734
9.861	2.1799
10.105	1.9179
10.352	2.4756
10.594	2.1751
10.833	2.6091
11.075	2.4009
11.268	1.6501
11.548	3.3696
11.781	3.3771
11.990	2.6402
12.231	4.2402
12.448	3.3511
12.678	4.2133
12.891	4.4378
13.103	4.8770
13.280	4.3452
13.535	4.8059
13.755	4.4587
14.044	4.7404
14.427	4.8417
14.679	8.1729
14.901	8.1386
15.120	9.3045
15.416	11.1614
15.594	11.1639

Run 65, 26.47 cc H_2 @ 0.1 Hz

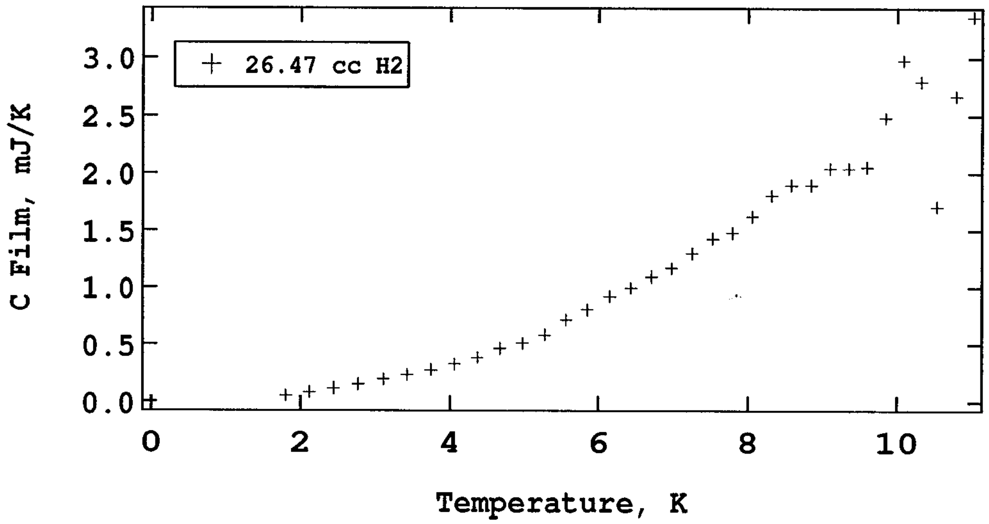

T (K)	C (mJ/K)	T (K)	C (mJ/K)
1.803	0.0524	6.981	1.1651
2.123	0.0814	7.256	1.2970
2.445	0.1148	7.526	1.4297
2.770	0.1511	7.794	1.4809
3.112	0.1938	8.060	1.6248
3.432	0.2317	8.323	1.8073
3.749	0.2757	8.583	1.8994
4.062	0.3268	8.842	1.8999
4.372	0.3862	9.099	2.0451
4.677	0.4653	9.349	2.0446
4.978	0.5142	9.598	2.0565
5.275	0.5846	9.843	2.4820
5.566	0.7168	10.083	2.9782
5.857	0.8033	10.324	2.7976
6.149	0.9194	10.537	1.7132
6.430	0.9960	10.795	2.6714
6.708	1.0919	11.024	3.3586

Background Heat Capacity @ 1.0 Hz

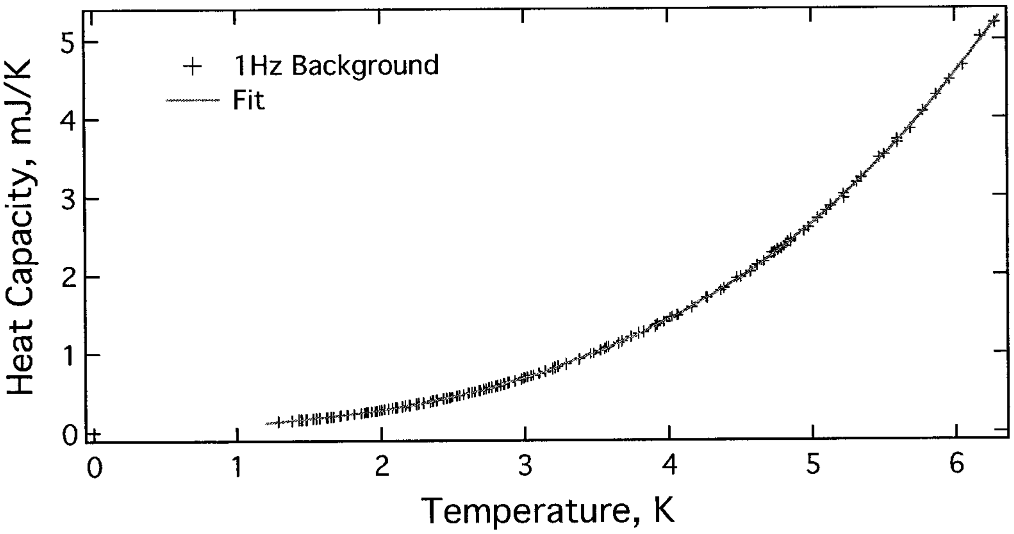

T (K)	C (mJ/K)
1.284	0.1365
1.383	0.1523
1.429	0.1614
1.429	0.1614
1.445	0.1614
1.450	0.1626
1.450	0.1635
1.451	0.1641
1.478	0.1673
1.486	0.1686
1.529	0.1777
1.550	0.1807
1.573	0.1836
1.623	0.1936
1.631	0.1943
1.631	0.1957
1.653	0.2001
1.653	0.2007
1.654	0.2014
1.669	0.2038
1.713	0.2132
1.716	0.2134
1.721	0.2186
1.763	0.2249
1.769	0.2264
1.810	0.2363
1.858	0.2487
1.858	0.2460
1.884	0.2539
1.897	0.2582
1.906	0.2583
1.932	0.2662
1.954	0.2719
1.967	0.2755
1.967	0.2755
1.986	0.2821
2.002	0.2858
2.021	0.2920
2.051	0.3004
2.077	0.3088
2.102	0.3153
2.111	0.3173
2.150	0.3298
2.151	0.3306
2.170	0.3372
2.198	0.3441
2.202	0.3452
2.246	0.3606
2.263	0.3683
2.293	0.3777
2.294	0.3765
2.341	0.3936
2.356	0.4013
2.362	0.4027
2.384	0.4069
2.387	0.4126
2.433	0.4298
2.450	0.4374
2.456	0.4365
2.474	0.4458

continued on next page

Background Heat Capacity @ 1.0 Hz Continued

T (K)	C (mJ/K)
2.480	0.4450
2.492	0.4533
2.519	0.4636
2.526	0.4637
2.542	0.4706
2.570	0.4831
2.604	0.5010
2.610	0.5009
2.628	0.5109
2.630	0.5122
2.650	0.5202
2.683	0.5355
2.691	0.5364
2.714	0.5490
2.731	0.5550
2.750	0.5692
2.771	0.5752
2.800	0.5894
2.812	0.5953
2.834	0.6075
2.853	0.6143
2.857	0.6139
2.885	0.6329
2.894	0.6371
2.935	0.6588
2.976	0.6823
2.993	0.6921
2.998	0.6959
3.017	0.7041
3.018	0.7045
3.045	0.7220
3.058	0.7265
3.096	0.7483
3.098	0.7500
3.138	0.7767
3.139	0.7731
3.192	0.8070
3.206	0.8173
3.228	0.8338
3.284	0.8635
3.375	0.9236
3.381	0.9349
3.459	0.9898
3.483	1.0044
3.529	1.0384
3.556	1.0586
3.570	1.0746
3.587	1.0809
3.656	1.1297
3.677	1.1490
3.740	1.2078
3.789	1.2502
3.824	1.2691
3.905	1.3350
3.905	1.3444
3.918	1.3570
3.966	1.3936
4.010	1.4467
4.025	1.4559
4.060	1.4799
4.066	1.4789
4.165	1.5829
4.165	1.5751
4.264	1.7050
4.273	1.7009
4.362	1.7902
4.385	1.8175
4.473	1.9562
4.499	1.9673
4.569	2.0378
4.616	2.1169
4.665	2.1679
4.721	2.2730
4.735	2.2773
4.744	2.2847
4.760	2.3273
4.766	2.3116
4.788	2.3341
4.810	2.3606
4.832	2.4162
4.854	2.4404
4.855	2.4534
4.855	2.4210
4.947	2.5580
4.976	2.6054
5.040	2.7184
5.099	2.8146
5.132	2.8804
5.222	3.0260
5.224	2.9763
5.315	3.1764
5.347	3.2377
5.472	3.4975
5.508	3.5381
5.595	3.7268
5.597	3.6871
5.685	3.8575
5.774	4.0835
5.867	4.2914
5.960	4.4786
6.056	4.6653
6.174	5.0342
6.271	5.2073
6.273	5.1996

Background Heat Capacity @ 0.1 Hz

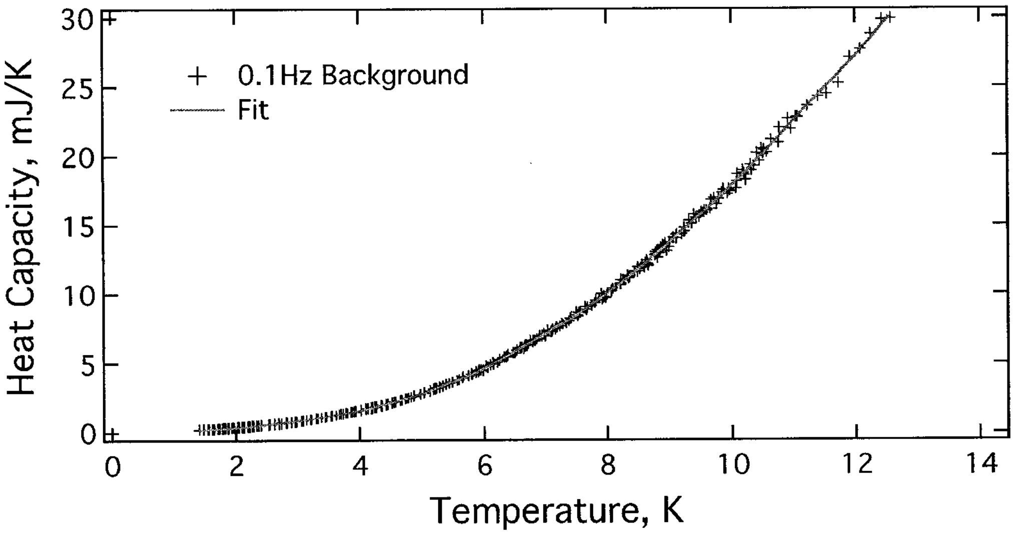

T (K)	C (mJ/K)
1.409	0.2152
1.475	0.2310
1.484	0.2312
1.548	0.2454
1.559	0.2488
1.567	0.2518
1.621	0.2651
1.633	0.2680
1.634	0.2652
1.646	0.2712
1.707	0.2867
1.721	0.2905
1.735	0.2916
1.780	0.3086
1.794	0.3125
1.810	0.3179
1.828	0.3203
1.868	0.3348
1.885	0.3415
1.889	0.3370
1.933	0.3563
1.941	0.3592
1.959	0.3649
1.977	0.3709
2.032	0.3876
2.035	0.3891
2.047	0.3897
2.051	0.3947
2.105	0.4148
2.125	0.4215
2.135	0.4268
2.145	0.4291
2.198	0.4499
2.207	0.4471
2.218	0.4575
2.233	0.4636
2.270	0.4799
2.291	0.4871
2.342	0.5088
2.370	0.5136
2.414	0.5425
2.534	0.5884
2.556	0.6069
2.630	0.6417
2.693	0.6753
2.699	0.6673
2.734	0.6961
2.814	0.7409
2.826	0.7491
2.894	0.7840
2.955	0.8235
2.975	0.8328
3.055	0.8837
3.080	0.8983
3.136	0.9367
3.203	0.9808
3.217	0.9886
3.298	1.0465
3.323	1.0597
3.379	1.1049

continued on next page

Background Heat Capacity @ 0.1 Hz Continued

T (K)	C (mJ/K)
3.441	1.1489
3.459	1.1634
3.540	1.2240
3.557	1.2390
3.621	1.2883
3.671	1.3302
3.701	1.3574
3.735	1.3828
3.782	1.4249
3.802	1.4402
3.862	1.4936
3.880	1.5067
3.912	1.5338
3.942	1.5656
4.022	1.6326
4.022	1.6467
4.102	1.7240
4.130	1.7493
4.181	1.8037
4.194	1.8002
4.202	1.8197
4.237	1.8592
4.260	1.8839
4.271	1.8992
4.343	1.9799
4.355	1.9693
4.418	2.0644
4.448	2.1075
4.514	2.1498
4.520	2.1832
4.552	2.2189
4.575	2.2584
4.655	2.3605
4.673	2.3561
4.731	2.4580
4.757	2.4859
4.779	2.5214
4.831	2.5797
4.872	2.6442
4.887	2.6734
4.988	2.7907
5.042	2.8981
5.052	2.9077
5.144	3.0357
5.196	3.1628
5.229	3.2179
5.245	3.2332
5.299	3.3004
5.349	3.4069
5.403	3.5196
5.454	3.5463
5.500	3.6622
5.574	3.7913
5.606	3.8121
5.651	3.9612
5.670	4.0430
5.753	4.1296
5.758	4.1078
5.800	4.2510
5.812	4.2278
5.872	4.3798
5.909	4.4003
5.919	4.4955
5.949	4.5398
5.985	4.5186
6.034	4.7877
6.059	4.7473
6.105	4.9030
6.147	4.9686
6.151	5.0522
6.153	4.9379
6.217	5.0783
6.251	5.2114
6.258	5.2863
6.339	5.4494
6.364	5.4612
6.369	5.5003
6.384	5.5510
6.397	5.6099
6.478	5.7571
6.507	5.7558
6.511	5.7676
6.541	5.9545
6.597	6.1266
6.622	6.1435
6.657	6.0747
6.673	6.2567
6.685	6.2641
6.704	6.3193
6.756	6.6738
6.803	6.5401
6.810	6.6531
6.829	6.6492
6.839	6.6241
6.864	6.7292
6.912	6.9523
6.946	6.9681
6.972	7.0954
6.995	6.9625
7.034	7.3415
7.089	7.2876
7.105	7.3540
7.113	7.4075
7.154	7.4465
7.173	7.5915
7.180	7.6208
7.228	7.6373
7.255	7.8311
7.275	7.8098
7.329	7.8595
7.373	8.0237
7.395	8.2432
7.403	8.2443
7.493	8.6568
7.514	8.4702
7.520	8.4097
7.534	8.6223
7.553	8.6242
7.638	9.0674
7.650	8.8449

continued on next page

Background Heat Capacity @ 0.1 Hz Continued

T (K)	C (mJ/K)	T (K)	C (mJ/K)	T (K)	C (mJ/K)
7.654	8.8486	8.817	13.1176	10.099	18.7033
7.673	9.0335	8.827	12.9451	10.184	18.9401
7.746	9.1247	8.840	12.9818	10.195	18.7421
7.794	9.3414	8.852	13.3595	10.204	18.6124
7.810	9.5293	8.880	13.5381	10.226	18.2304
7.867	9.6667	8.883	13.3988	10.304	19.3344
7.905	10.0130	8.916	13.5094	10.322	18.9541
7.916	9.6055	8.925	13.6404	10.354	19.2473
7.933	9.7306	8.952	13.1082	10.411	20.2284
7.948	9.7975	8.986	13.4088	10.449	19.6232
7.973	9.7315	8.993	13.7100	10.481	20.5205
8.070	10.2749	9.058	14.0408	10.509	20.1444
8.073	10.2027	9.102	14.0281	10.522	20.4246
8.085	10.3877	9.104	14.2569	10.568	20.2521
8.095	10.3977	9.114	14.3117	10.639	21.1712
8.208	10.7299	9.195	14.3129	10.766	20.9336
8.221	10.6898	9.232	14.7952	10.778	22.0309
8.222	10.8039	9.235	14.4622	10.916	22.6691
8.224	11.0527	9.245	14.5423	10.968	21.9262
8.256	11.0212	9.314	15.2943	11.047	22.7907
8.332	11.3453	9.357	15.1124	11.068	22.8026
8.345	11.1763	9.390	15.7396	11.078	22.7689
8.357	11.1941	9.431	15.4840	11.232	23.5811
8.362	11.2616	9.477	15.5519	11.406	24.2910
8.444	11.6378	9.519	15.9405	11.540	24.4605
8.481	11.6370	9.544	15.8941	11.726	25.2237
8.492	11.9511	9.563	16.0315	11.907	27.1351
8.523	11.8003	9.601	16.0449	12.082	27.6804
8.554	12.1312	9.658	16.1903	12.255	28.7936
8.590	11.9300	9.676	16.8084	12.431	29.8232
8.618	12.2498	9.721	16.9168	12.575	29.8883
8.626	12.4637	9.765	16.5177	12.755	30.9702
8.654	12.1977	9.799	16.8770	12.948	32.1737
8.656	12.0597	9.845	17.3615	13.122	33.9583
8.759	12.8075	9.873	17.5715	13.286	34.2066
8.770	12.8501	9.879	17.5053	13.461	35.8423
8.772	13.0307	9.937	17.2187	13.634	36.5293
8.787	12.8979	9.955	17.5769	13.797	38.1465
8.798	13.1631	9.974	17.4467	13.947	38.3432
8.805	12.6353	10.076	17.6424	14.153	40.0433
8.808	13.2130	10.085	18.1269	14.312	40.3256

VITA

Tate Wilson was born and raised in Denver, Colorado. He dropped out of high school at 16, because it was taking too much time away from learning. He has worked as a baker, pastry chef, welder, and musician, and has traveled extensively, despite an abiding comfort in the Northwest US.

Tate returned to school after many years, to take a few 'personal enrichment' courses at a community college. Having a voracious appetite for knowledge, he soon had taken almost all of the courses offered there, had a transfer degree, and had no reason not to go to the University. Ten happy and productive years later, he is ready to move on, and hopefully to give back richly to the scientific community.